Journal of Cardiovascular Magnetic Resonance (2007) **9,** 335–475

ISSN: 1097-6647 print / 1532-429X online
DOI: 10.1080/10976640601153077

informa
healthcare

Saturday Poster Session

Abstract Session XVII: Saturday, February 3, 2007

484. HIGH-RESOLUTION CARDIOVASCULAR MAGNETIC RESONANCE IMAGING OF THE CAROTID ARTERIES RELIABLY DETECTS VERY SIGNIFICANT EARLY ATHEROSCLEROSIS IN PATIENTS WITH ELEVATED LP(A)

Hamid Sattar, MD,[1] Kim Christian,[2] Mary P. Harmon,[2] H. Robert Superko, MD,[2] Szilard Voros, MD.[2] [1]***Wayne State University, Detroit, MI, USA,*** [2]***Fuqua Heart Center of Atlanta, Atlanta, GA, USA.***

Introduction: Atherosclerosis (AS) is the leading cause of death worldwide; elevated Lp(a) is an emerging risk factor. Cardiovascular magnetic resonance (CMR) can accurately assess AS plaque volume and composition in carotid arteries. Detection of early AS by CMR in patients with high Lp(a) has not been reported.

Purpose: To compare silent atherosclerotic burden, as measured by carotid arterial vessel wall thickness, between patients with elevated Lp(a) and normal subjects.

Methods: Ten patients with elevated Lp(a) and 10 normal subjects underwent high-resolution CMR of the carotid arteries at 1.5 T, using a commercial neck coil. After careful localization, 22 axial, non-gated, high-resolution T1-weighted turbo spin echo images of the carotid arteries were obtained, centered on the bifurcation (TR 1500 ms, TE 10 ms, field-of-view 15 cm, voxel size 0.5 × 0.5 × 3.0 cm, flip angle 180, number-of-averages 3). A subset of eight normal subjects also underwent T2-weighted imaging (TR 2500 ms, TE 92 ms, averages 4; otherwise same as T1) and proton density (PD) weighted imaging (TR 2500 ms, TE 10 ms, averages 2; otherwise same as T1). Total vessel area (TVA) and lumen area (LA) were manually planimetered and vessel wall area (VWA) was calculated (VWA = TVA-LA). %VWA was calculated as (VWA/TVA) × 100 and was averaged over all slices for the right and left internal and common carotids (APVWA). Maximum % VWA in each patient was also recorded. Demographics and clinical information were determined from charts retrospectively and through interviews with the subjects. Lipid measurements were done with standard enzymatic methods. Statistical analysis was done using unpaired t-test; values expressed as mean ± SD. APVWA by T1, T2 and PD imaging was compared using ANOVA analysis.

Results: Of the 10 patients with elevated Lp(a), known coronary disease was present in 40%. Projected 10-yr risk was 1 to 5%. Mean Lp(a) was 60 ± 34 mg/dL. Other lipid values were (mg/dL): total cholesterol 204 ± 44, LDL 114 ± 43, HDL 58 ± 24, ApoB 118 ± 48, fibrinogen 406 ± 106, CRP 1.9 ± 2.0.

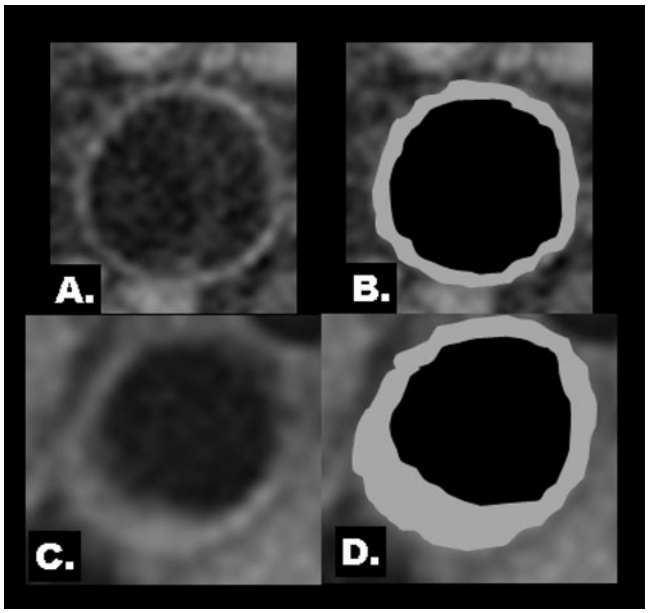

FIG. 1.

LDL peak particle diameter was 270 ± 11A. HDL 2b was 25 ± 17%. All patients were treated with lipid-lowering agents. APVWA and maximum %VWA in patients with high Lp(a) vs. normals were 42.9 ± 9.9% vs. 33.3 ± 2.6 ($p < 0.0001$) and 54.2 ± 15.1% vs. 39.1 ± 4.1 ($p = 0.012$). Maximum %VWA in patients vs. APVWA in normals was 54.2 ± 15.1% vs. 33.3 ± 2.6 ($p = 0.002$). Fig. 1 shows a representative example of a thin, normal carotid vessel wall in a normal subject (A, B), compared to thickened carotid arterial wall and an eccentric plaque in a patient with elevated Lp(a) (C, D). In the subset of eight normal subjects who were imaged with all three pulse sequences, APVWA with T1, T2 and PD weighted images were 33.1 ± 2.4%, 33.2 ± 4.9% and 33.4 ± 5.5%; there was no statistical difference between groups ($p = 0.66$).

Conclusions: Carotid arterial vessel wall thickness (APVWA) measured by high-resolution carotid CMR was significantly higher in patients with elevated Lp(a), compared to normal subjects. High-resolution carotid CMR imaging is a useful tool for the detection of very significant early AS in patients with elevated Lp(a). This imaging approach is very robust

APVWA with T1, T2 and PD weighted images in normal subjects

	T1	T2	PD
APVWA (%)	33.1 ± 2.4	33.2 ± 4.9	33.4 ± 5.5

with very low SD; this was seen with all 3 evaluated imaging pulse sequences and there was no statistically significant difference in APVWA between T1, T2 and PD imaging. The standard deviation was largest with PD imaging. Elevated Lp(a) remains a significant risk factor for early AS, despite successful treatment of the conventional lipoprotein parameters.

485. T1 MAPPING IN CARDIAC AMYLOIDOSIS REVEALS EARLY T1 SHORTENING AFTER CONTRAST

Ralf Wassmuth, MD, Daniel Messroghli, MD, Rainer Dietz, MD, Jeanette Schulz-Menger, MD. ***Franz-Volhard-Clinic, Charite, University Berlin, Berlin, Germany.***

Objectives: Using the delayed enhancement technique, unusual contrast patterns have been reported in cardiac amyloidosis. However, it is often difficult to achieve sufficient image quality. Therefore, we applied a high-resolution T1 mapping technique to measure post contrast T1 relaxation. We tried to elucidate contrast behavior in amyloid cardiomyopathy in comparison to normal volunteers.

Methods: We used a clinical 1.5 T MRI scanner (Magnetom Sonata, Siemens AG Medical Solutions, Erlangen, Germany). For T1 measurements we applied a modified Look-Locker inversion recovery sequence (MOLLI) with a flip angle of 35°, a minimum TI of 100 ms, a TI increment of 80 ms, and 3 pausing pulses. Each map was based on 11 mid-cavity short-axis images. Image sets were taken before and each minute after administration of Gd-DTPA 0.15 mmol/kg. A custom-made software generated T1-maps.

Two women with biopsy proven cardiac AL-amyloidosis (62 and 67 years) and one woman (46 years) with multiple myeloma, but no evidence of amyloidosis were investigated. Data were compared to results in 12 healthy volunteers (6 men, mean age 25 ± 5 years).

Results: In volunteers T1 decreased instantly after contrast and slowly recovered. The patient with multiple myeloma, but no amyloidosis did not differ from the control group. However, the patients with biopsy-proven amyloidosis showed lower T1 values than the controls at all time points, in particular in minute 0–4 after contrast. T1 was 60–90 ms shorter than the control group. The difference between patients and controls decreased over time (Fig. 1).

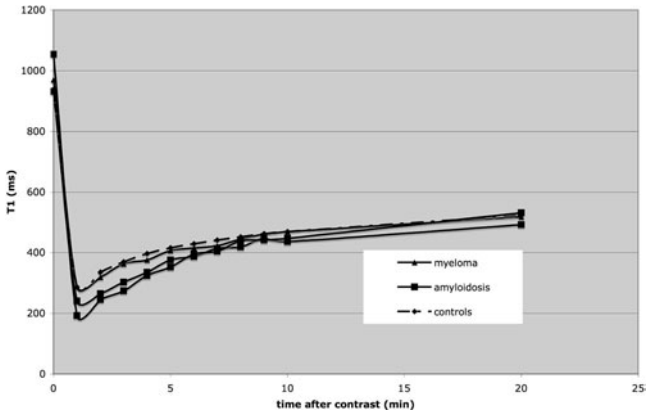

FIG. 1.

Conclusion: In cardiac amyloidosis T1-mapping reveals markedly shortened myocardial T1 early after contrast administration. This indicates that early rather than delayed contrast enhanced T1-weighted imaging might be useful to detect cardiac amyloidosis. T1 quantification might be of additional diagnostic value compared to contrast enhancement imaging alone.

486. AUTOMATED QUANTIFICATION OF SCAR TISSUE AND ITS CORRELATION WITH REGIONS OF STUNNED MYOCARDIUM

Henning Steen, MD,[1] S. Nowak,[2] D. Wald,[2] Constanze Merten,[1] Evangelos Giannitsis,[1] Stefan Wesarg.[2] ***[1]University of Heidelberg, Heidelberg, Germany, [2]Fraunhofer Institute Darmstadt, Darmstadt, Germany.***

Introduction: For a non-invasive cardiac analysis of myocardial function and morphology, MRI has become the reference standard. Volume data sets covering the whole cardiac cycle, allow the assessment of left and right ventricular volumes, wall motion, function and mass.

In patients (pts.) after acute myocardial infarction (AMI), myocardial necrosis is not directly visible in conventional cine MRI. However, after gadolinium application, non-cine contrast enhanced MRI (CE-MRI) enables detection of non-viable tissue by late enhancement (LE) of necrotic areas. The amount of necrotic tissue is a significant surrogate for clinical outcome and cardiovascular mortality. Yet, scar quantification proves to be cumbersome by manual delineation of LE areas in non-cine images.

Interestingly, the distribution of wall motion abnormalities in cine images often exceeds the areas of LE in non-cine images leading to the concept of myocardial stunning. Therefore, a direct comparison of necrotic areas and distribution of wall motion abnormalities would be important to further quantify myocardial stunning after AMI.

Purpose: In this work, we propose a method that provides an automatic fusion of standard cine MRI with CE-MRI data to determine the correlation between regions of viable but stunned and non-viable tissue. In addition, an automatic extraction of scar regions from LE data and the computation of its physical parameters are presented.

Methods and Results: Our approach combines information from cine MR and LE data. For standard left ventricular assessment, we have developed an automated method adhering to the recommendations of the AHA. In order to automatically extract scar tissue, the endocardial and epicardial borders, which have been delineated in the cine data, are transferred to the LE data. Considering the fact that the LE data set is normally acquired at around 80% between two consecutive diastolic phases, it is automatically registered to the corresponding

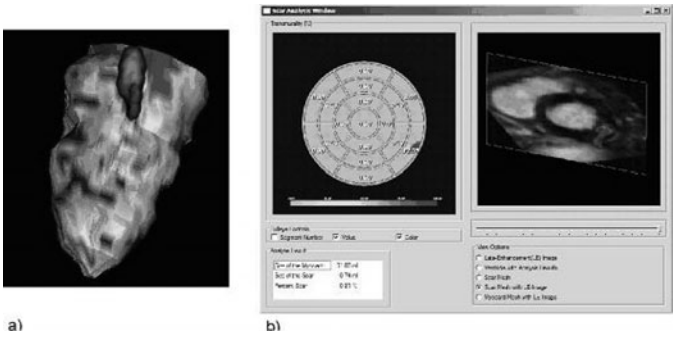

FIG. 1. a) The parameter wall motion has been mapped to a mesh that approximates the endocardial border. That mesh is merged with the LE data where anything outside the myocardium has been masked out. Thus, the correlation between scar location and the region of stunned myocardium (red) can easily be detected. b) The transmurality of the scar is visualized in a bull's-eye display (left). The outer border of the extracted scar is visualized together with the original slices of the LE data set (right).

volume of the cine data employing a normalized correlation metric.

This allows for masking out volume information outside the myocardium. The correlation between scar location and regions of stunned myocardium can be investigated combining a volume rendering of the LE data and the display of a polygonal mesh. That mesh has been extracted from the endocardial border positions in the cine data, and each vertex of the mesh a scalar value is assigned to (e.g., wall motion).

The scar tissue is automatically extracted from the masked LE data set employing a multilevel Otsu voxel classification—scar appears brightest in the LE images. Thus, its size relative to that of the myocardium can be determined. Employing a radial ray approach starting at the left ventricle's long axis the scar's transmurality is computed and visualized.

Conclusions: An automated scar analysis technique has been presented. The computation of clinical important parameters and their presentation in a commonly known bull's-eye display simplifies the decision process for the cardiologist. The newly introduced combined visualization of dynamic left ventricular parameters and the scar location goes beyond existing approaches that can be found in the literature.

487. DOBUTAMINE STRESS CARDIOVASCULAR MR IMAGING IN PATIENTS AFTER CORONARY REVASCULARISATION WITH STENT PLACEMENT

Thomas Schlosser, MD,[1] Fabian Meier,[1] Oliver Bruder, MD,[2] Peter Hunold, MD,[1] Jörg Barkhausen, MD.[1]
[1]University Hospital Essen, Essen, Germany, [2]Elisabeth Hospital, Essen, Germany.

Introduction: Dobutamine stress cardiovascular MR imaging for detection of ischemia-induced wall-motion abnormalities has become a mainstay for noninvasive diagnosis and risk stratification of patients with suspected coronary artery disease (CAD). Several studies have demonstrated that dobutamine stress MR provides high sensitivities and specificities for the detection of ischemia and is superior to dobutamine stress echocardiography. Furthermore, it has been shown that it can be used for risk stratification and it allows predicting patients' prognosis. However, most studies included patients with suspicion of coronary artery disease, whereas larger studies on CAD patients after stent placement have not been published yet.

Purpose: In our study we investigated the value of high-dose dobutamine stress MR imaging in CAD patients after percutaneous coronary interventions (PCI) for the detection of restenoses using invasive coronary angiography as the standard of reference.

Methods: Fifty patients (mean age 62 ± 7 years) with known coronary artery disease who had undergone PCI with stent placement were examined with high-dose dobutamine stress MR imaging and invasive coronary angiography. MR imaging was performed on a 1.5 T MR scanner (Magnetom Sonata, Siemens, Erlangen, Germany). A dobutamine/atropine stress protocol (10, 20, 30 and 40 μg/kg per min dobutamine and up to 1 mg of atropine) was used until the age-predicted target heart rate was achieved. Imaging at each stress level was performed in at least 3 long and 3 short axis views using a segmented steady state free precession sequence (TrueFISP, TR 3 ms, TE 1.5 ms, FA 60°). All examinations were evaluated by an experienced radiologist and a cardiologist in consensus. Myocardial ischemia was defined by new or worsening stress-induced wall motion abnormalities in more than one myocardial segment.

Results: In the 50 patients, coronary stents were placed in 74 coronary arteries. Seven in-stent stenoses were found by use of invasive coronary angiography; six of these cases were correctly diagnosed by MRI, one in-stent stenosis was missed by MRI which resulted in a sensitivity of 86%. Sixty-seven coronary arteries with implanted stents showed no significant stenoses in invasive coronary angiography, however, in seven of these vessels the MRI examination was false positive, which resulted in a specificity of 89%. The positive predictive value was 46%, the negative predictive value was 98%. Diagnostic accuracy was 89%.

Conclusion: High-dose dobutamine stress MRI allows for a reliable detection of significant in-stent stenoses: Due to a high diagnostic accuracy the technique appears to be helpful in the selection of patients who need to undergo control invasive coronary angiography.

488. COMPARISION OF UNSUPERVISED FULLY AUTOMATED INLINE VENTRICULAR FUNCTION ANALYSIS VS. MANUAL CONTOURING IN CMR EVALUATION OF GLOBAL SYSTOLIC AND DIASTOLIC FUNCTION

Anup Bhargava,[1] Bernd J. Wintersperger,[1] Carmel Hayes,[2] Jens Guehring,[3] Olaf Dietrich,[1] Armin Huber,[1] Stefan

O. Schönberg,[1] Maximilians F. Reiser.[1] ***[1]Klinlkum Grosshadern, LMU, Munich, Germany, [2]Siemens Medical Solutions, Erlangen, Germany, [3]Siemens Corporate Reseach, Princeton, NJ, USA.***

Introduction: Evaluation of cardiac function is one of the main referrals for CMR as its accuracy and reliability has been proven in numerous studies. While necessary post-processing for evaluation of global systolic parameters such as end-diastolic volume (EDV), end systolic volume (ESV) and ejection fraction (EF) is straight forward, accurate contouring of each individual frame, which is necessary for evaluation of diastolic parameters, is rather time consuming. The use of semi-automated software algorithms has reduced necessary post processing efforts although evaluation of both, systolic and diastolic parameters still takes ∼20 minute on average. Hence, evaluation of a reliable fully automatic segmentation method becomes a necessity.

Purpose: Evaluation of the accuracy of an unsupervised fully automated inline analysis of systolic and diastolic left ventricular (LV) function based on cine SSFP MRI in comparison to manual segmentation and contouring in healthy volunteers and patients with LV dysfunction.

Methods: Twenty-five patients with LV dysfunction and 4 volunteers underwent cine MR analysis at 1.5 T (Magnetom Avanto; Siemens Medical Solutions) with retrogated cine TrueFSIP along the cardiac short axis. Cine TrueFISP provided a spatial resolution of 1.4×1.9 mm^2, a slice thickness of 8mm and a temporal resolution of 42 ms (GRAPPA $R = 2$). Ventricular coverage was based on 9–12 short axis slices ranging from the mitral valve annulus to the apex with 2 mm gaps. Fully automated segmentation and contouring was included into the ICE image reconstruction environment without the need for any user interaction. In addition acquired cine data sets were also manually segmented using semiautomated post-processing software (ARGUS; Siemens Medical Solutions). Results of fully automated evaluation were compared with results of manual segmentation in regard to end-diastolic volume (EDV), end-systolic volume (ESV), ejection fraction (EF), myocardial mass (MM) as well as peak ejection rate (PER) and peak filling rate (PFR).

Results: Volumetric results of the automated inline analysis for EDV ($r = 0.95$), ESV ($r = 0.95$) EF ($r = 0.93$) and MM ($r = 0.97$) showed high correlation with results of manual segmentation (all $p < 0.001$). Head-to-head comparison though did

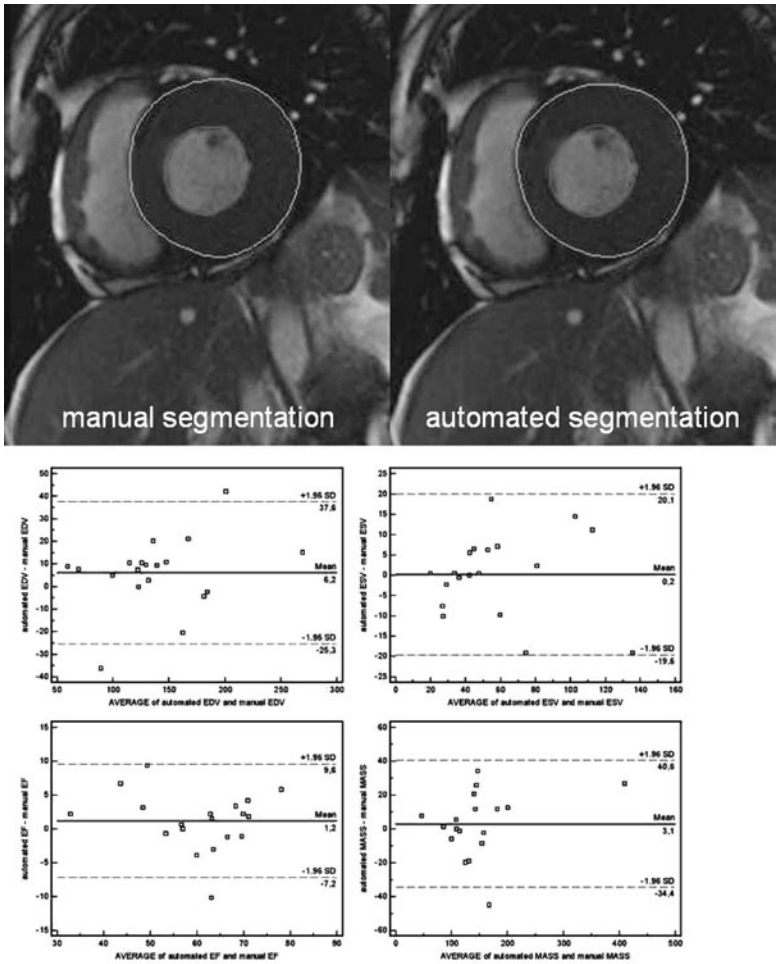

not show significant differences between automated and manual evaluation for EDV (142.7 ± 51.7mL vs. 136.5 ± 47.0 mL; p = 0.11), ESV (57.1 ± 31.8 mL vs. 56.8 ± 32.1 mL; p = 0.92), EF (61.1 ± 11.0% vs. 59.8 ± 11.7%; p = 0.23) and myocardial mass (149.5 ± 77.7 g vs. 146.5 ± 72.4 g; p = 0.50). The results of the fully automated evaluation of PER and PFR showed good correlation in comparison to the manual approach, while fully automated inline analysis allowed for significant reduction in post-processing time.

Conclusions: Unsupervised fully automated segmentation and contouring performed during image reconstruction enables accurate inline evaluation of global ventricular performance, providing also information of diastolic parameters in addition to end-diastolic and end-systolic volumes. This initial study has proven the accuracy of this approach in patients with LV dysfunction. In regard to the workflow of CMR clinical implementation of inline functional analysis would allow for a substantial time saving.

Further studies are necessary evaluating the performance of the fully automated approach in a wide range of clinical scenarios.

489. WHOLE-HEART CORONARY ANGIOGRAPHY USING A 3D CONES TRAJECTORY AND ALTERNATING-TR BALANCED SSFP

Paul T. Gurney, Phillip C. Yang, Bob S. Hu, Dwight G. Nishimura. ***Stanford University, Stanford, CA, USA.***

Introduction: Whole-heart imaging using the 3D Cones trajectory (1) has many benefits over 3DFT methods, such as robustness to motion artifacts, a higher readout duty cycle, and reduced scan time. However, since it is a radial trajectory and, therefore, does not support centric encoding, it is incompatible with standard periodic fat saturation techniques. Previous work has used phase-based fat suppression (2), but this results in a reduction in achieved resolution due to partial-volume effects and off-resonance blurring of the fat signal. The recently proposed alternating TR (ATR) balanced SSFP sequence (3) is more appropriate for radial trajectories since it suppresses fat in the steady state.

Methods: Figure 1a shows the pulse sequence used, with TR1/TR2 = 0.7 ms/4.1 ms. The effective RF flip angle for each TR (TR1/TR2) was 80°(40°/40°), with a phase difference of 135° between TR1 and TR2. The standard 180° phase cycling was applied after each TR1/TR2 sequence. The slab width was set to 15 cm FWHM with a TBW of 2.2. The 3D Cones trajectory was designed for a resolution of $1.1 \times 1.1 \times 1.5\ mm^3$, a field of view of $28 \times 28 \times 20\ cm^3$, and a readout plus rewinder length of 3 ms, resulting in a requirement of 10,000 readouts. On every heartbeat, steady-state is achieved with a 20 TR raised cosine ramp of flip angles, followed by an 8-interleaf 2D coronal projection pre-navigator, 80 TRs of 3D Cones readouts, an 8-interleaf 2D coronal projection post-navigator, and a raised cosine ramp down of flip angles over 10 TRs. A complete dataset is acquired every 125 heartbeats. Cross-correlation over a region of interest of the navigator images near the proximal left coronaries gives an estimate of the S-I position of those vessels. The 3D Cones dataset was acquired 8 times (for a total scan time of 1000 heartbeats) with each readout placed in a different cardiac phase (giving a best-case temporal resolution of 48 ms). Lower resolution 3D time-resolved reconstructions were performed with gating based on either cardiac phase or navigator respiratory position, showing cardiac motion during the acquisition window or motion caused by breathing. These reconstructions enable retrospective selection of an appropriate cardiac window (typically 120 ms), respiratory window (typically 3 mm) and respiratory compensation factors for a full-resolution reconstruction. Respiratory compensation was performed by applying appropriate linear phase to each readout in the S-I and A-P directions. All scans were performed on a GE Excite 1.5T system using an 8-channel cardiac coil, and informed consent was obtained from all volunteers.

Results: The resulting contrast generated with this pulse sequence is shown in Figure 1b. Excellent (3:1) fat suppression is seen over a range of off-resonance frequencies from −50 to 50 Hz. Figure 2 shows several reformats of the acquired 3D dataset, verifying good fat suppression around the proximal vessels. The fat suppression is compromised at the distal regions of the RCA,

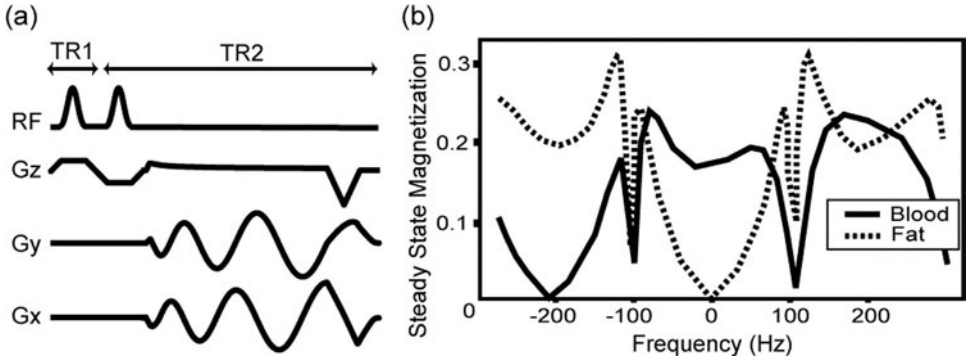

FIG. 1. (a) The ATR SSFP 3D cones pulse sequence used, and (b) the frequency response of the sequence.

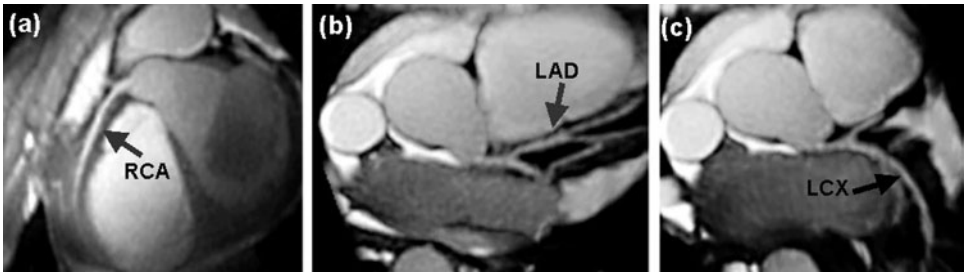

FIG. 2. Curved multi-planar reformats of the 3D dataset, showing the (a) RCA, (b) LAD, and (c) LCX coronary arteries. Note the excellent fat suppression in the proximal vessels.

probably due to off-resonance. Nonetheless, this method results in very high quality angiography covering large portions of both the left and right coronary trees.

REFERENCES

1. Magn Reson Med 2006; 55:575–582.
2. 14th ISMRM 2006; program 2156.
3. Magn Reson Med 2006;55:557–565.

490. ECG-GATED CONTRAST ENHANCED ANGIOGRAPHY WITH PARALLEL IMAGING AND SLICE PARTIAL FOURIER FOR IMPROVED PULMONARY VEINS AND LEFT ATRIUM IMAGING

Maggie M. Fung, MSc,[1] Ehud Schmidt, PhD,[2] Godtfred Holmvang, MD.[3] [1]***GE Healthcare, Bethesda, MD, USA,*** [2]***GE Healthcare, Boston, MA, USA,*** [3]***Cardiology, Massachusetts General Hospital, Boston, MA, USA.***

Introduction: Ungated 3D contrast-enhanced MR angiography (ceMRA) has been extensively used to provide a 3D model of the left atrium and pulmonary veins for pre-operative planning in electro-physiology (EP) mapping and ablation procedures. However, intra-cardiac structures may be blurred and pulsatility artifacts are also observed in those patients with a strong pulsatile flow. An ECG-gated ceMRA sequence might reduce these artifacts, but the breath-hold time is usually elongated. In this study, we utilized SENSE parallelized acquisition in-plane and partial-Fourier techniques in the slice direction to reduce the breath-hold time in an ECG-gated 3D ceMRA technique. We undertook to demonstrate the improvement in the visualization of the pulmonary veins (PV), the left atrium (LA) and the intra-arterial septal wall using this ECG-gated technique, compared to the conventional ungated approach.

Methods: ceMRA was performed on 16 patients in a 1.5T whole-body MR system with an 8 channel cardiac coil (GE Healthcare, Waukesha, USA), using both ungated and gated ceMRA. The first 5 patients underwent conventional ungated ceCMRA (TR/TE = 3.3/0.9 ms, Flip = 40°, 1 NEX, resolution 1.1 × 1.8 × 2.2 mm^3 (0.6 × 0.6 × 1.1 mm^3 after interpolation), elliptic centric acquisition, scan time = 32 ± 3 s for 60 uninterpolated slices). A second group of 5 patients underwent an ECG-gated ceMRA with a 3D vascular TOF SPGR sequence (TR/TE = 3.4/0.9 ms, Flip 45-50°, SENSE factor 1.5–1.75, 1NEX, resolution 1.1 × 1.8 × 3.2–3.6 mm^3 (0.6 × 0.6 × 1.6–1.8 mm^3 after interpolation), gating delay 160 ms, centric acquisition in the slice direction, scan time = 37 ± 5 s for 30 uninterpolated slices). To further reduce the breathhold time, ECG-gated ceMRA with 70% partial-Fourier encoding in the slice direction was performed on a third group of 6 patients (scan time = 31 ± 4 s). All scanning was performed with first pass contrast (0.2 mmol/kg Gd-DTPA, 2–3 cc/s) and the trigger delay, from the time of injection, was determined by the peak bolus arrival at the left atrium. For the longer breathhold scans, patients were instructed to hyperventillate for 20 seconds before breathholding. Vessel sharpnesses (defined as 1/distance between 25% and 75% maximum intensity) of the 4 pulmonary veins and the left atrial wall were analyzed separately, to assess the effect of cardiac motion on different cardiac structures. The visualization of the intra-arterial septal wall was also compared to assess the possibility of performing intra-septal puncture using ceMRA-guided images.

Results: The results (Figs. 1 and 3) showed that the reduction of cardiac motion due to ECG-gating, as compared to ungated acquisition, significantly improved the delineation of: the right superior PV (RSPV) (0.54 ± 0.15 vs. 0.77 ± 0.23, $p < 0.05$); the left superior PV (LSPV) (0.51 ± 0.08 vs. 0.92 ± 0.13, $p < 0.05$); the left inferior PV (LIPV) (0.64 ± 0.16 vs. 0.91 ± 0.20, $p < 0.05$); the anterior LA wall (0.24 ± 0.06 vs. 0.61 ± 0.18,

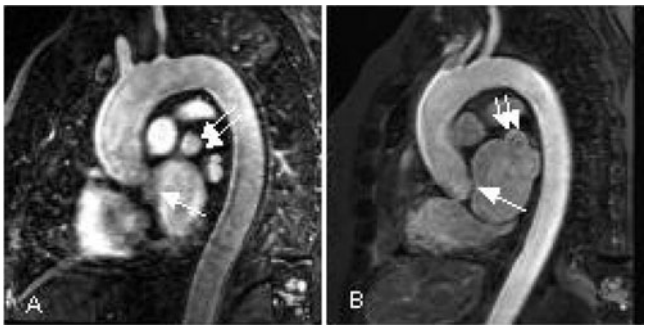

FIG. 1. Anterior left atrial wall (single arrow) and pulmonary veins (double arrows) were better visualized with ECG-gated ceMRA (B), compared to ungated ceMRA (A). Images A & B were from separate patients.

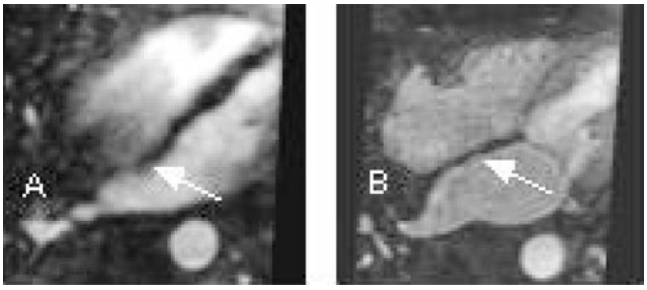

FIG. 2. Intra-atrial septal wall (arrow) was clearly delineated in ECG-gated ceMRA (B) while it was poorly visualized in ungated ceMRA (A). Images A & B were from separate patients.

$p < 0.05$). Wall sharpness was also observed to be superior in the right inferior PV (RIPV) (0.74 ± 0.14 vs. 0.89 ± 0.25, $p = 0.17$) and posterior LA wall (0.61 ± 0.10 vs. 0.72 ± 0.29, $p = 0.27$), although this did not reach statistical significance. This lack of significance might be explained by the relative distance of these structures from cardiac structures with significant cardiac-related motion such as the aortic root and left ventricle. The intra-arterial septal wall was also more clearly observed with the ECG-gated technique (Fig. 2). Further comparison, between ECG-gated ceMRA sequences with and without partial Fourier in the slice direction, showed that the partial Fourier did not reduce the contour sharpness for all 4 PVs ($p > 0.05$).

Discussion: It has been demonstrated that ECG-gating can substantially improve the delineation of the pulmonary veins, left atrium and intra-arterial septal wall in ceMRA, which may allow for improved naivgation in the EP lab using these images. Utilization of parallelized SENSE imaging and partial Fourier encoding in the slice direction can reduce the breathhold time of the ECG-gated ceMRA sequence, thus making this technique a practical alternative to the conventional un-gated scan.

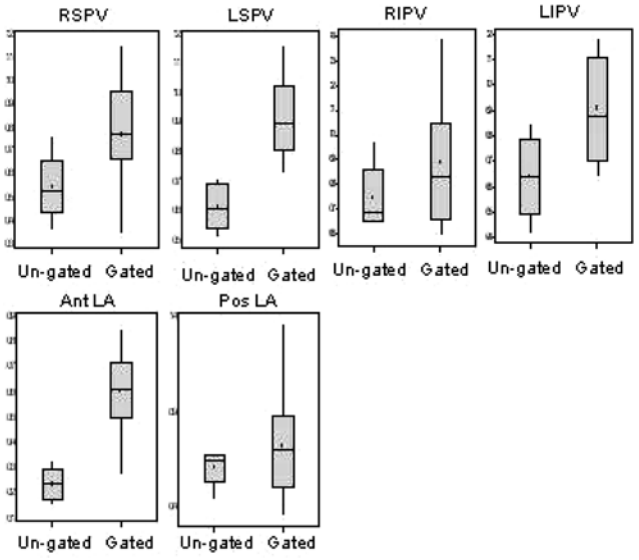

FIG. 3. Edge sharpness comparison on 16 patients between gated and ungated ceMRA at 4 pulmonary veins and left atrial walls. ECG-gated ceMRA improved the delineation of pulmonary veins and the contours visualization of the arterior left atrial wall.

491. SERIAL ACUTE MRI PERFUSION MEASUREMENTS FOR DETECTION OF REDUCED MICROVASCULAR PERFUSION DESPITE COMPLETE RESTORATION OF EPICARDIAL BLOOD FLOW IN PATIENTS WITH ST ELEVATION MYOCARDIAL INFARCTION

Constanze Merten, MD, Henning Steen, MD, Hugo A. Katus, Evangelos Giannitsis, MD. ***University Heidelberg, Heidelberg, Germany.***

Introduction: In patients (pts) with acute ST elevation myocardial infarction (STEMI), epicardial vessel occlusion leads to microvascular perfusion (MVP) failure. Despite normal epicardial flow after PCI of the infarct related artery (IRA), a reduced MVP is often observed. Few data exists on MVP-time course after STEMI. We hypothesized that MVP recovery is prolonged but can be evaluated by cardiac MR (CMR) MVP imaging.

Methods: We performed gadolinium CMR first-pass perfusion in 28 STEMI pts at day 1of 7 after successful PCI by employing two semi-quantitative parameters from signal intensity (SI)-curves: 1. = contrast enhancement ratio (CER = [peak SI–baseline SI]/baseline SI); and 2.= upslope = SI–increase/frame.

Results: Day 1 after reperfusion all pts showed a significantly reduced MVP in infarcted compared to remote myocardium (CER:1.1 ± 0.1vs.2.2 ± 0.1, $p < 0.001$; upslope: 0.6 ± 0.1vs.1.5 ± 0.2,< 0.001). At day 7, MVP in the infarcted area was still significantly reduced (CER:1.8 ± 0.1 vs.2.4 ± 0.1, $p < 0.001$; upslope:1.0 ± 0.1 vs. 1.6 ± 0.1, $p < 0.001$) but also revealed a significant increase compared to the infarct MVP at day 1 ($p = 0.004$).

Conclusion: After successful STEMI recanalization, MVP remains significantly impaired at day1 and, although again significantly improved, at day 7. CMR is a sensitive diagnostic tool to visualize STEMI-induced MVP deficits which could have profound impact on further post recanalization risk stratification and treatment strategies.

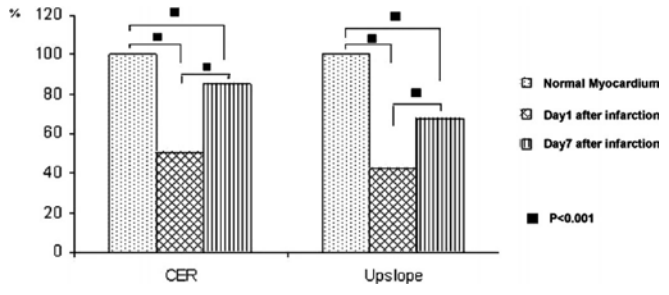

492. ROBUST TRACKING OF IRREGULAR SHAPE REGION OF INTEREST IN THE MYOCARDIUM USING MR TAGGING

Ayman M. Khalifa,[1] Abu Bakr M. Youssef, PhD,[1] Nael F. Osman, PhD.[2] [1] *Cairo University, Cairo, Egypt,* [2] *Johns Hopkins University, Baltimore, MD, USA.*

Introduction: The harmonic phase (HARP) technique is used for fast and automated analysis of tagged cardiac magnetic resonance images (1). HARP can track the motion of individual points through a sequence of tagged images. Because of regional fading of tags, too rapid motion and through-plane, motion tracking of some individual points would fail resulting in miscalculation of strain. It is useful to track irregularly shaped contours, marking specific regions of interest in delayed enhancement or first pass perfusion images, in order to study the strain inside and adjacent to them. A modified HARP technique (2, 3) was proposed to correct for mistracking errors by preserving the shape of contour while tracking, by combining HARP with active contour methods (ACM) (4). The modified HARP worked successfully for tracking regular, smooth contours as circular ones; however, it was less successful in case of irregular shaped contour, and another modification to the technique is needed.

Purpose: We propose a modification to the HARP technique to reduce the tracking error in case of irregular contours by embedding them in circular contours that are tracked by the modified HARP technique.

Methods: Three circular contours (epicardial, endocardial and mid wall) are manually drawn as white contours shown in Fig. 1B. Each contour consists of 24 points. These contours are tracked using the modified HARP. Any irregular contour is then set on top of the circular contours as red contour shown in Fig. 1B. The motion of the points on the circular contours are used to create the displacement field of arbitrary points inside the myocardium. This is done by assuming that the number of tracked points inside the myocardium is high enough to capture the motion information of the left ventricle. In other word, the motion of an arbitrary point (of the irregular shape) inside the myocardium can be estimated from the motion of points of the three circular contours. Bicubic-Spline (5) is used for interpolation and it efficiently estimates the motion of each point of the irregular shape contour from the motion of the circular shape contours.

Results: Fig. 1A shows the first timeframe of heart. Fig. 1B Shows an irregularly shaped contour (red) on top of the three circular contours (white). All these contours are manually drawn at this timeframe. Fig. 1C shows irregular contour tracked at the mid-diastole timeframe using two methods. The first method is HARP (red) and the other is the new technique (cyan). Both contours are identical except at the lower left part where HARP causes mistracking and the new technique corrects it. Fig. 1D shows the location of the irregularly shaped contour at the mid-diastole tracked using the new technique with respect to the circular contours tracked using the modified HARP. It is obvious that the mistracked points were corrected.

Conclusion: Estimating the motion of any irregularly shaped contour from the motion of the three circular contours tracked using the previously modified HARP is a robust technique against mistracking of motion. This will consequently improve the calculations of regional strain and make it less prone to error.

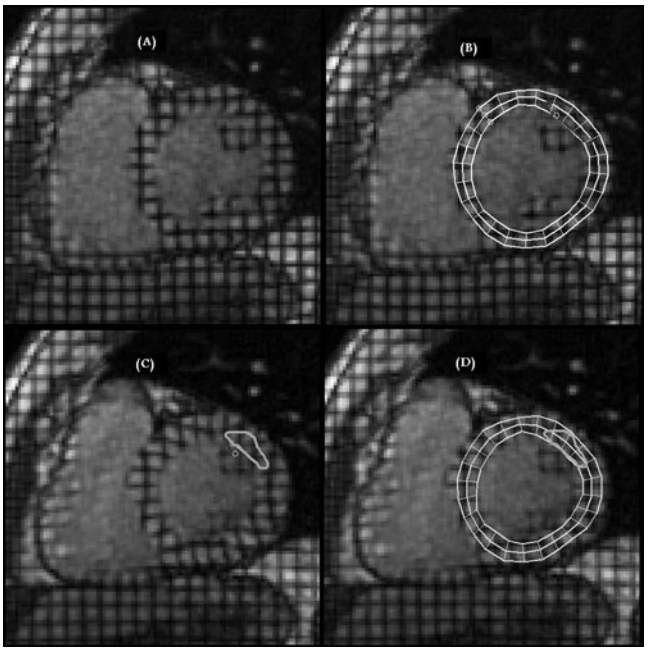

FIG. 1.

REFERENCES

1. Osman, et al. 1999; 42:1048–1060.
2. Khalifa, et al. SCMR 2004.
3. Khalifa, et al. SCMR 2005.
4. Kass, et al. IJCV 1998; 1:321–331.
5. Farin G. Curves and Surfaces for Computer Aided Geometric Design.Academic Press.

493. EVALUATION OF MYOCARDIAL LESIONS IN PATIENTS WITH TRANSIENT LEFT VENTRICULAR APICAL BALLOONING (TAKOTSUBO CARDIOMYOPATHY) BY STUDY OF DELAYED ENHANCEMENT OF GADOLINIUM WITH MAGNETIC RESONANCE IMAGING

Xavier H. Lyon,[1] Christophe Imsand,[1] Frank Renders,[1] Salah D. Qanadli,[2] Eric Eeckhout.[1] [1] *Service of Cardiology-CHUV, Lausanne, Switzerland,* [2] *Department of Radiology-CHUV, Lausanne, Switzerland.*

Introduction: Transient left ventricular apical ballooning (Takotsubo cardiomyopathy, TLVAB) is an acute transient left ventricular (LV) dysfunction, which is typically triggered by emotional or physical stress. The phenomenon is increasingly reported and is characterized by ECG alterations mimicking an acute coronary syndrome in the absence of obstructive

coronary disease on angiography. Pathophysiology is not understood, and it is not known if myocardial damages persist after the acute event; biopsies performed in a small number of patients ranged from normal myocardium, interstitial fibrosis to mononuclear infiltrate. Differential diagnosis could be difficult as an atherothrombotic coronary event without residual lesion on angiography, a prolonged spasm of an epicardial artery or a severe acute myocarditis could share the same clinical presentation.

Purpose: To evaluate if myocardial lesions could be detected in TLVAB by evaluating the delayed enhancement of gadolinium (DE) with magnetic resonance imaging (MRI) which is known to be specific and sensitive for the presence of myocardial fibrosis. These data could help better understanding the pathophysiology and contribute to a more accurate diagnostic of TLVAB.

Methods: Evaluation of DE by MRI (15' after IV injection of 0.1 mmol/L of Gd) was performed in 10 consecutive patients fulfilling diagnostic criteria for TLVAB after cardiac function had fully recovered (delay from acute event 45 ± 24; mean ± SD).

Results: Patients were predominantly female (sex ratio w/m: 9/1; mean age 73 ± 9 y) A triggering stress was identified in 9/10 (3 emotional, 6 concomitant acute illness). All patients have ECG alterations mimicking an acute ischemic event (ST elevations/T wave inversion: 5/5). Initial LV ejection fraction (EF) was 31 ± 7 % with complete normalization at MRI follow up (61 ±5%). Peak troponine I level range from 0.17 to 5.04 ng/L. Coronary angiography show normal arteries in 3 patients and mild atherosclerosis (without angiographically significant lesion) in 7 patients with TIMI 3 flow in every vessels. Vasoactive amines were transiently needed in half of cases. All patients were free of cardiac symptoms at 1 year with 1 case of recurrence. There was no DE enhancement observed in any patient.

Conclusions: This study has demonstrated the absence of DE in consecutive patients having suffered of TLVAB. This support the hypothesis of a diffuse constriction of the microvasculature due to cathecolamines excess as no myocardial fibrosis could have been detected although elevation of troponine was measured during the acute event. It is suggested that DE evaluation should be performed in every TLVAB case as it would help differentiating this entity from myocardial infarction (subendocardial DE) or severe myocarditis (subepicardial DE) with important implications in terms of treatment, follow up and prognosis.

494. MRI PERFUSION CHANGES IN THE HYPOTHERMIC ISOLATED PORCINE HEART: IMPLICATIONS FOR EXTENDED DONOR HEART PRESERVATION AND CARDIAC TRANSPLANTATION

Andrew L. Rivard, MD, MS,[1] Cory M. Swingen, MS, PhD,[2] Forum D. Kamdar, BA, BS,[3] Jonathan W. Holstad,[3] Zachary Demorest,[3] Erin J. Cordova,[3] John E. Foker, MD, PhD,[3] Michael Jerosch-Herold, PhD,[4] Ranjit John, MD,[3] Richard W. Bianco, BA.[3] [1]***University of Florida, Gainesville, FL, USA,*** [2]***University of Minnesota, Minnesota, MN, USA,*** [3]***University of Minnesota, Minneapolis, MN, USA,*** [4]***Oregon Health Sciences University, Portland, OR, USA.***

Purpose: Preservation of the donor heart is currently limited by ischemic changes that have well known biochemical and histological effects. Unfortunately whole heart assessment using those techniques renders the organ not useable for transplantation. We chose MR imaging to determine the global changes in myocardial perfusion with prolonged hypothermic storage. Peak contrast enhancement was used as a measurement of viable microvasculature.

Materials and Methods: Porcine hearts were excised (n = 24), flushed with Ribosol cardioplegic and stored at 7 °C for either 6.1 ± 0.6 hours (n = 13) or 15.6 ± 0.6 hours (n = 11). T-1 weighted imaging was performed in the short axis view. Approximately 80 serial images were acquired at a rate of 1/s during administration of 0.006 mmol/mL Gd-DTPA (500 mL, 1 L/min). Endo- and epicardial borders were manually drawn using the MASS® software (Version 4.2, Medis Medical Systems, The Netherlands). Signal intensity curves vs. time were generated for each heart to determine the percent contrast enhancement of the myocardium as compared to a reference. Average slope, peak slope, average enhancement, and peak enhancement parameters were measured for each heart. Average slope was calculated using a linear regression fit connecting the foot to the peak of the SI curve. Peak slope was calculated as peak slope of a smoothing spline fit to the entire SI curve. The average distribution of contrast was calculated as the average stable signal intensity during the gadolinium infusion, while the peak distribution parameter was defined as the peak signal intensity from the stable portion of the SI curve.

Results: Peak myocardial contrast enhancement at 15.6 hours was much less than at 6.1 hours (30% vs. 67%, $p < 0.005$). No correlation of peak or average up-slope of the intensity curve (as a surrogate of flow) to storage time was found. Scanner time averaged 16 min.

Conclusion: This is the first report of a global assessment of perfusion changes in the isolated heart using perfusion MRI

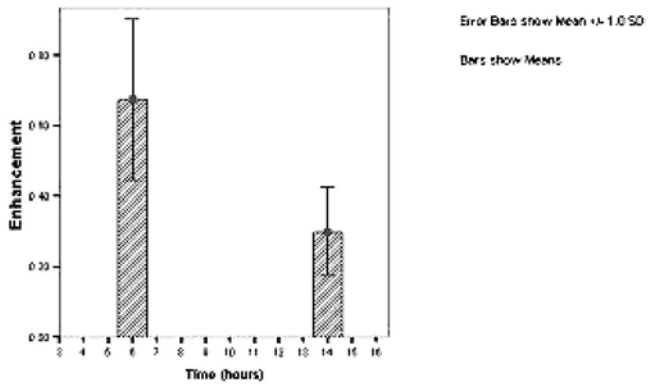

technology. Significant time-related alterations occur in the microvasculature as the heart ages in hypothermic storage. This new method can be used to assess new preservation solutions, preservation methods, or donor heart quality. A major advantage is that this technique allows a practical and feasible myocardial evaluation of donor heart ischemia using the same modality used in post transplant follow-up.

495. TIME-RESOLVED CHANGES IN LEFT VENTRICULAR SHAPE, MYOCARDIAL AND INTRACAVITARY VOLUMES CONTRIBUTE TO IMPROVED CONTRACTILITY IN SURGICAL VENTRICULAR RESTORATION

Thu-Thao Le,[1] Liang Zhong,[2] Dhanjoo N. Ghista,[1] Si-Yong Yeo,[2] Ru-San Tan.[2] [1]*College of Engineering, Nanyang Technological University, Singapore, Singapore,* [2]*Department of Cardiology, National Heart Centre, Singapore, Singapore.*

Introduction: By excluding akinetic or dyskinetic left ventricular (LV) segments, surgical ventricular restoration (SVR) is believed to reduce LV volume, restore normal LV geometry and improve LV contractility in patients with ischemic cardiomyopathy. The mechanism of LV functional recovery is not well understood. Zhong et al (1) described a novel shape-based contractility index (*CONT*) based on instantaneous generated LV wall stress (σ) normalized to LV intracavitary pressure (P), σ^*:

$$\sigma* = \sigma/\mathrm{P} = (2+\mathrm{S})\{1 - \mathrm{S}^2(2 + \mathrm{S})/[2(2+\mathrm{S}) + \mathrm{V}^*]\}/\mathrm{V}^*\mathrm{CONT} = |\mathrm{d}\sigma^*/\mathrm{dt}|_{\max}$$

where shape ratio, S = B/A, is the ratio of LV minor (B) and major radii (A), A being defined as two-thirds of the long-axis distance from LV base to apex and B is the LV short-axis radius at the junction of the basal and middle thirds of the same LV long-axis; $V^* = V_m/V$ is the ratio of LV myocardial volume at end-diastole (V_m) and instantaneous LV intracavitary volume (V). Normalizing σ to P eliminates the requirement for invasive LV pressure measurement, enabling CONT to be estimated from non-invasive imaging.

Purpose: We aimed to measure and compare pre- and post-operative LV volumes, function, shape, σ^* and *CONT* in patients undergoing SVR.

Methods: Patients underwent cardiac magnetic resonance (CMR) on a 1.5T MR scanner (Siemens, Avanto) less than 2 weeks before SVR, and 4 months after. V at all time instants during LV ejection and V_m were measured from manually drawn contours on trueFISP short-axis cine images (retrospective EKG-gating, 25 phases per cardiac cycle) using standard methodology. Radii A and B were determined at each time instant from long-axis 4-chamber cine images. For each patient, calculated σ^* values at all time instants were input into Matlab 7.0 software and CONT was determined from the first time-derivative.

Results: Four patients (all male; mean age 53.0 ± 9.2 years), diagnosed with ischemic cardiomyopathy and scheduled to undergo SVR, were studied. Their preoperative and 4-month postoperative ejection fractions (LVEF), S, V*, dS/dt, dV*/dt and CONT, as well as body surface area-indexed LV end-diastolic (LVEDVI) and end-systolic volumes (LVESVI) are tabulated (values expressed as mean ± SD). The preoperative and 4-month postoperative $\sigma*$and $d\sigma*/dt$ of one patient are shown in the Fig.

Conclusions: Although LV volumes reduce and LVEF increases after SVR, LV conformation becomes more spherical (*S* increases). The latter is suboptimal for LV contractile efficiency. Despite this, LV contractility, as determined by maximal generated pressure-normalized wall stress (CONT), actually

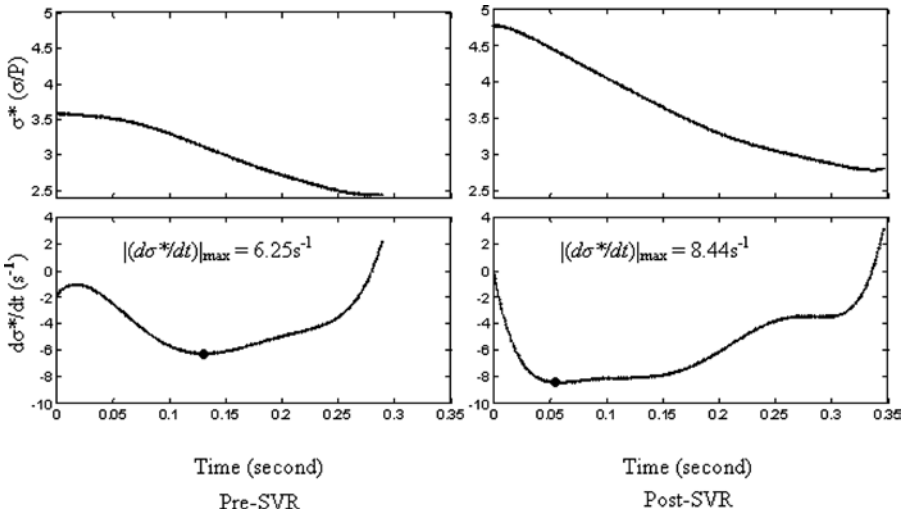

FIG. 1. Preoperative and 4-month postoperative LV pressure-normalized stress, σ^*, and its first time-derivative, $d\sigma*/dt$, at all time instants during ejection in one patient.

TABLE
CMR-derived preoperative and 4-month postoperative LV functional parameters

Parameter	Pre-surgery	Post-surgery	Percentage change
LVEDVI (mL/m^2)	123.9 ± 18.1	97.1 ± 12.8	−21.6%
LVESVI (mL/m^2)	91.3 ± 28.0	59.1 ± 7.5	−35.2%
LVEF (%)	27.5 ± 12.4	38.4 ± 10.0	+ 39.7%
S	0.49 ± 0.04	0.57 ± 0.06	+ 16.3%
V*	0.55 ± 0.07	0.61 ± 0.15	+ 10.9%
dS/dt (s^{-1})	0.42 ± 0.16	0.67 ± 0.17	+ 59.5%
dV*/dt (s^{-1})	1.21 ± 0.51	2.12 ± 0.80	+ 75.2%
CONT (s^{-1})	6.45 ± 1.66	7.44 ± 1.28	+ 15.4%

improves. It is not LV shape alone that defines LV contractility. Rather, a complex interaction of the rates of change of shape (dS/dt) and LV myocardial volume-intracavitary volume ratio (dV*/dt)—both of these increase in magnitude post-SVR–may explain the improvement in LV contractility after SVR. CMR yields accurate geometrical measurements and is a useful tool for quantifying these alterations.

REFERENCE

1. Zhong, et al. J Biomech 2006; 39:2397–2409.

496. EXERCISE CMR WITH REAL-TIME IMAGING OF WALL MOTION AND PERFUSION

Mihaela Jekic, Eric Foster, Subha V. Raman, Orlando P. Simonetti. ***Ohio State University, Columbus, OH, USA.***

Introduction: Stress testing is extensively used to diagnose coronary artery disease, a leading cause of death from cardiovascular disease worldwide. Stress may be induced by intravenous infusion of a pharmacologic agent or by exercise. In addition to reproducing symptoms related to exertion, exercise stress provides valuable clinical information on exercise capacity and ECG changes. Imaging modalities typically used with exercise testing (echocardiography and nuclear scintigraphy) have limitations in signal-to-noise and resolution, and image quality can be highly dependent on both operator and patient. Combining the physiologic advantages of exercise with the superior image quality of MRI should result in improvements in the diagnosis and treatment of coronary artery disease (1).

Purpose: To develop a protocol for real-time non-breathhold MRI of cardiac function and myocardial perfusion within 60 and 90 seconds, respectively, following maximal treadmill exercise and test its feasibility in healthy volunteers.

Methods: Seven healthy volunteers underwent MRI exercise testing using a novel real-time acquisition protocol. After resting cine images were acquired, the volunteers exercised on a treadmill positioned just outside the magnet room. The speed and grade of the treadmill were increased following the standard Bruce protocol. Twelve lead ECG and blood pressure were monitored during exercise. After reaching the target heart rate, the subjects were quickly escorted to the magnet table for stress cine imaging. A real-time SSFP sequence with TSENSE acceleration factor of 3 was used. Temporal resolution of approximately 57 ms and spatial resolution of 3.0 mm × 3.9 mm × 8 mm were achieved with no breath-hold and no ECG gating. Twelve lead ECG was recorded again immediately following imaging.

Three volunteers underwent a similar protocol with the addition of stress perfusion imaging immediately after stress function. 0.1 mmol/kg gadolinium-DTPA was administered intravenously as a contrast agent. GRE-EPI with TSENSE acceleration rate of 2 was used to obtain three short-axis slices each cardiac cycle. Resting perfusion was imaged after recovery to obtain the myocardial perfusion reserve index (MPRI).

Results: At peak exercise, the seven volunteers undergoing stress function tests reached 98.1 ± 2.4% of their age-determined maximum heart rate. By the start of imaging, the heart rate decayed to 81.1 ± 7.3% of the age-determined maximum. LV ejection fraction increased by 11.4 ± 4.3% from rest to post-exercise imaging, while cardiac output increased by a factor of 3.4 ± 0.3. The time between the end of exercise and the completion of imaging was 52.4 ± 11.6 seconds.

Stress function and perfusion scans were completed within 90 seconds post-exercise for the three volunteers. MPRI by quantitative perfusion analysis was 1.5 ± 0.1.

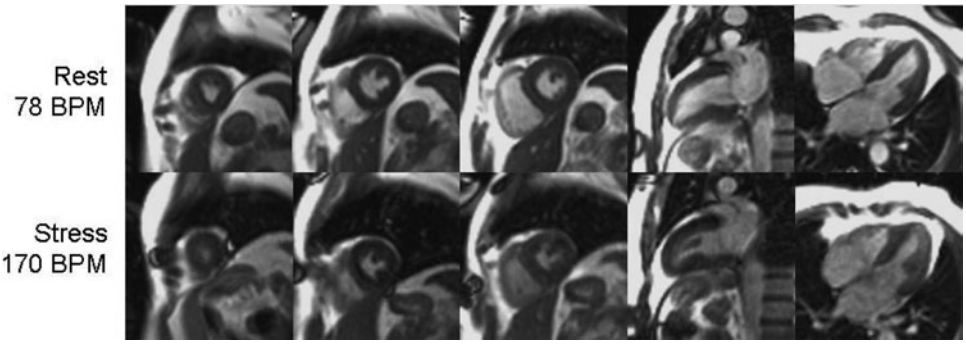

FIG. 1. End-systolic images shown at rest (top row) and immediately post-exercise (bottom row) in one normal subject. Increased contractility clearly depicted using real-time imaging with no ECG gating and no breath-hold.

Image quality was sufficient for visual assessment of wall motion and perfusion in all LV segments for visual assessment, and no subject had ischemic abnormality with stress.

Conclusions: This study demonstrates the feasibility of MRI exercise testing to capture function and perfusion at stress with real-time MRI. Efforts are being made to develop a magnet-safe treadmill for use inside the magnet room in order to further reduce the time between exercise and imaging, and consequently minimize heart rate decay.

REFERENCE

1. Rerkpattanapipat P, Gandhi SK, et al. Feasibility to detect severe coronary artery stenoses with upright treadmill exercise magnetic resonance imaging. Am J Cardiol 2003; 92:603–606.

497. USEFULNESS OF INTEGRATION OF DELAYED ENHANCEMENT MAGNETIC RESONANCE AND CORONARY COMPUTED TOMOGRAPHY ANGIOGRAPHY IMAGES IN REVASCULARIZATION PLANNING

Jolanta H. Misko, Sr, MD, PhD,[1] Marcin Basiak, Jr, MD,[1] Barbara Paraniak, Jr, MD, PhD,[1] Rafal Ulczok, Jr, MD,[2] Michal Krejca, Sr, MD, PhD,[2] Tomasz Banasik, Jr,[3] Jacek Skarysz, MD, PhD,[2] Jacek Brzezinski, MD, PhD,[1] Marek Konopka, MD, PhD,[1] Andrzej Bochenek, MD, PhD, Professor.[2] [1]***HELIMED, Silesian Centre for Diagnostic Imaging, Katowice, Poland,*** [2]***Medical University of Silesia, Katowice, Poland,*** [3]***Institute of Nuclear Physics, Polish Academy of Sciences, Kraków, Poland.***

Introduction: New techniques of cardiac imaging, coronary computer tomography angiography (CTA) and cardiovascular magnetic resonance (CMR) are undergoing rapid technological developement with constantly growing usefulness of boths methods in diagnosis of coronary artery disease (CAD). The combination of imaging of coronary arteries by CTA and myocardial viability by CMR could be a noninvasive and highly effective way of the assessment of CAD patients before revascularization.

Purpose: We hypothesis that post processing and software fusion of CTA and CMR images has the potential for better visualization and analysis of viability and necrosis in myocardial areas supplied by stenotic coronary artery.

Methods: For evaluation of potential role of image fusion of CTA and CMR we used software program for post processing and image fusion—PMOD. CTA (16-slices CT) with standard protocol for coronary arteries imaging and CMR (1.5T scanner) with protocol for myocardial viability imaging were performed in 5 patients with CAD before planned revascularization. CTA images were used as reference data, CMR images were processed and two and three dimensional color-coded maps of myocardial viability as input data were corregistrated with CTA images.

Results: All matched CTA and CMR images were analyzed by four experienced cardiac surgeons. In two patients there was no viable myocardium in area supplied by stenotic coronary artery-patients were rejected from revascularization procedure. In remaining three patients we have found no necrosis or subendocardial necrosis below 50% of transmural extension in regions supplied by stenotic arteries-in this group revascularization was performed with good results (improvement of myocardial function and stabilization of CAD).

Conclusions: Combination of two noninvasive imaging techniques; coronary CTA and CMR viability imaging seemed to have specific role in the assessment of patients with CAD before revascularization.

498. DOSE DEPENDENT SHADOW ARTIFACT IN HIGH RELAXIVITY CONTRAST ENHANCED CORONARY MRA AT 3T MAY OBSCURE VESSEL

Melanie S. Kotys, DSc,[1] Ahmed Gharib, MD,[1] Daniel Herzka, PhD,[2] Roderic Pettigrew, MD, PhD.[1] [1]***National Institutes of Health, Bethesda, MD, USA,*** [2]***Philips Medical Systems, Bethesda, MD, USA.***

Introduction: Although an SNR increase in coronary MRA is realized at 3T, this remains insufficient to support a resolution comparable to X-ray angiography. The addition of T1-shortening agents can increase vascular SNR and contrast (1). Higher relaxivity agents may further increase these benefits, however artifacts seen at higher dosages due to local field changes may result in poor coronary images.

Purpose: To evaluate a dark shadowing artifact observed in high relaxivity contrast-enhanced coronary MRA with slow infusion.

Methods: Four normal volunteers (NVs) were imaged on a 3T whole-body scanner(Achieva, Philips, Best, Netherlands) using an FFE T2-preparation coronary MRA sequence (2). Data were collected using a cardiac coil with SENSE. Acquisitions were cardiac-triggered and respiratory navigator-gated with TR/TE = 7.8/2.2 ms, $\alpha = 20^{\circ}$, FOV = 384 × 268 mm, matrix = 512 × 512, and 20 slices each 3 mm thick.

A 0.2 mmol/kg body weight of Gd-BOPTA(Multihance, Bracco, Princeton, NJ, USA) was power-injected (Spectris, Medrad, Indianola, PA, USA) at 0.1 mL/s or 0.2 mL/s followed by an equal volume and rate of saline solution. Coronary MRA of the RCA was performed at four time points: immediately before contrast injection (TP0), during contrast infusion (TP1), twice following infusion (TP2 and TP3). Each acquisition required 2:18 minutes with 40–50% gating efficiency.

For each time point, artery width and signal intensity were determined using five line profiles measured perpendicular to the RCA. Table 1 shows the acquisition parameters and profile analysis for all four NVs. The vessel width and intensity ratios with respect to TP0 were averaged over the five line profiles.

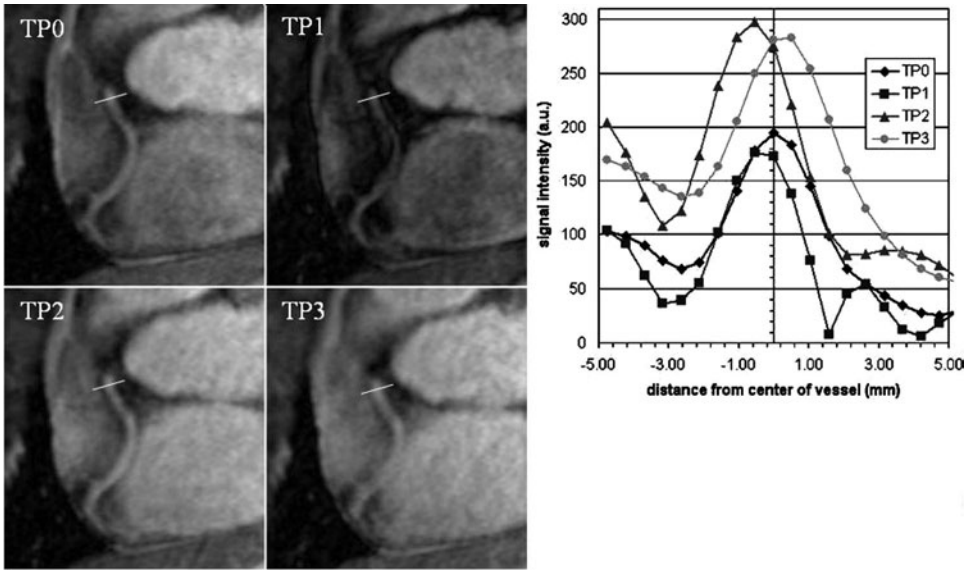

FIG. 1. Coronary MRA at four time points and corresponding line profiles through the RCA for NV2. Signal intensity plots for profiles on right. Note underestimated width and decreased intensity of TPI compared to TP0.

Results: The four time points collected for NV2 and a coronary line profile are shown in Fig. 1. A severe shadowing artifact can be observed on either side of the artery at high concentrations (TP1), reflected in the TP1 line profile. The shadowing was greatest when the artery was positioned perpendicular to the phase encoding (PE) direction. This artifact was consistent with that seen in NV1 (not shown).

The shadowing artifact led to a significant underestimation of the vessel width and decreased SNR compared to the pre-contrast vessel (NV1 and NV2, TP1). At TP2 and TP3, the artifact disappeared and SNR increased considerably. This artifact is consistent with the Gibbs phenomenon (truncation artifact) which was first described in MRI for the spinal cord (3) and recently in cardiac perfusion studies (4), where the artifact was reduced by one of two means: switching the PE direction or increasing the spatial resolution. We chose the former, being already close to the limits of spatial resolution. As expected, a parallel PE direction eliminated the shadowing (NV3, width, TP1), although it reduced the signal intensity by 10% prior to injection. This resulted in an overall decrease in SNR benefit from the contrast agent (NV3, intensity). According to the Gibbs theory, reducing the large discontinuity in intensity between the vessel and surrounding tissue should ameliorate or eliminate the artifact. Thus, we chose to simply reduce the injection rate to deliver the contrast agent volume over a longer period of time (NV4). Even for TP1, this scheme eliminated the artifact while retaining a high SNR benefit.

Conclusion: A prominent signal loss shadowing artifact along the coronary margins occurs with high Gd concentrations at 3T. Shadowing artifacts in coronary MRA can result in incorrect assessment of the coronary artery width, and may potentially obscure narrowing from vessel wall plaque. This artifact can be reduced by switching the phase encoding direction to be parallel to the vessel, but this results in a decreased SNR benefit. This shadowing artifact is dependent on concentration at the time of imaging and, therefore, may be avoided by optimizing dose or injection duration.

TABLE 1
Imaging parameters and profile analysis for coronary MRA studies

NV	PE direction relative to artery	Duration of injection (sec)	Average vessel width ratio†			Average vessel intensity ratio†		
1	Perpendicular	140	0.84	1.00	0.97	0.78	1.46	1.53
2	Perpendicular	200	0.83	1.03	1.02	0.81	1.82	1.60
3	Parallel	200	0.96	0.98	1.01	0.96	1.37	1.44
4	Perpendicular	350	1.10	1.16	1.25	1.49	1.80	1.98

†Vessel width and intensity with respect to TP0.

REFERENCES

1. Li, et al. Radiology 2001; 219:270–277.
2. Nezafat, et al. MRM 2006; 55:858–864.
3. Bronskill, et al. Radiology 1988; 166:485–488.
4. DiBella, et al. MRM 2005; 54:1295–1299.

499. CARDIAC MR MEASURES OF LEFT ATRIAL SIZE: COMPARISON OF BLACK BLOOD, SPIN ECHO AND BRIGHT BLOOD GRADIENT ECHO IMAGING

Runa Bhattacharya, MD, Erin Goheen, PA, Peter Kokkinos, PhD, Syed Zaidi, Gregory Trachiotis, MD, Michael D. Greenberg, MD. ***Washington DC VA, Washington, DC, USA.***

CMR measures of left atrial dimensions

	LA dimension	p value
T1 black blood	3.9 ± 10	
Bright blood 2 ch, major axis	5.5 ± 8	0.001
Bright blood 2 ch, minor axis	4.0 ± 8	0.045
Bright blood 4 ch, minor axis	3.9 ± 9	ns
Bright blood 4 ch, major axis	5.7 ± 11	0.0001

Introduction: Left atrial (LA) size is an independant predictor of cardiac morbidity and mortality. Traditional measures of LA dimensions have utilized echocardiographic parameters and more recently cardiac MR (CMR). The relationship between LA size made in the various CMR imaging planes has not been well defined.

Purpose: To compare conventional assessment of LA size using T1 black blood imaing with measures of the LA obtained from both two and four chamber views acquired with the bright blood, cine-FIESTA protocol.

Methods: Ninty-three patients (62 ± 14 years) underwent CMR (Signa CV/i;1.5T, GE Medical Systems) with LA dimensions obtained from standard T1 black blood images mesuring the maximal transverse dimension. The reference value was compared to LA dimensions (major and minor axis) measured from 2 and 4 chamber planes with the bright-blood, FIESTA-cine sequence.

Results: Compared to the traditional CMR measures of LA dimensions (T1 black blood images; maximal transverse dimension) the 4 chamber (minor axis) imaging plane yielded almost identical results (p = ns). Other imaging planes however yielded statistically different values for LA size with considerable variability.

Conclusions: Equivelent measures LA size can be made from the maximal transverse dimension using the traditional T1 black blood image sequence or from a 4 chamber (minor axis) using the FIESTA-cine sequence.

500. WHOLE HEART CORONARY ANGIOGRAPHY TO DETERMINE THE COURSE OF ANOMALOUS CORONARY ARTERIES—A FEASIBILITY STUDY

John F. Younger, MB BCh, Andrew Crean, MB, Sven Plein, PhD, John P. Greenwood, PhD. ***Leeds University, Leeds, United Kingdom.***

Background: Anomalous coronaries are present in 1% of the population and may be associated with sudden death, particularly if the aberrant vessel courses between the aorta and right ventricular outflow tract (RVOT) to supply the left coronary distribution. Although the course of these vessels can be demonstrated by cardiovascular magnetic resonance, traditional magnetic resonance coronary angiography (MRCA) is a time consuming examination that requires multiple, double oblique, three-dimensional (3D) acquisitions that are targeted to the likely course of the coronary. In the case of anomalous coronaries, where the course will by definition be uncertain, multiple acquisitions are often required to adequately demonstrate their path.

A recently introduced technique allows visualization of all three coronary arteries with a single 3D volume acquisition. This 'whole heart' imaging involves a navigator-gated, 3D steady-state free precession sequence to generate a volume stack, which can subsequently be analyzed as axial slices or reformatted to produce multi-planer, or volume rendered images.

Aims: The purpose of this study was to evaluate the utility of a single three dimensional volume, consisting of multiple transverse slices, (whole heart coronary angiography or WHCA) to define the proximal course of anomalous coronary arteries.

Methods: Between April 2006 and July 2006 five patients who were referred for CMR because of known or suspected anomalous coronaries were evaluated by both traditional targeted acquisitions which were either navigated free breathing or breath hold, and with whole heart coronary imaging. WHCA was performed with a sufficient number of transverse slices to cover the proximal course of the anomalous coronary using an SSFP sequence with a fat suppression and T2 preparation prepulses TR/TE/flip angle 4.6/2.3/100 and spatial resolution was 1.18 × 1.18 × 1.80 mm. A single diaphragmatic navigator was used. Both sets of images were then assessed independently for visual quality of the coronary images and diagnostic ability. The sequence which most clearly and unequivocally defined the course of the vessel was judged superior.

Results: Twenty-seven sequences were used in the 5 patients, of which 17 were targeted. Eight of these targeted acquisitions provided unambiguous diagnostic images, but in two patients the multiple targeted sequences were unable to adequately demonstrate the course of the anomalous vessel. Seven WHCA sequences were performed, of which 6 provided diagnostic images. Image quality was assessed as superior for the targeted sequences in 2 patients, for the WHCA in 2 patients and equivalent in 1 patient.

Conclusions: Magnetic resonance WHCA is feasible in patients with anomalous coronary arteries. It provides diagnostic quality images in the majority of cases which are of similar quality to traditional targeted acquisitions. Unlike targeted coronary imaging, WHCA does not require complex planning, and hence may be preferable as the initial sequence to demonstrate anomalous vessels.

Number and type of sequences, both diagnostic and non-diagnostic, performed on each patient

Patient	A	B	C	D	E
Total sequences	8	3	5	3	8
Diagnostic WH	1	1	2	1	1
Non-diagnostic WH	0	0	1	0	0
Diagnostic T	4	0	0	2	2
Non-diagnostic T	2	2	2	0	5
Superior	Equivalent	WH	WH	T	T

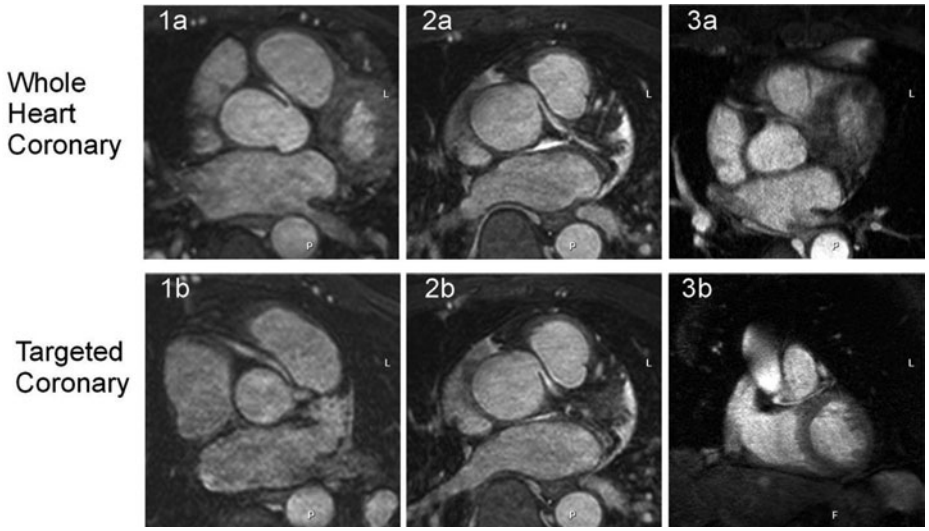

501. FREQUENCY OF T2 ENHANCEMENT IN PATIENTS UNDERGOING CARDIAC MRI ADENOSINE STRESS PERFUSION IMAGING

Vikram Raya, MD,[1] Subodh B. Joshi, MD,[2] Anthon R. Fuisz, MD.[2] [1] ***Georgetown University Hospital, Washington, DC, USA,*** [2] ***Washington Hospital Center, Washington, DC, USA.***

Background: Increased signal on T2-weighted images of the myocardium has been shown to correlate with myocardial ischemia. The T2 changes are thought to represent edema associated with peri-infarct ischemia and last days after the initial insult. The frequency of these changes seen in a population of patients referred for stress perfusion CMR, however, is not known. We hypothesized that T2 enhancement would be present in an unselected series of patients undergoing stress perfusion.

Methods: Twenty-six consecutive patients referred for CMR stress perfusion were studied using a Philips Intera CV 1.5T imaging system. In addition to standard adenosine perfusion and delayed enhancement (DE) sequences, T2 weighted black blood (BB) spin echo images were acquired in a short axis orientation. Eight slices were acquired as individual breath-holds with a slice thickness 8 mm with adjusted gap for coverage, TR of ~1765 ms, TE of 100 ms, and a matrix of 205/512 reconstructed. T2 images were acquired before the adenosine stress portion of the exam.

Results: The patients had an average age of 59 and a mean ejection fraction of 60%. All patients were referred for a history of chest pain. T2 enhancement of the left ventricular subendocardium, most prominent at the apex was present in 25 of 26 (96%) patients. Seven patients also exhibited more prominent T2 enhancement extending from the epicardial surface to the mid wall myocardium. In 5 patients with these mid wall T2 abnormalities, there were corresponding stress perfusion defects in the same vascular territory. There was no relationship between mid wall T2 enhancement and areas of delayed hyper-enhancement after gadolinium administration (infarction was seen in a remote area in 6 patients).

Conclusions: T2 enhancement restricted to the apex and subendocardium is almost universal in patients referred for stress perfusion imaging when using a standard T2 BB sequence. The mid wall T2 enhancement was seen in 26% of patients and in most cases correlated with stress perfusion defects but not areas of infarction. The persistence of post-ischemic edema identified by T2 weighted CMR may be novel imaging approach in localizing at risk myocardium.

502. PRE-TEST SCREENING BY PHYSICIANS RESULTS IN LOW CANCELLATION RATES FOR PEDIATRIC OUTPATIENTS UNDERGOING CARDIAC MRI WITH ANESTHESIA

Naum Shaparin, MD, Johanna C. Schwarzenberger, MD, Beth F. Printz, MD, Ashwin Prakash, MD. ***College of Physicians & Surgeons of Columbia University, New York, NY, USA.***

Introduction: While other authors have demonstrated the safety of general anesthesia (GA) for children with congenital heart disease (CHD) in the CMR environment (1), there has been no analysis of children with CHD undergoing CMR as an outpatient. In our institution, we instituted an algorithm to screen patients prior to CMR with anesthesia. The CMR performing cardiologist screens the patient for sequencing of CMR, possible additional cardiac imaging and the need for breath holding during CMR. The management of children with craniofacial syndromes, tracheal abnormalities, history of prematurity, severe lung disease and/or decreased cardiac reserve is discussed with

an attending anesthesiologist. The risk-benefit ratio for performing CMR under GA is ascertained prior to scheduling the child for CMR.

Methods: As part of a quality-assurance analysis seeking to investigate factors that lead to cancellations on the day of the scheduled test, anesthesia records of all cardiac MRIs performed under general anesthesia between May 2004 and February 2006 were reviewed. The age of the patient, ASA status, presence of cyanosis (room air saturation < 90%), need for endotracheal intubation, airway abnormalities as well as disposition of the patient after the test was recorded. In addition, we reviewed the case records of patients who were cancelled for cardiac MRI study on the day of the test.

Results: A total of 121 anesthetic records were reviewed. The age ranged from 20 days to 26 years. Thirty-five patients (35/121; 29%) were less than 1 year old: 18 patients (18/121: 15%) were less than 6 months old and 17 (17/121: 14%) between 6–12 month. Apart from four (4/121: 3%) adult patients who were between 23–26 years of age, the average age for patients older than one year was 4.17 years old. ASA status was as follows: 30 (30/121: 25%) patients ASA 2, 78 (78/121: 64%) patients ASA 3, and 13 (13/121: 11%) ASA 4. Eight patients had compromised airways due to vascular rings. Thirty-five (35/121: 29%) patients were cyanotic at the time of the test. Fifty- two (52/121: 43%) patients required endotracheal intubation. One hundred six (106/121: 88%) procedures were performed on an outpatient basis, while 10 (10/121: 8%) patients were inpatients and 5 (5/121: 4%) were same day (SD) admits. Of the SD admits, only one patient (vascular ring) required admission for observation of her respiratory status. The remaining SD patients were admitted to proceed with corrective surgery. Three of 124 patients were cancelled on the day of surgery (2%): one outpatient due to active URI, and two patients in whom chest CT without need for general endotracheal anesthesia was deemed safer following discussion with the family. For comparison, the cancellation rate for non-cardiac MRI patients requiring GA at our institution averages 15%.

Conclusion: Our review demonstrates that cardiac MRI can be performed safely on an outpatient basis in patients of all ages with CHD with a low cancellation rate. This is despite the fact that our outpatients are not evaluated in person in an anesthesia pre-op clinic. In addition, shunt-dependent lesions are not admitted the night before for pre-test hydration, as suggested by other institutions performing pediatric cardiac MRI (2). Pre-test screening by an interdisciplinary team of cardiologists and anesthesiologists, including risk assessment with planning of optimal anesthetic technique and post-test disposition, provides safe and efficient CMR evaluation of the complex CHD patient.

REFERENCES

1. Odegard KC. Pediatric Anesthesia 2004; 14:471.
2. Tsai-Goodman, JACC 2004; 94:69.

503. DELAYED-ENHANCEMENT MAGNETIC RESONANCE IMAGING AND MULTIDETECTOR COMPUTED TOMOGRAPHY IMAGING FOR THE ASSESSMENT OF CHRONIC COLLAGENOUS SCARS OF REPERFUSED INFARCTS

Karl Heinz Schuleri, MD, Marco Centola, MD, Richard George, MD, Robert Evers, Kristina Evers, Joshua Hare, MD, Albert C. Lardo, PhD. ***Johns Hopkins University, Baltimore, MD, USA.***

Background: Delayed-enhancement magnetic resonance (MR) is the current clinical 'gold standard' to assess acute and chronic myocardial infarcts (MI).

Delayed contrast-enhanced multidetector computed tomography (MDCT) is an evolving technology, and can accurately characterize myocardial necrosis and microvascular obstruction following acute MI. The ability of MDCT to characterize chronic collagenous scar (CCS) resulting from a healed reperfused MI, however, is unknown. Therefore, we hypothesized that MDCT can accurately identify and quantify CCS in a porcine model of chronic reperfused MI compared to delayed-enhancement MR and postmortem pathology.

Methods and Results: Eight Göttingen minpigs underwent 120 to150 minute coronary artery occlusion followed by reperfusion. MDCT and MRI studies were performed on the same day 6 months after MI induction followed by animal sacrifice. Delayed contrast-enhanced MDCT images were acquired on a 64-slice CT scanner (Toshiba) with an axial slice thickness of 0.5 mm five minutes after 150 mL iodine contrast injection. For infarct size analysis CT-images were reconstructed at 2 and 8 mm. Delayed enhancement MRI was performed 15–20 minutes following 0.2 μm/kg Gd-DTPA the same day using an inversion-recovery gradient-echo pulse sequence and slice thickness of 8 mm on a 1.5 T csanner (GE). Semi-automated quantitative analysis were performed using a uniform threshold technique of the remote myocardium to the infarct areas. Post-mortem hearts were fixed and cut into 2 mm slices. MRI showed excellent correlation with pathology($r = 0.961$; $p < 0.01$) even though MRI overestimated pathology derived infarct sizes up to 30%. MDCT at 8 mm slice thickness correlated well with pathology and MRI ($r = 0.672$; $p < 0.05$ and $r = 0.659$; $p < 0.05$). Subsequent analysis in 4 animals could demonstrate that the reduction of slice thickness to 2 mm improved the correlation to MRI dramatically ($r = 0.837$; $p < 0.05$)

Conclusion: Delayed contrast enhanced- MDCT provides an accurate measure of the spatial extent of CCS compared to MRI and pathology. However, the accuracy is dependent on the used slice thickness. This is likely due to substantial reduction in partial volume effects for MDCT. The ideal slice thickness of delayed enhancement MDCT imaging needs to be determined for accurate infarct sizing.

504. DETECTION OF PERI-INFARCT ZONE BY DELAYED-ENHANCEMENT MAGNETIC RESONANCE AND MULTIDETECTOR COMPUTED TOMOGRAPHY IMAGING IN POST-MYOCARDIAL INFARCTION CARDIOMYOPATHY

Marco Centola, MD, Karl Heinz Schuleri, MD, Richard George, MD, Robert Evers, Kristina Evers, Andrea Vavere, Joshua Hare, MD, Albert C. Lardo, PhD. ***Johns Hopkins University, Baltimore, MD, USA.***

Background: The extent of peri-infarct zone characterized by delayed-enhancement magnetic resonance (DE-MR) provides an incremental prognostic value besides the left ventricular systolic volume index and the ejection fraction in post-myocardial infarction cardiomyopathy. The recent advent of delayed contrast-enhanced multidetector computed tomography (MDCT) is expanding its potential for an accurate evaluation of myocardial necrosis, microvascular obstruction and collagenous chronic scar following the MI. However, the ability of MDCT to detect and quantify the peri-infarct zone is unknown. Accordingly, we hypothesized that MDCT can accurately identify the peri-infarct zone in occlusion/reperfusion animal model of chronic MI compared to DE-MRI.

Methods and Results: Eight Göttingen minipigs underwent 120 to 150 minute coronary artery occlusion followed by reperfusion. MDCT and MR studies were performed on the same day 6 months after MI induction followed by animal sacrifice. Delayed contrast-enhanced MDCT images were acquired on a 64-slice CT scanner (Toshiba) with an axial slice thickness of 0.5 mm five minutes after 150 mL iodine contrast injection. For infarct size analysis CT-images were reconstructed at 2 and 8 mm. Delayed enhancement MR was performed 15–20 minutes following 0.2 μm/kg Gd-DTPA the same day using an inversion-recovery gradient-echo pulse sequence and slice thickness of 8 mm on a 1.5 T scanner (GE). Semi-automated quantitative analyses were performed using a uniform threshold technique of the remote myocardium to the infarct areas. The peri-infarct zone was normalized as a percentage of the infarct size. Mean DE-MR-defined infarct size at 6 months post-MI was 19.6 $\pm$ 2.1% of left ventricular (LV) volume. The infarct size characterized by MDCT at 8 mm slice thickness correlated well with MR ($r = 0.659$; $p < 0.05$). The peri-infarct size detected by MRI showed a good correlation with MDCT at 8 mm (0.9 $\pm$ 0.4% versus 1.1 $\pm$ 0.2, mean difference 0.2%). Interestingly, subsequent analysis in 4 animals could demonstrate that the peri-infarct size characterized by MDCT at 2 mm (0.2 $\pm$ 0.06%) did not match well with that measured by MR and MDCT 8 mm.

Conclusion: The spatial extent of chronic myocardial infarction and peri-infarct zone can be determined and quantified accurately with delayed contrast enhanced-MDCT compared to MR. However, the reduction of slice thickness by MDCT can better characterize the peri-infarct zone because of the decreasing in partial volume effects. Further studies will elucidate the ideal slice thickness of delayed enhancement MDCT imaging for accurate peri-infarct zone measurements.

505. COMPARISON OF SPAMM, HARP AND DENSE IN A DEFORMABLE PHANTOM

Sujeewa N. Hettiwatte, PhD,[1] Robert S. Kirton, PhD,[1] Joost P. A. Kuijer, PhD,[2] Frederick H. Epstein, PhD,[3] Brett R. Cowan, MBChB,[4] Alistair A. Young, PhD.[5] ***[1]Bioengineering Institute, University of Auckland, Auckland, New Zealand, [2]Vrije Universiteit Medical Center, Amsterdam, The Netherlands, [3]Departments of Radiology and Biomedical Engineering, University of Viginia, Charlottesville, VA, USA, [4]Centre for Advanced MRI, Faculty of Medical and Health Sciences, University of Auckland, Auckland, New Zealand, [5]Department of Anatomy with Radiology and Bioengineering Institute, University of Auckland, Auckland, New Zealand.***

Introduction: A number of techniques are available for the measurement of displacement and strain in the heart including SPAtial Modulation of Magnetization (SPAMM) (1) followed by tag line detection, CSPAMM followed by HARmonic Phase (HARP) analysis (2), and Displacement ENcoding with Stimulated Echoes (DENSE) (3). However, it is unclear which method gives the most accurate results in practice.

Purpose: This study compared SPAMM, HARP and DENSE imaging of a deformable gel phantom by comparing the accuracy of pixel-based displacement and strain measurements from each technique with a known analytical solution.

Methods: A deformable, silicone gel cylindrical annulus with a fixed outer cylinder (radius 50 mm) and movable inner cylinder (radius 20 mm) was cyclically driven at 1Hz by a stepper motor to rotate the inner cylinder by 45 deg in a sinusoidal fashion. The deformation has an analytical solution independent of material properties of the gel (4). Images were obtained on a 1.5T Siemens Avanto.

TrueFISP SPAMM tagging (1) used FOV 300 $\times$ 300 mm, grid tagging 45 deg to readout direction with 7 mm spacing, image matrix 256 $\times$ 154 interpolated to 256 $\times$ 256, slice thickness 8 mm, TR 18.64 ms, TE 2.33 ms, flip 20 deg, 8 segments, bandwidth 370 Hz/pixel, tag flip 122 deg, 5 LISA cycles, 49 frames, single $\sim$ 20 s acquisition. TrueFISP 1-1 CSPAMM HARP (2) used FOV 300 $\times$ 300 mm, line tagging in the readout direction at 7 mm spacing, image matrix 256 $\times$ 77 interpolated to 256 $\times$ 256, slice thickness 8 mm, TR 18.64 ms, TE 2.33 ms, flip 20 deg, 8 segments, bandwidth 370 Hz/pixel, tag flip 140 deg, 5 LISA cycles, 49 frames, single $\sim$20 s acquisition (two encoding directions). CineDENSE imaging (3) used FOV 300 $\times$ 225 mm, 1-1 CSPAMM at kenc = 0.2 cycles/mm, image matrix 128 $\times$ 96,

TABLE
Errors (mean ± sd) in displacements and Eulerian strains

	Angular displacement (Uth, degrees)	Radial displacement (Ur, mm)	Radial strain (Err)	Circumferential strain (Ecc)	Shear strain (Erc)
SPAMM	−3.80 ± 1.28	−0.72 ± 0.60	−0.05 ± 0.09	−0.02 ± 0.03	0.07 ± 0.06
HARP	−0.34 ± 0.27	0.02 ± 0.14	−0.01 ± 0.04	0.00 ± 0.01	0.01 ± 0.03
DENSE	−0.29 ± 0.70	−0.12 ± 0.39	−0.01 ± 0.05	0.00 ± 0.03	0.01 ± 0.03

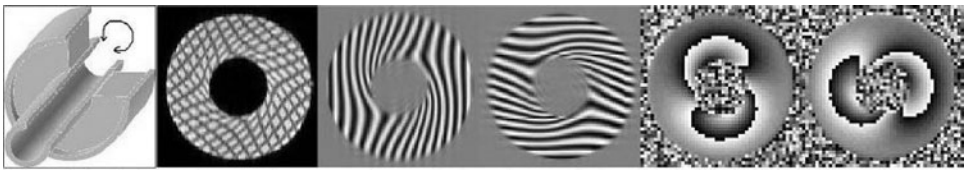

FIG. 1. Left to right: Cut-away view of phantom, deformed SPAMM grid-tagged image, x and y complementary-SPAMM images used in HARP, and x and y phase images used in DENSE.

slice thickness 8 mm, TR 20 ms, TE 5.75 ms, flip 15 deg, 14 segments, EPI factor 7, bandwidth 798 Hz/pixel, tag flip 180 deg, 23 frames, two ∼20 s acquisitions (one for each encoding direction).

In SPAMM, the grid-tagged images were convolved with the 2nd derivative of a Gaussian to obtain tag lines in each direction. The distance from each pixel to the closest tag minimum was obtained by searching along a straight line normal to the initial undeformed tags. Displacement maps were then calculated as the difference from the first frame. Such displacements are accurate only at tag line centers; at all other points, the displacements were calculated using a thin-plate spline interpolation. In HARP, the phase of the filtered image provided position information at each pixel and displacements were calculated from the phase differences from the first frame. The k-space filter was circular, centered at the harmonic peak at d = 1/7 cycles/mm, with radius 0.8 d, and Gaussian roll off. In DENSE, the image phase gave the displacements directly at each pixel (no filters were applied). With all three methods phase unwrapping was required to obtain the actual displacements in two orthogonal directions, which were then used to calculate Eulerian strain using a pixel based algorithm.

Results: The mean and standard deviation of errors between phantom results and the analytic solution were calculated at every pixel within a mask of R = 25 mm to 45 mm (Table). Fig. 1 shows a cut-away view of the phantom, and images obtained by each technique, and Fig. 2 shows the variation in radial Eulerian strain (Err) averaged at each radius.

Conclusions: Phantom experiments showed that errors in displacements and strains were small in DENSE and HARP, and highest in SPAMM. Errors in SPAMM were likely due to the very simple pixel based tag tracking algorithm used.

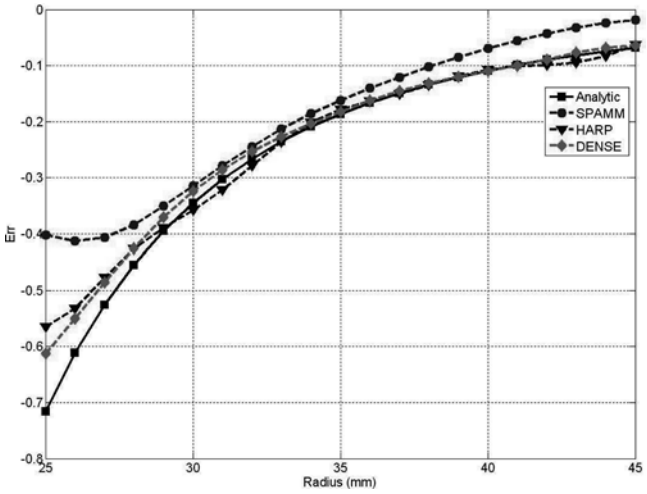

FIG. 2. Variation of Eulerian radial strain (Err) with radius.

REFERENCES

1. Zwanenburg et al. MRM 2003; 49:722–730.
2. Kuijer et al. MRM 2001; 46:993–999.
3. Kim et al. Radiology 2004; 230:862–871.
4. Young et al. Radiology 1993; 188:101–108.

506. WALL THICKNESS IN HUMAN CAROTID ARTERIES CORRELATES NEGATIVELY WITH PLAQUE INFLAMMATION AS DETERMINED BY FDG PET

James H. F. Rudd, MD, PhD, Karen Weinshelbaum, Venkatash Mani, PhD, Kelly Myers, Sameer Bansilal, MD, Michael Farkouh, MD, Josef Machac, MD, Silvia Aguiar, MD, Valentin Fuster, MD, PhD, Zahi A. Fayad, PhD. ***Mount Sinai School of Medicine, New York, NY, USA.***

Background: Atherosclerosis is an inflammatory disease, where the degree of inflammation, not the plaque size, determines risk of rupture and therefore likelihood of a clinical event.

MRI can image atherosclerotic plaque with high resolution, and several MRI parameters of disease extent in the carotid arteries and aorta have been shown to correlate with atherosclerotic risk factors (1).

By providing a metabolic image of macrophage activity, FDG PET can image atherosclerotic plaque inflammation in patients and in animal models of disease, with a strong correlation between FDG uptake and plaque macrophage content. In addition, autoradiography has confirmed that the FDG signal originates from activated macrophages within the lipid core and fibrous cap of the plaque (2). This has led to the suggestion that FDG-PET might have a role in identifying 'high risk' plaques and monitoring their response to therapy.

We imaged patients with established vascular disease (post-PCI or CABG) using both MRI and FDG-PET to assess the relationship between vascular FDG uptake and MRI indices of disease burden.

Methods: Twenty-two patients underwent PET/CT imaging on a GE Discovery LS with 10mCi FDG. Aortic (from arch to diaphragm) and carotid images were acquired 90 minutes after FDG injection. CT was used for co-registration of the PET images and for attenuation correction. To estimate FDG uptake into plaque, standardized uptake values (SUV) were calculated for each arterial slice and averaged for the whole vessel, using ROI applied to the fused PET/CT images. SUV values were divided by averaged blood pool activity to give a plaque/blood SUV ratio.

MR imaging was performed on a Siemens Sonata 1.5T scanner. 12 to 24 non-overlapping 3 mm cross sectional slices centered around the carotid bifurcation and 24-36 non-overlapping 5 mm cross sectional slices from the level of the aortic arch to diaphragm were obtained using the rapid extended coverage double inversion recovery turbo spin echo black blood (REX) pulse sequence. Imaging parameters were as follows: proton density weighted (PDW) non-gated sequence imaging 12 slices simultaneously (TR/TE = 2130/5.6 ms), with a field of view of 12 × 12 cm, bandwidth of 488 Hz/pixel, matrix size of 256 × 256, a turbo factor of 15 and 2 signal averages. We calculated mean and max wall thickness, along with wall area/vessel area (atherosclerotic disease index-ADI), using previously validated methods.

Results: The mean age was 62 years; 40% of the patients were female.

The mean (± SEM) carotid FDG SUV determined by PET was 1.51 (0.05), with a mean MRI-derived ADI of 0.45 (0.01).

There was a significant negative correlation between mean carotid FDG SUV and the ADI ($r = -0.43$, $p < 0.05$).

Additionally, the mean carotid artery wall thickness was negatively correlated with mean FDG uptake ($r = -0.38$, $p < 0.05$). In the descending thoracic aorta, there was no significant correlation between the FDG and MRI results.

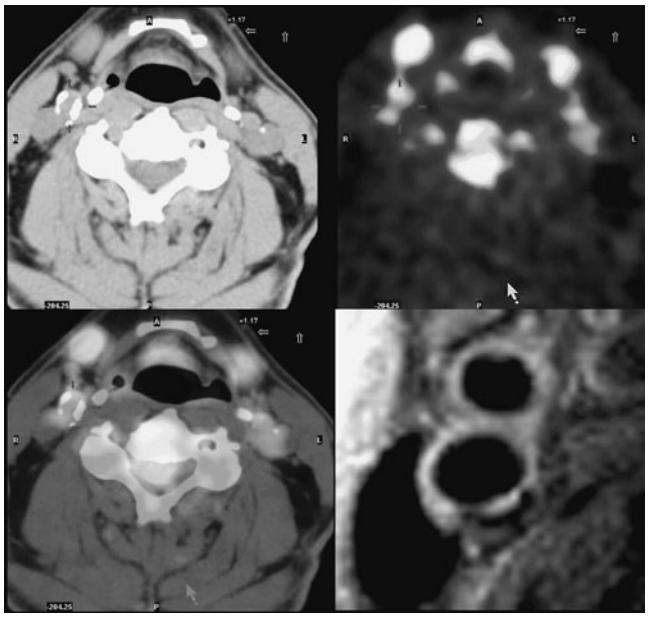

Conclusions: This study used non-invasive multimodality imaging (MR and FDG PET/CT) to show a negative correlation between atherosclerotic plaque size and degree of inflammation in the carotid arteries. This result reinforces the view that plaque rupture events may be caused by small highly inflamed lesions. Another potential for this method may be study of plaque regression early after treatment.

Upper row shows CT (left) and FDG-PET (right) carotid images. Lower row shows combined PET/CT and close-up MRI image of the right carotid artery. Calcification, inflammation and wall thickening are all illustrated multimodality imaging.

REFERENCES

1. Yuan C, Zhang SX, Polissar NL, et al. Identification of fibrous cap rupture with magnetic resonance imaging is highly associated with recent transient ischemic attack or stroke. Circulation 2002; 105:181–185.
2. Rudd JHF, Warburton EA, Fryer TD, et al. Imaging Atherosclerotic Plaque Inflammation With [18F]-Fluorodeoxyglucose Positron Emission Tomography. Circulation 2002; 105:2708–2711.

507. CMR DEMONSTRATES THAT A POTENT ANTI-INFLAMMATORY AGENT IS AS EFFECTIVE AS THE COMBINATION OF ACE-INHIBITION AND BETA-BLOCKADE AT REDUCING POST-INFARCT LEFT VENTRICULAR REMODELING IN MICE AFTER REPERFUSED MYOCARDIAL INFARCTION

Ronald J. Beyers, MSEE, Yaqin Xu, MD, PhD, Stuart S. Berr, PhD, Frederick H. Epstein, PhD, Joel Linden, PhD, Brent A. French, PhD. ***University of Virginia, Charlottesville, VA, USA.***

Introduction: CMR-based studies have previously demonstrated that potent agonists of the adenosine A2A Receptor (A2AR) can help preserve left ventricular (LV) contractile function early after reperfused myocardial infarction (MI) in mice (1). However, the long term effects of such anti-inflammatory agents on the progression of LV remodeling have not been explored, nor have the long-term effects of these agents ever been compared with the most effective clinical treatment regimen currently available – the combination of ACE-inhibition and beta-adrenergic receptor blockade (AI + BB).

Purpose: The purpose of this study was to test the hypothesis that selective A2AR activation could help preserve cardiac structure and function after reperfused MI similar to that provided by the combination of AI+BB.

Methods: All mice were studied by CMR before and at 1, 7, and 28 days after experimental MI. MI was induced by a 1 h occlusion of the LAD followed by reperfusion. Study groups were composed of untreated C57Bl/6J wild-type mice (WT, n = 6), mice treated with ATL313 (a potent A2AR agonist, n = 5) and mice treated with the combination AI + BB (n = 7). ATL313 was administered (10 ng/kg-min) starting 1h post-reperfusion until Day 14 post-MI using implanted Alzet micro-osmotic pumps (Durect Corp). The AI + BB combination of Captopril and Metoprolol (each at 35 ug/kg-min) was delivered similarly starting 1 h post-reperfusion until Day 28. CMR studies included localizer scanning, 6-8 short-axis slices of black-blood cine imaging to cover the entire heart, and at Day 1, 6–7 gadolinium-enhanced, high flip-angle (60–90°) short-axis slices. Gd-DTPA was infused after cine imaging through an indwelling IP line. All imaging was performed on a 4.7 T scanner with a custom-built Litz RF-coil (Doty Scientific). All images had a field-of-view of 2.56 cm, a matrix size of 128 × 128, and zero-filled pixel size of 0.1 × 0.1 mm^2. Post acquisition analysis performed on Matlab yielded myocardial LV end-diastolic (ED), end-systolic (ES) volumes and ejection fraction (EF) from the cine images. Day 1 infarct size was measured as percent of LV mass from the gadolinium enhanced images.

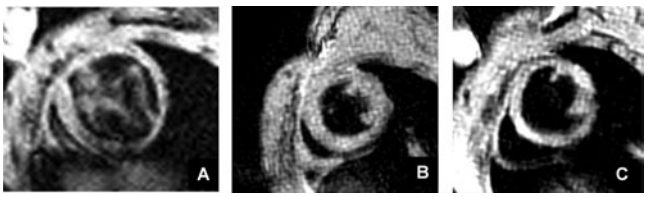

FIG. 1. Mid-ventricular short-axis images 28 days post-MI of (A) an untreated WT mouse, (B) a WT mouse treated with ATL-313, an (C) a WT mouse treated with AI+BB. Reduced cavity ize and circumferential extent of all thinning are evident in (B) and (C).

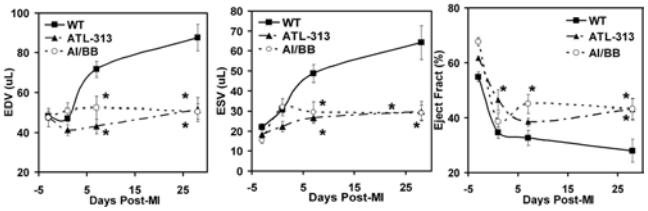

FIG. 2. End diastolic volume (EDV), end systolic volume (ESV) and jection fraction (EF) at baseline and during first 28 days following MI. Selective activation of the A2AR (ATL-313) reduces ESV and increases EF to a degree similar to that seen in Al+BB mice compared to untreated wild-ty;e (WT) mice. Note * indicates $p<0.05$ in comparison to WT.

Results: Gadolinium-enhanced CMR demonstrated similar Day 1 infarct sizes in untreated (40 ± 4%), ATL313-treated (41 ± 3%) and AI+BB-treated mice (44 ± 5%) with p = NS by ANOVA. Fig. 1 shows example Day 28 ED images illustrating the effect of drug treatments. Specifically, LV cavity dilation and circumferential wall thinning are evident in the untreated mice (Fig. 1A). In contrast, preservation of cavity size and minimal wall-thinning in the anterior segment were seen in the ATL313- and AI + BB-treated groups (Figs. 1B&C). Fig. 2 shows the EDV, ESV and EF results from the present study. Both ATL313 and AI+BB significantly reduced both EDV and ESV at Days 7 and 28 post-MI compared to WT. ATL313 improved EF on Days 1 and 28 post-MI, whereas AI + BB improved EF on Days 7 and 28 post-MI. All comparisons reported here met $p < 0.05$ by ANOVA.

Conclusions: Using CMR, we have shown that selective activation of the A2AR reduces post-infarct LV remodeling to an extent similar to that provided by the combination of ACE-inhibition and beta-adrenergic receptor blockade. In addition, A2AR-stimulation preserves EF on Day 1 post-MI significantly better than the combination of AI + BB, a property that may prove beneficial to survival in patients with large anterior MI. More generally, these results demonstrate the utility of serial CMR in mice for evaluating the efficacy of new therapies against heart failure and for comparing new therapeutic approaches with conventional clinical paradigms.

REFERENCE

1. Toufektsian MC, Yang Z, Prasad KM, Overbergh L, Ramos SI, Mathieu C, Linden J, and French BA. Stimulation of A2A-adenosine receptors after myocardial infarction suppresses inflammatory activation and attenuates contractile dysfunction in the remote left ventricle. AJP Heart & Circ Phys 2006; 290:H1410–1418.

508. GENERALIZED ANALYSIS FRAMEWORK FOR SPAMM, HARP AND DENSE

Sujeewa N. Hettiwatte, PhD,[1] Brett R. Cowan, MBChB,[2] Alistair A. Young, PhD.[3] ***[1]Bioengineering Institute, University of Auckland, Auckland, New Zealand, [2]Centre***

for Advanced MRI, Faculty of Medical and Health Sciences, University of Auckland, Auckland, New Zealand, [3]Department of Anatomy with Radiology and Bioengineering Institute, University of Auckland, Auckland, New Zealand.

Introduction: A number of MR imaging techniques are used to measure deformation in the heart including SPAtial Modulation of Magnetization (SPAMM), HARmonic Phase (HARP) and Displacement ENcoding using Stimulated Echoes (DENSE). In SPAMM, a line or grid tag pattern is created magnetically in the tissue and displacement is measured from this reference by tracking the tags. In HARP, position information is encoded into the phase of a filtered image and this is used to calculate displacement. In DENSE, displacements are directly encoded into the phase of the image.

Purpose: We show how all methods can be analyzed using a single generalized framework. We test this framework by numerically creating SPAMM, HARP and DENSE images with known deformations and comparing the results with the analytical solution.

Methods: A known deformation was defined comprising axial shear in a cylindrical annulus (1). SPAMM grid-tagged images were generated with a tag spacing of 7 mm at 45 deg and 135 deg with the first five terms of a Fourier expansion used to approximate a square wave tag profile. CSPAMM cosine modulated images and DENSE images were generated with displacement encoding in both the × and y directions. All images were generated in DICOM format; SPAMM and CSPAMM at 256 × 256 and DENSE at 128 × 128 resolution, all with FOV = 300 mm.

Displacement images were calculated as follows. In SPAMM, grid tagged images were interpolated to 512 × 512, and convolved with a 2nd derivative of a Gaussian to obtain line tags in each direction. Tags were detected by searching from each pixel along a line normal to the initial undeformed tags. Each pixel value was equated to the distance from that pixel to the nearest tag centre in the tag direction to obtain a wrapped image of initial position X as a function of current position x. The displacement u(x) was then given by x-X(x). This displacement is only accurate at tag line centers; at other points displacement was obtained using a thin plate spline interpolation. In HARP, the Fourier transform of CSPAMM images gave spectral peaks, which were filtered using a circular filter centered at the harmonic peak d = 1/7 cycles/mm with radius 0.8 d and Gaussian roll off. The phase of the inverse Fourier transform gave the X(x) map, and displacement u(x) was again given by x-X(x). In DENSE, the image phase gave displacement u(x) directly. The displacement maps from each method were unwrapped (2) and used to calculate angular and radial displacements and Eulerian strains, using the same pixel based calculation.

Results: The figure shows the unwrapped displacement maps from each technique in the × and y directions. The mean and standard deviation of differences with the analytic solution were calculated for all pixels at least 5 mm from the inner or outer edge (Table).

Conclusions: A generalized analysis framework demonstrates the similarity in displacement encoding methods. Simulated errors in displacements and strains were lowest in DENSE, intermediate in HARP and highest in SPAMM. SPAMM had the highest errors due to the simple pixel based tracking algorithm and the interpolation scheme used. In HARP, the errors are largely due to the choice of filter parameters used in Fourier domain.

REFERENCES

1. Radiology 1993; 188:101–108.
2. J Opt Soc Am A 1994; 11:107–117.

TABLE
Errors (mean ± sd) in displacement and Eulerian strains

	Angular displacement (degrees)	Radial displacement (mm)	Radial strain	Circumferential strain	Shear strain
SPAMM	−1.88 ± 0.46	−0.35 ± 0.29	0.00 ± 0.07	−0.01 ± 0.02	0.03 ± 0.03
HARP	1.11 ± 0.77	0.06 ± 0.07	0.05 ± 0.05	0.00 ± 0.00	−0.04 ± 0.02
DENSE	0.00 ± 0.01	0.00 ± 0.01	0.00 ± 0.00	0.00 ± 0.00	0.00 ± 0.00

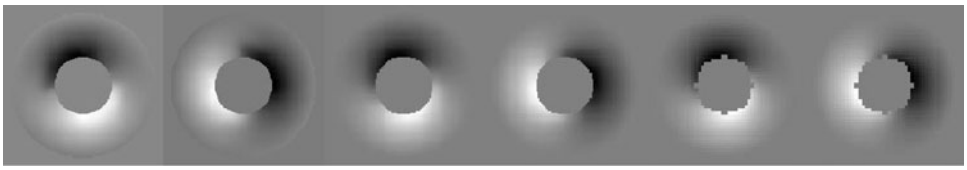

FIG. 1. Unwrapped displacement maps: Left to right: SPAMM (x and y), HARP(x and y) and DENSE (x and y).

509. A STUDY OF AORTIC DISTENSIBILITY AND AORTIC DILATION PREVALENCE IN A POPULATION OF TURNER SYNDROME PATIENTS WITHOUT ASSOCIATED CONGENITAL HEART DISEASES: ROLE OF CARDIOVASCULAR MAGNETIC RESONANCE FOR THE EARLY IDENTIFICATION OF AORTIC INVOLVEMENT

Luigi Lovato,[1] Daniela Prandstraller,[2] Vincenzo Russo,[1] Cesare La Palombara,[1] Katia Buttazzi,[1] Valentina Gostoli,[1] Maurizio Montalti,[1] Laura Mazzanti,[3] Rossella Fattori.[1] ***[1]S. Orsola Hospital-Cardiovascular Radiology Unit-Cardiovascular Department, Bologna, Italy, [2]S. Orsola Hospital-Pediatric Cardiology and Adult Congenital Unit-Cardiovascular Department, Bologna, Italy, [3]S. Orsola Hospital-Pediatric Department, Bologna, Italy.***

Introduction: Cardiovascular diseases are a common cause of mortality in Turner syndrome (TS), that is in fact frequently associated with bicuspid aortic valve, aortic coarctation, aortic stenosis but also with aortic dissection and subsequent rupture.

Purpose: We have evaluated with cardiovascular magnetic resonance (CMR) the aortic dilation prevalence and the possible aortic distensibility alterations in a population of TS without associated congenital heart diseases to assess both the necessity for a close cardiovascular monitoring and the possible role of CMR in the identification of a an early aortic involvement.

Methods: Sixty-two patients with TS (range 15-35.2 years) underwent a clinical and imaging study, which consisted of a cardiologic visit and a CMR study. CMR morphological evaluation was performed by axial and sagittal spin-echo images and CMR angiography to measure aortic root and ascending aorta diameters, while a CMR functional study was performed with the acquisition of a phase-contrast sequence on a plane perpendicular to ascending aorta to quantify aortic distensibility.

Results: There is a 12.9% (9/62) prevalence of ascending aorta dilation and a 17.7% (11/62) prevalence of aortic root dilation. Aortic distensibility was not significantly different compared to normal population mean values (0.04 ± 0.002 vs 0.025 ± 0.006). Aortic distensibility was inversely related to systolic arterial blood pressure ($p < 0.00001$) and significantly different in the presence or absence of aortic dilatation (ANOVA, $p = 0.01$). CMR occasionally identified associated arterial or venous vascular anomalies (persistent left superior vena cava, aberrant right subclavian artery, elongation of the aortic arch) in the 11.2% of cases.

Conclusions: The high prevalence of aortic dilation compared to the normal population and the negative influence of arterial blood pressure on aortic distensibility recommend a continuous monitoring of arterial blood pressure and aortic dimensions. CMR has a great potential in the follow-up of patients with TS as an absolutely non invasive, high reproducible and extremely accurate imaging technique, which also has a superior capacity in the visualization of associated vascular anomalies and finally offers the most complete morphological and functional evaluation of TS.

510. EFFICACY OF LATE GADOLINIUM ENHANCEMENT CARDIOVASCULAR MAGNETIC RESONANCE OF THE SYSTEMIC RIGHT VENTRICLE FOR THE IDENTIFICATION OF MYOCARDIAL STRUCTURAL ALTERATIONS: PROGNOSTIC VALUE IN THE FOLLOW-UP OF ADULT PATIENTS WITH CONGENITAL COMPLETE OR CONGENITALLY CORRECTED TRANSPOSITION OF THE GREAT ARTERIES

Luigi Lovato,[1] Alessandro Giardini,[2] Vincenzo Russo,[1] Cesare La Palombara,[1] Katia Buttazzi,[1] Valentina Gostoli,[1] Maurizio Montalti,[1] Fernando M. Picchio,[2] Rossella Fattori.[1] ***[1]S. Orsola Hospital, Cardiovascular Radiology Unit-Cardiovascular Department, Bologna, Italy, [2]S. Orsola Hospital, Pediatric Cardiology and Adult Congenital Unit-Cardiovascular Department, Bologna, Italy.***

Introduction: In patients with Congenital Complete or Congenitally Corrected Transposition of the Great Arteries with the atrial switch technique the right ventricle is submitted to systemic pressure (systemic right ventricle) and their natural history is characterized by a progressive ventricular dysfunction.

Purpose: We evaluate with cardiovascular magnetic resonance if areas of late gadolinium enhancement (LGE) as expression of myocardial damage would be present in adults with systemic right ventricle and if LGE areas would be associated with markers of adverse clinical outcome.

Methods: Thirty-four adults (age 25 ± 8 years, range 17–55 years) with a systemic right ventricle (23 patients with atrial repair (Senning technique-age at repair of 9 ± 4 months) for transposition of the great arteries, 11 with congenitally corrected transposition) have been studied by cardiopulmonary exercise test and cardiovascular magnetic resonance which consisted in ventricular function parameters evaluation (cardiac volumes and mass) and myocardial late gadolinium enhancement study. Twelve patients with worsening of heart failure symptoms were re-evaluated after a mean period of 16 months. Presence of LGE areas were compared to age and cardiopulmonary and ventricular functional parameters.

Results: LGE areas were present in 14 patients (41%). Presence of LGE areas was associated with older age ($p = 0.037$), lower right ventricular (RV) ejection fraction (34 vs. 45%, $p = 0.006$), higher RV wall stress ($p = 0.0001$), reduced peak oxygen uptake (47 vs. 56%, $p = 0.001$) and history of arrhythmia ($p = 0.005$). Right ventricular ejection fraction correlated with RV wall stress ($r = -0.81$, $p < 0.0001$), and peak oxygen uptake

($r = 0.74$, $p < 0.0001$). Twelve patients experienced worsening of clinical condition. This was associated with a decrease in biventricular function, and increase in prevalence and number of LGE areas.

Conclusions: Patients with a systemic right ventricle have areas of LGE presumably due to myocardial fibrosis that can be seen by contrast-enhanced MRI. LGE areas are associated with RV dysfunction, poor exercise tolerance, arrhythmia, and progressive clinical deterioration in these patients. This morphological parameter constitutes a useful prognostic index for the follow-up of adults with Congenital Complete or Congenitally Corrected Transposition of the Great Arteries.

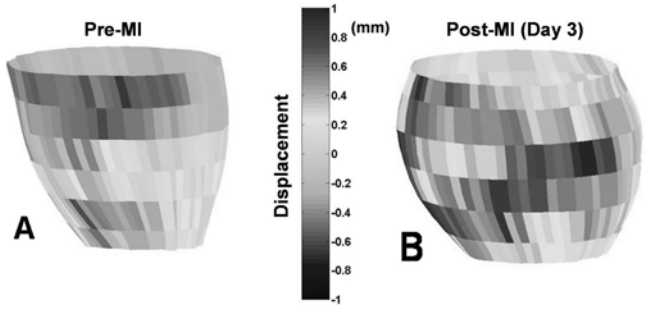

FIG. 1. Pre and post-MI (day-3) color surface plots of the measured mid-wall longitudinal displacement. The pre-MI mouse (A) shows approximately 1 mm of base-to-apex motion near the base, a gradient of longitudinal motion along the long axis, and approximate 0.25 mm of apex-to-base motion near the apex. The post-Mi heart (B) shows neither coherent displacement nor gradient in the anterior wall infarct region.

511. COMPREHENSIVE SYSTOLIC FUNCTION ASSESSMENT USING VOLUMETRIC DENSE MRI IN MICE AFTER MYOCARDIAL INFARCTION

Ronald J. Beyers, MSEE, Florent C. Sureau, MS, Wesley D. Gilson, PhD, Zequan Yang, PhD, R. Jack Roy, Brent A. French, PhD, Frederick H. Epstein, PhD. ***University of Virginia, Charlottesville, VA, USA.***

Introduction: The recent application of cardiac MRI to study transgenic and knockout mice after the experimental induction of myocardial infarction (MI) has provided new insights into the basic mechanisms underlying MI, left-ventricular (LV) dysfunction and LV remodeling (1). While cine MRI, tagging, and two-dimensional DENSE have been previously demonstrated, the present study aimed to develop a volumetric DENSE sequence with three-dimensional displacement-encoding (DE) to comprehensively measure pre- and post-MI regional systolic function over the entire murine LV.

Methods: A 3D DENSE sequence was implemented on a 4.7 T MR scanner and used to image C57Bl/6J mice before and after experimental MI. MI was induced by a 1-hour occlusion of the LAD followed by reperfusion. Upon ECG trigger, DE was sequentially applied to each of the three orthogonal short (2) and long-axis (1) directions. DE frequencies of 0.85 and 0.34 cycles/mm were used for measuring in-plane and through-plane motion, respectively. Additional phase reference data sets were also acquired with no DE applied. *C*osine *and s*ine modulation were used to *e*liminate (CANSEL) artifact generating echoes by phase-cycling the second RF pulse in the DE module as previously described (2). The DE longitudinal magnetization was sampled at end-systole using a double-oblique, slab-selective, 3D gradient-echo sequence. The slab thickness was 5.5 mm to cover the entire longitudinal length of the mouse heart. The 3D matrix size was $128 \times 96 \times 12$ and field-of-view was $30 \times 22 \times 7$ mm^3 for a voxel size of $0.23 \times 0.23 \times 0.58$ mm^3. The TE was 3.1 ms, and a TR of 800 ms was used between each DE pulse set to enable sufficient T1 relaxation. Image reconstruction and data analysis were conducted off-line using Matlab. A 3D inverse Fourier transform was then performed, and the resulting complex volumetric data were phase-corrected using the phase reference data. After manual segmentation of the LV from the magnitude-reconstructed 3D volume, a comprehensive assessment of LV systolic function was automatically computed from the segmented phase-reconstructed 3D volume including 3D displacement, myocardial strain, twist and torsion. Mice were studied in accordance with protocols approved by the animal care and use committee at our institution. During MRI, mice were anesthetized with 1% isoflurane in O_2, temperature was maintained at 37°C using circulating hot water and ECG was monitored for use in cardiac gating.

Results: The scan time varied from 2 to 2.5 hours. The SNR of the LV myocardium averaged 13.5 ± 0.7. Images demonstrating the 3D measurement of LV regional systolic function are shown in Figs. 1 and 2. Specifically, Figs. 1A and 1B are color surface plots of the measured mid-wall longitudinal displacement of the pre-MI and post-MI (Day 3) mice, respectively. The pre-MI mouse (1A) shows approximately 1 mm of base-to-apex

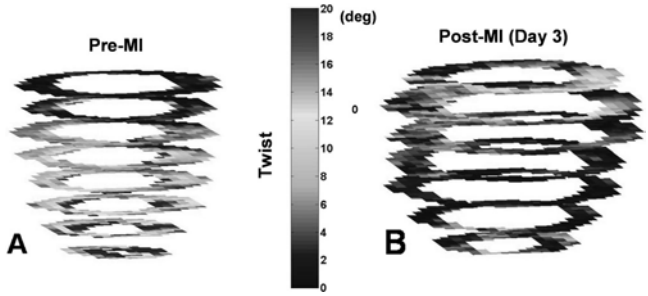

FIG. 2. Pre and post-MI (day-3) color short-axis slices of regional myocardial twist. For the pre-MI heart (A), the systolic longitudinal torsion pattern is visualized as a change in twist angle along the longitudinal direction. Meanwhile the post-MI mouse (B) indicates a drastically reduced twist and torsion pattern.

motion near the base of the heart, a gradient of longitudinal motion along the long axis, and approximately 0.25 mm of apex-to-base motion near the apex. The post-MI mouse (1B) shows neither coherent displacement nor gradient in the anterior wall infarct region. Figure 2 presents the regional myocardial twist of the same pre- and post-MI mice, respectively. In the pre-MI mouse (2A), the systolic longitudinal torsion pattern is visualized as a change in twist angle along the longitudinal direction. Meanwhile the post-MI mouse (2B) displays dramatically reduced twist and torsion patterns.

Conclusions: Three dimensional DENSE enables a comprehensive evaluation of systolic function throughout the entire mouse heart. This technique may be used to assess basic mechanisms underlying regional LV dysfunction in transgenic and knockout mouse models of ischemic heart disease.

REFERENCES

1. Gilson WD, Epstein FH, Yang Z, Laubach VE, Berr SS, French BA, Circ 2003;108:IV-700.
2. Epstein FH, Gilson WD, Proc Int Soc Magn Reson Med 2003;11:1645.

512. VISUALISATION OF THE CORONARY VENOUS SYSTEM WITH A THREE DIMENSIONAL SINGLE VOLUME CARDIAC MAGNETIC RESONANCE PROTOCOL

John F. Younger, MB BCh, Andrew Crean, MB, Sven Plein, PhD, John P. Greenwood, PhD. ***Leeds University, Leeds, United Kingdom.***

Objectives: We sought to evaluate the ability of cardiac MRI to demonstrate coronary venous anatomy.

Background: Cardiac MRI is useful in the diagnosis and management of patients with impaired left ventricular (LV) function, providing information about anatomy, function, perfusion, viability and coronary disease. Cardiac resynchronisation therapy (CRT) with biventricular pacing is now an established treatment of LV dysfunction. It requires the deployment of a left ventricular (LV) pacing lead via the coronary sinus, to a branch of the cardiac venous system. However in some patients the venous anatomy will not be appropriate for CRT, due to an absence of large veins over the left ventricle. Hence knowledge of coronary venous anatomy, and the presence or absence of suitable veins for CRT, may be useful in the management of patients referred for CMR to investigate heart failure. Although coronary veins can be seen on cardiac CT scan performed for coronary artery imaging, they are not routinely demonstrated with conventional targeted cardiac MRI coronary artery protocols.

Methods: The cardiac MRI scans of 15 patients (9 men) were studied. All scans had been performed for the diagnosis or assessment of coronary artery disease on a 1.5 T MR scanner (Gyroscan Intera CV, Philips Medical Systems, Best, The Netherlands), and were judged suitable for coronary artery imaging. A 3-dimensional volume stack was acquired, using a single diaphragmatic navigator, with sufficient slices to cover the entire heart (whole heart coronary angiography-WHCA), using an SSFP sequence with a fat suppression and T2 preparation prepulses (TR/TE/flip angle 4.6/2.3/100 and spatial resolution was $1.18 \times 1.18 \times 1.80$ mm).

All scans were commenced after first pass perfusion imaging with intravenous administration of 0.05mmol/kg of a gadolinium based contrast agent. The sequences were reviewed on a ViewForum Workstation (Philip's Medical Systems) equipped with a dedicated cardiac analysis package. The quality of venous imaging, the ability to visualise the coronary sinus (CS), anatomical variants and the presence of an LV branch after volume rendering were recorded. The diameter of the CS ostium on the axial images, and the uninterrupted distance from this point to the most distal demonstrable end of a cardiac vein on the volume rendered image was measured.

Results: Continuous data are presented as mean $\pm$ standard deviation. The coronary sinus was demonstrated in all patients. The average diameter of the CS was 13.9 ± 4.3 mm. The mean distance for which continuous vein could be visualised from the ostium of the CS was 75.8 ± 52.6 mm. An LV branch was demonstrated in 11 (73.3%) patients and an anterior interventricular branch was seen in 8 (53.3%) patients.

Conclusions: Definition of the coronary veins has practical applications particularly for patients undergoing consideration

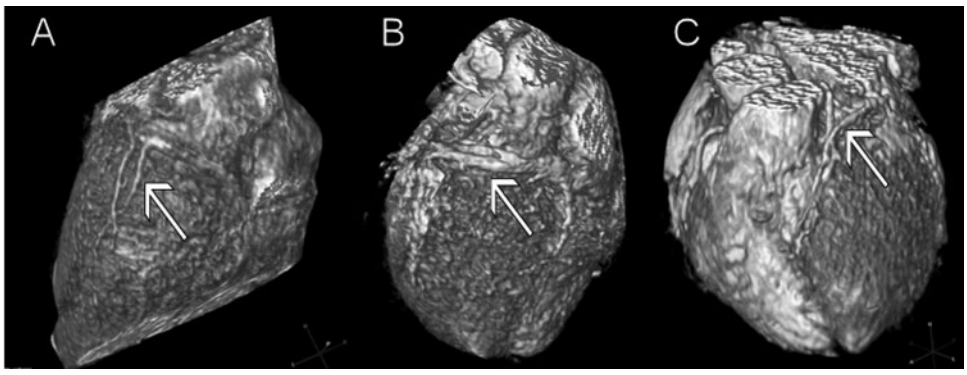

FIG. 1. Example images from 3 patients showing; A—Left marginal vein; B—Coronary sinus; C—Anterior interventricular vein.

of biventricular pacing. This study shows that cardiac MRI can be used to demonstrate the branches and anatomy of the coronary venous system using volume rendered 3D images in a manner similar to EBCT and multi-slice CT. This technique can be performed during the same examination as viability and functional imaging, and may prove a useful addition to the already impressive armamentarium of cardiovascular MRI for the assessment of patients with left ventricular impairment.

513. ACCELERATED MAGNETIC RESONANCE IMAGING OF RAT HEARTS IN VIVO AT 9.4 T

Jurgen E. Schneider,[1] Titus E. Lanz, PhD,[2] Sean Smart, PhD,[3] Mark A. Griswold, PhD,[4] Stefan Neubauer, MD.[1]
[1]Oxford University, Oxford, United Kingdom, [2]Rapid Biomedical, Rimpar, Germany, [3]Varian NMR & MRI, Oxford, United Kingdom, [4]Case Western University, Cleveland, OH, USA.

Introduction: Cardiac functional studies in surgically or genetically modified mice and rats are typically performed using dedicated volume coils or with a volume coil/transmit-surface coil/receive setup. Required experimental time is about one hour or longer to cover the entire heart. However, the availability of dedicated coil-arrays would improve the sensitivity, and allow the use of parallel imaging techniques (such as SENSE or GRAPPA). These techniques use spatial information from the array to more rapidly encode the image. While well established in the clinic, their use has not been reported in experimental cardiac MRI. This work presents methods and first results for accelerated cardiac MRI in rats at 9.4T using GRAPPA and a dedicated four channel receive array.

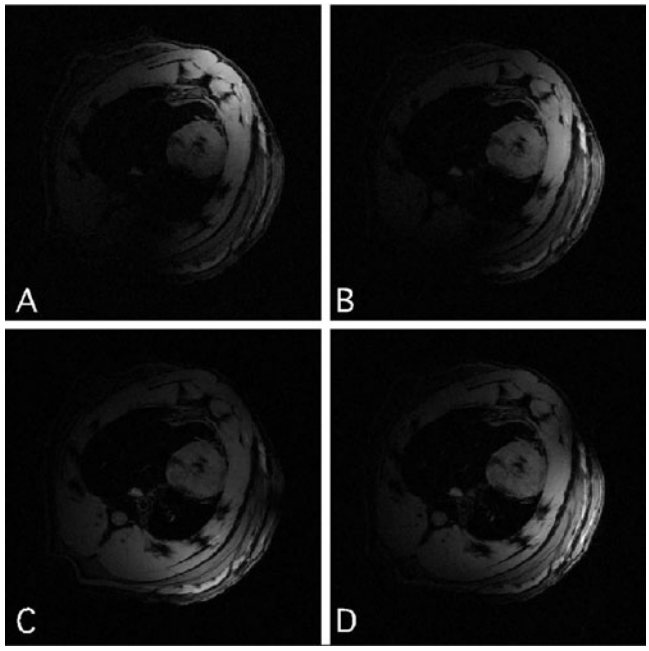

FIG. 1.

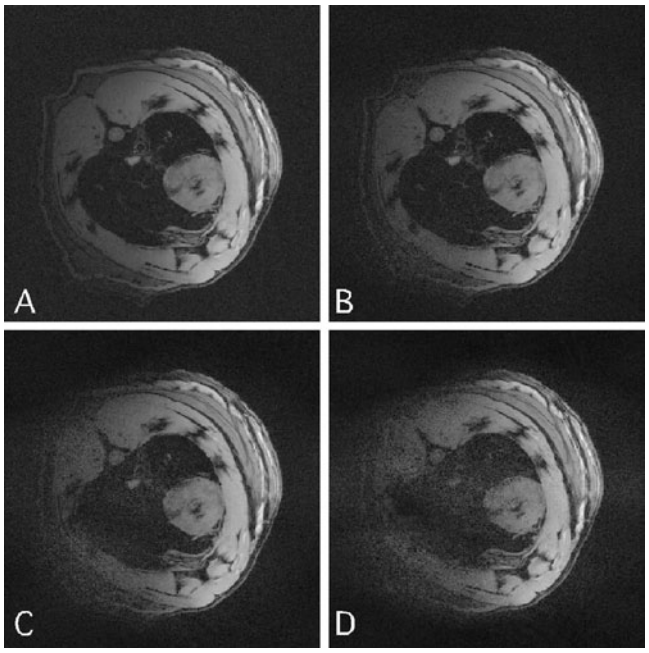

FIG. 2.

Methods: We designed a four-element coil-array optimized for rat hearts. All coil elements were decoupled using a combination of shared inductors and preamplifier decoupling. Imaging was performed on a horizontal 9.4T MR system (VNMRS, Varian Inc.). Ex vivo MR images were acquired using a fast gradient echo (GE) sequence and the parallel imaging method GRAPPA to accelerate data acquisition (24 auto calibration lines, acceleration factors R = 2, 3 and 4). For in vivo experiments, a fast multi-frame GE sequence (TE/TR = 1.79/4.6 ms) was used.

Results & Discussion: Single coil elements showed high isolation and therefore good encoding properties. Overall decoupling of each pair of coil elements was better than -20dB. In Fig. 2A the sum of squares of the ex vivo images from Fig. 1A-D is shown. Results of GRAPPA are shown in Fig. 2B-D (acceleration factors R = 2, 3 and 4, respectively). Note, even a

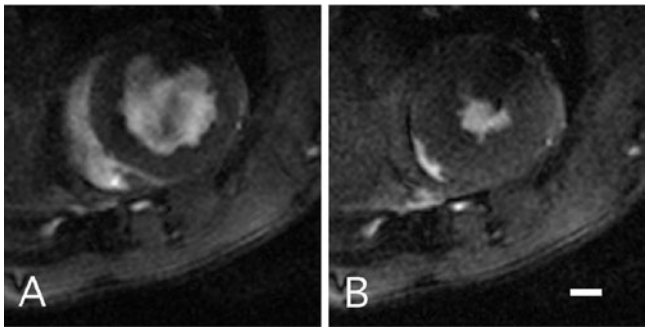

FIG. 3.

threefold reduction in scan time provides sufficient image quality in the heart region (Fig. 2C). Fig. 3 shows the sum-of-square (A) end-diastolic and (B) end-systolic frames of the rat heart in vivo (in plane resolution 100 μm, slice thickness 1.5 mm. scale bar: 2 mm).

Conclusions: This is the first study to report on the development of a dedicated cardiac coil array and GRAPPA in the rat heart. Further improvements of the in vivo method should allow cardiac exams in rodents to be performed in about 15 minutes.

Acknowledgement: This work was supported by the British Heart Foundation (BHF). We would like to thank Miss L. Stork, Miss D. Medway and Miss H. Barnes for technical assistance.

514. THE ADJUNCTIVE ROLE OF CARDIOVSCULAR MAGNETIC RESONANCE (CMR) IN PATIENTS WITH AN ABNORMAL RESTING ELECTROCARDIOGRAM (ECG) AND NON-DIAGNOSTIC TRANSTHORACIC ECHOCARDIOGRAPHY (TTE)

Ravi Assomull, MRCP, William M. Bradlow, MRCP, Niall G. Keenan, MRCP, Jonathan C. Lyne, MRCP, Dudley J. Pennell, MD FRCP FACC FESC, Sanjay K. Prasad, MD MRCP. ***Royal Brompton Hospital, London, United Kingdom.***

Introduction: In the absence of chest pain, an abnormal resting electrocardiogram (ECG) raises the suspicion of structural cardiac disease. Transthoracic echocardiography (TTE) is the initial investigation of choice due to its widespread availability and low unit cost. A proportion of patients presenting with an abnormal ECG will, however, have "normal" or non-diagnostic TTE. These patients present a difficult clinical dilemma for physicans as no diagnosis can be ascribed. This has important implications for subsequent management, including treatment and risk stratification. Possible explanations for the lack of diagnosis by TTE are that image quality is often operator-dependent and acoustic windows may be inadequate in up to 10% of patients. Cardiovascular magnetic resonance (CMR) is free from these restrictions and is a modality capable of providing consistently high resolution imaging of cardiac structure, function and tissue character. Previous studies have already shown a role for CMR in a highly selected group for detecting cardiomyopathy where TTE has been non-diagnostic.

CMR Findings

Diagnosis	Value (%)
Hypertrophic cardiomyopathy	6 (11)
Dilated cardiomyopathy	6 (11)
Myocardial infarction	4 (7)
Myocarditis	3 (6)
Other	4 (7)
Normal	32 (58)

Purpose: In this prospective study we hypothesized that CMR has incremental diagnostic value beyond that provided by TTE in patients with an abnormal ECG and no structural abnormalities detectable by TTE in a consecutive, unselected group of patients from general cardiology clinics.

Methods: Fifty-five consecutive patients presenting with an abnormal ECG in whom subsequent TTE had been labelled as normal or non-diagnostic were recruited between January 2004 and July 2006. All patients underwent ECG and TTE in the 3 months prior to enrolment. No patients had a previous history of coronary artery disease, coronary intervention or cardiac surgery. Any patients with a prior cardiac history, for example of myocarditis, myocardial infarction, known cardiomyopathy or impaired LV function were also excluded.

Standard 12 lead ECGs (25 mm/s, 10 mm/mv) were recorded with the patient supine during shallow respiration. The primary ECG abnormality was ascribed by a single blinded interpreter in accordance with the Minnesota code. TTE was performed at the referring centre by qualified technical staff. Clinically generated reports were acquired for all patients and checked to ensure that the findings included normal chamber sizes, normal wall thickness and non-significant valvular pathology (no more than mild valvular regurgitation or stenosis) and that the findings were reported either as normal or inconclusive for any definitive diagnosis.

CMR (Siemens Sonata 1.5T, Erlangen, Germany) was performed within 3 months of ECG/TTE. Long axis and short-axis

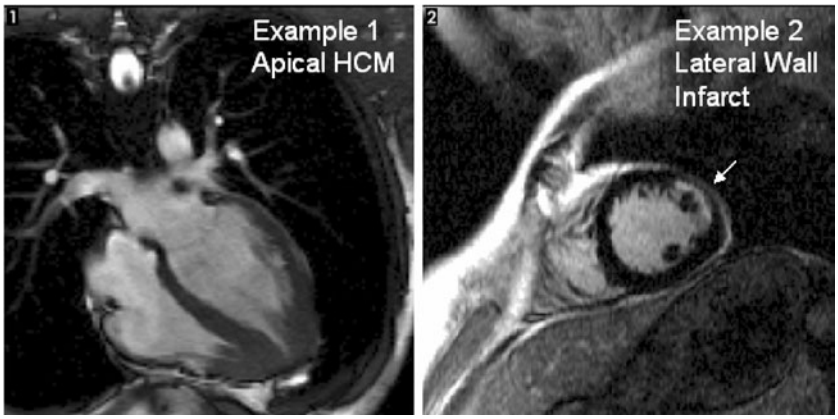

cine images were acquired in the standard way. Late gadolinium enhancement (LGE) images were acquired 10 minutes after intravenous gadolinium-DTPA (Schering; 0.1 mmol/kg) in identical long and short-axis planes using an inversion-recovery gradient echo sequence.

Results: CMR provided a new diagnosis in 23 patients (42% of cohort). In the remaining patients, no new diagnosis was made as LV and RV parameters were within normal limits and there was no detectable myocardial infarction or fibrosis. Cardiomyopathy was the most common diagnosis and was ascribed on the basis of WHO diagnostic criteria (Table 1). Other diagnoses included myocardial infarction, myocarditis and severe aortic regurgitation (Fig. 1).

Conclusions: This study reveals a role for CMR as an adjunct to TTE in patients with an abnormal ECG. In our cohort, CMR provided a new diagnosis in 42% of cases and more confidently excluded significant structural pathology in the remainder.

515. FUNCTIONAL RECOVERY AFTER ACUTE MYOCARDIAL INFARCTION IN HUMANS—STRAIN BY VELOCITY-ENCODED MAGNETIC RESONANCE IMAGING

Erik Hedström, PhD,[1] Erik Bergvall, MSc,[1] John Molvin, BSc,[1] Gunnar Sparr, PhD,[2] Håkan Arheden, MD, PhD.[1]
[1]Lund University, Lund, Sweden, [2]Faculty of Engineering, Lund University, Lund, Sweden.

Introduction: Quantitative measurements of regional myocardial function is of high diagnostic and prognostic value. Strain as a quantitative measurement of regional myocardial function can be calculated from velocity-encoded magnetic resonance imaging (VE-MRI).

Purpose: We sought to investigate the functional recovery of human myocardium, regarding strain, during the year after an acute myocardial infarction.

Methods: Nine patients (median age 66 years, range 41–71 years), who had a first time myocardial infarction treated by acute primary percutaneous coronary intervention (PCI) with stenting, underwent VE-MRI and delayed contrast-enhanced MRI (DE-MRI) at 1 day after the infarction, and follow-up at 1 week, 6 weeks, 6 months, and 12 months thereafter. Long-axis images in the 2-, 3-, and 4-chamber views were acquired. Velocity data was integrated with respect to time to obtain the displacement field in the myocardium. The Cauchy-Green strain tensor was calculated by numerical differentiation of the displacement field. Strain was decomposed in longitudinal and radial strain, and end-diastole was used as reference configuration (zero strain). Extent of infarction was determined by DE-MRI in a 21-segment model. The segments were classified in six groups as remote (no infarction and not adjacent to an infarcted segment), adjacent (adjacent to an infarcted segment or extent of infarction less than 10 %),

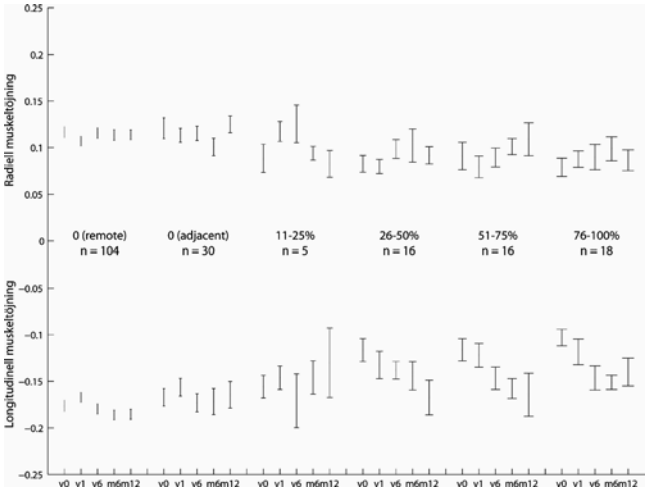

and extent of infarction of 11–25%, 26–50%, 51–75%, and 76–100%.

Results: A trend of less magnitude of strain was found with increased extent of infarction at day 1, especially for longitudinal strain. In segments with more than 25% extent of infarction, a gradual increase in longitudinal strain was found from the acute setting to 12 months thereafter (0.05 units). This trend was also found for radial strain; however, it was not as pronounced (0.02 units). In the segments without infarction, the magnitude of strain was constant.

Conclusions: Analysis and presentation of strain data was performed automatically in below 30 seconds on a standard PC, indicating clinical usefulness. During up to 12 months after an acute infarction, a gradual recovery of myocardial regional function was found. At 12 months after the acute infarction the regional function had recovered towards that of segments without infarction, also in segments with the highest degree of extent of infarction (75–100%).

516. TE DEPENDENCE OF FLOW MEASUREMENTS IN STENOTIC JETS

Kieran R. O'Brien, BE(hons),[1] Brett R. Cowan, MBChB,[2] Alistair A. Young, PhD.[3] **[1]*Bioengineering Institute, University of Auckland, Auckland, New Zealand,* [2]*Centre of Advance MRI, University of Auckland, Auckland, New Zealand,* [3]*Department of Radiology, Bioengineering Institute, University of Auckland, Auckland, New Zealand.***

Introduction: Phase contrast (PC) measurement of velocity and flow is an important component of the CMR assessment of congenital and acquired valvular heart disease. It is known that these jets can be very turbulent and that intra-voxel dephasing can cause significant errors in this setting. In clinical and trial data we have found that PC measurements of stroke volume (SV) in aortic stenosis are frequently lower than SV obtained from volumetric measurements at end-diastole and end-systole.

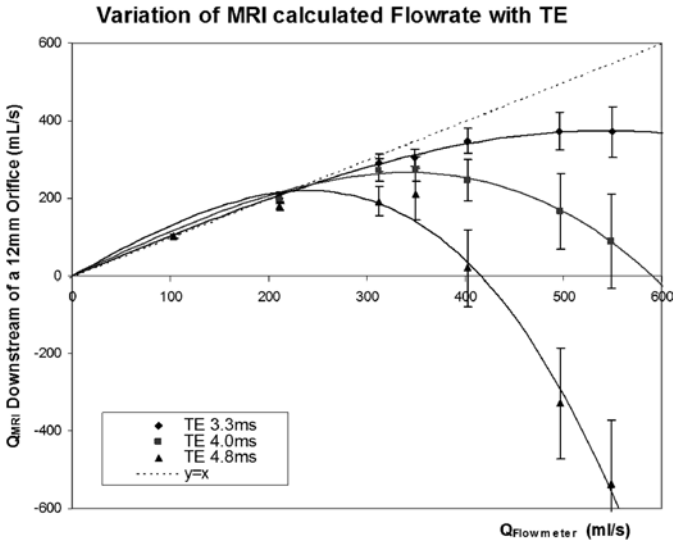

FIG. 1. Shows the increase of error in PC with increasing flow rate at various TEs, 35 mm into the jet.

Purpose: To determine the cause of the underestimation of SV by PC by constructing an experimental phantom to model a stenotic aortic valve and resulting flow jet. The aim was then to investigate the magnitude of the errors and effect of the PC pulse sequence parameters in this controlled environment.

Methods: Two phantoms were constructed. The first consisted of a straight PVC pipe (internal diameter [ID] 17 mm) without any narrowing. The second (ID = 28 mm) had a concentric circular obstruction (ID = 12 mm) placed in the flow to simulate a stenotic valve.

Water was pumped through a closed circuit at constant flow rates ranging from 100–1100 mL/s. An electromagnetic flow meter with an accuracy of 1% was placed in the circuit and outside the 5 Gauss line to provide a gold standard measurement of flow.

All experiments were conducted on a Siemens 1.5T Avanto system. A retrospectively gated velocity encoding technique used an artificial ECG trace for triggering. Parameters were TE/TR of 3.3-4.8 ms/66 ms, typical voxel size of 1.17 × 1.17 × 8, matrix size 192 × 256 and LVOT and AR VENCs of 250/500 cm/s.

Results: Flow in the small pipe showed that the scanner was capable of accurately measuring high velocity fully developed turbulent flow (Reynolds number 80,000) with peak velocities of 587cm/s. for all TEs the linear regression anaylysis between the scanner and the Gold standard had an R2 value of 1.000 and the maximum error experienced was 2.8% with an average error of 1.8 ± 0.6%.

Fig. 1 shows that in the jet, 35 mm downstream of the constriction, with increasing flow rate the PC underestimation of flow worsens. As flow is increased, the turbulence in the flow increases. Intravoxel dephasing caused by turbulence increases as a result and leads to the increasing error experienced at high flow rates in the jet. At the long TE of 4.8 ms, investigation of the magnitude image reveals that considerable signal loss and salt and pepper noise in the phase image is characteristic of complete intravoxel dephasing induced flow errors, Figs. 2A and 2D.

Shortening the TE to 4.0 and 3.3 reduces the extent of intravoxel dephasing that occured during image acquisition and results in an improvement in the PC flow estimate. Figs. 2E and 2F show that salt and pepper noise is removed from the phase

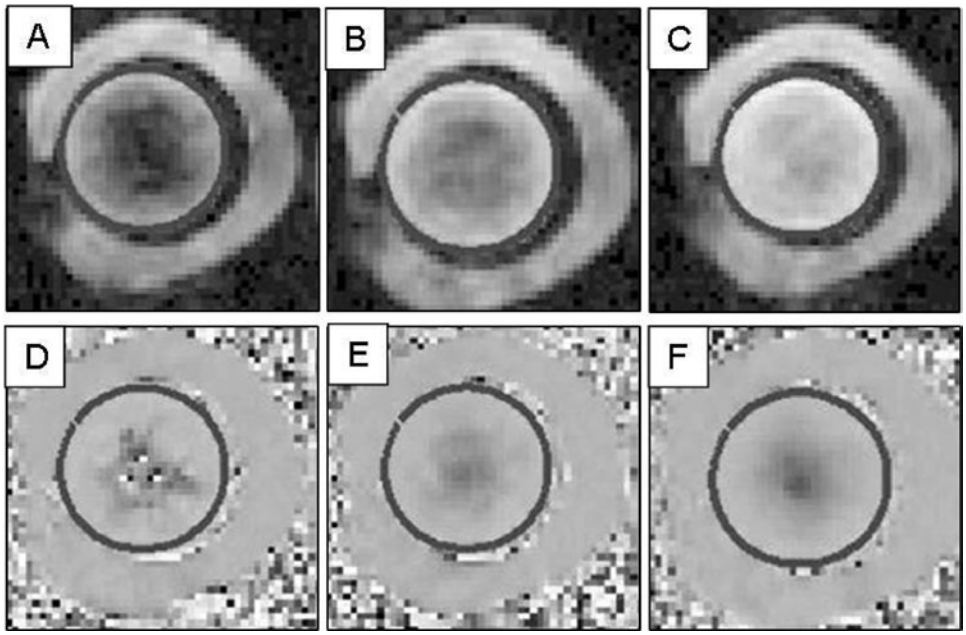

FIG. 2. Shows the magnitude and phase image of the jet formed at a flow rate of 400 mL/s, 35 mm from the constriction at various TEs, 4.8 (A/D), 4.0 (B/E) and 3.3 (C/F).

image associated with the reduction in intravoxel dephasing. But comparing Figs. 2B and 2C reveals that at the longer TE of 4.0 ms significant signal loss is still apparent, evident that intravoxel dephasing caused by turbulence is still a source of error.

Conclusions: Intra-voxel dephasing leads to signal loss in the magnitude image and can result in underestimation of flow in stenotic jets. Shorter TE's reduce this effect but shorter TE's than are currently available on many systems are required for reliable measurements at high flows.

517. MYOCARDIAL INFARCT SIZE IN RELATION TO MYOCARDIUM AT RISK VERSUS DURATION OF ISCHEMIA IN HUMANS: COMPARISON WITH DIFFERENT SPECIES

Erik Hedström, PhD, Fredrik Frogner, MD, Karin Åström-Olsson, MD, Hans Öhlin, MD, PhD, Håkan Arheden, MD, PhD. ***Lund University, Lund, Sweden.***

Objectives: The impact of duration of ischemia on infarct size related to myocardium at risk has been demonstrated in several species, but not yet in humans. We, therefore, sought to investigate how duration of ischemia affects infarct size in humans, and to compare the results to earlier animal studies of different species.

Methods and Results: In order to study the impact of duration of ischemia on infarct size while minimizing the influence of confounding factors, more than 700 patients admitted for acute primary percutaneous coronary intervention (PCI) were screened and excluded if they had signs of previous infarction, visible collaterals, or release of biochemical markers, resulting in a study population of 16 patients. Myocardium at risk was assessed by acute perfusion scintigraphy, and infarct size was measured by delayed contrast-enhanced magnetic resonance imaging 1 week later. We found that infarct size in humans increased with duration of ischemia, however, more slowly than in rat and pig, and similar to or more slowly than in canine and baboon.

Conclusions: The present study is the first to provide direct measurement of the time course of acute infarct evolution in relation to myocardium at risk in humans. Infarct evolution in humans was similar to, or slower, compared to experimental infarct in animals. The findings suggest that the major part of myocardium at risk may be salvaged if treated early, but also that late reperfusion may be of value for limiting infarct size.

518. APOLIPOPROTEIN E DERIVED PEPTIDE CONTAINING GADOLINIUM MIXED MICELLES FOR MACROPHAGE IMAGING IN ATHEROSCLEROTIC PLAQUE OF APOE −/− MICE

Esad Vucic,[1] Karen C. Briley-Saboe, PhD,[1] Juan Gilberto Aguinaldo, MD,[1] Vardan Amirbekian, MD,[1] Sandro Keller, PhD,[2] Edward A. Fisher, MD, PhD,[3] ,Margitta Dathe, PhD,[2] Zahi A. Fayad, PhD.[1] ***[1]Mount Sinai School of Medicine, New York, NY, USA, [2]Leibniz Institute of Molecular Pharmacology, Berlin, Germany, [3]New York University School of Medicine, New York, NY, USA.***

Introduction: Lipid nanoparticles containing Apolipoprotein E derived peptide (P2A2) have been shown to be effectively incorporated in various endothelial cell types in vitro. P2A2 consists of a 20 amino acid tandem dimer comprising binding sites for the low-density lipoprotein receptor and for cell surface heparan sulfate proteoglycan. Untargeted Gadolinium mixed micelles have been shown previously by our group to be an effective magnetic resonance contrast agent for atherosclerotic plaque imaging in ApoE −/− mice. Untargeted micelles localize to areas rich in extracellular matrix in atherosclerotic plaque without cellular interaction. This study tests the hypothesis that the incorporation of P2A2 into Gadolinium mixed micelles will shift the properties of untargeted micelles from a non-cellular to cellular interaction in atherosclerotic plaque with the potential of specific macrophage imaging.

Methods: Gadolinium mixed-micelles were prepared and P2A2 was incorporated during preparation. This lead to formation of P2A2 containing Gadolinium mixed micelles (ApoE Micelles). Fifteen-month-old ApoE −/− mice (n = 5) underwent in vivo MRI of the abdominal aorta using a 9.4T MR system. Lissamine Rhodamine (red chromophore) containing APOE Micelles (0.038 mmol Gd/Kg) were injected in the tail vein and pre- and post-contrast enhanced MR at 24 h using a T1W black blood sequence was performed. As a control ApoE −/− mice (n = 6) were injected with NBD (green chromophore) containing untargeted micelles (0.038 mmol Gd/Kg) and were imaged as described. Another control group (n = 6, Apo E −/− mice) was injected with Gd-DTPA and imaged at 1 h and 24 h post-injection.

After MRI, the aortas were removed and fixed. Frozen sections were obtained and where indicated stained with CD68 for macrophage staining. The sections were then imaged using confocal microscopy for co-localization studies.

Results: Relative to muscle (as described by the %NENH), administration of untargeted and ApoE micelles resulted in a significant enhancement of the vessel wall of ApoE−/− mice. % NENH: 62% ± 5 for untargeted micelles, and 113% ± 5 ApoE micelles. Following administration of GdDTPA, transient signal enhancement was observed in the vessel wall of ApoE−/− mice one-hour post injection. No significant enhancement of the vessel wall of ApoE−/− or WT mice was observed 24 hour post injection.

Confocal fluorescence imaging demonstrates the localization of untargeted micelles primarily to perivascular areas and areas rich in extracellular matrix without significant cellular interaction. Aortic Sections after ApoE micelle injection demonstrate localization of ApoE micelles to core areas of atherosclerotic plaque with specific co-localization to macrophages.

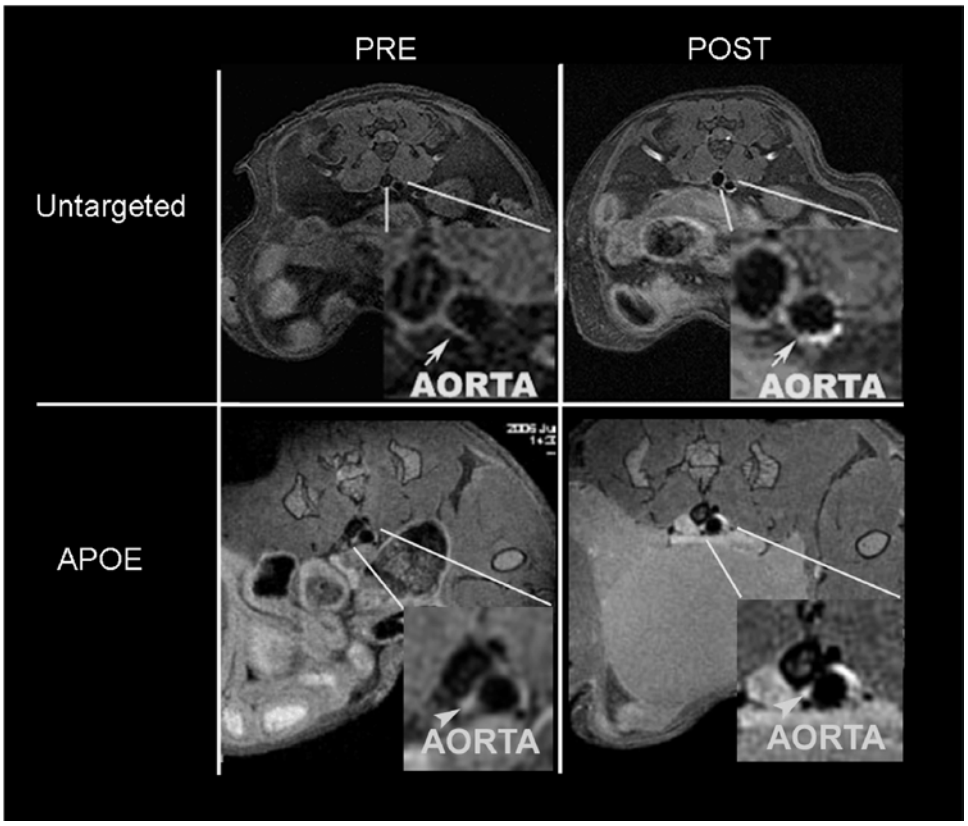

FIG. 1. MR images of ApoE−/− mice pre and 24 hours after the administration of 0.038 mmol Gd/Kg of untargeted or APOE targeted micelles at 9.4T.

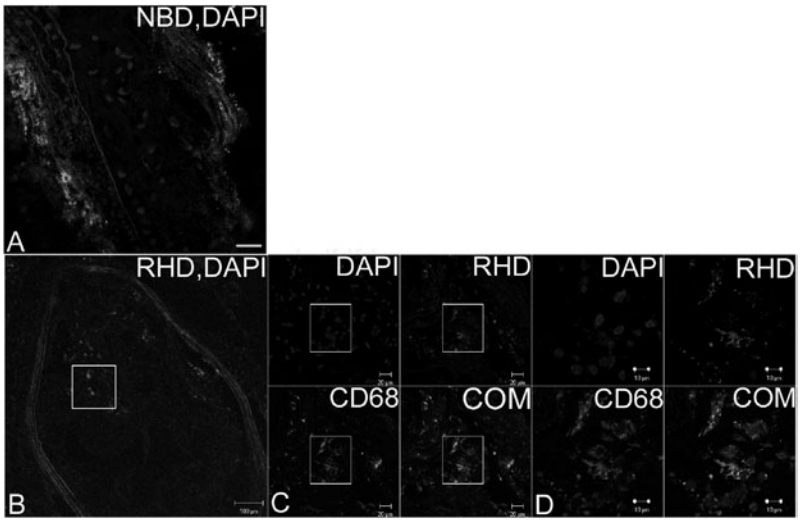

FIG. 2. Fluorescence Confocal microscopy of aortic sections 24 h post injection of untargeted NBD-tagged micelles (A) and Lissamine Rhodamine-tagged APOE micelles (**B–D**). **A)** Untargeted micelles display diffuse extracellular and perivascular distribution (green areas) with no apparent cellular interaction. Grey bar = 20 μm. **B)** Two channel image overlay shows at low power magnification, an aortic section with APOE micells (red) localizing to core areas of atherosclerotic plaque. **C)** RGB and composite image of an adjacent section to B with higher magnification A core plaque area as seen on image B with CD 68 staining (green) for Macrophages. Areas of comparable distribution of APOE micelles (red) and Macrophages (green) on individual channel images. A close association shown between Macrophages and APOE micelles (yellow-orange areas) on composite image. **D)** RGB and composite image with magnification of marked area from image B. Both APOE micelle and macrophage are dected in congruent areas of the plaque as seen on individual channel images. The composite image reveals punctate cellular localization of APOE micelles in tissue macrophages. DAPI nuclear stain: blue, on individual and composite images.

Summary of the in vivo efficacy in ApoE−/− mice and WT mice 24 hours after the administration of a 0.038 mmol Gd/kg dose. The normalized signal enhancement (%NENH) reflects the signal increase of the vessel wall relative to muscle. All imaging was performed at 9.4 T using T1-weighted black blood (SE) sequences with TR/TE/flip = 600 ms/8.6 ms/30, NEX = 14, FOV = 2.6 cm × 2.6 cm. Bold-faced values represent statistically significant values relative to wild type mice

	0.038 mmol Gd/kg micelles 24 hours post injection			GdDTPA 0.1 mmol/kg	
	Untargeted Apo−/− (n = 6)	Targeted Apo−/− (n = 5)	Untargeted WT (n = 3)	Apo−/− 1 hr. p.i. (n = 6)	Apo−/− 24 hrs. p.i. (n = 6)
%NENH	62 ± 5	113 ± 5	10 ± 11	20 ± 12	−2 ± 7

Conclusion: We demonstrate the specific molecular imaging of macrophages using ApoE derived peptide containing gadolinium mixed micelles. Further studies need to be added to establish the molecular nature of the interaction of ApoE micelles with macrophages in atherosclerotic plaque.

519. PHASE CONTRAST FLOW ERRORS IN STENOTIC JETS

Kieran R. O'Brien, BE(hons),[1] Andrew J. Kerr, MBChB,[2] Ralph Stewart, MBChB,[3] Brett R. Cowan, MBChB,[4] Alistair A. Young, PhD.[5] [1]***Bioengineering Institute, University of Auckland, Auckland, New Zealand,*** [2]***Department of Cardiology, Middlemore Hospital, Auckland, New Zealand,*** [3]***Department of Cardiology, Auckland Hospital, Auckland, New Zealand,*** [4]***Centre of Advance MRI, University of Auckland, Auckland, New Zealand,*** [5]***Department of Radiology and Bioengineering Institute, University of Auckland, Auckland, New Zealand.***

Introduction: Phase contrast (PC) MR measurements of velocity and flow in stenotic jets provide valuable diagnostic and pre-operative information in patients with valvular heart disease. It has been suggested that due to intra-voxel dephasing, PC measurements in turbulent jets may not be completely reliable. We conducted a clinical trial to investigate the accuracy of PC measurements in aortic stenosis (AS) followed by phantom experiments on a jet in a straight pipe.

Purpose: To compare aortic PC flow measurements against left ventricular stroke volume (SV) in patients with isolated AS and (ii) to evaluate PC accuracy in a jet in a straight pipe.

Methods: Patients (n = 38, 26 males, age range of 50–80 years and weight 52–120 kgs and an average AVA of 0.94 ± 0.31 cm^2) with AS were scanned using a free breathing retrospectively gated velocity encoding technique. Two image planes with through-plane velocity encoding were acquired: one in the aortic root (AR) and a second in the left ventricular outflow tract (LVOT). Typical pulse sequence parameters were TE/TR of 4.8/25 ms, typical voxel size of 1.25 × 1.25 × 8 mm, matrix size 192 × 256 and LVOT and AR VENCs of 250/500 cm/s.

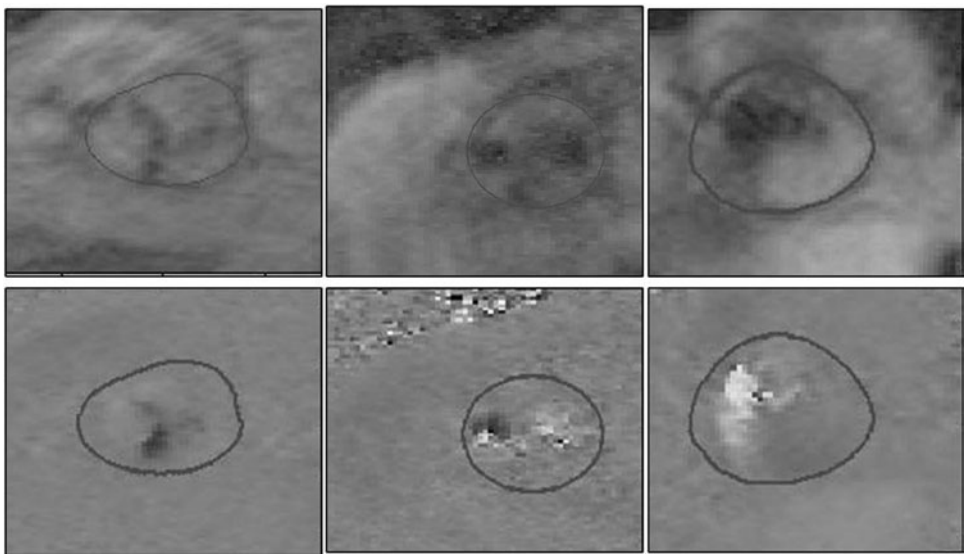

FIG. 1. Shows the magnitude images of three different patients with errors −28.2% (A/D), −98.3% (B/E) and −55.7% (C/F). The magnitude images all display signal loss from intravoxel dephasing though salt and pepper noise in the phase image is only seen in E and F.

Six short and three long axis true-FISP cines of the left ventricle were also acquired to provide a validated estimate of stroke volume (SV).

In the phantom experiments, a stenotic jet was created by placing a 12 mm concentric circular constriction in a straight PVC pipe with an internal diameter of 28 mm. Water was circulated around the circuit by a pump at a constant flow rate of 400 mL/s. Gold standard flow measurement was provided by an electromagnetic flow meter with an accuracy of 1% situated outside the 5 Gauss line. An artificial ECG was used to trigger the same sequence as used in the clinical trial.

All images were obtained on a 1.5T Siemens Avanto.

Results: Using the true-FISP SV as the gold standard, PC consistently underestimated SV in the AS patients. The error in the LVOT was -27.4 ± 21.0% and in the AR -41.6 ± 21.7%. The magnitude images from the clinical trial suffered from signal loss with salt and pepper noise in the phase image (Fig. 1), characteristic of intra-voxel dephasing.

In the straight pipe phantom, the PC results were also consistently less than the gold standard. Reducing the TE from 4.8 to 4.0 and 3.3 ms decreased the error from −95.1 ± 24.4%, to -38.5 ± 13.1% and -13.5 ± 8.2% respectively, confirming the anticipated critical dependence of accuracy on TE.

In a case study, an AS patient was imaged at the minimum TE available on the Avanto system (2.8 ms) using a breath-hold acquisition. Images were acquired in the middle of the LVOT, at the valve plane and 10mm above the valve plane. Even at this minimum TE, there is still underestimation of flow compared to the volumetric gold standard. The errors increase in the patient from −0.4% at the LVOT, −11.6% at the valve plane, to −25.1% 10 mm above the valve plane. This result was confirmed in the phantom (Fig. 2) which shows that at TE = 3.3 ms, that the errors are worst between 40 and 100 mm from the constriction.

Conclusions: PC techniques underestimate flow (and therefore velocity) in stenotic jets due to intra-voxel dephasing caused by turbulence. TE minimisation is critical to minimising error, but with current hardware and sequences the minimum values available may still not be low enough for clinically acceptable results.

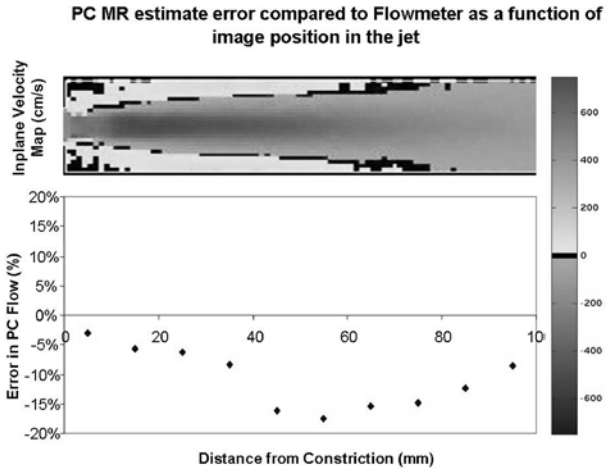

FIG. 2. Error as a function of distance from the constriction in the phantom.

520. ASSESSMENT OF SYSTOLIC PARAMETERS IN DOBUTAMINE STRESS CMR (DSMR) USING AUTOMATIC ENDOCARDIAL CONTOUR TRACING FOR LEFT VENTRICULAR VOLUME TIME CURVES (VTCS)

Tarinee Tangcharoen, MD,[1] Osama Gomaa, MD,[1] Harry Peusen,[2] Eckart Fleck, MD,[1] Eike Nagel, MD.[1] [1]*German Heart Institute, Berlin, Berlin, Germany,* [2]*Philips Medical System, Best, The Netherlands.*

Purpose: To evaluate systolic function at rest and different dobutamine stress levels by using automatic endocardial contour tracing.

Methods: Twenty-three subjects with invasive coronary angiogram (no coronary artery disease; CAD−ve = 11; significant

TABLE

Parameters	Normal CAG (N = 11)	Abnormal CAG (N = 12)	*p*value
1. EDV (mL) delta	−6.98 ± 11.33	−0.23 ± 5.86	0.083
rest/low dose delta	−17.72 ±12.27	−4.95 ± 6.05	< 0.01
rest/high dose	−16.35 ± 6.66	−8.23 ± 5.73	< 0.01
		−9.64 ± 6.38	< 0.01
2. ESV (mL) delta	−19.02 ±7.05	8.00 ±5.57	0.629
rest/low dose delta	9.36 ± 7.67	4.69 ± 6.37	< 0.01
rest/high dose	1.3 ± 7.79		
3. SV (mL) delta rest/low		1.82 ± 1.01	0.477
dose delta rest/high dose		3.18 ± 1.09	0.530<
	2.08 ± 0.68		
	3.46 ± 1.01		
4. CO (L/minute) delta			
rest/low dose delta			
rest/high dose			

coronary artery disease; CAD+ve = 12) and low and high dose DSMR(1.5 T, Philips Intera CV) were included. Three short axis and 3 long axis planes (2- , 3- and 4- chamber view) were acquired under rest, low and high doses dobutamine stress levels. The endocardial contours were automatically traced and, if required, manually corrected using View-Forum Workstation R 4.2. L. Systolic parameters in each stress level were automatically calculated including, end-diastolic volume (EDV), end-systolic volume (ESV), stroke volume (SV) and cardiac output (CO). The difference of each parameter between rest and low dose and rest and high dose dobutamine were calculated. All values are expressed as mean + SD.

Results: CAD-ve and CAD +ve did not differ in EDV, ESV, SV and CO at rest. The results for different stress levels are shown in the table.

Conclusion: Patients with CAD showed significant abnormalities of ESV during low dose dobutamine and EDV, ESV and SV during high dose dobutamine. Assessment of global LV function and volume provides a quantitative parameter which may allow to objectify DSMR analysis. Its accuracy for the detection of ischemia needs to be evaluated.

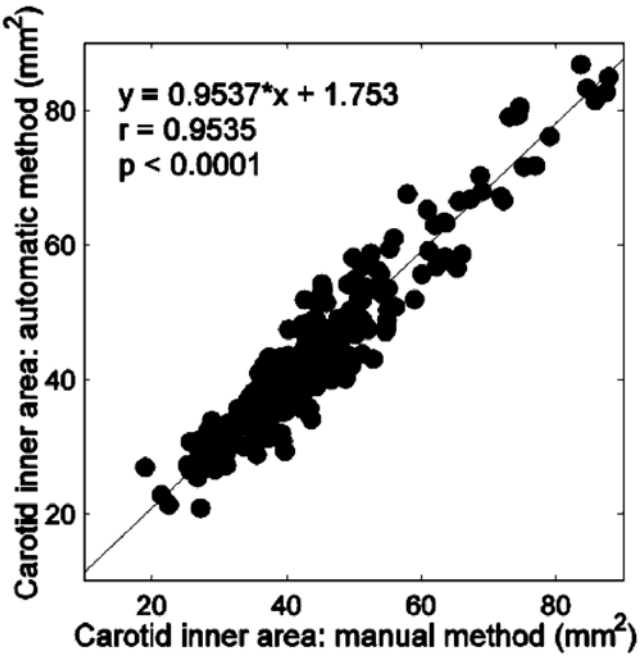

FIG. 1. Comparison of results of automatic method with actual manually traced vessel dimensions for the carotid arteries.

521. VALIDATION OF AUTOMATED MEASUREMENT OF DYNAMIC ARTERIAL LUMEN AREA BY CMR

Clare E. Jackson, PhD, Cheerag C. Shirodaria, MRCP, Justin M. S. Lee, MRCP, Robin P. Choudhury, DM, MRCP, Keith M. Channon, MD, FRCP, Stefan Neubauer, MD, FRCP, Matthew D. Robson, PhD. ***University of Oxford Centre for Clinical Magnetic Resonance Research, Oxford, United Kingdom.***

Introduction: Increased vessel stiffness shown by decreased arterial compliance has been shown to correlate to a number of disease states (1). Vessel compliance is calculated from the ratio of the change in vessel area to the change in blood pressure between two time points. The change in vessel lumen area can be measured over the cardiac cycle using cardiovascular magnetic resonance (CMR) for a series of cine images. Manually tracing the vessel lumen area in a series of cine CMR images is time consuming and prone to error. We, therefore, developed an automated method for measuring the vessel lumen area from cine CMR images (2), and here extend that approach to the smaller carotid vessels.

Purpose: To build a tool for the cardiovascular community for automated vascular analysis. This paper focuses on validation of the accuracy and repeatability of the automated method presented at SCMR 2006 (2).

Methods: All studies were performed on a 1.5T clinical MR scanner (Siemens Sonata). Bright blood SSFP cine MR images were acquired of 33 newly diagnosed coronary artery disease patients, who were each imaged on two separate occasions. Left and right carotid artery lumen area was found using the automated method for each of the images from each of the 66 examinations. The areas at end diastole and end systole were found by manual tracing and the results from both the manual and automatic methods were compared.

The repeatability of the method was also tested using bright blood SSFP cine MR images of the aorta of 6 volunteers who were each imaged 5 times. The automated measurement method was implemented under Matlab (Mathworks Inc, Natick, MA).

Results: Inner areas of the carotid arteries were found at end diastole and end systole using both manual tracing and the automated method. A close correlation (r = 0.9535) was found between these two approaches (Fig. 1).

The repeatability of the automated method was tested by analysing one data set from each of the 6 volunteers 5 times in succession. Five data sets were acquired for each volunteer and each one was analysed using the automated method.

TABLE 1
R values for the correlation of the results of the analysis of the repeatability data

	1	2	3	4	5	6	Mean
Same acquisition	0.99884	0.99730	0.99845	0.99935	0.99936	0.99829	0.998598
Different acquisition	0.98957	0.98896	0.98851	0.99631	0.99601	0.99081	0.991695

Correlation coefficients were found between each possible pair of corresponding area curves for each volunteer. Mean correlation coefficients are given in Table 1 for each of the 6 volunteers. The mean correlation was high ($r > 0.99$) for both the repeated analysis of the same data set and analysis of repeatedly acquired data from the each volunteer.

Conclusions: The carotid arteries were a factor of ~10 smaller than the average areas of the aorta (45 mm^2 vs. 500 mm^2), the automated method still worked well.

The higher correlation coefficients from the repeatability measurements demonstrate that, measurements of this sort are dominated not by the measurement error, but by physiogical variability in the subject, and hence the automated analysis is not a significant source of error. This method provides a robust and accurate method for measuring dynamic changes in the lumen area of the carotid artery.

REFERENCES

1. Wiesmann F, Petersen SE, Leeson PM, Francis JM, Robson MD, Wang Q, et al. Global impairment of brachial, carotid, and aortic vascular function in young smokers—Direct quantification by high-resolution magnetic resonance imaging. Journal Of The American College Of Cardiology 2004; 44:2056–2064.
2. Jackson CE, Shirodaria CC, Lee JMS, Choudhury RP, Channon KM, Neubauer S,. Robson MD. Accurate Automated Measurement of Dynamic Arterial Lumen Area by CMR, 8th SCMR, Poster #488, January 2006.

522. MODULATION OF CARDIAC T2* MEASUREMENTS BY MYOCARDIAL LIPID AT 3.0 TESLA

Declan P. O'Regan, FRCR, Martina F. Callaghan, PhD, Marzena Wylezinska-Arridge, PhD, Julie Fitzpatrick, Rossi Naoumova, PhD, Jo V. Hajnal, PhD, Stephan A. Schmitz, PhD. ***Imperial College, London, United Kingdom.***

Introduction: T2*-weighted multiecho sequences, used for the assessment of iron-overload, have the potential to be modulated by the effects of fat-water cancellation at opposed-phase echo times. Such sequences may be optimised to allow the calculation of fat content within the myocardium which is believed to play a role in diabetic cardiomyopathy.

Purpose: Our aim was to develop a spatially-resolved multiecho sequence at 3.0 Tesla to quantify myocardial lipid content and compare this to proton spectroscopy.

Methods: We developed a cardiac-gated multiecho sequence on a 3.0 Tesla Philips Intera (Best, The Netherlands) system with 7 echoes. A multiecho turbo field gradient echo sequence was used with an echo interval of 1.15 ms—allowing acquisition of alternate in-phase and out-of-phase images. A navigator echo was used for respiratory gating and two signal averages were used to improve signal to noise ratio. A black blood prepulse was used to suppress flow artifact. Images of the left ventricular short axis were acquired at mid-diastole, as well as an axial section of the liver.

Signal intensities were measured in the septum and peripheral liver. An iterative curve-fitting model was used to derive the relative proportions of fat and water within the tissue. In the heart global T2* was derived, and in the liver T2* for both the fat and water components. Five subjects underwent additional point-resolved proton magnetic resonance spectroscopy (MRS) of the liver and a further subject cardiac-gated spectroscopy of the interventricular septum-both without water suppression. The integrals of the lipid and water peaks were used to derive a fat fraction with a correction made for T2 decay.

Results: The image quality of the cardiac and liver multiecho sequences was good with minimal motion artefact (Fig. 1). The curve-fitting model converged on a best-fit in each case, for both liver and cardiac studies. A range of hepatic fat fractions between 1.1 and 15.1% were imaged which showed a good correlation with MRS measurements ($R^2 = 0.99$). In cardiac tissue

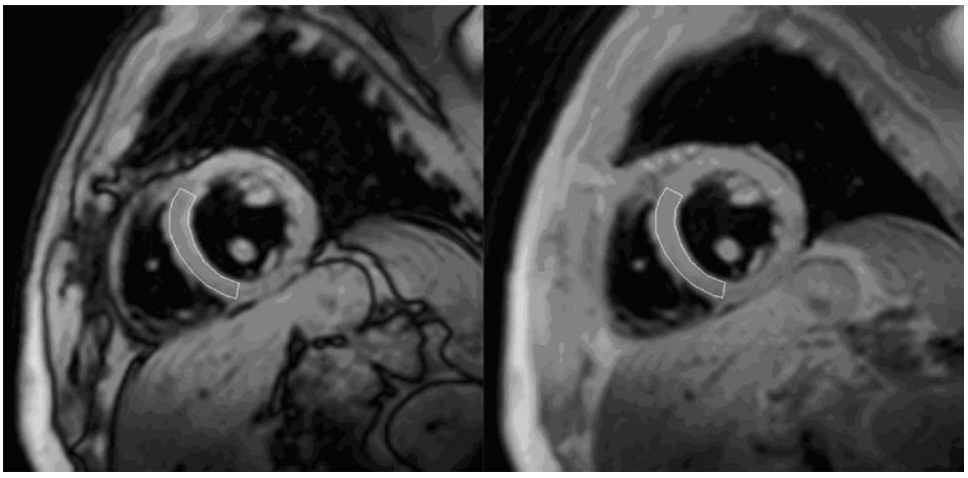

FIG. 1. The first two echoes from the multiecho sequence—opposed-phase on the left, and in-phase on the right. A region of interest is drawn on the interventricular septum.

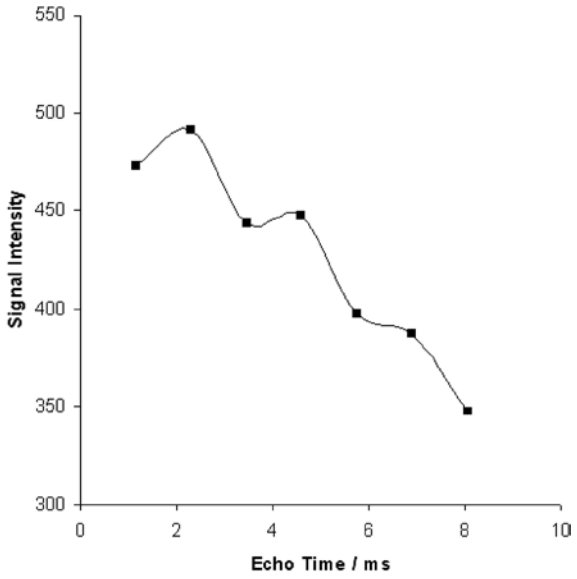

FIG. 2. A graph to show the modulation in exponential signal intensity decay in the septum at increasing echo times. The oscillation in the curve reflects the the presence of lipid and water within the voxels.

the multiecho sequence showed a modulation of the exponential decay of signal intensity in one subject with diabetes and obesity (Fig. 2). The presence of intra-myocardial lipid was confirmed on MRS with a fat fraction of 2% (Fig. 3).

Conclusions: Opposed-phase multiecho imaging is a promising tool for the measurement of both T2* and fat fraction within both liver and cardiac tissue. The acquisition of spatially-resolved images may be of value in the investigation of cardiac lipotoxicity. Furthermore, T2* sequences used for the measurement of tissue iron may be modulated by the effects of tissue lipid.

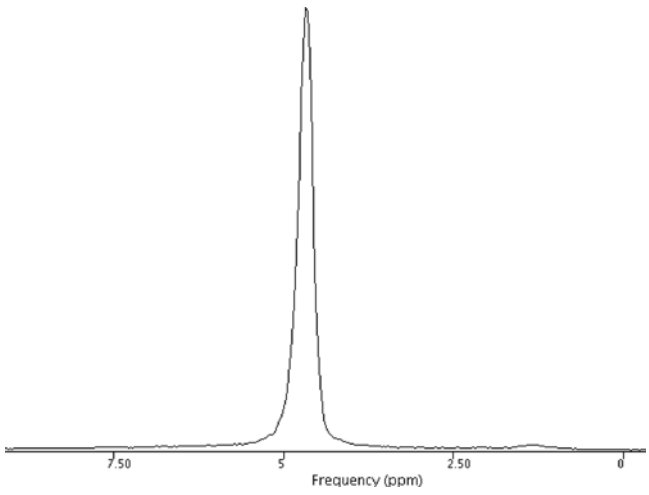

FIG. 3. A multibreath-hold cardiac triggered MRS spectrum of the septum showing a small lipid resonance at 1.4 ppm in the same patient.

523. MYOCARDIAL STRESS PERFUSION IMAGING AT 3T: COMPARISON OF SEMI-QUANTITATIVE AND QUALITATIVE ASSESSMENT IN PATIENTS WITH SUSPECTED CORONARY ARTERY DISEASE

Theodoros D. Karamitsos, MD, Adrian S. H. Cheng, MBBS, MRCP, Tammy J. Pegg, MBChB, MRCP, Matthew D. Robson, PhD, Stefan Neubauer, MD, FRCP, Joseph B. Selvanayagam, Dphil, FRACP, FESC. ***University of Oxford, Oxford, United Kingdom.***

Background: Assessment of myocardial perfusion using Cardiovascular Magnetic Resonance (Perfusion CMR) is increasingly used as an alternative to nuclear medicine techniques for the evaluation of inducible myocardial ischemia. Previous studies at 1.5 Tesla (T) have shown that perfusion CMR has moderate diagnostic accuracy for detection of coronary artery disease (CAD), but little data exist on the respective performance of semi-quantitative methods of perfusion assessment versus visual assessment in the same group of patients. Improved signal-to-noise ratio and contrast enhancement afforded by recently available 3T systems can potentially be used to improve spatial resolution and image quality. The aim of this study was to assess the clinical utility of CMR perfusion at 3T, by comparing the diagnostic accuracy of semi-quantitative against qualitative analysis, in the same population of patients with suspected CAD.

Methods: Twenty-five patients (21 men, mean age 62.8 ± 8.6 years) referred for diagnostic cardiac catheterization for suspected CAD were recruited. All patients underwent perfusion CMR imaging at 3T (T_1-weighted fast gradient echo sequence -echo time 1.04 ms, repetition time 2 ms, voxel size $2.1 \times 2.6 \times 8$ mm^3 with parallel imaging). Images were acquired both at rest and during adenosine stress during the first pass of 0.04 mmol/kg of a gadolinium-based contrast agent (Gadodiamide, Omniscan, GE Healthcare). Three short-axis planes were imaged, covering the left ventricle from the base to the apex. Perfusion CMR scans were visually interpreted by two observers acting in consensus, blinded to all data and using the AHA 17-segment model. For semi-quantitative analysis, a 3rd observer plotted the relative upslope of the signal intensity-time profiles for 16 myocardial segments defined on the three short-axis image sections, and calculated a myocardial perfusion reserve index (MPRI) between stress and rest, normalized to the input function from the blood pool. Receiver operating characteristic (ROC) curve analyses were performed to compare the diagnostic performance of perfusion CMR at 3T, using either visual or semi-quantitative assessment. Any segments with MPRI less than the defined cut-off value were classified as ischemic. If more than 1 segment within the territory of a coronary artery was classified as ischemic, CMR was regarded as positive for that region. Significant CAD was defined angiographically as the presence of at least one stenosis of $> 50\%$ diameter.

Results: Significant CAD was present in 84% (21/25) of the patients. As expected, visual assessment was significantly less

TABLE 1
Diagnostic performance of 3 Tesla perfusion imaging with visual and semi-quantitative assessment

	Sensitivity	Specificity	AUC ± SE	Diagnostic accuracy
Overall detection of CAD				
Visual	91% (19/21)	75% (3/4)	0.83 ± 0.1*	88% (22/25)
Semi-quantitative	95% (20/21)	75% (3/4)	0.85 ± 0.09*	92% (23/25)
Left Anterior Descending Artery				
Visual	77% (10/13)	83% (10/12)	0.80 ± 0.09*	80% (20/25)
Semi-quantitative	100% (13/13)	67% (8/12)	0.83 ± 0.08*	84% (21/25)
Left Circumflex Artery				
Visual	70% (7/10)	93% (14/15)	0.82 ± 0.09*	84% (21/25)
Semi-quantitative	91% (10/11)	79% (11/14)	0.85 ± 0.08*	84% (21/25)
Right Coronary Artery				
Visual	100% (11/11)	93% (13/14)	0.96 ± 0.04*	96% (24/25)
Semi-quantitative	100% (11/11)	79% (11/14)	0.89 ± 0.07*	88% (22/25)

AUC = Area Under the ROC Curve; SE = Standard Error; *$p > 0.05$ for comparison of AUC with the 2 methods of assessment.

time-consuming (8 minute per patient) than semi-quantitative analysis (60 minute per patient). Of the 400 myocardial segments available for semi-quantitative analysis, 30 (7.5%) were excluded because of mis-triggering or artefacts. A significant difference in MPRI between ischemic and normal segments (0.77 ± 0.21 and 1.79 ± 0.76, $p < 0.01$) was found that resulted in a cut-off value of 1.12. Visual and semi-quantitative assessment of CMR perfusion imaging provided similar diagnostic accuracies for the detection of CAD (Fig. 1) and the determination of disease location (Table 1). When evaluating the ability to detect disease in each coronary artery distribution, semi-quantitative analysis resulted in higher sensitivity and slightly lower specificity compared to visual assessment. This may reflect the ability of semi-quantification analysis to detect differences in myocardial tissue enhancement not always evident visually, possibly reflecting microvascular and not epicardial coronary disease.

Conclusions: Both visual and semi-quantitative assessment of CMR perfusion at 3T have high diagnostic accuracy for the detection of significant coronary artery stenoses, despite the latter being more time consuming. Although larger numbers of patients need to be studied, our findings underline the concept that visual assessment of CMR perfusion studies may be adequate in clinical practice, especially when imaging at higher field strengths.

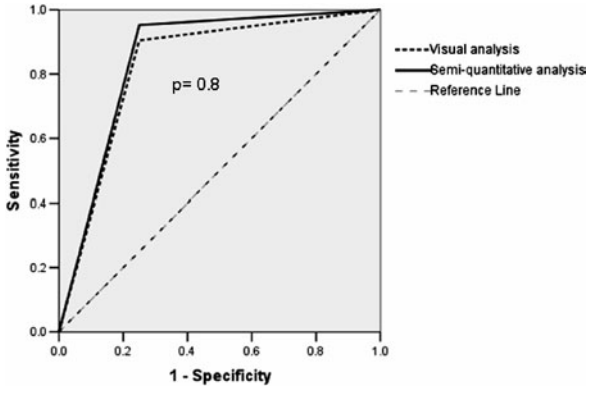

FIG. 1. Receiver-operator-characteristic curve analysis comparing visual with semi-quantitative analysis for the detection of coronary artery disease.

524. LEFT VENTRICULAR FUNCTION AND REMODELING AFTER INTRACORONARY INFUSION OF BONE MARROW—DERIVED PROGENITOR CELLS AFTER ACUTE STEMI: MRI SUBSTUDY OF THE DOUBLE-BLIND, RANDOMIZED, PLACEBO-CONTROLLED MULTICENTER REPAIR-AMI TRIAL

Thorsten Dill, MD,[1] Susanne Moellmann, MD,[1] Andreas Rolf, MD,[1] Guido Conradi, MD,[1] Holger Thiele, MD,[2] Volker Schaechinger, MD,[3] Andreas Zeiher, MD,[3] Christian W. Hamm, MD.[1] [1]***Kerckhoff-Heart Center, Bad Nauheim, Germany,*** [2]***Leipzig Heart Center, Leipzig, Germany,*** [3]***Frankfurt-University, Dep. Cardiology, Frankfurt, Germany.***

Introduction: The Reinfusion of Enriched Progenitor Cells And Infarct Remodeling in Acute Myocardial Infarction trial (REPAIR-AMI) has established a beneficial effect of intracoronary infusion of bone marrow-derived progenitor cells (BMC) on left ventricular function, assessed by quantitative left ventricular angiography. A prespecified analysis revealed, that especially patients with large infarcts (below the median ejection fraction) derived the most benefit from therapy.

Purpose: The goal of the present substudy is to scrutinize these findings by MRI as the gold standard technique to assess myocardial function, wall motion, and infarct size.

Methods: In this double-blind, randomized, placebo-controlled multicenter trial, patients with successful reperfusion therapy of a STEMI were randomized into intracoronary

infusion of bone marrow-derived progenitor cells or placebo medium. Sixty of the randomized 204 patients participated in the MRI substudy (n = 30 BMC, n = 30 Placebo). LV function, wall motion, and dimensions were quantitated using SSFP-cine sequences and multi-slice volumetry at the index hospitalization and after 4 months. Infarct size and transmurality were measured by using a contrast enhanced inversion recovery TurboFLASH sequence covering the whole ventricle in multiple short axis slices.

Results: Baseline ejection fraction (EF) was similar in the BMC and Placebo group in patients with an EF below the median of 48.9% (BMC = 38.7 ± 8.1%, Placebo = 40.5 ± 8.0%, p = 0.54) and those above the median (BMC = 56.5 ± 4.1%, Placebo = 55.1 ± 6.2 %, p = 0.45). In patients with baseline EF below the median, ejection fraction increased by 5.0 ± 5.7% (p = 0.014), whereas there was no change in ejection fraction in the placebo group (−0.82 ± 7.8 %, p = 0.68). Thus, BMC treatment effect on EF was 5.8 absolute % increase in EF (95% CI 0.5 to 11 %, p = 0.034). In contrast, patients with smaller infarcts (≥ median of baseline EF), derived no benefit from the therapy (treatment effect −0.9%, 95%CI−6.4 to 4.5 %). Likewise, BMC therapy was associated with a significant decline of enddiastolic volumes (treatment effect −29 mL, 95% CI −0.7 to −58 mL, p = 0.045) and endsystolic volumes (treatment effect −28 mL, 95% CI−2.1 to −53 mL, p = 0.035) in patients with baseline EF < median. Wall motion in the infarct area increased in the BMC group (p = 0.019) better than in the placebo group (n.s.) and infarct size decreased more pronounced (BMC group p < 0.012 vs. placebo group p < 0.2).

Conclusions: In patients with a large ST elevation myocardial infarction, intracoronary infusion of bone marrow-derived progenitor cells significantly enhances recovery of left ventricular contractile function and beneficially interferes with left ventricular remodeling processes in the 4 months follow-up. Therefore, MRI findings confirm that bone marrow-derived progenitor cell therapy holds great promise to limit post infarction heart failure.

525. STANDARDIZED T2* MAP OF NORMAL HUMAN HEART IN VIVO TO CORRECT T2* SEGMENTAL ARTEFACTS: A MULTISLICE, MULTIECHO T2* MRI APPROACH FOR CARDIAC IRON OVERLOADED PATIENTS

Alessia Pepe,[1] Vincenzo Positano,[1] Maria Filomena Santarelli,[1] Barbara Scattini,[1] Anna Ramazzotti,[1] Eliana Cracolici,[2] Daniele De Marchi,[1] Petra Keilberg,[1] Massimo Midiri,[2] Luigi Landini,[1] Massimo Lombardi.[1] ***[1]MRI Laboratory, Institute of Clinical Physiology-CNR, Pisa, Italy, [2]Department of Radiology, University of Palermo, Palermo, Italy.***

Introduction: A segmental, multislice, multiecho T2* MRI approach could be useful in cardiac iron overloaded patients in order to account for heterogeneous iron distribution, demonstrated by histological studies. However, segmental T2* assessment in heart could be affected by the presence of geometric and susceptibility artifacts, that may act on different segments in different way.

Purpose: Aim of our study was to assess the T2* value distribution in the left ventricle (LV) and to develop and verify a correction procedure to compensate the artefactual variations in segmental analysis.

Methods: MRI was performed in 4 groups of 22 subjects each: healthy subjects (I), controls (II) (thalassemia intermedia patients without iron overload), thalassemia major patients with mild (III) and heavy (IV) iron overload. Three short axis views (basal, medium, and apical) of the LV were obtained and analyzed using a custom-written. The myocardium was automatically segmented into a 16-segments standardized heart model, and T2* mean value on each segment was calculated. Punctual distribution of T2* over the myocardium was assessed and T2* inhomogeneity maps for the 16 segments were obtained. Using the mean segmental deviations as correction factors, an artefacts correction map was developed. The map was used to normalize segmental data respect to the mid-ventricular septum, that is the standard location for T2* measurements in heart, assuming the artefacts minimal in this region.

Results: In group I, no significant variation of the mean T2* among slices was found. T2* shows a characteristic circumferential variation among the segments. Only 9 segment couples were detected as significantly different by Scheffè post hoc grouping analysis. The effect of susceptibility differences induced by cardiac veins was evident, together with low-scale variations induced by geometrical artefacts. The correction procedure was validated on the group I and II. The T2* segmental correction map was able to compensate middle and low resolution variations in T2*, correcting for cardiac/visceral geometric and susceptibility artefacts The group IV showed no significant presence of segmental artefacts, confirming the hypothesis that susceptibility artefacts are additive in nature and become neglectable for high levels of iron overload. Group III showed a greater variability respect to normal subjects. The correction map failed to compensate these variations if both additive and percentage-based correction were applied.

Conclusions: We produced a standardized, 3D 16-segments map of the circumferential distribution of T2* value artefactual variations in normal subjects. The developed T2* correction map can be exploited to correct segmental measurements in patients with different levels of myocardial iron burden. In mild iron overloaded patients, the correction map failed to compensate segmental variations reinforcing the hypothesis of the true heterogeneity in cardiac iron deposition. Thus, using an optimized MRI acquisition technique joined with an appropriate post processing analysis, the segmental approach is robust and can be effectively used to extend the T2* assessment to the entire heart.

526. SIMULTANEOUS QUANTIFICATION OF MYOCARDIAL DEFORMATION AND T1-RELAXATION USING TAGGING DATA

Andrea K. Rutz,[1] Sebastian Kozerke,[1] Sven Plein,[1] Jürg Schwitter,[2] Salome Ryf,[1] Roger Luechinger,[1] Peter Boesiger.[1] [1]***University and ETH, Zurich, Switzerland,*** [2]***Division of Cardiology, University Hospital, Zurich, Switzerland.***

Introduction: Myocardial scar detection plays an important role in the clinical diagnosis of various heart diseases. Quantitative T_1-maps acquired late after contrast agent injection can be used to identify regions with myocardial scar. Additionally, quantification of cardiac deformation using CSPAMM (1) or N-SPAMM (2) tagging can give valuable insight in the resulting functional changes of the heart. A new method is introduced that allows obtaining T_1-maps of the myocardium as well as deformation parameters in a single scan. The approach exploits the inherent properties of the tagging preparation sequence which partly inverts/saturates the magnetization prior to the acquisition.

Methods: The signal intensity I_{Tk} for the kth ($k = 1 \ldots n$) heart-phase image of a CSPAMM acquisition can be described as (1):

$$I_{\mathrm{Tk}}\alpha \exp(-t_k/T_1^*)\ \Pi_{j-1}^{k-1}\cos(a_j)\sin(a_k), \qquad [1]$$

with t_k: time after tagging preparation and $a_1 \ldots a_k$: variable flip angles. By using an optimized flip angle train, a constant tagging signal throughout the cardiac cycle can be obtained for a tissue with known T_1 (1, 3). However, for tissues with a different T_1 value, a change in signal amplitude is still observed over the cardiac cycle (Fig. 1).

After dividing I_{Tk} by

$$\Pi_{j-1}^{k-1}\cos(a_j)\sin(a_k), \qquad [2]$$

the T_1*-value of any imaged tissue can be calculated using a two-parameter fit according to: $I = A\exp(-t_k/T_1^*)$. In order to use signal intensities from the same (moving) tissue points, HARP-tracking (4) needs to be applied prior to T_1*-calculation.

To obtain sufficient spatial resolution of the T_1-maps, a TFEPI-sequence as described in (5) was used and phase-cycling of the first tagging RF-pulse ('3-SPAMM', (2)) was applied to separate the harmonic peaks. Furthermore, RF phase cycling was implemented in the acquisition to suppress coherent transversal signal across heart phases. Slice-following tagging images with a tag-line distance of 8mm were acquired in two navigator controlled breath-holds on a 1.5 T Scanner (Philips Medical Systems, Best, The Netherlands): FOV: 320 × 272 mm^2, matrix: 160 × 84 (recon. 512 × 512), EPI-factor:7, turbo-factor:14, flip angle train adjusted for T_1= 870 ms, flip angle for last heart phase: 20°, 20 cardiac phases, temporal resolution: 28 ms, total scan time: 28 s.

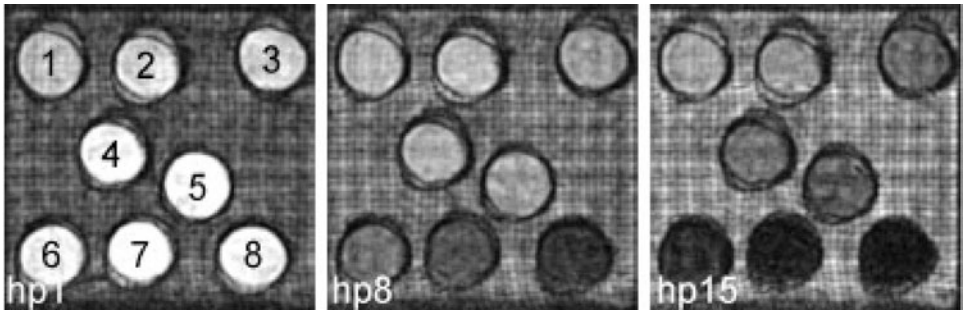

FIG. 1. Three SPAMM magnitude images for different heart phases (phantom).

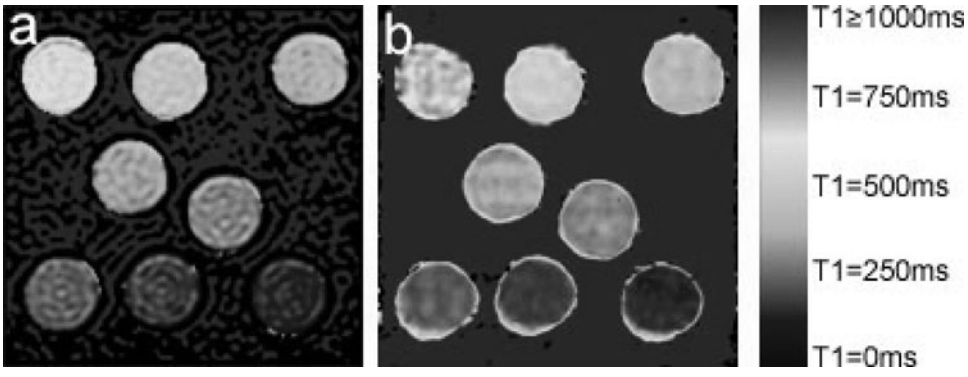

FIG. 2. T_1* maps obtained from the saturation recovery sequence (a) and the tagging sequence (b).

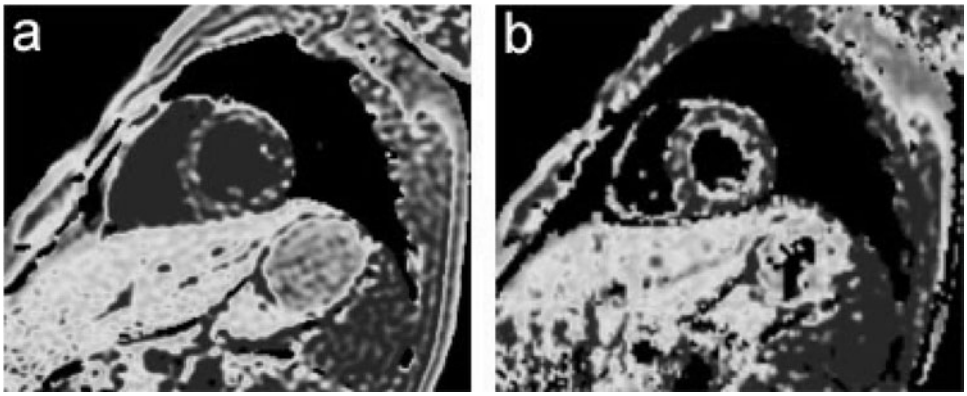

FIG. 3. In vivo T_1*-maps calculated from the data of the saturation recovery sequence (a) and the tagging sequence (b) with the same color coding as in the phantom.

Both phantom data and in vivo images from a healthy volunteer were acquired. The obtained T_1*-values were compared with the results from a Mix-sequence (interleaved spin-echo and inversion recovery) as the reference and the results from a modified SSFP saturation recovery sequence (6). The saturation recovery data were measured in one breath-hold and an additional non-saturated image was acquired to get an estimation of M_0 for the following two-parameter fit: $I = M_0(1-\exp[-\{T_S+dt\}/T_1^*])$ with T_S denoting the time interval between saturation and acquisition and dt taking into account non-idealities of the B_1-field.

Results: By applying RF phase cycling during tagging acquisition the underestimation of T1-values could be reduced ($T_1^* =$ 693 ms with RF phase cycling for phantom 1 vs. $T_1^* = 517$ ms without). The obtained T_1*-values from the phantom and the in vivo measurements are summarized in Table 1 and 2. The corresponding T_1* maps are shown in Figs. 2 and 3.

Conclusion: T_1* values obtained from the phantom measurements showed good agreement with the reference values. An underestimation of T_1 values was already reported in (6) for the saturation recovery sequence and could also be observed to a lesser extent for the tagging data. Initial in vivo results showed the feasibility of the proposed method. However, further studies will be necessary to reduce artifacts and to further improve spatial resolution.

TABLE 1
Measured T_1*-values (phantom)

	T1* [ms]		
Phantom	Ref. scan	Sat. recovery	Tagging
1	736	605	693
2	558	473	520
3	447	396	411
4	394	357	354
5	335	301	306
6	256	243	234
7	197	185	181
8	160	151	152

TABLE 2
Measured T_1*-values (in vivo)

	T1* [ms]		
Tissue	Literature	Sat. Recovery	Tagging
Myocardium	870	866	910
Liver	500	557	580
Fat	250	268	313
Muscle	870	848	942

REFERENCES

1. Fischer SE, et al. MRM 1993;30:191–200.
2. Tsao J, et al. Proc. ISMRM 2005;273.
3. Stuber M, et al. MRM 1999;9:85–91.
4. Osman N, et al. MRM 1999;42:1048–1060.
5. Ryf S, et al. JCMR 2005;7:693–703.
6. Stehning C, et al. Proc. ISMRM 2006;922.

527. WIRELESS, SELF-GATED MULTISLICE CINE MR OF MOUSE HEARTS *In Vivo*

Cees J. A. Van Echteld, PhD,[1] Bernard C. M. Te Boekhorst, MD,[2] Marcel G. J. Nederhoff, MSc,[2] Kees W. A. Van de Kolk, MSc,[1],Arno Nauerth, MSc.[3] [1]***University Medical Center Utrecht, Utrecht, The Netherlands,*** [2]***Interuniversity Cardiology Institute of the Netherlands, Utrecht, The Netherlands,*** [3]***Bruker Biospin MRI GmbH, Ettlingen, Germany.***

Introduction: In conventional cardiac cine MRI, ECG and respiratory gating is required. In animal cardiac MRI, the quality of the ECG signal is variable and sometimes deteriorates over time, in particular with mice with myocardial infarction or cardiac hypertrophy. Sometimes ECG gated cardiac MRI is not possible at

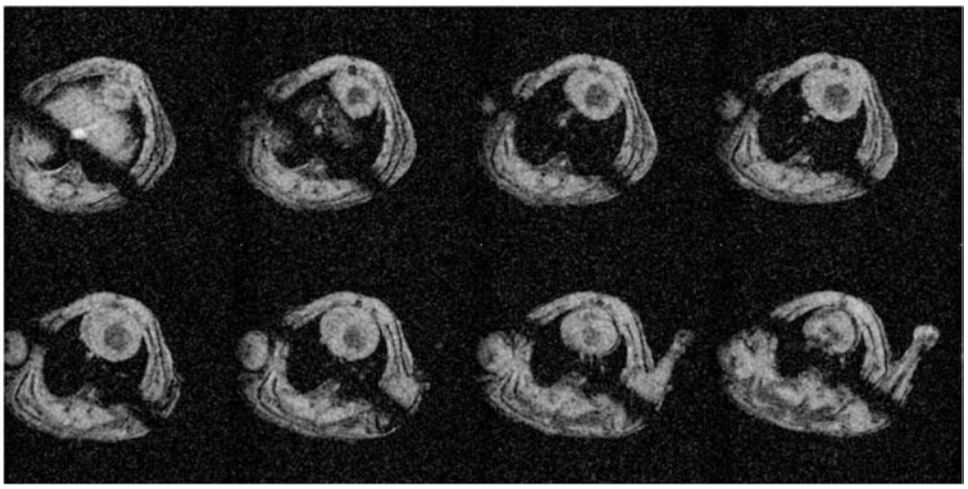

FIG. 1.

all due to severe cardiac conduction disturbances. Also, breath holding is quite common in clinical cardiovascular MR, but yields little time in mouse cardiac MRI and requires intubation. Therefore, we have explored a newly developed navigator-based retrospective gating technique, using a gradient echo sequence with very high temporal resolution on adult control mice and mice with large myocardial infarctions.

Methods: Myocardial infarction was induced in mice by proximal ligation of the left coronary artery. After 4 weeks mice were fitted with ECG electrodes and a respiratory sensor and positioned inside a 30 mm birdcage coil. Conventional ECG and respiratory gated (Rapid) cine CMR images were obtained on a vertical 9.4 T, Avance 400 DRX MR system (Bruker BioSpin) using a flow compensated gradient echo method with TE 1.9 ms, TR 9.8 ms, pulse angle 18°, matrix size 256 × 256, FOV 30 mm, slice thickness 1 mm. The number of frames in the cardiac cycle usually varied between 12 and 14, depending on the heart rate. Self-gated, navigator based cine MR images were obtained using a gradient echo method with TE 1.8 ms, TR 3.0 ms, pulse angle 10°, matrix size 128 × 128, FOV 30 mm, slice thickness 1 mm and for multi slice acquisition a 25° navigator/saturation pulse with a slice thickness of 2 mm. The number of frames in the cardiac cycle was chosen upon reconstruction to be 10 or 20.

Results: Fig. 1 shows self-gated short axis cine MR images from a multi-slice experiment (8 slices, 10 reconstructed frames), which were obtained in a total time of 2 min. The diagonal black stripes correspond with the navigator/saturation plane, which was positioned in such a way that both optimal motional information and optimal contrast between blood and myocardium were obtained. Cardiac function of healthy control mice derived from self-gated cine MRI was similar to cardiac function derived self-gated MRI, yielding an left ventricular ejection fraction (EF) of 57.2 ± 2.6 % (SEM, n = 8). From a mouse with a large myocardial infarction no ECG and respiratory gated cine MRI images could be obtained whatsoever, since the ECG was highly irregular and showed multiple R-waves. However, very satisfactory self-gated short-axis cine MRI images could be obtained, which yielded an EF of 18.4 %, which was comparable to the ejection fraction of mice with large infarcts, that could be analyzed with conventional ECG and respiratory gated MR.

Conclusions: Self-gated, wireless cine MRI allows accurate analysis of mouse heart function when ECG and respiratory gated cine MRI fails.

Self-gated, wireless cine MRI allows a higher throughput, since instrumentation with ECG electrodes is unnecessary.

Although perhaps not immediately obvious from the images, the self-gated method shows less flow artifacts.

528. INCREASED TEMPORAL RESOLUTION FLOW IMAGING BY INTERLEAVED REFERENCING

Mark Doyle, PhD,[1] Geetha Rayarao,[1] Eduardo Kortright, PhD,[2] Andreas Anayiotos, PhD.[3] Longchuan Li, PhD,[3] Diane A. Vido,[1] Kethes Caruppannan, MD,[1] Vikas K. Rathi, MD,[1] Robert W. W. Biederman, MD.[1] [1]***Allegheny General Hospital, Pittsburgh, PA, USA,*** [2]***University of New Orleans, New Orleans, LA, USA,*** [3]***University of Alabama at Birmingham, Birmingham, AL, USA.***

Introduction: In highly accelerated jet flow, accuracy of quantitative velocity measurements suffers as data segmentation factors increase. However, sufficiently low segmentation factors lead to excessively long scan times. We note that the phase compensated data used to correct phase distortions in the velocity encoded data exhibit a known relationship to the velocity-encoded data. This additional information can be used to increase the temporal rate and improve fidelity of velocity data without increasing the scan time.

Hypothesis: We hypothesize that phase compensated data acquired in a temporally sparse manner can be used to correct the more rapidly acquired velocity encoded data when an appropriate correction factor is applied.

Methods: Jet flow data were generated in a cylindrical phantom (10 cm diameter) using blood mimicking fluid (60% glycerin, 40% water) passing through a circular orifice (1 cm diameter) with a reproducible cyclic waveform (Shelly, Vancouver, Canada). A gradient echo phase velocity scan was used (TR/TE/Flip 7.7/2.5/20°) to acquire a reference data set without segmentation and with flow compensated and flow encoded data sets acquired in separate cycles to realize the highest possible temporal rate (7 ms per data set). These data were used to simulate conventional segmented scans with segmentation values of 2 and 4. Additionally, simulations were run in which the velocity compensated data were acquired sparsely while the velocity encoded data were acquired rapidly in the ratio of 5:1. The sparsely sampled velocity compensated reference data sets were used to phase correct the nearest velocity compensated data to produce an intermediate data set of apparent velocities. The apparent velocities do not in general represent the true velocity; the exception being where the velocity compensated and velocity encoded data sets were adjacent to each other. The true velocity was generated by applying a correction algorithm dependent on the ratio of first moments of the velocity compensated and velocity encoded gradients: corrected velocity = (apparent velocity × 3 + reference velocity)/4. In this case the ratio of first moments was 3:1.

Conventional (CON) and interleaved referencing (INT) scans were simulated for segmentation factors of 2 and 4. The velocity time curves were compared to the reference (REF) scan from two corresponding regions of the flow field: 1) high acceleration during onset of jet flow and 2) low acceleration in the post jet flow.

Results: Using the reference scan, maximal jet velocity was 2.08 m/s. Correlation r values showed that during high acceleration (maximum acceleration 105 m/s/s) the CON scans consistently underrepresented the slope of the velocity-time curve compared to the INT scans: segmentation factor 2 ($r = 0.84 \pm 0.12$ vs 0.93 ± 0.08, $p < 0.01$) and segmentation factor 4 ($r = 0.87 \pm 0.05$ vs 0.94 ± 0.05, $p < 0.001$). However, the low acceleration decaying flow (average deceleration 9.3 ± 23 m/s/s) was equally well represented by the CON and INT scans for segmentation factor 2 (0.97 ± 0.04 vs 0.96 ± 0.04, $p = 0.06$) and 4 (0.96 ± 0.03 vs 0.97 ± 0.04, $p = 0.8$). Fig. 1 shows the tendency for the CON scan to lag the rapid onset of jet flow for segmentation factor 2, while the INT scan more accurately follows the rapid jet onset.

Conclusion: Increasing the temporal rate of quantitative velocity data can be achieved by interleaving sparsely sampled phase compensated data with more rapidly acquired velocity encoded data. A correction algorithm was successfully applied to extract the accurate velocity data at each time point. The higher data rate allowed improved fidelity in following the rapid onset of highly accelerated jet flow without increasing scan time.

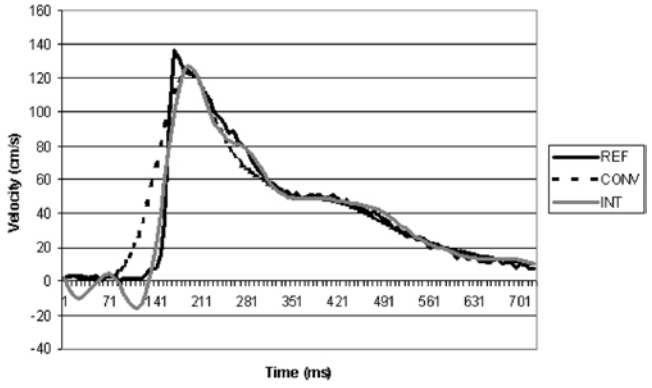

FIG. 1. Velocity time curves for reference data (REF), conventional segmented data (CONV) with segmentation factor 2, and data with interleaved referencing (INT) also using segmentation factor 2.

529. VALIDATION OF FREE SOFTWARE FOR AUTOMATED VESSEL DELINEATION AND MRI FLOW ANALYSIS

Einar Heiberg, PhD,[1] Karin Markenroth, PhD,[2] Håkan Arheden, MD, PhD.[1] [1]***Department of Clincial Physiology, Lund, Sweden,*** [2]***Philips Medical Systems, Lund, Sweden.***

Background: We have developed a software package for cardiac image analysis that is freely available for non commercial research purposes (http://segment.heiberg.se). The purpose of this study was to validate the flow quantification tools in this software.

Methods: Flow measurements were performed both *in vitro* and *in vivo*. Flow was measured using a non segmented gradient echo pulse sequence on a 1.5 T Philips Intera CV system (Philips, Best, The Netherlands). Maxwell and eddy current compensation were performed by the MRI scanner. *In vitro* measurements were performed using gravity driven flow at 5 different flow

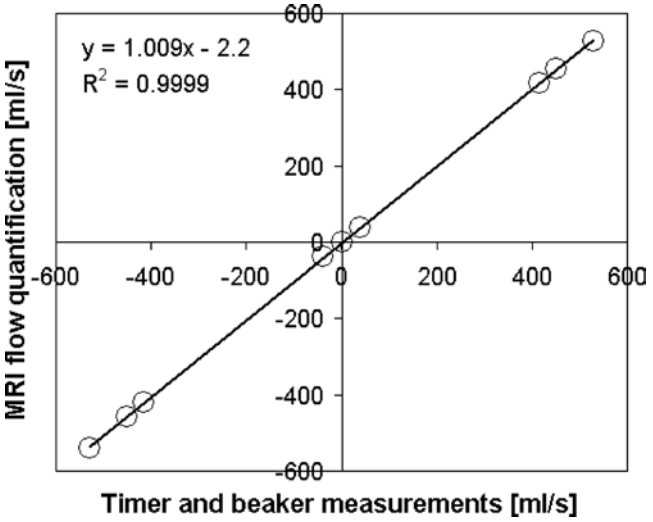

FIG. 1. Correlation plot between time and beaker flow measurements versus velocity encoded MR flow quantification.

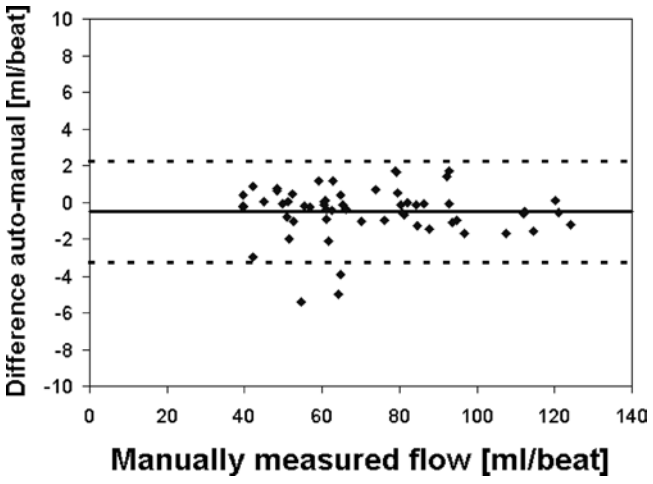

FIG. 2. Difference in total net flow comparing automated and manual vessel delineation. Bias ± 2SD is indicated in the plot.

rates through a silicon gel with two holes with a diameter of 26 mm. Flow rate was measured by timer and beaker method.

For the *in vivo* experiments, one experienced observer outlined ascending and descending aorta in 12 patients and 20 patients from the clinical routine. In total 64 vessel region of interests were analyzed both manually and using automated vessel delineation. In the automated vessel delineation the manually outlined vessel contour from the first time frame were taken as input to the algorithm. The algorithm first tracks the vessel throughout the heart cycle using an optical flow based method. Thereafter, a deformable model approach is used to refine the vessel contour. Total net flow through the vessel were measured for the automatically delineated vessels and were compared to the manual vessel delineation.

Results: MRI flow measurements corresponded well with timer and beaker measurements (Fig. 1). In 4 of the 64 vessels (6%) the automated vessel tracking failed due to poor image contrast and imaging artifacts, and resulted in a difference larger than 10 mL and large overestimation in vessel area. These vessels were excluded from further analysis. Bias and variability between total net flow for the manual vessel delineation and automated vessel delineation were -0.50 ± 1.4 mL/beat. Fig. 2 shows a difference plot between manual delineation and automated delineation.

Conclusion: The suggested method for automated vessel quantification have a low bias and variability.

530. RIGHT ATRIAL VOLUME AND EJECTION FRACTION ASSESSMENT IN HEALTHY SUBJECTS AND PATIENTS WITH RIGHT HEART FAILURE: INTERSTUDY VARIABILITY USING THE STANDARD SHORT AXIS METHOD

Burkhard Sievers, MD,[1] Marvin Addo,[2] Frank Breuckmann, MD,[1] Raimund Erbel, MD.[1] [1]***West German Heart Center, University Hospital Essen, Essen, Germany,*** [2]***Department of Cardiology, University Hospital Cologne, Cologne, Germany.***

Background: There is growing agreement that measurements of atrial volumes and ejection fraction (EF) are superior to diameters for both accurate determination of the atrial size and follow up studies. Right atrial volume and EF and their changes might have a prognostic impact in patients with right heart failure and may provide reliable data for follow up studies. We, therefore, sought to evaluate the interstudy variability of right atrial volumes and EF in healthy subjects and patients.

Methods: Right atrial volumes (maximum and minimum) and EF were measured in 10 healthy subjects and 10 patients with right heart failure using the standard short axis method. Images were acquired with a steady state free precession gradient-echo sequence on a clinical 1.5 Tesla magnetic resonance scanner (Siemens, Erlangen, Germany). Volumes were determined by the sum the outlined areas. The EF was calculated as follows: EF = (EDV−ESV)/EDV × 100. All patients were examined twice (scan 1 and 2). Both scans were performed at the same day.

Results: Maximum volumes, minimum volumes and EF for healthy subjects were 95.4 ± 19.9 mL, 47.9 ± 8.9 mL, 49.0 ± 8.1% in scan 1 and 95.8 ± 17.5 mL, 49.5 ± 11.2 mL, 48.1 ± 8.8% in scan 2 ($p \geq 0.285$). Volumes and EF for patients in scan 1 and 2 were 145.2 ± 28.2 mL, 106.9 ± 25.9 mL, 26.5 ± 9.7% and 146.3 ± 26.3 mL, 109.9 ± 23.9 mL, 24.9 ± 9.8%, respectively ($p \geq 0.139$). The interstudy variability was −0.3 ± 7.9 mL, -1.6 ± 4.9 mL and 0.9 ± 3.5% for healthy subjects (Fig. 1A) and −1.1 ± 6.8 mL, −3.0 ± 5.2 mL and 1.7 ± 2.7% for patients, respectively (Fig. 1B).

Conclusions: The standard short axis method provides good reproduciblility for right atrial volume and EF measurements. The assessment of right atrial volumes and EF may be useful to identify and follow up patients with various kinds of right heart disease.

531. A STUDY OF STRUCTURAL AND FUNCTIONAL HEART CHARACTERISTICS IN MALE TRIATHLETES COMPARED TO NORMALS

Mathilda Eliasson, Ms, BM,[1] Henrik Mosén, MD, PhD,[1] Marcus Carlsson, MD,[1] Torsten Buhre, MD, PhD,[2] Hakan Arheden, MD, PhD.[1] [1]***Department of Clinical Physiology, LUND, Sweden,*** [2]***Department of Sports Sciences, Malmoe, Sweden.***

Introduction: Only a few cardiovascular magnetic resonance (CMR) studies have focused on the endurance trained elite athlete's heart. Earlier studies have often used echocardiography as imaging technique, but modern CMR is in many respects a more accurate method yielding more precise data.

Purpose: The overall aim of this study was, therefore, to compare the athlete's heart with the normally trained heart, regarding structural and functional parameters measured with CMR. Some of these parameters have not been studied before, namely total heart volume (THV) and total heart volume variation (THVV) over the cardiac cycle.

Methods: Thirteen male Swedish elite triathletes, age 33.3 ± 5.7, underwent a maximal spiroergometer exercise test with gas analysis to assess their physical working fitness. To retrieve their heart parameters they were examined with steady state free precision (SSFP) and velocity-encoded CMR-sequences. The study consisted of four sub studies with the common objective to try to disclose if there were any differences in heart physiology between the athletes and the general population. Cardiac index (CI), ejection fraction (EF), left ventricular mass (LVM), left ventricular volumes (end diastolic volume [EDV] and end systolic volume [ESV]), THV and THVV were studied.

Results: CI was found to be slightly, but not significantly ($p = 0.10$), elevated in the athletes compared to controls. LVM, EDV and ESV were higher than available reference data, whereas EF was unchanged. The athletes had a significantly ($p < 0.001$) larger THV but did not differ in THVV from the control group.

Conclusions: We found the athlete's heart to be larger in size compared to the normal heart, both regarding the left ventricle and the whole heart, but with maintained normal physiological functions. All structural parameters were larger in the athletes compared to normals and all functional parameters remained the same as in normals. This led us to conclude that the endurance trained athlete's heart is a larger heart maintaining a well balanced working physiology as a result of the higher demand on the heart as a pump.

532. IS THE AREA-LENGTH METHOD ACCURATE ENOUGH FOR RIGHT ATRIAL VOLUME AND EJECTION FRACTION ASSESSMENT?

Burkhard Sievers, MD,[1] Marvin Addo,[2] Frank Breuckmann, MD,[1] Raimund Erbel, MD.[1] [1]***West German Heart Center, University Hospital Essen, Essen, Germany,*** [2]***Department of Cardiology, University Hospital Cologne, Cologne, Germany.***

Background: The standard short axis method for volume and ejection fraction (EF) assessment is still time consuming, and automated contour detection programs that can reliably measure atrial volumes and EF are currently commercially not available. The area-length method approach requires less analysis time and thus, may be more applicable in clinical practice. The accuracy of the area-length method for right atrial volume and EF assessment has not been studied.

Methods: We compared right atrial volumes (maximum and minimum) and EF calculated by the area-length method to those determined by the standard short axis method in healthy subjects ($n = 74$) and patients with right heart failure ($n = 24$) using a steady state free precession gradient-echo sequence and a clinical 1.5 Tesla magnetic resonance scanner (Siemens, Erlangen, Germany). Right atrial area and length was measured from the horizontal long axis view. Minimum and maximum volumes were calculated as follows: $(\text{Length}^2/\text{Area}) \times 0.85$, EF (%) = (Maximum volume-Minimum volume)/Maximum volume × 100.

Results: Maximum volumes, minimum volumes and EF for healthy subjects using the area-length method and standard short axis method were 102.3 ± 32.4 mL, 50.2 ± 20.2 mL, 51.7 ±

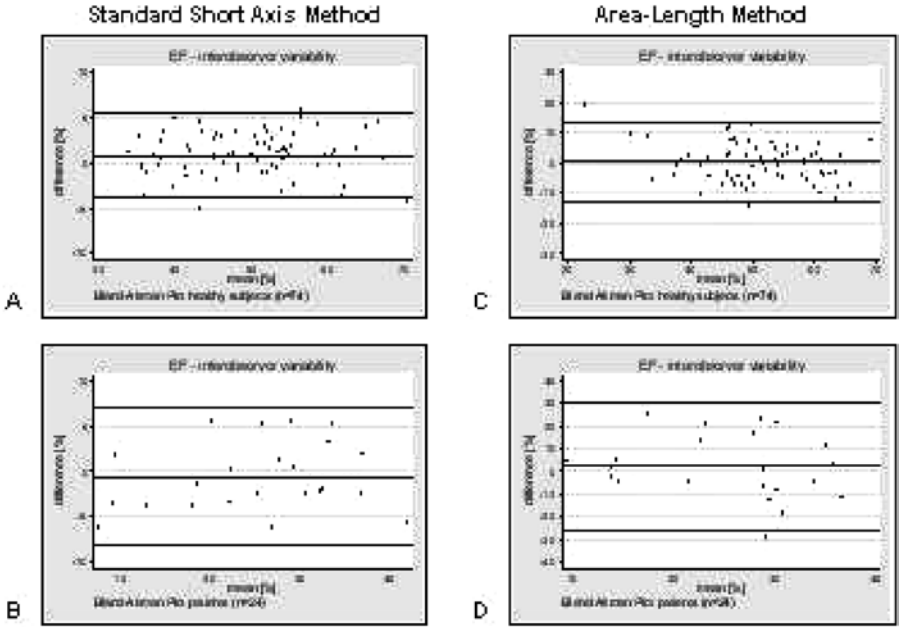

FIG. 1.

9.1% and 106.3 ± 31.9 mL, 53.2 ± 20.2 mL, 50.5 ± 8.9%, respectively ($p \leq 0.0001$ for all comparisons). Volumes and EF for patients were 148.3 ± 42.6 mL, 111.2 ± 39.8 mL, 26.1 ± 10.3% and 152.7 ± 44.1 mL, 116.0 ± 39.3 mL, 24.7 ± 10.0%, respectively ($p \leq 0.014$ for all comparisons). Interobserver variability was smaller for the standard method (Fig. 1 A, B) compared to the area-length method (Fig. 1 C, D) in both healthy subjects and patients (difference −2.6 ± 8.9 mL, −2.2 ± 6.2 mL, 0.9 ± 2.3% and −0.5 ± 16.3 mL, −0.6 ± 8.7 mL, 0.4 ± 6.6%, respectively, and 0.5 ± 8.3 mL, 1.4 ± 7.7 mL, −0.6 ± 3.8% and −2.9 ± 17.0 mL, −1.7 ± 16.2 mL, 2.1 ± 13.9%, respectively). The analysis time was 60 ± 20 s for the area-length method and 6 ± 2 min for the standard method.

Conclusions: Volumes and EF calculated by the area-length method are significantly different from those measured by the standard method. Different reference values and a higher interobserver variability compared to the standard method should be taken into account when using the area-length method for right atrial volume and EF measurements.

533. HYPERTROPHIC CARDIOMYOPATHY MUTATION CARRIERS EXHIBIT REGIONAL DIFFERENCES IN SYSTOLIC BUT NOT DIASTOLIC FUNCTION IN A VERY EARLY STAGE OF DISEASE

Tjeerd Germans, MD,[1] Jaco J. M. Zwanenburg, PhD,[1] Robin Nijveldt, MD,[1] Aernout M. Beek, MD,[1] Marco J. W. Goette, MD, PhD,[1] Arthur A. M. Wilde, MD, PhD,[2] Yigal M. Pinto, MD, PhD,[3] Pieter A. Doevendans, MD, PhD,[4] J Tim Marcus, PhD,[1] Albert C. van Rossum, MD, PhD.[1] [1] ***VU University Medical Center, Amsterdam, The Netherlands,*** [2] ***Academic Medical Center, Amsterdam, The Netherlands,*** [3] ***University Hospital, Maastricht, The Netherlands,*** [4] ***University Medical Center Utrecht, Utrecht, The Netherlands.***

Introduction: Hypertrophic cardiomyopathy (HCM) is caused by mutations in genes encoding for sarcomeric proteins and is characterized by left ventricular (LV) hypertrophy in the absence of increased external load. The hypertrophy mainly involves the septum. Several studies suggest that the mutations result in functional impairment of the myocardium and that the characteristic hypertrophy is merely compensatory for this loss of function. We hypothesized that regional functional differences exist between septal and lateral segments of myocardium in HCM mutation carriers (carriers), before frank hypertrophy has developed.

Purpose: Cardiac magnetic resonance imaging was used to evaluate if regional functional differences between the septum and lateral segments can be discerned in carriers without LV hypertrophy.

Methods: We selected 20 asymptomatic carriers who either had a 2373insG mutation in the gene encoding for cardiac myosin binding protein C (13 patients; 5 male) or a Glu62Gln mutation in the gene encoding for α-tropomyosin (7 patients; 4 male). The carriers did not have LV hypertrophy (wall thickness <12 mm on echocardiography) in the year prior to inclusion of the study. Also, we selected 20 age and gender matched healthy volunteers.

To evaluate regional wall thickness and thickening, global LV ejection fraction, volumes and mass, we acquired a stack of short-axis cines, that fully covered the LV, using a retro-triggered, balanced, steady state free precession sequence in all subjects. Additionally, we performed retro-triggered, high temporal resolution myocardial tissue tagging on basal, mid and apical short axis slices which were equally distributed over the end-systolic (Es) length of the LV on a 4-chamber cine. A 3-chamber cine was used as second localizer to exclude the LV outflow tract from the basal slice. The basal and mid slice were equally divided into 6 segments, and the apical slice was divided into 4 segments. Strain analysis was performed with in-house developed software and the following parameters were determined: peak systolic circumferential strain (Eccmax) and peak circumferential early diastolic lengthening rate (peak CEDLR).

Results: Four carriers were excluded from analysis (1 had developed hypertrophy, 1 had atrial fibrillation, and 2 tagging datasets were not analyzable). Tagging datasets of 2 healthy volunteers were also not analyzable. LV ejection fraction, mean LV end-diastolic (ED) and end-diastolic (ES) volumes and mass were comparable between the carriers and healthy volunteers. In healthy volunteers, wall thickness of all segments were comparable (5.4 ± 1.3 mm). In the carriers, the basal ánd mid inferoseptal segments were thicker than the remaining segments within the same slice (7.7 ± 1.5 mm versus 5.9 ± 1.1 mm, $p < 0.0001$, and 6.6 ± 1.5 mm versus 5.1 ± 0.8 mm, $p < 0.0001$ respectively). There were no differences in wall thickness of apical segments in carriers.

In healthy volunteers, wall thickening was lower in the basal inferoseptal segments compared to lateral segments (74.8 ± 26.4% versus 95.3 ± 21.1%, $p < 0.01$). However, in carriers, the difference in wall thickening between the basal inferoseptal segment and remaining segments in that slice was more profound (45.0 ± 10.8%, versus 96.9 ± 22.8% $p < 0.001$).

In healthy volunteers, Eccmax was smaller in the septum compared to the lateral segments in all slices (−15.5 ± 3.0% versus 19.8 ± 3.3%, $p < 0.05$). There were no differences in Eccmax between septal and lateral segments in carriers (−16.9 ± 3.6% versus 17.8 ± 2.4%). Although peak CEDLR was overall higher in healthy volunteers than carriers (114.7 ± 32.3 $\%\cdot s^{-1}$ versus 95.5 ± 26.6 $\%\cdot s^{-1}$, $p < 0.05$), no regional differences of peak CEDLR were observed between septal and lateral segments of carriers.

Conclusions: In carriers, systolic wall thickening of the inferoseptal segments relative to the lateral segments is decreased, whereas peak CEDLR is not. Thus, regional differences in systolic dysfunction but not diastolic dysfunction occur in a very early stage of disease in HCM mutation carriers.

534. NORMAL VALUES FOR RIGHT ATRIAL VOLUMES AND EJECTION FRACTION USING THE STANDARD SHORT AXIS METHOD AND A 1.5 TESLA CLINICAL MRI SCANNER

Burkhard Sievers, MD,[1] Marvin Addo, MD,[2] Frank Breuckmann, MD,[1] Raimund Erbel, MD.[1] [1]***West German Heart Center, University Hospital Essen, Essen, Germany,*** [2]***Department of Cardiology, University Hospital Cologne, Cologne, Germany.***

Background: There is growing consensus that measurements of atrial volumes and ejection fractions (EF) are superior to atrial diameters for both accurate determination of the atrial size and follow up studies. With the attention usually drawn to the left heart, little is known about right atrial volumes and EF. We, therefore, sought to establish normal values for the standard short axis method that may serve as reference values to identify patients with impaired right atrial function.

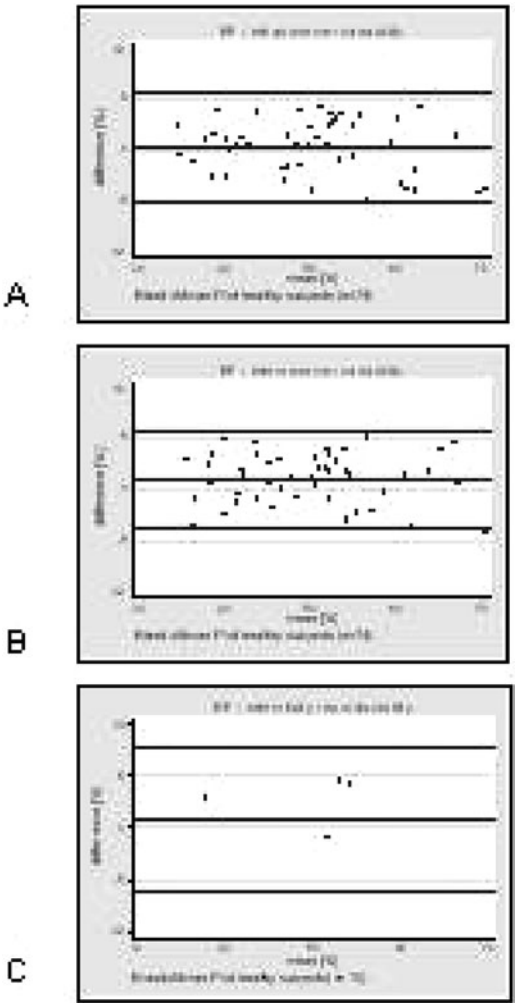

FIG. 1.

Methods: We calculated right atrial volumes (maximum and minimum) and EF with the standard short axis method in healthy subjects (n = 74) using a steady state free precession gradient-echo sequence and a clinical 1.5 Tesla magnetic resonance scanner (Siemens, Erlangen, Germany). Volumes were calculated from the sum of the outlined areas. EF was determined as follows: (EF (%) = (Maximum volume−Minimum volume)/Maximum volume × 100. In addition, intra-, interobserver (n = 74) and interstudy (n = 20) variability was assessed.

Results: Maximum volumes, minimum volumes and EF were 106.3 ± 31.9 mL, 53.2 ± 20.2 mL and $50.5 \pm 8.9\%$, respectively. There were no gender-related differences in volumes and EF (≥ 0.773). Intraobserver varaiblity was -0.6 ± 6.0 mL, -0.6 ± 4.9 mL and $0.2 \pm 2.8\%$ (Fig. 1A), interobserver variability -2.6 ± 8.9 mL, -2.2 ± 6.2 mL and $0.9 \pm 2.3\%$ (Fig. 1B), and interstudy varaiblity 3.6 ± 10.9 mL, 1.7 ± 7.3 mL and $-0.4 \pm 3.5\%$, respectively (Fig. 1C).

Conclusions: We established normal ranges for right atrial volumes and EF in healthy subjects that may be used as reference values in patients with right heart failure such as congential and valvular disease.

535. PIXEL-BASED RESPIRATORY MOTION CORRECTION IN FIRST-PASS MYOCARDIAL PERFUSION IMAGING FOR IMPROVING KEYHOLE RECONSTRUCTION

Henrik Pedersen, MSc, Steffen Ringgaard, PhD, W. Yong Kim, MD. ***Aarhus University Hospital, Aarhus N, Denmark.***

Introduction: Pixel-based analysis of first-pass MRI myocardial perfusion studies has the advantage of using the full underlying spatial resolution of the images, but requires accurate image registration in the presence of respiratory motion to maintain the true spatial resolution. We present an image registration algorithm that operates on a pixel-by-pixel level and does not require any user interaction. This makes it ideal for reducing motion aliasing artifacts in temporally accelerated imaging approaches, such as keyhole, because the entire field-of-view rather than a small region of interest can be corrected. To demonstrate its clinical potential the algorithm is applied to both fully sampled and undersampled keyhole data.

Methods: The main difficulty in automated registration of myocardial perfusion images is to differentiate between signal intensity changes caused by 1) motion and 2) the passage of the contrast agent. We used a well-established image registration method, which is based on optical flow, to determine the translation of each individual pixel in the last 30% of the image frames. In this part of the image series signal intensity changes caused by the contrast agent are insignificant. Thus, the motion can be reliably detected.

Principal component analysis of the estimated motion was used to calculate a motion template, as depicted in Fig. 1A. The motion template consists of a set of motion vectors-one for each pixel-and in general more than 99% of the respiratory motion can be described by a scaled version of this template. Hence, a single parameter or scale factor describes the motion over an entire image frame! In the former 70% percent of the images, where signal intensity changes are caused by both motion and the passage of the contrast agent, the motion template was used to estimate the motion. This was done for each image frame by warping the image according to different scalings of the motion template, until the scale factor bringing the image closest to a chosen reference image was found. The efficiency of the image algorithm is illustrated in figures 1B and 1C, which contain horizontal image time profiles aligned through the left ventricle (yt-profile) before and after image registration. In addition, myocardial signal intensity vs. time curves are shown figure 1.G1 before and after registration.

Keyhole reconstruction with a keyhole size of 25% (e.g. 32 phase encoding lines for a matrix of 128 or an acceleration factor of 4) was performed in the conventional way, where the remaining 75% of the phase encoding lines are replaced by the corresponding lines of a stationary reference image. Fig. 1E and 1H illustrates the result of conventional keyhole reconstruction. In this case, the displacement of the heart between the reconstructed image frame and the reference image is large. Fig. 1F and 1I shows keyhole reconstruction of the same image frame, but where the low-resolution image corresponding to the keyhole data was first registered prior to keyhole reconstruction. In this case, the displacement between the reconstructed image frame and the reference image is small.

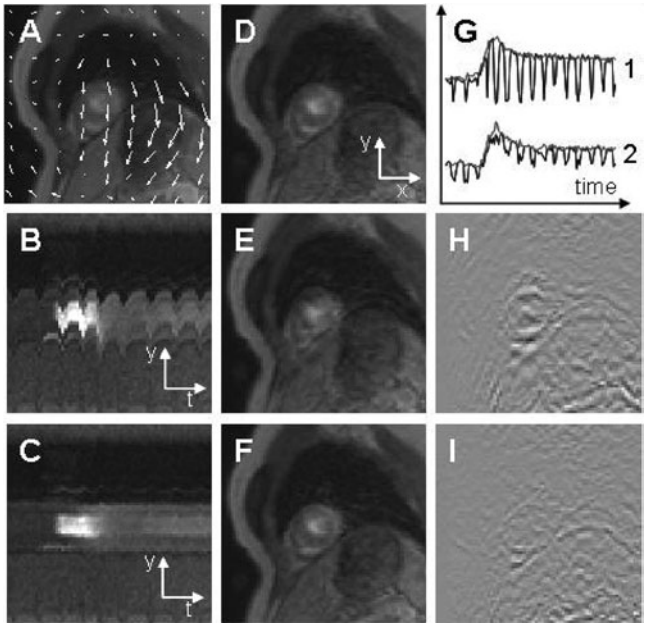

FIG. 1. Motion template (A). yt-profile of original data (B), yt-profile of corrected data (C), frame 60 of original data (D), frame 60 with conventional keyhole recon. (E) and recon error (H), frame 60 with corrected keyhole recon (F) and recon error (I), comparison of myocardial signal vs time curves (G), corrected (−) and non-corrected (−) original data (G1), corrected (−) and non-corrected (−) *keyhole* data (G2).

*Results:*The image registration approach has been successfully applied in a total of 32 myocardial perfusion data sets, including both rest and stress images. Visual analysis has demonstrated that the algorithm is highly robust with only a negligible level of residual in-plane motion. In all cases, keyhole reconstruction with motion registration led to less motion artifacts and good agreement the original fully sampled data (Figure 1).

*Conclusions:*An algorithm has been presented that allows fully automated pixel-based image registration in first-pass myocardial perfusion images. It has been demonstrated that such algorithms can be used to reduce motion artifacts in temporally accelerated keyhole data.

536. MAGNETIC RESONANCE TISSUE VELOCITY MAPPING DEMONSTRATES AN ENDOCARDIAL-EPICARDIAL RADIAL STRAIN RATE GRADIENT

Jana G. Delfino, BS,[1] Brandon Fornwalt, BS,[1] Robert Eisner, PhD,[2] Angel Leon, MD,[2] John N. Oshinski, PhD.[1]
[1]Georgia Institute of Technology/Emory University, Atlanta, GA, USA, [2]Emory University, Atlanta, GA, USA.

Introduction: Strain (ε) and strain rate (SR) imaging are measures of myocardial function that offer the possibility of non-invasively determining regional contractility and distinguishing between actively contracting myocardium and motion caused by passive tethering. Strain is the deformation of an object normalized to its original shape, and strain rate is the rate at which that deformation occurs (1). Strain rate has recently been shown to be an excellent indicator of underlying myocardial contractility (2).

Radial myocardial strain rates are particularly difficult to measure, since deriving strain rate from tagged MRI or ultrasound speckle-tracking involves the computation of two derivatives. Computing strain rate from Magnetic Resonance tissue velocity data is potentially advantageous since the computation is achieved through a single derivate. Furthermore, the high spatial resolution of the underlying velocity data offers the possibility of distinguishing between endocardial and epicardial strain rate values.

Purpose: To determine endocardial and epicardial radial strain rate values in the myocardium of healthy volunteers.

Methods: Experiments were performed on a 1.5T Philips Medical Systems Intera CV MRI scanner using a cardiac coil. A segmented, navigator-echo and ECG-gated sequence was used to acquire three-directional velocities within the myocardium. Velocity directions were interleaved by heartbeat and use of the navigator ensured that all three velocity directions were correctly

registered for post-processing. Velocity was acquired at three slice locations (apex, mid, base) in the myocardium and presaturation slabs were used on each side of the slab to null in-flowing blood. The VENC value was 30 cm/s, temporal resolution was 35 ms, and voxel size was 1.4 × 1.4 × 8 mm. Myocardial tissue velocity maps were acquired in 10 normal volunteers.

The acquired three-directional velocities (x, y, and z) were converted into a myocardial coordinate system (radial, circumferential and longitudinal). Strain rate was calculated directly from the radial velocity data. For each phase in the cardiac cycle, velocity difference along a line running radially through the myocardial wall was plotted vs. radial distance. Strain rate was determined as the slope of the regression line (3). Using all points across the myocardium yielded transmural strain rate. Subdividing the myocardium allows computation of endocardial and epicardial strain rates.

Strain rate values were computed along 48 equally-spaced radial lines in each phase of the cardiac cycle. In basal and mid slices, values were averaged into six segments and in the apical slice values were averaged into four segments to adhere to the AHA 17-segment model of the myocardium.

Peak systolic values were defined as the curve maximum between aortic valve opening and aortic valve closing. P values < 0.05 were considered statistically significant.

Results: Velocity maps were successfully acquired in all volunteers and strain rate curves were successfully computed. A difference was observed in the magnitude of peak systolic strain rate between the endocardium and the epicardium, with endocardial values being larger than epicardial values. This endocardial-epicardial strain rate gradient was observed consistently in all three slices, although the difference was significant only in the basal and mid slices (Fig. 1).

Conclusions: This study demonstrated the feasibility of computing endocardial and epicardial strain rates within the myocardium. Furthermore, the existence of an endocardial-epicardial radial strain rate gradient within the myocardium was demonstrated. The ability to differentiate endocardial and epicardial strain rate values may assist in the detection of subendocarial changes in contractility.

REFERENCES

1. D' Hooge J, et al. Eur J Echocardiogr 2000;154–70.
2. Sutherland GR, et al. J Am Soc Echocardiogr 2004;788–802.
3. Hanekom L, et al. Ultrasound Med Biol 2004;1451–60.

537. CONTRAST ENHANCED MRI FOR CHARACTERIZATION OF CARDIAC MASSES

Vincenzo Russo, MD, Luigi Lovato, MD, Cesare La Palombara, MD, Katia Buttazzi, MD, Valentina Gostoli, MD, Maurizio Montalti, MD, Rossella Fattori, MD. ***University Hospital S.Orsola, Bologna, Italy.***

Introduction: Primary cardiac neoplasms are rare and more commonly benign than malignant. However, the diagnosis of cardiac masses is still a relevant clinical problem. Magnetic resonance imaging (MRI) is an important tool in the evaluation of cardiac tumors. T1-weighted (T1-W) and T2-weighted (T2-W) sequences, used for anatomic definition and tissue characterization, are not always adequate to assess structures with similar relaxation times as cardiac masses. Gadolinium-enhanced (Gd-e) sequences and MR malignancy indicators (right side or pericardial involvement, tissue inhomogeneity, diameter greater than 5 cm and invasive behavior) are particularly useful to distinguish between benign and malignant neoplasm and to identify specific tumors. Cine gradient-echo imaging is used to assess functional effects.

Purpose: Our purpose was to analyze retrospectively MRI examinations of patients with suspected cardiac masses in the attempt to identify the usefulness of Gd-e sequences for the diagnostic value of MRI.

Methods: Forty-three patients (20 M and 23 F, mean age 41.3 Y, range 9–80) underwent cardiac MRI (1.5T Signa

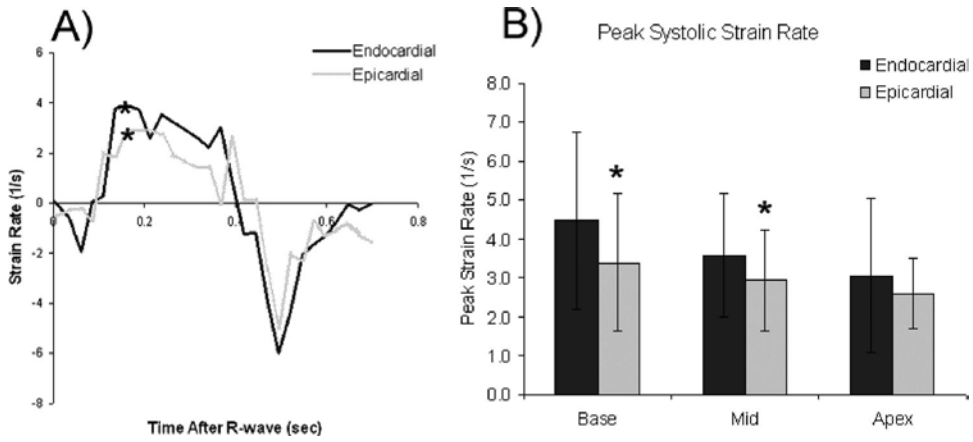

FIG. 1. A) Example endocardial and epicardial strain rate curves. Peak systolic values are denoted by *. B) Average systolic strain rate values by slice. *denotes p <</le > 0.05

Horizon, GE Medical Systems, Milwaukee, WI, USA) due to a suspected cardiac mass, from January 2003 to July 2006. For the basic scan protocol T1-W, T2-W and T1-W fat sat sequences were employed, as well as Gd-e sequences such as first pass (fast gradient echo-echo train imaging), T1-W post Gadolinium and delayed enhancement (inversion-recovery segmented fast gradient echo). Functional sequences (cine gradient echo) have been also performed.

Results: In most of the cases (36/43, 83.7%) information obtained from Gd-e sequences were essential for distinction between neoplasms (34) and thrombi (7) and, among tumors, from benign (26) to malignant (8) types. All of 7 thrombotic lesions and all of 8 malignant types were correctly depicted by cardiac MRI (100% of sensitivity and specificity). The histologic type suspected by MR was confirmed in 24 of 28 (85.8%) available histologic samples.

Conclusions: Gd-e MRI sequences have an essential role in the evaluation of suspected cardiac masses. MR signal variation after Gd administration, together with morphologic (T1-W and T2-W) and dynamic (gradient-echo) sequences allow a clear distinction between neoplasms and thrombi and, among tumors, between benign and malignant types. Furthermore, with MRI tissue characterization is possible to make a differentiation between histologic types of cardiac neoplasms, with a good correlation to histology. In the evaluation of a suspected cardiac mass a full MRI examination (non Gd-e and Gd-e sequences) could be considered, in selected cases, a suitable non-invasive alternative to myocardial biopsy.

538. RELATIONSHIP BETWEEN DELAYED ENHANCED MRI AND THE LOW VOLTAGE BORDER ZONE BY ELECTROANATOMIC MAPPING IN PORCINE MODEL OF VENTRICULAR TACHYCARDIA

Tetsuo Sasano, MD, PhD, Hiroshi Ashikaga, MD, Roselle Abraham, MD, PhD, Jun Dong, MD, Kevin J. Mills, BS, Henry Halperin, MD, PhD, Eduardo Marbán, MD, PhD, Albert C. Lardo, PhD. ***Johns Hopkins University, Baltimore, MD, USA.***

Introduction: The relationship between morphologic features of chronic myocardial scar detectable by delayed enhancement magnetic resonance imaging (DE-MRI) and the occurrence of monomorphic ventricular tachycardia (MVT) remain unclear.

Purpose: The purpose of this study compare DE-MRI and electroanatomic mapping (EAM) based assessment of myocardial scar and the infarct border zone region in a porcine model of MVT.

Methods: Seven pigs underwent anteroseptal myocardial infarction followed by reperfusion. DE-MRI was performed at 10 weeks after infarction and scar size and infarct boarder zone regions were defined by regions 2 and 1 SD above the mean remote myocardial signal, respectively. Scar transmurality was also assessed by DE-MRI. Bipolar voltage mapping studies were performed at the time of imaging to define low voltage scar (amplitude < 0.5 mV) and the infarct boarder zone region ($0.5 <$ amplitude < 1.5mV). Surface areas of these low voltage zones and DE-MRI infarct regions were measured and expressed as a percentage of the total LV mass and compared with the scar spatial extent and morphologic features by DE-MRI. Ratios of EAM scar and DE-MRI scar were also calculated and compared with MVT inducibility testing by programmed stimulation in each animal.

Results: Regions of myocardial scar by DE-MRI were significantly greater than the EAM defined scar region in all animals ($13.81 \pm 4.1\%$ vs. $6.92 \pm 4.5\%$, $p < 0.01$), but the border zone region by DE-MRI was much smaller that of the EAM defined border ($1.2 \pm 0.6\%$ vs. $14.8 \pm 7.9\%$, $p < 0.01$). Sustained MVT was induced in 6 of 7 animals by programmed stimulation and all 6 inducible animals had transmural infarcts. One pig that was not inducible for MVT was non-transmural and showed reduced scar by EAM compared with inducible animals (ratio $= 0.021$ vs. 0.57 ± 0.18).

Conclusions: DE-MRI defined scar area is significantly greater than that defined by EAM. Scar transmurality may be an important determinant of low voltage scar and substrate for MVT.

539. MYOCARDIAL PERFUSION IMAGING WITH GADOBUTROL: A COMPARISON BETWEEN 3 AND 1.5 TESLA WITH AN IDENTICAL SEQUENCE DESIGN

Daniel Theisen, Bernd J. Wintersperger, MD, Armin Huber, MD, Olaf Dietrich, PhD, Maximilian F. Reiser, MD, Stefan O. Schoenberg, MD. ***University of Munich-Grosshadern, Munich, Germany.***

Purpose: To implement myocardial first-pass perfusion imaging at 3 Tesla and to evaluate signal parameters in comparison to 1.5 Tesla using identical sequence settings and an intraindividual comparison.

Materials and Methods: In 17 volunteers, myocardial first-pass perfusion imaging was performed at 1.5 Tesla (Magnetom Avanto) and 3 Tesla (Magnetom TIM Trio) after injection of 0.05 mmol/kg BW Gadobutrol using an accelerated saturation recovery TurboFLASH technique (GRAPPA;$R = 2$) at 1.5 and 3 Tesla. Scan order was randomized and detailed sequence parameters (TR 2.3 ms, TE 0.93 ms, FA 15°, Δv 780 Hz/px) as well as spatial resolution were kept identical for both field-strengths. Signal-to-noise ratio (SNR) and contrast enhancement rate (CER) were calculated for all measurements from SI time curves and normalized to baseline signal intensity. A linear fit on the upslope was performed for semiquantitative perfusion analysis.

Results: SNR was significantly higher at 3 Tesla than at 1.5 Tesla (20.8 ± 6.2 vs. 9.0 ± 3.3, $p < 0.0001$). CER was significantly greater at 3 Tesla than at 1.5 Tesla (1.9 ± 0.5 vs. 1.4 ± 0.4). The maximum upslope of linear fitted SI time-curves was significantly higher at 3 Tesla than at 1.5 Tesla (2.3 ± 1.3 vs. 1.8 ± 1.0, $p < 0.0001$).

Conclusions: Three Tesla significantly improves contrast and SNR compared to an identical sequence design at 1.5 Tesla. In addition, most important semiquantitative perfusion parameters are significantly increased. This may allow for an improvement of spatial resolution and potentially for a better delineation of perfusion deficits.

540. MR DETECTION OF GADOFLUORINE-M LABELED MOUSE EMBRYONIC STEM CELLS: FEASIBILITY STUDY IN MOUSE KIDNEY CAPSULES

Karen C. Briley-Saebo, PhD,[1] Eric Adler, MD, PhD,[1] Venkatesh Mani, PhD,[1] Juan Gilberto Aquinaldo, PhD,[1] Joseph Frank, PhD,[2] Hanns-Joachim Weinmann, PhD,[3] Zahi A. Fayad, PhD.[1] ***[1]Mount Sinai School of Medicine, New York, NY, USA, [2]National Institute of Health, Bethsda, MD, USA, [3]Shering AG, Berlin, Germany.***

Introduction: Since embryonic stem cells (ESC) may offer a novel renewable source of lineage specific progenitors for cell replacement therapy, focus has been placed on development of magnetic labels to allow for *in vivo* cell tracking by MRI. Currently iron oxide based materials are being used to label ECSs. The presence of iron within cells results in signal loss by MRI. Due partial voluming and other artifacts, it is often difficult to determine the source of signal loss by MRI. As a result, stem cells labeled with paramagnetic materials that induce positive signal enhancement may be advantageous. Gadofluorine-M (GdFM) is a paramagnetic amphiphilic contrast used for MRI. Due to the lipophilic nature of GdFM it has been hypothesized that this material may be able to penetrate cell membranes.

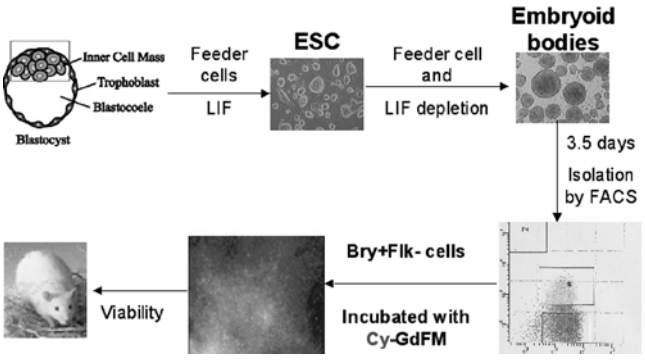

FIG. 1. ESCs were isolated from the inner cell mass and maintained undifferentiated in culture using embryonic feeder cells and leukemia inhibitory factor (LIF). Feeder cell depletion followed by withdrawl of LIF allowed for differentation and formation of embryoid bodies. After 3.5 days in culture FACS was performed and Bry^+ Fld^- es cells are isolated and re-aggregate overnight in serum free media with FGF and VEGF. The cells were plated onto gelatin and 4 days later spontaneous beating was observed. The beating cells are then incubated with cy-GdFM.

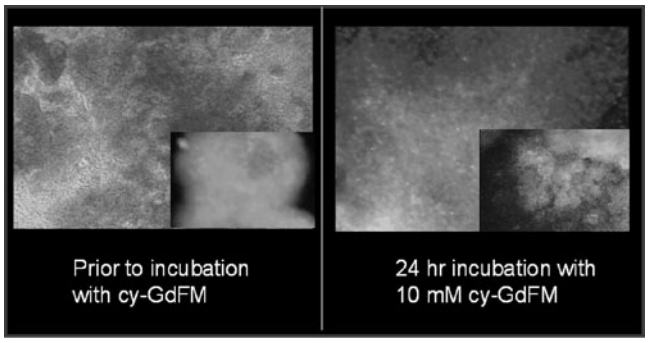

FIG. 2. Beating green fluorescent embryoid bodies prior to and after incubation with cy-GdFM. Presence of the cy-GDFM results in red color by FACS. Small bod reflects higher resolution image of the embryoid bodies.

*Purpose:*The aim of the current study was to evaluate the efficacy of GdFM labeling in mouse embryoid bodies and to evaluate the signal enhancement generated by labeled cells in mouse kidney capsules.

Methods: Green fluorescent protein cDNA ESC lines were used to target the primitive streak gene brachyury (Bry). ECS's from GFP-Bry ES cells carrying the lacZ gene in the Rosa locus were differentiated for 3.5 days to form embryoid bodies containing 3 distinct populations based on expression of GFP and the receptor tyrosine kinase Flk-1 (Bry^-/Flk-1^-, Bry^+/Flk-1^- and Bry^+/Flk-$1^{+)}$. After 3.25 days Bry^+/Flk-1^- cells are isolated by Fluorescence Assisted Cell Sorting (FACS) and allowed to re-aggregate for 24 hours, as shown in Fig. 1. The embryoid bodies were plated on gelatin wells in serum free medium. Within 4

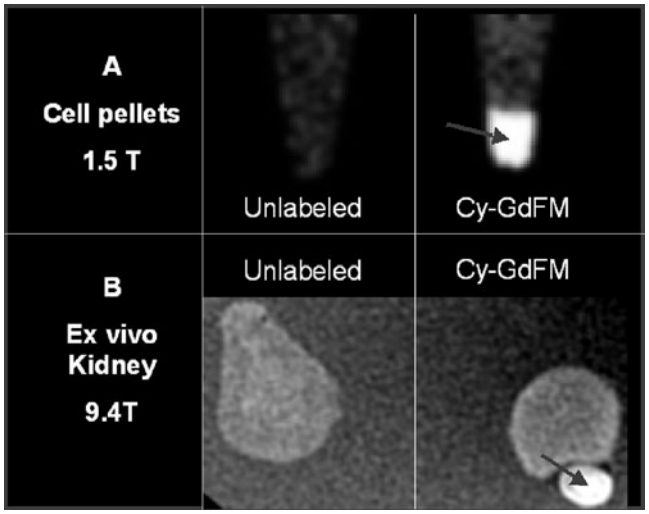

FIG. 3. A) Unlabeled and cy-GdFM labele embryold body pellets at 1.5T. B0 Ex vivo images of kidneys at 9.4T. Arrows shows cy-GdFM cells in pellet and in kidney capsule.

days cells within the culture beat spontaneously and expressed cardiac troponin t, cardiac alpha actin, connexin 43 and atrial natriuretic peptide and CD31. The beating cells were incubated at 37°C for 24 hours with 1, 5 or 10 mM of fluorescently labeled cy-GdFM. cy-GdFM labeled and unlabeled cells were concentrated into a pellet and imaged at 1.5T using T1-w sequences. 2 million unlabeled or cy-GdFM labeled cells were injected into the left kidney capsule of 8-month-old SCID mice (n = 6). Twenty-four hours after injection, the mice were sacrificed and the kidneys removed. The kidneys were fixed for 2 hours in paraformaldehyde, rinsed in PBS, and fixed in 2% agrose gel for MR imaging. Imaging was performed at 9.47 T using T_1-weighted spin-echo sequences (resolution = 200 um × 200 um × 1 mm). After imaging, the kidneys were fixed, cut, and confocal microscopy performed.

Results: No significant effect of cy-GdFM was observed on the function or viability of mESC's at concentrations less than 10 mM. Microscopy revealed that cy-GdFM was located within the cellular cytosol as shown in Fig. 2. Imaging of cell pellets resulted in strong signal enhancement at 1.5 T as shown in Fig. 3A. Cells injected into mouse kidney capsules were clearly visualized at 9.4 T, as shown in Fig. 3B. Confocal microscopy confirmed the presence of cy-GDFM within the kidney capsule. No significant attenuation of signal was observed in kidneys injected with unlabeled embryoid bodies.

Conclusions: Bry+/Flk-1$^-$ embroid bodies were able to incorporate cy-GdFM with limited affect on viability or function. The results of this study strongly suggest cy-GdFM may be used to label embryonic stem cells. In addition the results suggest that it may be possible to visualize the labeled cells *in vivo* based upon the MR signal increase generated by the labeled cells.

541. MYOCARDIAL EDEMA DURING THE ACUTE PHASE OF STRESS CARDIOMYOPATHY

Lorenzo Monti, MD,[1] Elena Corrada, MD,[1] Cristina Barbaro, MD,[1] Claudia Raineri, MD,[2] Alessandra Repetto, MD,[2] Arturo Raisaro, MD,[2] Mario Previtali, MD,[2] Roberto Dore, MD,[2] Luca Balzarini, MD.[1] [1]***I.R.C.C.S. Istituto Clinico Humanitas, Rozzano, Italy,*** [2]***I.R.C.C.S. Policlinico S. Matteo, Pavia, Italy.***

Introduction: Myocardial edema, detected with Cardiovascular Magnetic Resonance (CMR), has recently been described as a feature of myocardial stunning during an acute coronary syndrome. Myocardial stunning of unclear etiology is the main feature of Tako-Tsubo cardiomyopathy.

Purpose: To verify the ability of a T2-weighted-Short inversion Time Inversion Recovery (STIR) sequence in depicting myocardial edema in patients with an established diagnosis of Tako-Tsubo cardiomyopathy.

Methods: Seven consecutive patients (pts.) admitted to our hospitals because of chest pain occurred shortly after an emotional (6 cases) or physical stress (1 case). All pts. were womens, 65 ± 6,3 years. Cardiovascular Magnetic Resonance (CMR) with STIR sequences was performed 2 days after index event in 6 patients and after 8 days in one. Initial ECG showed ischemic ECG changes: 3 pts with deep negative T waves, 3 with ST elevation, 1 with ST depression. Coronary arteries were normal in all pts. Troponins reached a mean peak value of 1.91 (± 1.12) ng/mL, after a mean time of 12 hours from symptom onset.

Results: Four pts. showed akinesis of the mid- and distal left ventricle; two pts. showed akinesis of the mid-ventricle and normal function of the apex; one patient showed only hypokynesis of the mid- and distal left ventricle.In all patients but one, similar CMR features were documented during the acute phase of the disease: pre-contrast STIR sequences showed transmural high T2-signal of the dysfunctioning segments; in all cases the spatial distribution of the edema did not correspond to any specific single coronary artery territory. Contrast-enhanced imaging after gadolinium injection was negative for myocardial necrosis in all. Noteworthy, T2-weighted turbo spin-echo sequences, performed in two patients, gave equivocal results in depicting myocardial edema. The only patient without a clear myocardial edema in STIR sequences underwent CMR 8 days after symptom onset: at that time wall motion abnormalities already resolved. Three pts. were followed with CMR (mean 35 days) and demonstrated spontaneous normalization of wall motion and T2W signal.

Conclusions: STIR sequences allowed the visualization of myocardial edema only during the acute phase of Tako-Tsubo

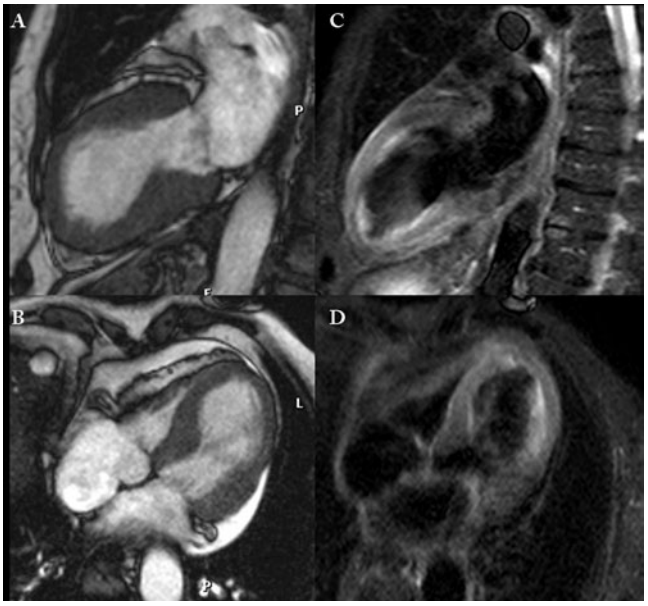

FIG. 1. Acute phase of stress cardiomyopathy. Panel A and B: steady-state free-precession (SSFP) images in the vertical (panel A) and horizontal (panel B) long axis view during the systolic phase show the typical ventricular shape of stress cardiomyopathy. Left ventricular ejection fraction (LVEF) was 39%. Panels C and D: STIR sequences acquired in mid-diastolic phase allow the visualization of edema of the akinetic myocardium. The bright signal of the spinal fluid in panel C confirms the T2-weighing of the sequence.

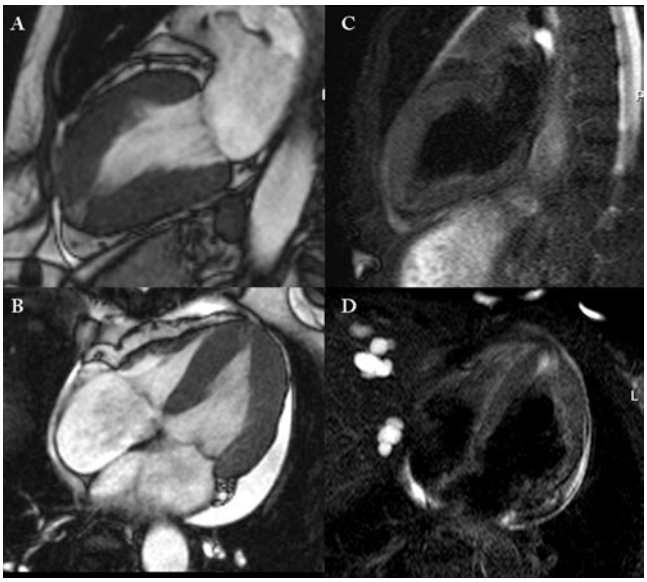

FIG. 2. Thirty day follow-up. Panels as in Fig. 1. Resolution of wall motion abnormalities with increase in LVEF (58%); high T2 signal is no longer detectable with STIR sequences.

cardiomyopathy in all dysfunctioning segments, typically with non-coronaric distribution of the edema and in absence of late gadolinium enhancement.

T2-weighted signal normalized with the resolution of the wall motion abnormalities. These findings can be useful for a non-invasive diagnosis of Tako Tsubo Cardiomyopathy.

542. MOLECULAR MRI OF POST-INFARCT MYOCARDIAL SCAR IN MICE USING A NOVEL COLLAGEN-TARGETED CONTRAST AGENT

Patrick A. Helm, PhD,[1] Brent A. French, PhD,[1] Peter Caravan, PhD,[2] Stephan Dumas, PhD,[2] Vincent Jacques, PhD,[2] Luhua Shen, MD,[2] R. Jack Roy, BS,[1] Christopher M. Kramer, MD,[1] Frederick H. Epstein, PhD.[1] [1] ***University Of Virginia, Charlottesville, VA, USA,*** [2] ***Epix Pharmaceuticals, Lexington, MA, USA.***

Introduction: Many cardiovascular diseases involve fibrosis and extracellular matrix remodeling, including atherosclerosis, hypertrophic cardiomyopathy, and myocardial infarction. We reasoned that molecular imaging of collagen could be valuable in the detection and monitoring of such diseases. A clinically-relevant animal model for evaluating a collagen-targeted molecular imaging agent is post-infarct myocardial scar. After myocardial infarction (MI), wound healing results in the generation of fibrotic scar tissue. In particular, scar formation post-MI is characterized by increased synthesis of the matrix proteins fibronectin, laminin, and collagen.

Purpose: To evaluate a novel gadolinium-based collagen-targeted contrast agent (EP3533, Epix Pharmaceuticals, MA) for improved scar imaging in a mouse model of chronic MI.

Methods: A collagen-specific contrast agent (EP3533) was designed by appending Gd-DTPA moieties for positive contrast imaging to a collagen-specific peptide for molecular targeting. MI was induced in five C57BL/6 mice by a 60 minute occlusion of the left anterior descending coronary artery followed by reperfusion. Two MRI studies per mouse were performed 40–45 days later, after scar formation was fully complete (1). Indwelling tail vein lines were used for I.V. injection of contrast agents during imaging. Conventional non-targeted Gd-DTPA, 0.2 mmol/kg (Magnevist, Berlex) was used during the first MRI study, and EP3533, 0.025 mmol/kg, was used for the second study, with the two studies being performed at least 3 days apart. Doses were chosen to give equivalent relaxivity of the two agents. Imaging was performed using a 4.7T MRI system (Varian, CA), and included ECG-gated localizer scans, cine MRI, and inversion-recovery (IR) imaging before and serially (every 5 minutes) after contrast agent injection. Contrast to noise ratios between scar and LV blood pool (CNR_{sb}) and between scar and normal non-infarcted myocardium (CNR_{sn}) were measured from IR images as a function of time post-injection.

Results: Serial IR imaging after Gd-DTPA injection showed immediate enhancement of the blood pool followed 10–30 minutes later by relatively mild enhancement of scar with peak CNR_{sn} at 20 minutes post-injection. Contrast washout from the blood and scar began at 20 minutes post-injection. EP3533 also immediately enhanced the blood pool with washout beginning 20 minutes after injection. Strong enhancement of scar began 10 minutes after injection with peak CNR_{sn} at 40 minutes; enhancement persisted for at least 60 minutes. Example images depicting enhancement of post-MI scar using Gd-DTPA and EP3533 at 20 and 40 minutes post-injection, respectively, are shown in Fig. 1. Summarizing the results from all mice, at 40 minutes post-injection for EP3533, CNR_{sb} was 22.3 ± 6.9 and CNR_{sn} was 21.7 ± 5.5, whereas at 20 minutes post-injection for Gd-DTPA, CNR_{sb} and CNR_{sn} were significantly lower at 3.9 ± 1.0 ($p < 0.01$) and 10.8 ± 2.7($p < 0.01$), respectively.

Conclusions: Molecular imaging of collagen with EP3533 provides high CNR for fibrotic scar vs. normal myocardium and blood in a mouse model of chronic, fully healed MI. High CNR

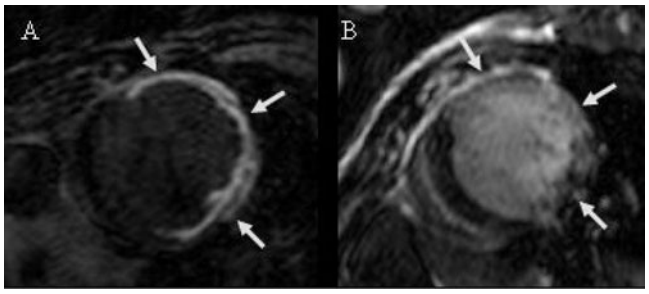

FIG. 1. (A) T1-weighted IR image acquired 40 min. post-injection of EP 3533 showing enhancement of scar in LV free wall. At 40 min. post-injection the scar remains bright, but contrast agent has washed out of the viable myocardium and blood pool, leading to excellent CNR. (B) An IR image of the same slice acquired using Gd-DTPA on another day.

at 40 minutes post-injection occurs because EP3533 binds to collagen, thus the contrast-enhanced scar remains bright after unbound contrast agent clears from the blood pool and normal myocardium. Beyond myocardial scar, this agent may find application in detecting and evaluating a broad array of diseases involving fibrosis and extracellular matrix remodeling.

REFERENCE

1. Ross, et al. MRM 2002; 47:1158–68.

543. VENTRICULAR END-DIASTOLIC VOLUME RATIOS CORRELATE HIGHLY WITH SHUNT SEVERITY: QUANTIFICATION USING MRI

Michael K. Atalay, MD, PhD, Philip L. Stockwell, MD, Lloyd R. Feit, MD, Thomas M. Drew, MD. ***Brown University, Providence, RI, USA.***

Introduction: Intra- and extracardiac shunts—particularly if mild—are often indolent and may cause vague, non-specific symptoms. They may go undetected well into adulthood, and are occasionally diagnosed incidentally. Moreover, increased right heart chamber sizes on imaging may be the first clue. By virtue of volume overload, shunt lesions are known to cause dilation of involved cardiac chambers and intervening vessels. It is unclear, however, if the chamber volumes increase in a predictable manner based on shunt severity.

Purpose: This study aims to determine if shunt severity correlates with chamber sizes and other anatomic metrics on MRI.

Methods: Referrals to our cardiac MRI service from December 1, 2003 to April 1, 2006 were reviewed. Patients who had an atrial septal defect (ASD) or anomalous pulmonary vein(s) (APV) clearly identified on MRI, with shunt severity quantified (Qp/Qs), were included in this study. Patients with left ventricular dysfunction or other significant congenital or valvular lesions were excluded. In each case, Qp/Qs was determined either by standard ventricular volume analysis (Simpson's method), by comparing blood flow in the main pulmonary artery and aorta using phase contrast techniques (PC-MRI), or by both. Correlations between Qp/Qs and various anatomic and volumetric measures were evaluated.

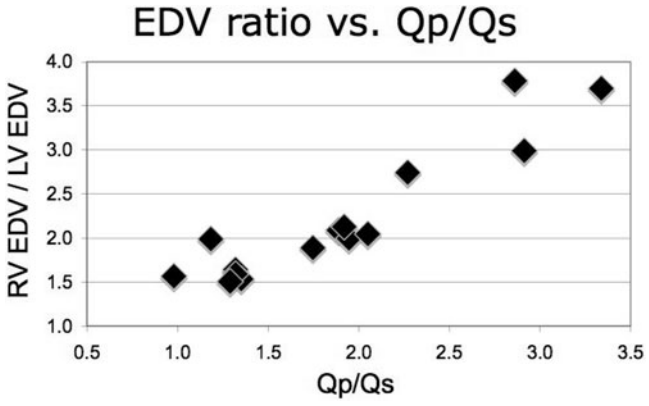

FIG. 1.

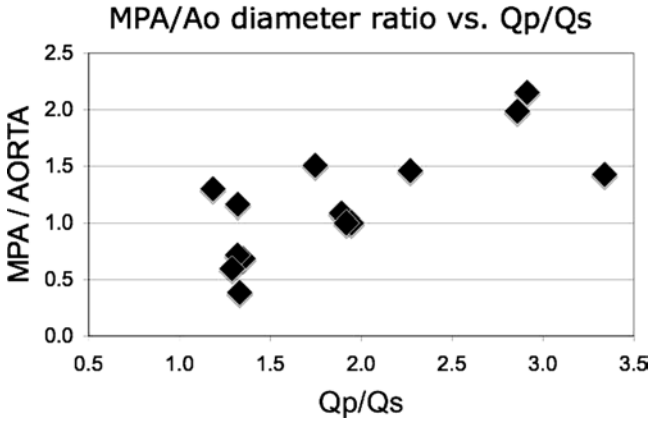

FIG. 2.

Results: Over the study period, 775 patients were imaged. In all, 27 (3.5%) patients with shunts were identified, 15 (2%) of whom met inclusion criteria (age range: 12–77 years; mean 49 years; 8 women). There were 7 cases of isolated ASD (1 sinus venosus, 5 secundum, 1 ostium primum), 5 cases of APV, and 3 cases of sinus venosus ASD combined with APV. Qp/Qs determined by PC-MRI has good correlation with that found using ventricular stroke volume data based on Simpson's method ($r^2 = 0.92$). Overall, the ratio of RV to LV end diastolic volumes varies linearly with Qp/Qs with high correlation ($m = 1.0$, $b = 0.3$, $r^2 = 0.93$) (Fig. 1). The ratio of pulmonary artery to aortic cross-sectional diameter also varies linearly with Qp/Qs ($m = 0.3$, $b = 0.6$, $r^2 = 0.72$) (Fig. 2). In pure ASDs, defect area roughly correlates with shunt severity ($m = 1.9\ cm^2$, $b = -1.9\ cm^2$, $r^2 = 0.72$).

Conclusion: Knowledge of shunt severity is important for clinical management. When available, PC-MRI can be used to accurately determine Qp/Qs. Various anatomic and volumetric measures are found to correlate with shunt severity. These may corroborate PC-data or serve as surrogates for estimating Qp/Qs on MRI or other modalities, such as computed tomography, when PC data is unavailable or spurious.

544. CARDIAC CINE MRI: RELATIONSHIP BETWEEN FAST GRADIENT ECHO AND STEADY STATE FREE PRECESSION FOR DETERMINATION OF MYOCARDIAL MASS AND VOLUMES

Ashkan A. Malayeri,[1] Craig Johnson, MS,[2] Robson Macedo, MD,[1] Joan Bathon, MD,[1] João A. C. Lima, MD,[1] David A. Bluemke, MD, PhD.[1] ***[1]Johns Hopkins Hospital, Baltimore, MD, USA, [2]University of Washington, Seattle, WA, USA.***

Introduction: Steady-state free precession (SSFP) cine MRI has replaced fast gradient echo (FGRE) cine due to faster imaging

and improved blood-tissue contrast. Differences in cardiac mass and volumes have been documented between the 2 sequences, but the methods to "convert" extensive existing databases of normal values of FGRE cine MRI data to equivalent SSFP values have not been determined.

Purpose: The purpose of this study is to assess the relationship between the FGRE and SSFP for myocardial mass and volume.

Methods: FGRE and SSFP cardiac cine MRI were acquired in the same MRI session for 26 participants (F: 18, M: 8) of the ESCAPE study of cardiac function. Cardiac cine MRI was acquired with < 50 ms temporal resolution and $6 - 8 \times 1.4 \times 1.9$ mm spatial resolution. Short axis endocardial and epicardial contours were determined using semi-automated analysis by experienced observers using QMASS MR 6.1.6 (Medis Medical System, Leiden, The Netherlands) to determine left ventricle (LV) mass and volumes.

Results: The overall mean age (SD) of the patients was 61 (9.44) years (45–80). The mean (SD) left ventricular end diastolic (LVED) volume measured by FGRE and SSFP were 120.08 (31.46) mL and 122.91 (27.18) mL, respectively ($p = 0.16$). Mean LV mass measured by FGRE and SSFP were 112.31 (24.47) and 106.85 (19.12) grams ($p = 0.002$). Importantly, the relationship between FGRE and SSFP measures appear linear and strongly correlated for both LVED volume (least squares $\beta = 1.102$, $p < 0.001$, Pearson $r = 0.952$) and LV mass (least squares $\beta = 1.226$, $p < 0.001$, Pearson $r = 0.958$).

Conclusions: Linear relationships exist for key LV function parameters when comparing FGRE and SSFP cine MRI. These results indicate that existing databases for FGRE LV function may be converted to corresponding LV function values for SSFP MRI. Because MRI is the standard of reference for LV mass and function, it is critical to understand the relationship of cardiac function measured by FGRE versus newer SSFP pulse sequences.

545. NONISCHEMIC LATE GADOLINIUM ENHANCEMENT BY CMR IN CHRONIC KIDNEY DISEASE CORRELATES TO SEGMENTAL AND GLOBAL LEFT VENTRICULAR HYPERTROPHY

Brian J. Schietinger, MD, Katherine W. Kwon, MD, Glenn M. Brammer, MD, Amy J. Mangrum, MD, J. Michael Mangrum, MD, Christopher M. Kramer, MD. ***University of Virginia Health System, Charlottesville, VA, USA.***

Background: The prevalence and distribution of late gadolinium enhancement (LGE) by cardiac magnetic resonance (CMR) in chronic kidney disease patients on hemodialysis (CKD) is not well described. Potential etiologies of LGE in CKD include myocardial infarction, fibrosis from left ventricular hypertrophy (LVH), or an inflammatory/infiltrative process. The relationship between LGE and hypertrophy is incompletely understood.

Methods: CMR was performed on CKD patients on a Siemens Avanto 1.5 T scanner. CMR included steady state free precession cine (TR 2.7 ms, TE 1.28 ms, flip angle 73^0, FOV 300–350 mm, resolution $1.8 \times 1.4 \times 8.0$ mm) and post-gadolinium phase sensitive inversion recovery sequences (TR 700 ms, TE 4.18 ms, inversion time 300 ms, flip angle 25^0, FOV 300–340 mm, resolution $1.8 \times 1.3 \times 8$ mm) 10–15 minutes after infusion of 0.15 mM/kg gadolinium -DTPA. Global and segmental left ventricular anatomic and functional measurements were performed with dedicated analysis software (Argus, Siemens Medical Solutions, Malvern, PA). LGE was defined as signal intensity greater than 2 S.D. that of remote myocardium. Infarct-related LGE was determined by subendocardial distribution and associated LV wall motion abnormalities with validation against known coronary anatomy. An AHA 16 segments analysis was performed to determine the extent of LGE present as a percentage of the segment. Linear regression analysis was performed between LGE and segmental and global LV mass and function.

Results: Twenty-four patients (age 59 ± 11 years, 54% males, 79% African American, dialysis for 45 ± 38 months, 100% hypertension, 71% diabetes, 42% known coronary artery disease by x-ray angiography) underwent CMR. LV ejection fraction was $48 \pm 15\%$ and LV mass (LVM) index 100 ± 52 g/m^2. LGE was seen in 79% (19 of 24) of patients in 3 distinct patterns; infarct-related, diffuse, and focal (Fig. 1). One patient had both infarct-related and diffuse nonischemic LGE. Infarct-related subendocardial LGE in a coronary distribution (Fig. 1, panel A) was present in 32% of patients (6 of 19). Diffuse nonischemic LGE (Fig. 1, panel B) was seen in 37% (7 of 19) and focal in 37% (7 of 19) (Fig. 1, panel C). LGE constituted 15 ± 18 percent of the total LVM. In all 24 patients, there was a significant relationship between LVM and LGE ($r = 0.443$, $p = 0.03$). Segmental analysis revealed a significant relationship between the extent of LGE and LV end diastolic wall thickness (ED) ($r = 0.315$, $p < 0.01$), end

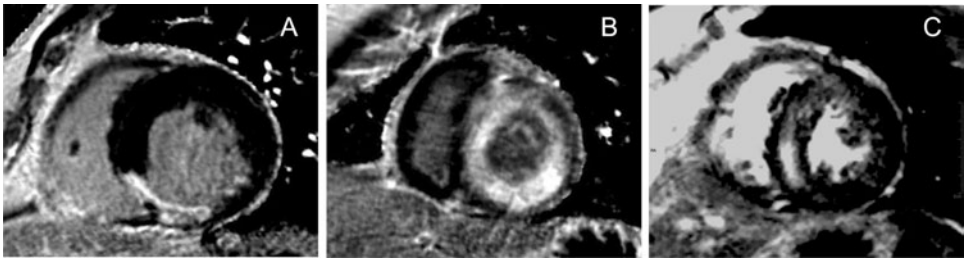

FIG. 1.

systolic wall thickness (ES) ($r = 0.18$, $p < 0.01$), and % thickening ($r = 0.0972$, $p < 0.01$). For ED and ES, these relationships were strengthened when only nonischemic segments were evaluated ($r = 0.425$, $p < 0.01$ and $r = 0.358$, $p < 0.01$, respectively).

Conclusion: LGE is prevalent in CKD patients and the extent is related to left ventricular hypertrophy. The majority of LGE is not infarct-related and may represent fibrosis due to LVH and/or an inflammatory/infiltrative process. Nonischemic LGE is more likely to be present in thicker LV segments. CKD patients are at high risk for sudden cardiac death and although risk factors such as left ventricular hypertrophy have been recognized, no mechanism or specific markers have been identified. Late gadolinium enhancement may be such a marker.

546. FEASIBILITY AND SAFETY OF DOBUTAMINE STRESS CARDIOVASCULAR MAGNETIC RESONANCE IMAGING IN CHILDREN

Sebastian Strigl, MD,[1] Rebecca Beroukhim, MD,[1] Laureen Sena, MD,[2] Tal Geva, MD,[1] Andrew J. Powell, MD.[1]
[1]Department of Cardiology, Children's Hospital Boston, Boston, MA, USA, [2]Department of Radiology, Children's Hospital Boston, Boston, MA, USA.

Background: Myocardial ischemia from coronary artery abnormalities is a rare condition in the pediatric age range. Accordingly, when faced with this important concern, there is a need for highly sensitive and specific testing; however, the optimal diagnostic pathway remains uncertain. Nuclear medicine techniques may be hampered by low-spatial resolution in the face of small structures as well as the potential deleterious effects of radiation exposure. Stress echocardiography may be limited by poor acoustic windows, particularly in post-operative patients, and the inability of young children to exercise effectively. Cardiovascular magnetic resonance (CMR) routinely provides high quality imaging of the ventricles; the ability to assess wall motion, myocardial perfusion, and viability; and visualization of the coronary arteries. However, there are very few reports on the use of CMR for these purposes in children. We report here our initial results on the feasibility and safety of dobutamine stress (DS) CMR to evaluate children at risk for myocardial ischemia.

Methods: A database search identified all patients < 18 years of age who underwent DS CMR at Children's Hospital Boston. Their medical records and DS CMR studies were retrospectively reviewed with particular attention to procedural parameters and medical complications. The DS MRI imaging protocol has evolved. In the most recent examinations, it has included the following: 1) baseline cine imaging (SSFP) in short-axis for complete ventricular coverage; 2) first pass perfusion imaging (FPP) at rest; 3) coronary artery imaging with VCG and navigator-gated 3D SSFP; 4) cine imaging (SSFP) in 3 short-axis and 3 long-axis locations at baseline and during incremental dobutamine infusion (beginning at 10 and up to 50 mcg/kg/min) with additional Atropine as needed, 5) FPP at peak stress; and 6) myocardial delayed enhancement (MDE) imaging.

Results: Seventeen DS CMR studies were performed on children < 18 years old over a 2.6 year period. Mean age was 7.3 years (range, 0.8–17.6), and 12/17 patients were male. Their principal diagnoses were Kawasaki disease with coronary artery aneurysms (n = 10), status-post cardiac transplant (n = 2), transposition of the great arteries status-post arterial switch procedure (n = 2), status-post repair of an anomalous left coronary artery from the pulmonary artery (n = 1), left coronary osteal stenosis (n = 1), and coronary aneurysms (n = 1). All but two patients had a left ventricular ejection fraction above 55%. Thirteen studies were performed with the patient receiving general anesthesia; the remainder were done without sedation. All examinations completed their pre-specified examination protocol; two were briefly interrupted because of scanner malfunction, but resumed. Atropine was administered in addition to achieve predicted heart rate in 15 patients. In 15 patients a heart rate of ≥160 beats per minute was reached; in two patients 85% of predicted peak heart rate for age was achieved.

Cine image quality was good allowing visualization of all cardiac segments in all but one patient who developed frequent premature atrial beats in her final stage. Four studies had wall-motion abnormalities at baseline; no patient developed new regional wall motion abnormalities during stress. One patient had a perfusion defect at baseline; none had new perfusion abnormalities with stress. Four patients were found to have regional of hyperenhancement on MDE, with corresponding regional wall-motion abnormalities in three. There were no serious adverse effects such as sustained arrhythmia, hemodynamic instability, or new post-test ECG abnormalities. One patient complained of nausea during stress.

Conclusion: DS CMR to evaluate for inducible myocardial ischemia can be effectively and safely performed in children. Even in an at-risk patient population, the incidence of inducible wall motion abnormalities is low. In this small case series, there were no serious adverse events. More investigation is warranted to better define the test characteristics of DS CMR in the pediatric age range.

547. GENDER DIFFERENCES ARE PRESERVED DESPITE IMAGING SEQUENCE-SPECIFIC DIFFERENCES IN MYOCARDIAL CONTRACTION FRACTION

Michael L. Chuang, MD,[1] Carol J. Salton, BA,[1] Susan B. Yeon, MD, JD,[1] Kraig V. Kissinger, BS, RT(R) (MR),[1] Daniel Levy, MD,[2] Christopher J. O'Donnell, MD, MPH,[2] Warren J. Manning, MD.[1]
[1]Beth Israel Deaconess Medical Center, Boston, MA, USA, [2]the NHLBI's Framingham Heart Study, Framingham, MA, USA.

Introduction: Ejection fraction (EF) is commonly used to summarize left ventricular (LV) systolic performance, but

compensatory changes in LV geometry, such as concentric remodelling, allow preservation of EF despite dysfunction at the level of myofibrillar contraction. Myocardial contraction fraction (MCF) is the ratio of LV stroke volume to myocardial volume and is a geometry-independent measure of myocardial performance. Using a TFE-EPI sequence, we have previously shown that MCF is greater in women than men (1). It is well established that LV volumes measured by SSFP ciné methods are greater than corresponding volumes by gradient-echo ciné methods, whereas LV mass (and thus myocardial volume) is smaller when determined using SSFP sequences. However, the effect of imaging sequence on MCF has not been determined.

Purpose: We sought to determine whether MCF differs systematically between SSFP and gradient-echo ciné methods and to examine whether gender-specific differences in MCF are preserved across sequences.

Methods: A convenience sample of 50 adults (25 women, 25 men) was selected randomly from among the members of the Framingham Heart Study offspring cohort. Subjects were normotensive (SBP < 140 mmHg, DBP < 90 mmHg) and there were no differences in mean age between women (56 ± 8 years) and men (55 ± 8 years), $p = 0.5$. Each subject underwent CMR twice, at widely separated timepoints, on a 1.5 Tesla system (Philips) using a contiguous multislice approach with 10-mm slice thickness in each study. The TFE-EPI sequence had 1.25×2.0 mm^2 in-plane resolution; the SSFP sequence was comparable at 1.56×1.92 mm^2. Images were analyzed at separate timepoints by a single expert observer who manually traced contours blinded to results of the other study. Data are summarized as mean $\pm$ standard deviation and differences between genders were assessed using Student's unpaired t test. The paired t test was used to assess the effect of imaging sequence on MCF.

Results: MCF was significantly greater in women than men for both imaging sequences (Table). SSFP-determined MCF was greater than MCF by TFE-EPI for both genders (both $p < 0.001$). As expected, LV stroke volume was greater with SSFP than TFE-EPI, whereas myocardial volume was lower with SSFP, regardless of gender ($p < 0.001$ for all sequence comparisons). Myocardial volume and stroke volume were significantly greater in men than women for each imaging sequence ($p < 0.001$ for all gender comparisons). LV end-diastolic and end-systolic volumes were greater with SSFP than TFE-EPI (all comparisons $p < 0.001$), although mean EF did not differ between SSFP and TFE-EPI ($p = 0.13$).

Conclusions: MCF is a measure of LV performance that detects myocardial dysfunction despite attempts at compensatory remodelling such development of concentric hypertrophy. MCF is greater in women than men, and this difference is consistent regardless of imaging sequence used. However, MCF determined by SSFP is significantly greater than MCF by gradient-echo ciné methods. CMR reference values for MCF must be not only gender-specific, but also imaging-sequence specific.

TABLE 1
MCF by Gender and Sequence

	SSFP	TFE-EPI	p vs. sequence
Women	0.93 ± 0.17	0.59 ± 0.12	<0.001
Men	0.79 ± 0.13	0.52 ± 0.07	<0.001
p vs. gender	0.003	0.027	

REFERENCE

1. Chuang, et al. JCMR 2003; 5:50.

548. INTRA-PLAQUE HEMORRHAGE QUANTIFICATION USING MORPHOLOGY-ENHANCED PROBABILISTIC PLAQUE SEGMENTATION (MEPPS) FOR IN VIVO CAROTID MRI

Fei Liu,[1] Marina Ferguson,[1] Baocheng Chu,[1] Wei Yu,[1] Minako Oikawa,[1] Hunter R. Underhill,[1] Dongxiang Xu,[1] Thomas S. Hatsukami,[2] Chun Yuan,[1] William S. Kerwin.[1]
[1]Dept. of Radiology, Unversity of Washington, Seattle, WA, USA, [2]Dept. of Surgery, VA Puget Sound Health Care System and University of Washington, Seattle, WA, USA.

Introduction: High-resolution MRI has been proven to reproducibly identify the plaque composition of carotid atherosclerotic lesions. We have previously presented a histologically validated technique, morphology-enhanced probabilistic plaque segmentation (MEPPS), for the automated detection of calcification, lipid-rich/necrotic core, loose matrix and fibrous tissue in the *in vivo* carotid plaque (1). In the original version of MEPPS, hemorrhage was included within the necrotic core.

The presence of intraplaque hemorrhage, frequently a subregion of the lipid-rich/necrotic core, has been implicated in accelerating progression in both the coronary (2) and carotid (3) arteries. Recently, we found that the presence of intraplaque hemorrhage was strongly associated with future cerebrovascular events (4). As such, identification and quantification of hemorrhage as a distinct entity within the atherosclerotic lesion is critical to evaluating plaque vulnerability and assessing overall risk.

Purpose: We sought to build upon our previous MEPPS technique to enable the automated quantification of intraplaque hemorrhage. Furthermore, we desired to further classify the hemorrhage by its appearance: Type I-consistent with more recent hemorrhage and Type II is consistent with more chronic hemorrhage.

Methods: By combining intensity information and morphology information (plaque thickness and distance to lumen), the

TABLE 1
Area correlation between MEPPS and HCMMS

	Nec. core	Hem I	Hem II	Hem I & II
CC (r)	0.92	0.95	0.62	0.90

CC, correlation coefficient.

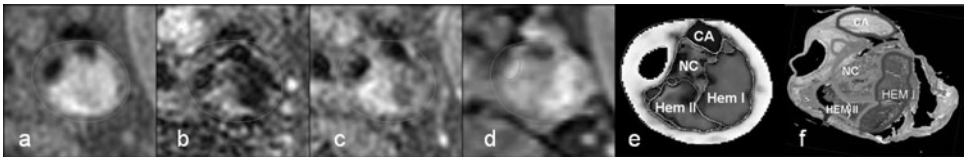

FIG. 1. (a)–(d) T1-, T2-, PD-weighted, and time-of-flight MR images; (e) MEPPS result; (f) matching histologic cross-section (H&E stain).

MEPPS algorithm segments the plaque region into calcification, lipid-rich/necrotic core, loose matrix and fibrous tissue. Within the lipid-rich/necrotic core, the probability of each pixel to be Type I hemorrhage, Type II hemorrhage and non-hemorrhage is further estimated based on the Bayesian rule

$$P(C_i|I) = P(I|C_i) \cdot P(C_i)/\text{sum}[P(I|C_i) \cdot P(C_i)], \quad \text{(eq1)}$$

where I is the set of image intensities, C is the component, and the probabilities are estimated from a training data set by the Parzen window method. Based on the generated probability map for each tissue, coupled active contours are applied to the lipid-rich/necrotic core region to assign each tissue with one active contour.

Nineteen patients scheduled for carotid endarterectomy (CEA) were imaged on a 1.5T GE Signa scanner with the following sequences: T1 (TR = 800 ms, TE = 11 ms), T2 (TR = 3150 ms, TE = 66 ms), proton density (PD; TR = 2770 ms, TE = 9.3 ms), time-of-flight (TOF; TR = 23 ms, TE = 2.8 ms). A total of 72 locations were selected with good image quality and matching histology that indicated the presence of hemorrhage. A trained carotid MRI reviewer identified the lumen and outer wall boundaries, and, referring to histology, manually contoured the lipid-rich/necrotic core, Type I and Type II hemorrhage at all locations. Forty-three locations from 12 patients were chosen for training and 29 locations from 7 patients for testing.

The areas of each component detected by MEPPS were then compared to the histologically confirmed MRI manual segmentation (HCMMS) by computing the correlation coefficients.

Results: An example of automated hemorrhage detection is shown in Fig. 1. Table 1 shows the area size correlation of the MEPPS segmentation result to HCMMS. Although the identification of Type II hemorrhage is not as robust as Type I hemorrhage, overall hemorrhage detection is highly correlated to HCMMS.

Conclusion: These results demonstrate that the reliable, automated, *in vivo* segmentation of intra-plaque hemorrhage is possible. These measurements can in turn be used to investigate the association of plaque features with plaque vulnerability or the changes in plaque composition over time due to therapy.

REFERENCES

1. Liu F, et al. MRM 2006; 55:659–668.
2. Virmani R, et al. ATVB 2005; 25:2054–2061.
3. Takaya N, et al. Circulation 2005; 111:2768–2775.
4. Takaya N, et al. Stroke 2006; 37:818–823.

549. SLICE-FOLLOWING CSPAMM MYOCARDIAL TAGGING IN RATS AND ON A HUMAN HIGH-FIELD SYSTEM

Khaled Z. Abd-Elmoniem,[1] John Terrovitis,[2] M. Roselle Abraham,[2] Jerry L. Prince,[1] Matthias Stuber.[1] [1]*Johns Hopkins University, Baltimore, MD, USA,* [2]*Johns Hopkins Hospital, Baltimore, MD, USA.*

Introduction: Small animal magnetic resonance imaging (MRI) is an invaluable tool for basic research in cardiology. More specifically, the response of local myocardial function to cellular or gene therapy is currently of considerable scientific interest. However, in order to quantify and characterize local myocardial function and changes thereof in a small animal model, both a high spatial and temporal resolution are required. For these reasons, MR myocardial tagging on small-bore animal systems has been implemented and successfully applied (1). However, the MRI methods developed on such experimental systems may not easily be adopted on human high field systems and both small dimensions and high heart rates pose major challenges, but recent advances in hardware (vector ECG) and software (spiral imaging) are not readily available on these animal systems. For these reasons, we have developed, implemented, and tested CSPAMM myocardial tagging in rats on a Human High-Field System.

Purpose: To establish a methodology that enables the assessment and quantification of local myocardial function in a small animal model (rat) on a human high-field MRI system.

Methods: Three male Wistar Kyoto rats (1–3 months old, 220–340 g) were imaged on a commercial human 3T system (Philips Achieva) equipped with a small-diameter (ø = 8cm) 4-element carotid surface (2 anterior and 2 posterior elements) coil (Pathway MRI), parallel receiver architecture, vector ECG triggering, and spiral imaging. In one rat, an anterolateral myocardial infarction was induced by coronary ligation 50 days prior to imaging. Animals were anesthetized by isoflurane inhalation (4% for induction, 2% maintenance). Four ECG leads for human use were tightly wrapped around the rats' paws for vector ECG triggering. The rats' position was head first and prone. Images were acquired from end-diastole, 11 ms after the R-wave; to end-systole in the subsequent R-wave. Vertically and horizontally tagged slice-following CSPAMM (1) cine images

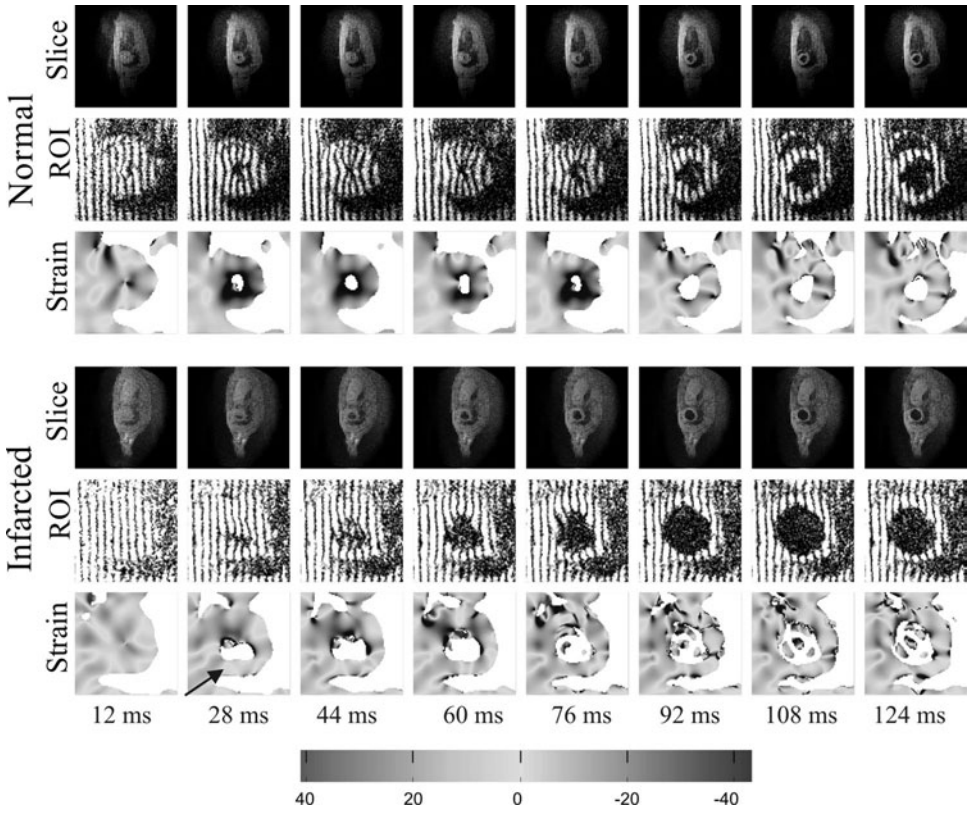

FIG. 1. Normal and infarcted rat SA myocardial functional imaging.

were acquired (16 cardiac phases, TR = 16 ms, FOV = 90 mm, slice thickness = 3 mm, 128 spiral interleaves (350 sample points each, 0.26 mm in-plane resolution), flip angle = 25°, tag spacing = 1.5 mm). On the resultant images, strain analysis was performed using the HARP method (2).

Results: In all animals, R-wave triggering was successful and CSPAMM tagged images could successfully be obtained. Hereby, a high visual tagging contrast supported HARP strain measurements and no fading of the tags was observed throughout the entire cardiac cycle. Fig. 1 shows the tagged images and the corresponding circumferential strain maps in both a normal (first three rows) and an infarcted (second three rows) rat heart. In the normal heart, the myocardium exerts up to 40% compression while in the infarcted case ~15% in the normal regions and 0% in the infarcted regions was measured.

Discussion and Conclusion: A methodology that enables the assessment and quantification of local myocardial function in a rat model on a commercial human high-field (3T) MRI system was developed, implemented, and successfully tested in both healthy and diseased states. Human high-field systems may, therefore, be well-suited for the quantification of local cardiac motion before and after intervention.

REFERENCES

1. Fischer. True myocardial motion tracking. MRM 1994.
2. Osman. Cardiac motion tracking using CINE harmonic phase (HARP) MRI. MRM 1999.

550. WHAT ARE THE HIGH RISK MARKERS OF ADVERSE CARDIAC OUTCOMES IDENTIFIED ON CARDIAC MAGNETIC RESONANCE IN PATIENTS WITH SUSPECTED PERICARDIAL DISEASE?

Mouaz Al-Mallah, MD, Alireza Maghsoudi, MD, Zelmira Curillova, MD, Sui Tsang, BSc, Raymond Y. Kwong, MD, MPH. ***Brigham and Women's Hospital, Boston, MA, USA.***

Introduction: Contrast-enhanced cardiac MR (CMR) can characterize changes in cardiac structure and physiology from pericardial disease. However, knowledge regarding the prognostic association of these changes with patient outcome remains limited.

Purpose: We aimed to explore the respective prognostic value of the alteration of cardiac structure and physiology in a patient cohort referred clinical for CMR assessment of pericardial disease.

Methods: We performed gadolinium-enhanced CMR in 100 patients (48 females, mean age 54 ± 15 years) with a clinical suspicion of pericardial disease. The CMR study was performed at a 1.5 T scanner (GE Signa CVi) and included short

and long-axis function with cine SSFP imaging, axial double inversion recovery FSE, phase contrast evaluation of the inferior vena cava, rest myocardial perfusion with 0.1 mmol/Kg of intravenous gadolinium, and T1 weighted inversion recovery FGRE pulse sequence 10-15 minutes after a cumulative dose of 0.15 mmol/kg of gadolinium. In all CMR studies, we assessed the global and regional bi- ventricular size and function, atrial sizes, vena caval sizes, pericardial thickness. We use Cox proportional hazard regression to assess the association of biatrial enlargement, pericardial thickness, alteration in RV shape, paradoxical septal motion, significant pericardial effusion, small ventricular size, and late gadolinium myocardial enhancement with major adverse cardiac events (MACE) which included mortality and admissions due to congestive heart failure.

Results: After a median follow-up period of 10 months (range 6 months to 4.8 years), 30 (30%) of patients experienced adverse events including 20 deaths and 10 heart failure admissions. The presence of small ventricles was associated with MACE (HR 8.63, $p = 0.0007$, 95% CI 2.46–29.86). Increased pericardial thickness demonstrates a non-linear association with MACE, and a pericardial thickness of more than 3 mm portended more than a 3-fold hazard increase (HR 3.19, $p = 0.02$, 95% CI 1.26–8.11). Dilated vena cava and biatrial enlargement trend towards worse outcomes (HR 5.66, $p = 0.08$, and HR 2.46, $p = 0.08$ respectively). Presence of late myocardial enhancement was also associated with a > 3 fold increase in hazards to MACE (HR: 3.09, $p = 0.04$, 95% CI 1.07–8.96) in patients without any history of myocardial infarction. However, paradoxical septal motion, tubular-shaped right ventricle and the presence of pericardial effusion were not predictive of patient outcome.

Conclusion: Increased pericardial thickness of > 3 mm and small ventricular size by CMR are associated with MACE in patients suspected to have pericardial disease. These markers reflect underlying constrictive physiology. Presence of late enhancement may represent myocardial extension from pericardial inflammation. These features should be routinely assessed by CMR referred in this clinical setting.

551. CONTRIBUTION TO LEFT VENTRICULAR STROKE VOLUME BY THE ATRIOVENTRICULAR PLANE DISPLACEMENT IN ADULTS, ATHLETES AND PATIENTS WITH DILATED CARDIOMYOPATHY

Marcus Carlsson,[1] Martin Ugander,[1] Henrik Mosén,[1] Torsten Buhre,[2] Hakan Arheden.[1] [1]***Clinical Physiology, Lund, Sweden,*** [2]***Department of Sport Sciences, Malmo University, Sweden.***

Introduction: Previous studies using echocardiography in healthy subjects have reported conflicting data regarding the percentage of the stroke volume (SV) of the left ventricle (LV) resulting from longitudinal and radial function respectively.

Purpose: To quantify the percentage of SV explained by atrioventricular plane displacement (AVPD) in controls, athletes and patients with decreased left ventricular function due to dilated cardiomyopathy (DCM) using cardiac magnetic resonance (CMR) imaging.

Methods: Twelve healthy subjects (mean age 24 years, 5 women), 12 elite triathletes (mean age 35 years, 4 women) and 12 patients with DCM and ejection fraction below 30% (mean age 54 years, 4 women) were examined by cine CMR. Maximum AVPD between end-diastole and end-systole was measured at two locations in each of three long axis planes and expressed as the average of the six locations. The SV was calculated from contiguous short axis images by established methods. The mean epicardial area of the two largest short axis slices in end-diastole was multiplied by the AVPD and divided by the SV to calculate the percentage of SV explained by longitudinal function (SV_{AVPD}).

Results: SV for controls was (mean $\pm$ SEM) 116 ± 6 mL. SV was higher in athletes (140 ± 4 mL, $p = 0.0086$) and lower in patients (72 ± 7 mL, $p = 0.0009$). AVPD for controls was 16 ± 0 mm, similar for athletes 17 ± 1 mm ($p = 0.453$) and lower for patients 7 ± 1 mm ($p < 0.001$). SV_{AVPD} for controls was $60 \pm 2\%$. SV_{AVPD} was similar both for athletes $57 \pm 2\%$ ($p = 0.507$) and for patients $67 \pm 4\%$ ($p = 0.237$).

Conclusions: Longitudinal AV-plane displacement is the primary contributor to LV pumping, accounting for about 60% of the stroke volume. Although AVPD is less than half in patients with DCM compared to controls and athletes, the contribution of AVPD to LV function is maintained, which can be explained by the larger short-axis area in the dilated LV.

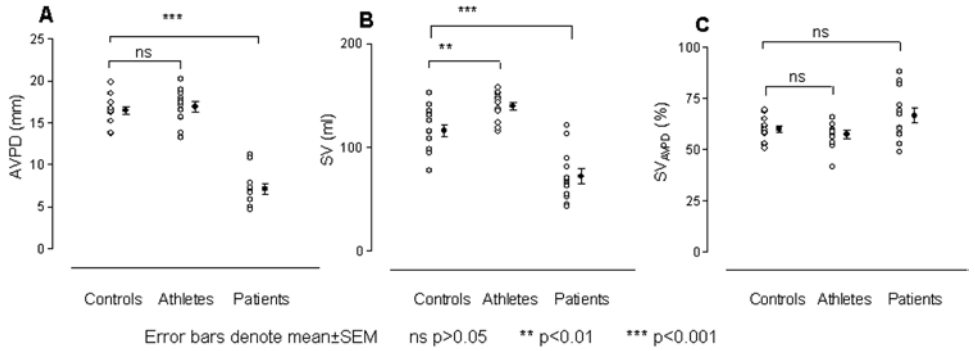

552. MULTIMODALITY IMAGING OF MYOCARDIAL CELL TRANSPLANTATION BY GENETIC LABELING WITH THE HUMAN SODIUM/IODINE SYMPORTER GENE AND MAGNETIC LABELING WITH IRON OXIDES

Takahiro Higuchi,[1] Martina Anton,[2] Sybille Reeder,[1] Katja Ahrens,[2] Bettina Wagner,[1] Marc Huisman,[1] Stephan Nekolla,[1] Markus Schwaiger,[1] Rene Botnar,[1] Frank Bengel.[1] [1]***Nuclear Medicine, Technical University of Munich, Munchen, Germany,*** [2]***Institute of Experimental Oncology and Therapeutic Research, Technical University of Munich, Munchen, Germany.***

Introduction: Intramyocardial progenitor cell transplantation is considered a promising therapy for cardiac regeneration. Multimodality non-invasive imaging may provide answers to unresolved questions concerning cell engraftment and viability.

Purpose: We assessed the feasibility of combined genetic labeling with the human sodium/iodine symporter (hNIS) for PET and magnetic labeling with iron oxides for MRI.

Methods: Human endothelial progenitor cells (EPCs) were transduced with the hNIS gene using a retroviral vector in conjunction with different reporter genes. Gene expression was confirmed by Northern blot and hNIS protein expression by fluorescence activated cell sorter (FACS) analysis. Functionality of the hNIS surface was confirmed by 99 mTc uptake studies. For MRI studies, EPCs were labeled with 50–100 ug of superparamagnetic iron oxides (SPIO) (Resovist, Schering, Berlin) per million cells in the presence of Lipofectin. Intramyocardial injection of 4 million EPCs (8 hNIS positive EPCs, 4 hNIS negative control EPCs) in nude rats was performed following thoracotomy. Both MRI and PET were performed in all rats. MRI was done using a clinical 1.5 T MRI scanner immediately or one day after cell transplantation. One day after cell transplantation, 18.5 MBq of I-124 were administrated via tail vein injection for small animal PET imaging. For localization of the heart, ammonia perfusion PET was performed following the I-124 PET. Subsequently, ex-vivo autoradiograhy and histological examination with Prussian blue stain were performed in a subset of animals.

Results: Gene and protein expression could be confirmed by radiotracer (I-124) uptake in-vivo, thereby demonstrating cell viability and normal cell proliferation capacity after magnetic labeling and myocardial injection. In all animals, iron labeled EPCs were readily detected with MRI at the site of injection and histologically confirmed by Prussian-blue staining. In vivo PET imaging demonstrated the presence of transplanted viable hNIS positive EPCs as a focal myocardial I-124 accumulation being equivalent to postmortem autoradiography. Control hearts with hNIS negative EPCs did not show any focal I-124 accumulations despite MRI confirmed successful cell injections into myocardium. I-124 uptake ratio in transplanted hNIS positive cells (10.5 ± 6.2) was significantly higher than in hNIS negative control cells (1.26 ± 0.25) as measured by autoradiograph ($p < 0.01$).

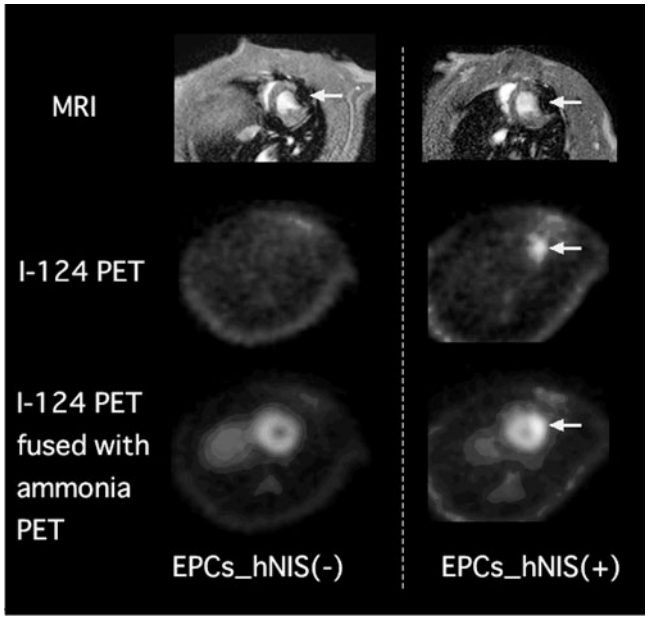

Conclusions: Combination of magnetic and genetic labeling allows for simultaneous non-invasive monitoring of cell localization and viability after myocardial cell transplantation using MRI and PET.

553. LATE ENHANCEMENT OF THE LEFT VENTRICULAR MYOCARDIUM IN PATIENTS WITH AORTIC VALVE STENOSIS AND LEFT VENTRICULAR HYPERTROPHY

Thomas Schlosser, MD, Peter Hunold, MD, Kai Nassenstein, MD, Frank Breuckmann, MD, Nasser Malyar, MD, Jörg Barkhausen, MD. ***University Hospital Essen, Essen, Germany.***

Introduction: Almost a decade ago myocardial late enhancement has been introduced to characterize myocardial damage in patients suffering from coronary artery diseases. Motivated by the promising results several research groups started investigating the late enhancement technique in non-ischemic cardiac disease. Several studies demonstrated that late gadolinium enhancement reflecting myocardial fibrosis can be detected in hypertrophic cardiomyopathy. However, late enhancement in other diseases associated with left ventricular hypertrophy has not been investigated in larger clinical trials so far.

Purpose: Our study aimed to investigate the prevalence of myocardial late enhancement in patients with left ventricular hypertrophy caused by aortic stenosis.

Methods: Fifty patients with known aortic valve stenosis were examined with MRI. Patients with a history of myocardial infarction were excluded from the study. In the remaining 31 patients, a significant coronary artery disease was ruled out by invasive coronary angiography.

In all patients MR imaging was performed on a 1.5 T MR scanner (Magnetom Avanto, Siemens, Erlangen, Germany) using cine SSFP sequences (TrueFISP, TR: 2.9 ms, TE: 1.3 ms, flip angle: 65°) for aortic valve planimetry and the assessment of left ventricular volumes, function and mass. Five contiguous slices (slice thickness: 4 mm) were measured parallel to the aortic valve and manual planimetry was performed on the slice showing the minimum aortic valve area. For the assessment of the left ventricular function and mass 10 to 15 slices (slice thickness: 6 mm, 2 mm gap) were collected. Fifteen min after injection of Gd-DTPA (Schering AG, Berlin, Germany) late enhancement MR imaging was performed using a segmented inversion-recovery gradient-echo sequence (TR: 8 ms; TE: 4.3 ms; flip angle: 25°).

Results: The mean aortic valve area measured by MRI was 0.85 ± 0.2 cm^2. The mean left ventricular mass was 128 ± 24 g/m^2 BSA. In 7 of 31 patients (22%), late enhancement was detected in the left ventricular myocardium mostly in the mid-myocardial basal regions (Fig. 1). The enhancement pattern was patchy and mainly found in the anteroseptal, septal, inferoseptal and lateral wall. In one patient, a diffuse, poorly demarcated enhancement was found in the entire left ventricular myocardium.

Conclusion: In accordance to patients with hypertrophic cardiomyopathy, focal areas of late enhancement can also be observed in about 20% of patients with hypertrophic left ventricles caused by aortic valve stenoses. The areas of late enhancement show a non-ischemic pattern with sparing of the subendocardial region, and are typically located in the basal anterior and anteroseptal segments. Larger studies with long-term follow-up are required to investigate the influence on patients' prognosis.

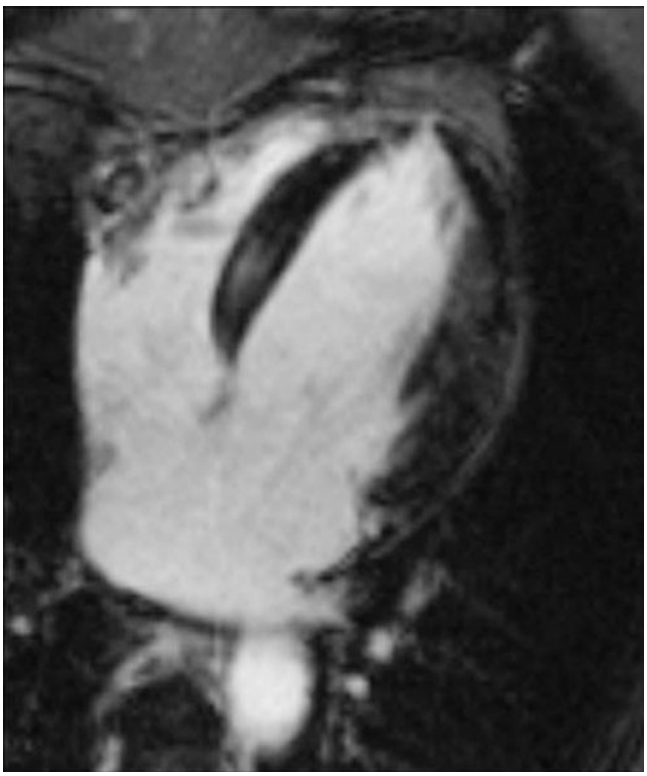

554. HEAT: A DEDICATED SOFTWARE FOR INTEGRATED EVALUATION OF DELAYED ENHANCEMENT AND CINE MRI DATA TO ANALYZE GLOBAL AND REGIONAL REMODELING AFTER ACUTE MYOCARDIAL INFARCTION

Gunnar K. Lund,[1] Dennis Sãring,[2] Stefanie Juchheim,[3] Kai Muellerleile,[4] Martin P. Bansmann,[3] Heinz Handels,[2] Gerhard Adam,[3] Alexander Stork.[3] [1]***Roentgeninstitut, Düsseldorf, Germany,*** [2]***Institut für Medizinische Informatik Zentrum für Experimentelle Medizin, Hamburg, Germany,*** [3]***Klinik für Radiologie, Hamburg, Germany,*** [4]***Klinik für Kardiologie, Hamburg, Germany.***

Introduction: Remodeling frequently occurs after acute myocardial infarction (MI), however, the regional processes, which occur in the border zone of the infarction are not well understood.

Purpose: To develop a Heart Analysis Tool **(HeAT)** for integrated evaluation of delayed enhancement (DE) and cine MRI data for evaluation of global and regional remodeling in patients with myocardial infarction (MI).

Material and Methods: Cine and DE-MRI were obtained in 10 patients at baseline (5 ± 3 days after acute MI) and at follow-up (9 ± 5 months after MI). Corresponding short axis images were acquired from apex to basis on 10–12 slices with an interslice distance of 10 mm. Epi- and endocardial contours were manually traced on cine MRI and automatically transferred to corresponding DE-MR images. A threshold method was used for DE-MRI to delineate only infarcted myocardium, which had a signal intensity $>+2.0$ SD of remote normal myocardium. A centerline method was used for regional analysis of wall motion and of infarct transmurality. The circumference of the LV was subdivided in 100 chords and data for regional wall thickening, diastolic wall-thickness, infarct transmurality and infarct extension are exported to a spread-sheet for graphical display.

Results: Fig. 1 shows the graphical display of regional wall motion analysis using HeAT in a patient with a transmural inferior infarction. At baseline, wall thickening was severely depressed in the infarcted area (light blue curve). At follow-up, wall thickening improved mainly in the border zone of the infarcted region (dark blue curve). The core of the infarction showed no recovery in function. The amount of recovery can be quantified by integration of the area between the two wall motion curves (red shaded area).

Conclusion: HeAT enables regional analysis of wall motion and infarct transmurality using information from cine and DE-MRI. Use of this software will enable to study the regional changes of wall motion and infarct transmurality occurring after AMI. Evaluation of larger number of patients will result in precise description of regional remodeling after AMI.

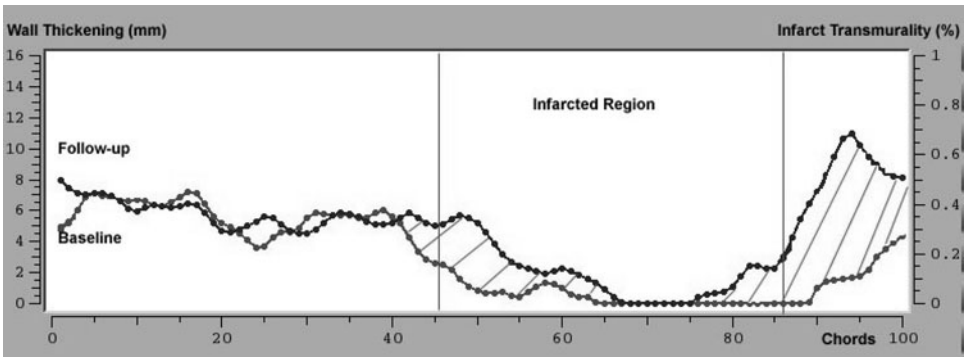

555. MYOCARDIAL FIBROSIS DETECTED BY MRI IS ASSOCIATED WITH VENTRICULAR TACHYARRHYTHMIA IN HYPERTROPHIC CARDIOMYOPATHY

Deboarh Kwon, MD, Randy M. Setser, PhD, Maran Thamilarasan, MD, Srikanth Sola, MD, Paul Schoenhagen, MD, Mario J. Garcia, MD, Harry Lever, MD, Milind Y. Desai, MD. ***Cleveland Clinic Foundation, Cleveland, OH, USA.***

Introduction: Patients with hypertrophic cardiomyopathy (HCM) are predisposed to ventricular tachyarrhythmia (VT). The etiology of VT in such patients is likely due to myocardial fibrosis, myocardial disarray, or small vessel disease. Magnetic resonance imaging (MRI), including delayed hyper-enhancement (DHE) is highly sensitive in measuring left ventricular (LV) myocardial thickness and detecting areas of myocardial fibrosis (scar) (1).

Purpose: We sought to determine the association between LV (and septal) thickness, scar and VT and/or history of sudden cardiac death (SCD).

Methods: Forty-nine patients (mean age 43 $\pm$ 16 years, 65% males) with documented HCM underwent MRI (Siemens 1.5 T scanner, Erlangen, Germany) and Holter monitoring. Maximal regional LV thickness (including septal thickness) was recorded at end-diastole on balanced steady state free precession (TrueFISP) cine images with retrospective ECG-triggering (TE = 1.6 ms, TR = 65 ms, flip angle = 70°, slice thickness = 6 mm (long axis images) or 8–10 mm (short axis images), matrix = 256 X 256). Three short axis delayed hyper-enhancement (DHE-MR) images (8–10 mm thick) were obtained at base, mid LV & apex, ~20 minutes after injection of 0.2 mmol/kg of Gadolinium DTPA (inversion recovery spoiled gradient echo sequence with phase sensitive reconstruction, TE 4 msec, TR 8 msec, flip angle 30°, 23 lines acquired every other RR-interval, slice thickness 8–10 mm). Endocardial and epicardial myocardial edges were manually delineated. Scar was determined semi-automatically (as % of myocardium) using VPT software (Siemens Research) and defined as having intensity >2 SD above viable myocardium. VT was documented on Holter monitoring, along with history of SCD and medication usage.

Results: Two patients had history of SCD, and 5 had VT on Holter monitor. No patients had ventricular fibrillation. Septal hypertrophy (maximal thickness > 1.2 cm) was present in all patients (mean septal thickness 2.4 $\pm$ 0.7 cm). On DHE-MRI, 29 (59%) patients had myocardial scar. Scar was distributed in multiple patchy areas (16 in septum, 14 in inferior wall, 7 in anterior wall and 5 in lateral wall). Concordance between scar location and hypertrophied areas was seen in 76% patients. There was significant correlation between scar % and septal thickness ($r = 0.41$, $p = 0.003$). Patients with VT and/or SCD had significantly higher scar %, compared to those without (16 $\pm$ 14% vs. 6 $\pm$ 7%, $p = 0.01$). On logistic multiple regression (which included scar, septal thickness and use of beta-blockers

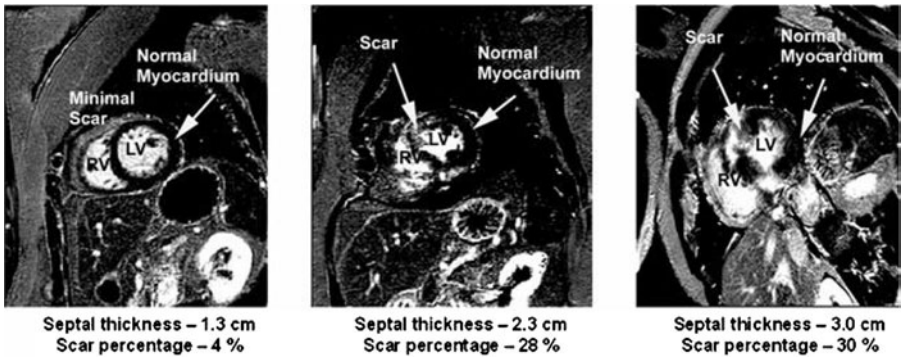

FIG. 1. Correlation between scar percentage and septal thickness on MRI.

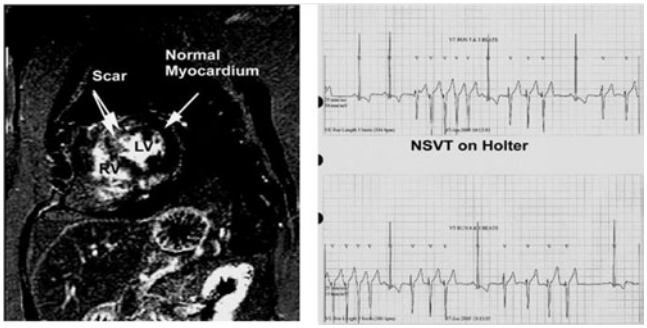

FIG. 2. Extensive myocardial fibrosis on MRI in a patient with NSVT on holter monitoring.

in the model), only the presence of scar was significantly associated with VT and SCD ($p = 0.02$). Septal thickness of 2.3 cm had highest sensitivity and specificity (76% and 70% of detecting myocardial scar on receiver-operating characteristic curve (area under curve 0.78, $p < 0.001$).

Conclusions: In HCM patients, the degree of septal thickness is significantly associated with myocardial scar %. Patient with evidence of VT and/or history of SCD have a significantly higher scar % on DHE-MRI compared to those without. Presence of scar is an independent predictor of VT and/or SCD. Furthermore, septal thickness of >2.3 cm (as opposed to a higher cutoff value) has the highest predictability for presence of scar (and perhaps increased risk of VT/SCD). Further studies are needed to determine if the % and/or myocardial scar location stratifies HCM patients at increased risk for SCD or VT.

REFERENCE

1. Simonetti OP, Kim RJ, Fieno DS, Hillenbrand HB, Wu E, Bundy JM, et al. An improved MR imaging technique for the visualization of myocardial infarction. Radiology 2001;218:215–223.

556. CARDIAC FUNCTIONAL EVALUATION OF CONNEXIN-30 DEFICIENT MICE BY CINE MRI

Frank Kober, PhD,[1] Daniel Gros, PhD,[2] Patrick J. Cozzone, PhD,[1] Monique Bernard, PhD.[1] [1]***Centre de Résonance Magnétique Biologique et Médicale, Marseille, France,*** [2]***Institut de Biologie du Développement de Marseille Luminy, Marseille, France.***

Introduction: Connexin-30 (cx30) has previously been shown to be expressed in the cardiac conduction system of normal mice and to play a role in the coordination of the atrial and ventricular contraction. Cx30lacZ/LacZ mice are deficient in cx30 and might show cardiac alterations induced by partial inhibition of conduction in the sinoatrial and atrioventricular nodes. Even if no expression of cx30 was shown in the left ventricle itself, one could expect that the deficiencies in atrial and ventricular synchronization and function might lead to ventricular adaptation.

In this study, myocardial function and morphology in cx30lacZ/LacZ mice were studied with cineMRI and compared to cx30+/+ mice.

Materials and Methods: Twelve cx30lacZ/LacZ mice underwent a cine MRI protocol at ages ranging from 2 to 4 months. Eleven aged-matched cx30+/+ mice were used as control group.

Experiments were carried out on a 4.7 T horizontal magnet (Bruker Biospec) using a 6 cm diameter volume TX coil and an actively decoupled mouse surface RX coil. Animals were anesthetized with 1.7% isoflurane administered in a continuous flow of oxygen/nitrous oxide (0.5/0.5 L/min) through an adapted nose cone. Heart and breath rates were monitored during the MRI protocol.

Cine MRI was performed in three slices strictly perpendicular to each other and to the long axis of the left ventricle. MRI Parameters were FOV 2.5 × 2.5cm, slice thickness 1.5 mm, matrix 128 × 128, one phase encoding step per cardiac cycle, repetition time (frame rate) 5.1 ms, echo time 1.6 ms.

Left ventricular parameters were determined by manually delineating inner and outer areas on the short axis views and by measuring ventricular inner and outer lengths on the four-chamber long axis view. These measurements were performed in diastole and systole. Inner and outer volumes were calculated using an ellipsoid model, where $V = 2/3\ A\ L$, with A being the respective areas and L the respective lengths.

Statistical comparison was done using Student's t-test, and differences were considered significant when $p < .05$.

Results and Discussion: The table summarizes the different morphologic and functional parameters measured with cine MRI.

LacZ mice had a lower body weight and a higher heart rate compared with the control animals. Absolute volume and function measures were not different between control and LacZ. Relative to body weight, the LacZ mice, however, showed a higher cardiac index and increased end-diastolic volume.

Conclusion: We observed relative cardiac enlargement in connexin-30 LacZ/LacZ mice. However, at least under our experimental conditions, myocardial function was slightly increased in these animals with respect to their weight.

TABLE 1
All values are expressed as means ± SD

	BW (g)	HR (bpm)	EF (%)	EDV/BW (uL/g)	LVW/BW (mg)	SV/BW (uL)	CI mL/g/min
cx30Lacz/Lacz	24 ± 5*	540 ± 55*	67 ± 6	2.8 ± 0.4*	3.9 ± 0.5	1.9 ± 0.3	1.0 ± 0.2*
cx30+/+	28 ± 6	488 ± 59	69 ± 6	2.4 ± 0.4	3.8 ± 0.3	1.7 ± 0.3	0.8 ± 0.2

557. ATHEROSCLEROTIC PLAQUES CONTRAST-ENHANCED MAGNETIC RESONANCE IMAGING IN RABBITS USING GADOCOLETIC ACID TRISODIUM SALT (B-22956)

Jean-Christophe Cornily, Sr, MD, Jean-Christophe Cornily, MD, Fabien Hyafil, Karen C. Briley-Saebo, Juan-Gilberto S. Aguinaldo, MD, Claudia Calcagno, Venkatesh Mani, Zahi A. Fayad. ***Mount Sinai School of Medicine, New York, NY, USA.***

Introduction: Pathological neovascularization of the vessel wall is a constant feature of atherosclerotic plaque development and progression of the disease. Different MRI techniques for plaque neovessel assessment have been described recently: Injection of $\alpha_v\beta_3$-Integrin -targeted, paramagnetic nanoparticles or dynamic contrast-enhanced MRI using conventional gadolinium-based paramagnetic agent.

Purpose: Gadocoletic Acid Trisodium Salt (B-22956) (Bracco Imaging) is a new blood pool contrast agent highly bound to serum albumin. Our main objective was to test B-22956 as a atherosclerotic plaque contrast agent and to determine a model of calculation of plaque partial blood volume (νp), and transfer constant (K^{trans}). Our hypothesis is that B-22956 has an early, strictly intravascular phase allowing a simple determination of the wall partial blood volume[1] (neovessel density) and then, a second phase of slow diffusion through activated plaque endothelium with a transfer constant that correlates to plaque inflammation via macrophage density (2).

Methods and Results: Seven atherosclerotic rabbits and 3 control rabbits underwent MRI (T1 Weighted Fast Spin Echo Sequence) on a 1.5 T system, before and up to 2 hours after Gd-DTPA (100 μmol/kg) IV injection on day one. On day two, pre- and post-contrast (up to 2 hours) after B-22956 (75 μmol/kg) IV injection. Mean Signal to Noise Ratio (SNR) was measured for each plaque on axial image at different time points (before contrast agent injection, 5 mn after injection, 15 mn, 30 mn, 60 mn, 90 mn, 120 mn).

We determined blood and tissue Gadolinium concentrations using calibration curves. Assuming that B-22956 has an early, strictly intravascular phase, νp is directly proportional to the increase in arterial wall intensity measured on the initial T1 Sequence. Applying a two compartment model of contrast agent, $K^{trans} = (Ct(t) - \nu p\, Cp(t))/\int Cp(u)du$. K^{trans} has been calculated 2 hours after injection by applying the following formula:. $K^{trans} = (Ct(2h) - \nu p\, Cp(2h)) / \Delta\, (Cp\ (2h–5\ mn))$.

Immunohistology was performed on each section of aorta using a anti-CD 31 antibody (endothelial cells) and a anti-RAM 11 antibody (macrophages).

T1 high resolution sequences showed a highly significant plaque enhancement 2 hours after B22956 versus Gd-DTPA in the atherosclerotic group (39.75% vs 9.5%, $p < 0.0001$). There was no difference between the 2 compounds in the control group (15% vs 15%, p = ns).

On the 146 aorta segments studied, plaque partial blood volume positively correlates with neovessel density: $r = 0.733$, $p < 0.001$; as well, K^{trans} positively correlates to macrophage density: $r = 0.704$, $p < 0.001$.

Conclusion: B-22956-enhanced MRI improves plaque detection compared to Gd-DTPA. During the early phase after injection, the intravascular properties of B-22956 allows the determination of the plaque partial blood volume using a simple model. Then, B-22956 diffuses from the neo-vessels into the plaque with a transfer constant that is correlated to the macrophage density of the plaque.

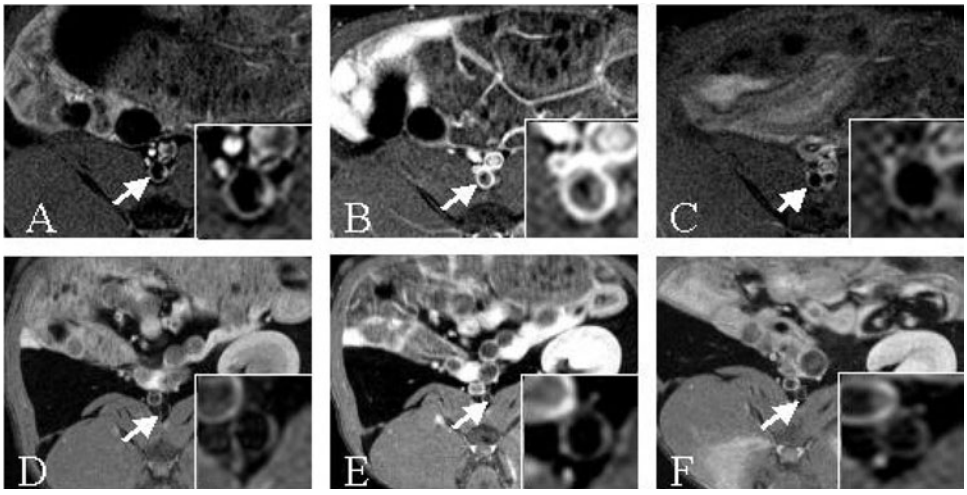

FIG. 1. Axial T1-Weighted MR images of atherosclerotic (*A*, *B*, *C*) and control (*D*, *E*, *F*) rabbit abdominal aortas: Pre contrast imaging (*A*, *D*) and 2 hours after B-22956 (*B*, *E*) or Gd-DTPA (*C*, *F*). *B* shows a strong enhancement of the atherosclerotic plaque 2 hours after B-22956 injection; there is no detectable enhancement after Gd-DTPA; there is no detectable enhancement of the control rabbit's wall after either B-22956 or Gd-DTPA.

REFERENCES

1. Kerwin W, Hooker A, Spilker M, et al: Quantitative magnetic resonance imaging analysis of neovasculature volume in carotid atherosclerotic plaque. Circulation 2003;107:851–6.
2. Kerwin WS, O'Brien KD, Ferguson MS, et al. Inflammation in Carotid Atherosclerotic Plaque: A Dynamic Contrast-enhanced MR Imaging Study. Radiology 2006.

558. COMPARISON OF MRI AND ECG FOR PREDICTION OF MYOCARDIAL FIBROSIS AND VENTRICULAR HYPERTROPHY IN PATIENTS WITH HYPERTROPHIC CARDIOMYOPATHY

Deboarh Kwon, Randy M. Setser, PhD, Maran Thamilarasan, MD, Srikanth Sola, MD, Paul Schoenhagen, MD, Mario J. Garcia, MD, Harry Lever, MD, Milind Y. Desai, MD. ***Cleveland Clinic Foundation, Cleveland, OH, USA.***

Background: On electrocardiography (ECG), presence of pathologic Q-waves in patients with hypertrophic cardiomyopathy (HCM); is thought to be related to myocardial fibrosis (scar) or right/posterior left ventricular hypertrophy (LVH).[1] ECG-criteria for LVH have a reasonable degree of accuracy in prediction of ventricular hypertrophy. Magnetic resonance imaging (MRI) accurately measures LV thickness and is highly sensitive in detecting/localizing myocardial scar and hypertrophy, and is considered to be a gold standard for scar quantification and LV dimension measurement.[2]

Purpose: We sought to determine the accuracy of ECG in predicting and localizing myocardial scar and hypertrophy in HCM patients, using MRI as the gold standard.

Methods: Forty-one patients (mean age 43 ± 17 years, 66% males) with echocardiography (echo)-confirmed HCM had MRI on 1.5T scanner (Siemens Sonata, Erlangen, Germany). Maximal regional LV thickness (including septal thickness) was recorded at end-diastole on balanced steady state free precession (TrueFISP) cine images with retrospective ECG-triggering (TE = 1.6 ms, TR = 65 ms, flip angle = 70°, slice thickness = 6 mm (long axis images) or 8–10 mm (short axis images), matrix = 256 × 256]. Three short axis delayed hyper-enhancement (DHE-MR) images (8–10 mm thick) were obtained at base, mid LV & apex, ~20 minutes after injection of 0.2 mmol/kg of Gadolinium DTPA (inversion recovery spoiled gradient echo sequence with phase sensitive reconstruction, TE 4 ms, TR 8 ms, flip angle 30°, 23 lines acquired every other RR-interval, slice thickness 8–10 mm). Endocardial and epicardial myocardial edges were manually delineated. Scar was determined semi-automatically (as % of myocardium) using VPT software (Siemens Research) and defined as having intensity >2 SD above viable myocardium. On ECG, pathologic Q-waves were defined as 1/3rd the height of QRS & 4 msec in duration in ≥2 contiguous leads. ECG diagnosis of LVH was made by Sokolow-Lyon indices criteria (3).

Results: While 24 patients (59%) had myocardial scar on DHE MRI, only 8(20%) had Q-waves on ECG. Seven out of 8 patients with Q-waves had scar on DHE-MRI. Accuracy of ECG in scar detection (with DHE-MRI as gold-standard) was as follows: 22% sensitivity, 89% specificity, 71% positive predictive value (PV) and 47% negative PV (Fig. 1). ECG demonstrated LVH in 22 patients. MRI noted evidence of hypertrophy in 40 patients. For detection of LVH in these HCM patients, the sensitivity of ECG was 51% and positive PV was 95%. Negative PV and specificity could not be calculated, as there were no true negatives. ECG correctly localized scar and LVH in only 3 and 1 patient(s) respectively. On MRI, the scar was most commonly present in hypertrophied areas of the ventricle (76% cases). Incidentally, in the study population, septal thickness was significantly underestimated by echo compared to MRI (2 vs. 2.4 cm, $p < 0.001$).

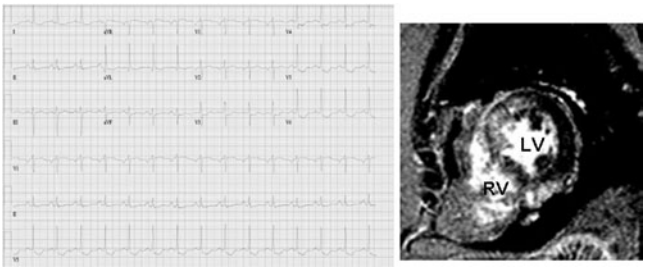

FIG. 1. EKG of HCM patient with no Q waves and corresponding MRI of the same patient demonstrating.

Conclusion: Using MRI as the gold standard, ECG has low accuracy in detection and localization of scar or hypertrophy in patients with HCM. MRI should be considered in HCM patients for precise calculation of ventricular thickness as well as accurate scar quantification. The clinical significance of scar assessment in HCM patients remains to be proven.

REFERENCES

1. Maron B. Q waves in Hypertrophic Cardiomyopathy: A Reassessment. J Am Coll Cardiol 1990;16:375–376.
2. Simonetti OP, Kim RJ, Fieno DS, Hillenbrand HB, Wu E, Bundy JM, et al. An improved MR imaging technique for the visualization of myocardial infarction. Radiology 2001;218:215–223.
3. Mirvis, DM. Electrocardiography: A Physiologic Approach, Mosby, St Louis 1993.

559. IMPROVED SNR IN CINE DENSE USING SPIRAL ACQUISITIONS

Xiaodong Zhong, MS,[1] Bruce S. Spottiswoode, MS,[2] Craig H. Meyer, PhD,[1] Frederick H. Epstein, PhD.[3] [1]***Department of Biomedical Engineering, University of Virginia, Charlottesville, VA, USA,*** [2]***MRC/UCT Medical Imaging Research Unit, University of Cape Town, Cape Town, South Africa,*** [3]***Department of Biomedical Engineering and Radiology, University of Virginia, Charlottesville, VA, USA.***

Introduction: Displacement encoding with stimulated echoes (DENSE) is a quantitative myocardial wall motion imaging technique that encodes tissue displacement into the phase of the stimulated echo (1). Two-dimensional (2D) cine-DENSE provides a time series of pixel-wise displacement and strain measurements for the myocardium through the cardiac cycle. Previous implementations of breathhold cine DENSE have employed a rectilinear bottom-up echo-planar k-space trajectory for rapid data sampling (2). Because stimulated echoes sacrifice half of the available signal, spatial and temporal resolution in cine DENSE are generally limited by signal-to-noise ratio (SNR).

Purpose: To improve SNR in cine DENSE by sampling the stimulated echo using a spiral k-space trajectory.

Methods: All studies were performed on a 1.5T MRI system (Avanto, Siemens Medical Solutions, Germany). An ECG-gated cine DENSE sequence that uses complementary spatial modulation of magnetization for artifact suppression and echo planar imaging (EPI) for data acquisition was modified to use a spiral k-space trajectory (3). The spiral gradient waveforms were designed with a maximum amplitude of 8.00 mT/m to meet the desired specifications. Single-shot images with two different TEs were acquired for each slice and at each cardiac phase to estimate field maps. The image reconstruction was performed on-line using gridding and linear inhomogeneity compensation. For cine DENSE with an EPI readout, the EPI readout gradient waveform was modified using the flyback technique to reduce flow and ghosting artifacts (4). In accordance with protocols approved by our institutional review board, and with informed consent, 6 healthy volunteers were imaged using both sequences. Whenever possible, identical parameters were used for both sequences, including pixel size $= 2.81 \times 2.81$ mm^2, slice thickness $= 8$ mm, flip angle $= 15^\circ$, TR $= 17$ ms, total imaging heartbeats $= 16$, and cardiac phases $= 22$. Also, both sequences used displacement encoding frequency $= 0.1$ cycles/mm, through-plane dephasing frequency $= 0.8$ cycles/mm for improved artifact suppression (5), and fat suppression pulses applied prior to the displacement-encoding pulses (6). Other parameters for spiral included TE $= 1.9$ ms, number of interleaves $= 10$, interleaves scanned per heartbeat $= 2$, and total sampling time per image $= 112$ ms. Other parameters for EPI included TE $=$ 8.9 ms, ETL $= 9$, segments $= 18$, and total sampling time per image $= 74$ ms. Lagrangian displacement and strain maps were calculated for all cine DENSE images as described in (7). The SNR of both sequences was calculated using the magnitude-reconstructed images.

Results: Example short-axis Lagrangian displacement and strain maps at end systole acquired using spiral cine DENSE are shown in Fig. 1(A) and Fig. 1(B), respectively. SNR results summarized for all 6 volunteers as a function of cardiac phase are shown in Fig. 1(C), where the SNR of spiral increases by about 34% at early cardiac phases and about 67% at late cardiac phases compared to EPI. Approximately 20% of the SNR difference is attributed to the difference in sampling time, with the remaining difference attributed to shorter TE.

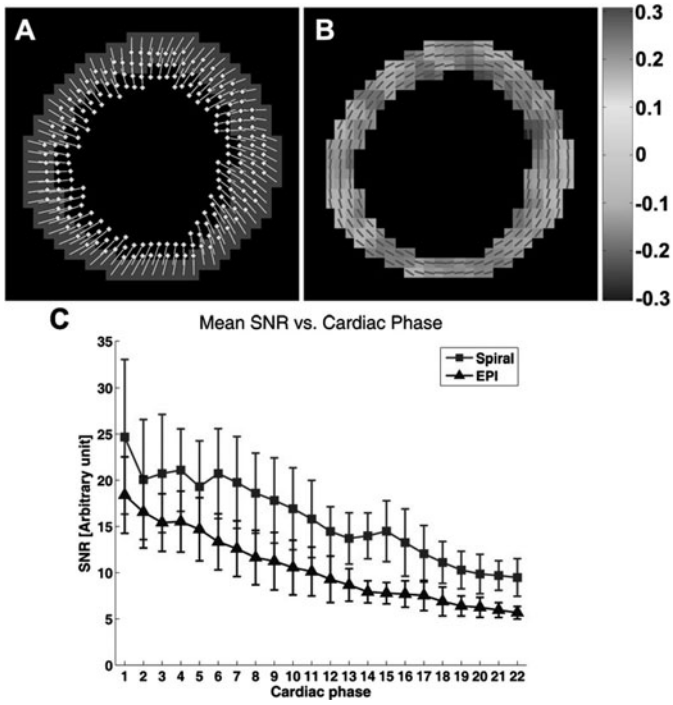

FIG. 1. (A) Lagrangian displacement map at end systole, where the line tail represents the position of the myocardium element at the beginning of the cardiac cycle (end diastole), and the line head represents the current position of this element. (B) Lagrangian second principal strain map at end systole, where the bar represents the strain direction. (C) Mean SNR of spiral and EPI cine DENSE as a function of cardiac phase for 6 volunteers.

Conclusions: The use of a spiral k-space trajectory for data acquisition in cine DENSE improves SNR compared to bottom-up flyback EPI. Because (a) fat suppression can be applied once per heartbeat before application of the displacement-encoding pulses (6), (b) TE is reduced, and (c) data are acquired efficiently, a spiral k-space trajectory may be advantageous for cine DENSE.

1. Aletras, et al. JMR 1999;137:247–252.
2. Kim, et al. Radiology 2004;230:862–871.
3. Meyer. Spiral Echo-Planar Imaging . In: Echo-Planar Imaging: Theory, Technique, and Application, eds. 1998.
4. Kim, et al. MRM 2003;50:813–820.
5. Zhong, et al. MRM 2006; in press.
6. Fahmy, et al. JCMR 2005;7:524.
7. Spottiswoode, et al. IEEE-TMI; in press.

560. WALL MOTION AND SIGNAL ABNORMALITIES IN RIGHT VENTRICULAR WALL DETECTED BY MRI ARE ASSOCIATED WITH HIGHER INCIDENCE OF VENTRICULAR TACHYCARDIA IN PATIENTS WITH FREQUENT PVCs WITH LBBB MORPHOLOGY AND INFERIOR AXIS.

Giovanni Donato Aquaro, MD,[1] Strata Elisabetta, MD,[1] Gianluca Di Bella, MD,[2] Daniele De Marchi, TSRM,[1]

Emanuele Grassedonio, MD,[3] Alessandro Pingitore, MD, PhD,[1] Massimo Lombardi, MD.[1] [1] *Institute of Clinical Physiology, pisa, Italy,* [2] *University of Messina, Messina, Italy,* [3] *University of Palermo, Palermo, Italy.*

Introduction: Premature ventricular complexes (PVCs) with left bundle branch block morphology (LBBB)and inferior axis can be a manifestation of Idiopathic Right Ventricular Tachycardia or Arrhythmogenic Right Ventricular Cardiomyopathy (ARVC). Magnetic Resonance (MR) is the ideal imaging technique to perform this differential diagnosis.

Purpose: To evaluate the incidence of right ventricular (RV) abnormalities in patients with frequent PVCs of LBBB morphology and inferior axis and without other pre-existing criteria for ARVC.

Methods: We enrolled 396 patients (258 male, mean age, 35 years) with frequent PVCs (> 2000 in 24 h) of LBBB morphology and inferior axis, exercise test negative for ischemia, a normal echocardiogram, a normal rest 12-leads ECG. All the patients underwent CMR examination. Right and left ventricular (LV) wall motion and volumes were evaluated with short axis cine images (30 phases for slice) from mitral valve plane to the apex (thickness 8 mm, no gap between slices). Regional right wall motion (WM) was also evaluated in axial cine images acquired from diaphragm to right ventricular outflow tract (thickness 5 mm, no gap between slices). Cine image were acquired using a SSFP pulse sequence (FIESTA). T1-weighted Fast Spin Echo images in the same short axis and axial slices were also acquired. Right ventricle WM was classified as normal, hypokynetic, akinetic, and bulging. Signal from right ventricular wall was classified: no alteration (grade 0); minor alteration (grade 1): abnormalities without complete agreement between three independent investigators; alteration compatible with fat infiltration (grade 2): abnormalities with full agreement between the investigators.

Results: In 117 (29.5%) patients RV abnormalities were found (RVA group), 279 (70.5%) patients showed no RV abnormalities (no-RVA group) (Fig. 1). Thirty (7.5%) patients had signal grade 2 combined with major WM abnormalities (akinetic or bulging).

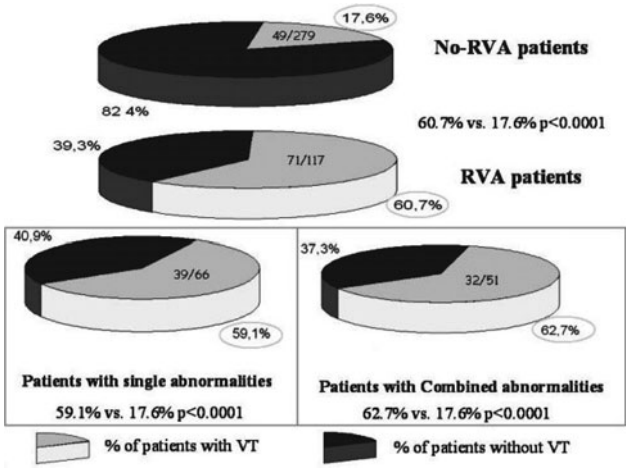

WM RV abnormalities were found in 97 (24%) patients, 12 (3%) showed WM abnormalities in left ventricle not detected by previous echocardiogram. In 71 (17.9%) patients signal abnormalities were found: grade 1 in 27 (6.8%), grade 2 in 44 (11.1%). Two patients (0.51%) had fat infiltration in LV wall. No differences between RVA and no-RVA group were found about the number of PVCs, couplet or triplet at holter monitoring. In 120 (30.3%) patients episode of ventricular tachycardia (VT), mostly non-sustained VT (96%), were recorded . RVA group showed higher incidence of VT than no-RVA group (17.6% vs 60.7% , $p < 0.0001$, Fig. 1). RVA group showed also higher REDVi than no-RVA group (84.5 ± 16.4 vs 77.8 ± 15.7 mL/m^2 $p < 0.0008$). Significant higher incidence of VT and higher RV volumes were found in the two subgroup (patients with single and with combined abnormalities) when compared with the no-RVA group (Table).

Conclusions: Combined major WM and signal abnormalities, allowing a diagnosis of ARVC, were found in less than 8% of patients. The "grey zone" of patients with single abnormalities or combined minor abnormalities can be distinguished from no-RVA group because of initial structural change in right ventricle and higher incidence of VT.

TABLE 1
Main results

	No-RVA group	RVA	Single abnormalities	Combined abnormalities
Patients	279 (70.5%)	117 (29.5%)	66 (16.7%)	51 (12.8%)
RVEDVi (mL/m^2)	77.8 ± 15.7	84.5 ± 16.4 $p < 0.0008$	86.6 ± 17.5 $p < 0.0002$	84.2 ± 15.9 $p < 0.002$
RVESVi (mL/m^2)	30.8 ± 9.1	34.1 ± 11.3 $p < 0.0008$	35.2 ± 11.4 $p < 0.005$	33.5 ± 11.6 $p < 0.005$
LV mass index (g/m^2)	67.8 ± 12.8	73.8 ± 14 $p < 0.002$	74.3 ± 13.4 $p < 0.001$	73 ± 14.9 $p < 0.05$
Septal thickness (mm)	9.1 ± 1.5	9.6 ± 2.2 $p < 0.05$	9.3 ± 2.3 n.s.	10 ± 2.2 $p < 0.01$
RV EDD (mm)	35.9 ± 5.6	44.7 ± 7.6 $p < 0.0001$	44.7 ± 7.1 $p < 0.0001$	45.2 ± 8.1 $p < 0.0001$
RV ESD (mm)	24.2 ± 4.4	31.1 ± 8.6 $p < 0.0001$	30.1 ± 7.1 $p < 0.0001$	32.6 ± 10 $p < 0.0001$
LV EDD (mm)	49.2 ± 4.4	51.1 ± 6.1 $p < 0.03$	51.3 ± 6.2 $p < 0.03$	50.3 ± 5.9 n.s.
Ventricular Tachycardia	49/279 (17.6%)	71/117 (60.7%) $p < 0.0001$	39/66 (59.1%) $p < 0.0001$	32/51 (62.7%) $p < 0.0001$

561. EVALUATION OF AORTIC VALVULAR STENOSIS WITH MAGNETIC RESONANCE IMAGING: A COMPARATIVE STUDY WITH ECHOCARDIOGRAM AND CARDIAC CATHETERIZATION

Aloha Meave, MD,[1] Martha Hernández-González, MD,[2] Maria Elena Soto, MD,[1] Nilda Espinola-Zavaleta, MD,[1] Silvia Siu, MD,[1] Sergio Solorio, MD,[2] Carlos Sierra, MD,[1] José Antonio Talayero, MD,[1] Patricio Cruz, MD,[1] Erick Alexanderson, MD.[1] [1]***Instituto Nacional de Cardiologia, Mexico D.F., Mexico,*** [2]***Unit of Clinical Epidemiology, Medical Unit of High Speciality 1, Mexican Institute of Social Security, León, Guanajuato, Mexico.***

Introduction: Evaluation of severity and extent of myocardial damage in aortic stenosis (AS) is necessary before valve replacement. Transthoracic echocardiography (TTE) has been used as the noninvasive method of choice for evaluation of the hemodynamic behavior of the disease, despite inter and intraobserver variability. Cardiac Catheterization (CC) is the gold standard for the assessment of hemodynamic and functional repercussion of this valvulopathy. Recently cardiac magnetic resonance (CMR) has become an alternative for diagnosis and can potentially evaluate valve morphology, stenosis degree, transvalvular gradient and left ventricular function.

Purpose: Compare CMR, TTE and CC in the study of patients with pure aortic valvular stenosis.

Methods: Twenty-one patients with AS were included in this study. TTE, CC and CMR were performed to all patients. We compared the results obtained by these methods using Pearson, Spearman and Bland-Altman statistical analysis.

Results: Similar measures of peak gradients were made with all methods (52.5 mm Hg $\pm$ 27.7 with CC, 53.3 mm Hg $\pm$ 23.2 with TTE and 44.7 mm Hg $\pm$ 12.2 with CMR) Spearman r was used for comparing peak gradients measurements; the r obtained for CC compared with CMR and CC with TTE was the same: 0.90, $p < 0.001$. According to Bland-Antman analysis, CMR underestimates and TTE overestimates the peak gradient. Aortic valve area calculated with CMR correlates better with CC than TTE (Spearman r 0.89, $p < 0.01$ vs 0.67 $p < 0.01$). In Bland-Antman analysis, CMR/CC has a better agreement than CC/TTE in the assessment of left ventricle ejection fraction. CMR diagnosed six subjects with bicuspid aortic valve; only one was identified with TTE and none with CC.

Conclusions: CMR is a useful non invasive diagnostic method for the evaluation of patients with aortic valve stenosis when compared with TTE and CC. The best morphologic assessment was done with CMR when compared with the other methods.

562. CMR EVALUATION IN PATIENTS WITH HIGH GRADE VENTRICULAR ARRHYTHMIAS

Luigi Natale, MD, Agostino Meduri, MD, Stefano Palmucci, MD, Donatella Brisinda, MD, Fenici Riccardo, MD, Lorenzo Bonomo, MD. ***Catholic University of Sacred Heart, Rome, Italy.***

Introduction: High grade venticular arrhythmias are life-threatening conditions whose causes are difficult to discover.

Purpose: To assess by cardiac MR the prevalence of myocardial alterations in arrhythmic patients.

Methods: We examined 43 patients with non ischemic ventricular arrhythmias. Premature ventricular complexes had left bundle branch block morphology (LBBB) in 29 cases, in 7 a right bundle branch block contour (RBBB) and 7 had polymorphic patterns (PV). US was negative in 78.4% of patients, while CMR was negative in only 13% of patients.Studies were performed on a 1.5 MR scanner with Cine sequences (Fastcard or FIESTA), bb-FSE and IR-prep FGRE 15 minutes after injection of 0.2 mmol/Kg of Gd-DTPA.

Results: CMR found a high prevalence of morphological, signal intensity and functional myocardial abnormalities. RV dilatation was found in 85% of patients with PV arrhytmias, 48.3% of patients with LBBB morphology, 12.5% of patients with RBBB morphology. LV dilatation was present in 28.6%, 25% and 24.1% of patients with LBBB, PV and RBBB type arrhytmias respectively. RV wall motion abnormalities were identified in 50% and 36.7% of patients with PV and LBBB pattern respectively; LV wall motion abnormalities in 25% and 10.3% of patients with PV and LBBB pattern, respectively. Free wall RV signal/thickness abnormalities were found in 23.3% of patients (18.6% with LBBB pattern and 4.7 with PV pattern); LV signal abnormalities were found in 11.6% of patients(9.3% with LBBB pattern and 2.3% with PV pattern). Seven patients underwent myocardial biopsy: 5 positive for myocarditis, 1 positive for ARVD, one had a negative biopsy.

*Conclusions:*In patients with primary ventricular arrhythmias MR documented high prevalence (87%) of morphological, signal intensity and wall motion abnormalities even with negative echocardiogram.

563. A NOVEL RADIO-OPAQUE BARIUM/ALGINATE MICROENCAPSULATION TECHNIQUE FOR ALLOGENEIC MESENHYMAL STEM CELL DELIVERY AND LOCALIZATION

K. M. Cosby,[1] L.V. Hofmann,[3] B.P. Barnett,[1] D.A. Kedziorek,[1] W. Gilson,[1] G. Korosoglou,[1] G. Huang,[1] JWM Bulte,[1,2] D.L. Kraitchman.[1] [1]***Russell H. Morgan Department of Radiology and Radiological Science,*** [2]***The Institute for Cell Engineering, Johns Hopkins University School of Medicine, Baltimore, MD,*** [3]***Stanford University, Palo Alto, CA.***

Introduction: Stem cell therapy for the treatment of ischemic heart and peripheral arterial disease (PAD) has produced limited results. In part, due to the inability to localize stem cells and

rapid cellular destruction. The development of new techniques that circumvent these limitations would enhance the efficacy of cellular therapy and improve the quality of life for many.

Purpose: We have developed a novel modification of alginate cellular encapsulation method employing Barium sulfate, which enables direct localization of mesenchymal stem cell (MSCs) with x-ray fluoroscopy. The properties of Alginate when cross-linked with poly-cations Calcium and Barium produce a composite capsule ideal for visualization and immuno-protection following cellular transplantation. This study will assess MSCs viability after encapsulation to determine the clinical utility for allogeneic stem cell delivery in PAD.

Methods: Protanal HF alginate (2.0%), Barium sulfate (10% w/v), and Poly-L-lysine (0.05%) were used to fabricate Xcaps on the order of 200–400 μm. The alginate was purified via a 0.2 μm and 0.45 μm pore-size filters and 10 mM HEPES was used to maintain a constant pH of 7.4. Allogeneic bone marrow derived rabbit MSCs were encapsulated with the purified alginate and allowed to gel in a 100 mM calcium chloride bath via an electrostatic droplet generator method. A rabbit endovascular model of hind limb ischemia was used with platinum coils to occlude the superficial femoral artery (SFA). Female rabbits were randomized to receive 5000 Xcaps (n = 5), Xcaps w/o MSCs (n = 5), naked MSCs (n = 1), or sham (n = 2) divided into 6 injections in the medial thigh compartment at 24 hours post-occlusion. Xcaps visibility and immunoprotection were assessed via x-ray fluoroscopy and histology. In vitro MSCs viability was assessed with confocal microscopy.

Results: MSCs viability was 70–80% at day 1 and remained at 50–60% after 1 week following encapsulation. Xcaps injection site were visible at 2 weeks in all 10 rabbits on X-ray and post-mortem, suggesting a feasible means for long-term tracking. There were no significant adverse effects (fibrotic overgrowth) noted at injection sites following 2 weeks of implantation.

Conclusion: We report the design and synthesis of a novel microencapsulation technique, which allows direct visualization and tracking of MSCs for the treatment of PAD. This cellular delivery system could also reduce the need for immunosuppressive agents, which may mute the response of MSCs. Given our present results, we believe that continued advancement of this technology is warranted.

564. FRACTIONATED FERUMOXIDE FOR *IN VIVO* IMAGING OF ATHEROSCLEROSIS

Karen C. Briley-Saebo, PhD, Venkatesh Mani, PhD, Fabien Hyafil, MD, Jean-Christophe Cornilly, PhD, Zahi A. Fayad, PhD. ***Mount Sinai School of Medicine, New York, NY, USA.***

Introduction: Macrophages are believed to be important in the progression of atherosclerotic plaque. Vulnerable plaques (or plaques prone to rupture) have been characterized by high intraplaque macrophage density. As a result, there is a need for the development of molecular imaging agents that are able to target functionalized intraplaque macrophages. Ultrasmall iron oxide particles (USPIOs) have been used to target intraplaque macrophages. For dextran based USPIOs, such as Combidex (also known as Sinerem/AMI-227/ferumoxtran) intraplaque macrophage uptake is modulated by particle size. Pre-clinical studies have indicated that macrophage uptake is increased as the size of the particle is reduced. Enhanced macrophage uptake is critical so that the dose of USPIO and time point of imaging after injection may be reduced. Currently, Combidex is administered at high dosages (20–56 mg Fe/kg) and is MR imaged at late time points (3–5 days post injection).

Purpose: The aim of the current study was to test the efficacy of fractionated Ferumoxide for macrophage uptake using atherosclerotic rabbits.

Methods: The USPIO was prepared by vacuum filtration of Ferumoxide (Feridex/AMI-25) through a 25 nm pore. The mean hydrated particle size was determined at 25°C using laser light scattering. Longitudinal (r_1) and transverse (r_2) relaxivities were determined using a Bruker Minispec operating at 60 MHz and 40°C. T_1 NMRD profiles were obtained in aqueous solution at 25°C (NIH, Bethesda MD).

The blood half-life and liver uptake was evaluated in NZW rabbits (3.2–3.6 kg) following administration of a 4.6 mg Fe/kg dose. Blood was collected at 7 times points post injection, and the half-life determined based upon T_1 values in blood. The liver was excised 44 hours post injection (n = 3) and the percent-injected dose in the liver was determined using established methods.

Balloon injury in the aorta was performed on NWZ rabbits (3.2–3.4 Kg). After injury the rabbits were placed on a high cholesterol diet for 4 months. Animals were administered either

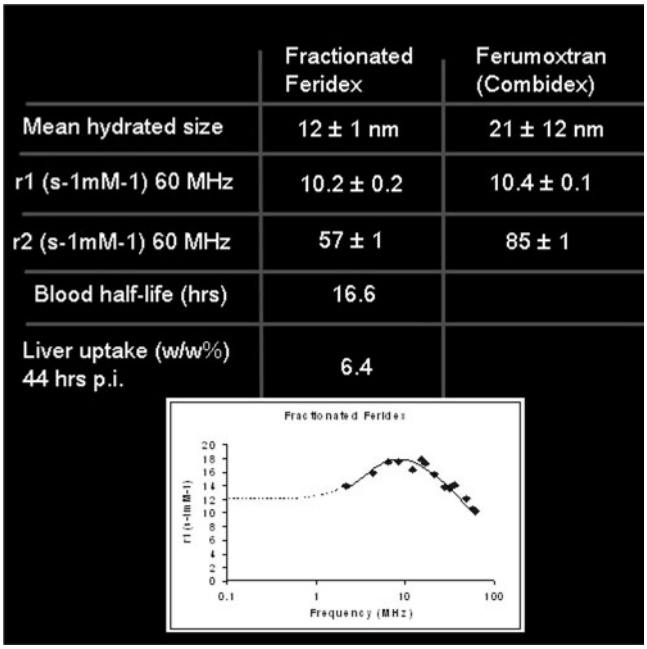

FIG. 1. Summary of physcial and chemical properties.

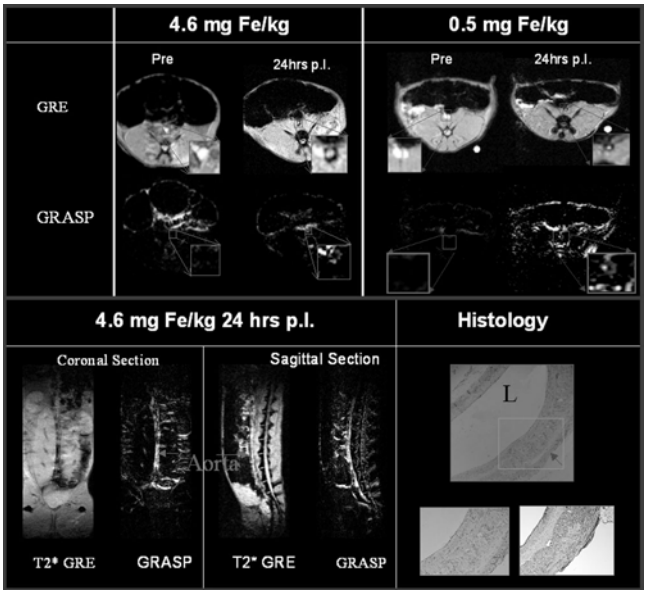

FIG. 2. Coronal and sagittal view of the aorta 24 hours post injection. Location for histology indicated by orange arrow. L reflects the position of the lumen.

0.5 mg Fe/kg (n = 1) or 4.7 mg Fe/Kg (n = 3) of fractionated Ferumoxide via i.v. injection into the ear vein. One control rabbit (non-injured) was administered the high dose. Imaging was performed using a conventional GRE sequence at 1.5T (TR/TE/flip = 300 ms/5 – 20 ms/90°, NEX = 1, FOV = 2.5 cm × 2.5 cm, and pixel size = 0.97 × 0.97 × 5 mm^3). The positive contrast technique (GRASP), which allows for the generation of positive signal in the presence of iron oxide particles, was also performed. After imaging, the aorta was removed, fixed and stained for iron using Perls Prussian Blue.

Results: Figure 1 summarizes the physical and chemical properties of fractionated Ferumoxide relative to other iron oxide particles. The MR imaging showed a dose dependent signal loss using conventional GRE sequences as shown in Fig. 2. Even at low dose, significant signal loss was observed that correlated well with histology. No enhancement of the vessel wall was observed in control non-injured rabbits. The GRASP sequence was able to generate positive signal enhancement in regions that correlated with signal loss by GRE and in regions containing iron-laden macrophages (by histology) as shown in Fig. 2.

Conclusions: Fractionated Ferumoxide shows in vivo macrophage uptake at clinically relevant dosages (<5 mg Fe/kg) and time points post injection (within 24 hours). This method may, therefore, prove to be useful for macrophage density characterization in atherosclerotic plaque.

565. PREVENTING HEART RUPTURE DURING TOPICAL NEGATIVE PRESSURE VAC THERAPY: ASSESSMENT OF A RIGID BARRIER OR PRESSURE TRANSDUCTION TO THE BOTTOM OF THE WOUND BY REAL TIME MRI

Martin Ugander, MD, PhD,[1] Rainer Petzina, MD,[1] Arash Mokhtari, MD,[1] Henrik Engblom, MD,[1] Roland Hetzer, MD,[2] Richard Ingemansson, MD, PhD,[1] Hakan Arheden, MD, PhD,[1] Malin Malmsjo, MD, PhD.[1] [1]***Lund University Hospital, Lund, Sweden,*** [2]***Berlin Heart Center, Berlin, Germany.***

Introduction: Heart rupture is a devastating complication to topical negative pressure therapy (VAC) of mediastinitis following cardiac surgery. However, little is known about the macroscopic effects of VAC therapy on the intrathoracic anatomy.

Purpose: To examine the effect of negative pressure application on the heart using real time MRI in a porcine sternotomy wound model.

Methods: Six pigs underwent median sternotomy. Real time MRI (1.5 T Philips Intera, balanced fast field echo sequence, TR 2.7 ms, TE 1.4 ms, spatial resolution 1.4 × 1.4 × 10 mm, 10 images/s) was performed in a midventricular transverse and a midsagittal plane during the application of 125 mm Hg negative pressure. Imaging was performed after the insertion of two different devices: a roughly 10 × 20 × 0.2 cm perforated plastic rigid barrier placed inside the thorax between the heart and the sternal edges and an open porous structure material (1 cm thick) was placed underneath the heart with preserved communication to the intersternal foam to facilitate pressure transduction to the bottom of the wound.

Results: Two potentially hazardous events were observed during the application of negative pressure. First, the anterior portion of the right ventricular free wall was sucked up towards the anterior thoracic wall and bulged into the space between the sternal edges, and then the sharp edges of the sternum jutted into and deformed the anterior surface of the heart. These events were prevented by the application of either of the two devices described above.

Conclusions: Inserting a rigid barrier prevents the heart from being sucked up into or deformed by the sternal edges. Pressure transduction to the bottom of the wound seems to hinder the heart from being sucked up into the intersternal space and against the sharp sternal edges. These two approaches may help avoid heart rupture. These events were observable for the first time by using real time MRI. Previously unknown mechanisms for heart rupture and the prevention thereof have been revealed in this study.

566. INTERCENTRE REPRODUCIBILITY OF THE BREATH-HOLD T2 TECHNIQUE FOR MYOCARDIAL IRON MEASUREMENT IN THALASSEMIA

Taigang He, PhD, Paul Kirk, MD, Mark A. Tanner, MD, Peter D. Gatehouse, Ph.D., Dudley J. Pennell, MD, David N. Firmin, PhD. ***Royal Brompton Hospital and Imperial College London, London, United Kingdom.***

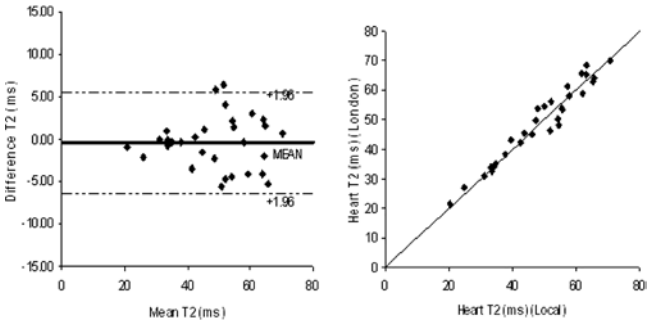

FIG. 1. Intercentre reproducibility of the T2 measurements for all of the 30 subjects: Bland-Altman plot and scatter plot with the line of identity.

Purpose: To assess the intercentre reproducibility of the developed breath-hold T2 sequence for myocardial iron measurement and its transferability to different MRI scanners.

Introduction: The measurement of cardiac iron is essential for preventing disease and managing iron-chelating treatment in thalassemia patients. Previously, a T2* technique has been developed and clinically validated for this purpose (1, 2). A more recent study has shown that the T2 technique also allows non-invasive and reproducible quantification of myocardial iron (3). Unlike T2*, T2 is unaffected by problems such as local susceptibility artifacts and, hence, has the potential to provide additional useful information in conjunction with T2* analysis. Although the interstudy reproducibility of this T2 technique was reported (3), challenges include its validation across multiple sites of different countries.

Methods: The breath-hold black blood spin echo T2 sequence (3) was installed and validated on three 1.5 T Siemens MRI scanners at different centres. Scans were synchronized to the cardiac cycle using standard ECG gating, and images were acquired during late diastole at a single slice oriented to give a short axis view of the left ventricle. The sequence parameters were the following: 10 mm slice thickness, field of view (FOV) was 40 cm with in-plane rotation applied to reduce the phase encoding FOV in order to keep the scan time to an acceptable duration. Other parameters were: turbo factor 3, 12 effective TE images (TE = 4.8–163.2 ms in 14.4 ms steps), and a 128 * 64 matrix.

Scanner details were as follows: Site 1, Siemens Sonata (Hong Kong, China), Site 2, Siemens Avanto (Philadelphia, USA), Site 3 Siemens Avanto (Singapore). Ten thalassemia patients were scanned at each individual site. All 30 patients (mean age 32 $\pm$ 8 years) were subsequently re-scanned at the standardization centre (Siemens Sonata, London, UK) within 1 month of their local site scans. The study was approved by the local ethics committee and all patients gave informed consent.

Results: The T2 sequence was successfully implemented on three different scanners. Myocardial T2 values ranged from 20 ms to 71 ms (48 $\pm$ 13 ms). The mean difference between T2 values at the standardization London centre and visited sites was 0.43 ms. The coefficient of variation for inter reproducibility was 6.3% (Fig. 1).

Conclusion: This study has demonstrated the good intercentre reproducibility of the breath-hold T2 technique between 1.5T MR scanners at different sites across different countries. We believe that this can provide additional reference data for the quantification of myocardial iron and has important clinical implications. These findings suggest the potential to transfer this technique worldwide to improve the diagnosis and monitor the treatment of patients with iron overload conditions such as thalassaemia.

ACKNOWLEDGEMENT

This work was supported by NIH Grant: R01 DK66084-01.

REFERENCES

1. Anderson LJ, et al. Eur Heart J 2001;22:2171–2179.
2. Westwood M, et al. J Magn Reson Imag 2003;18:33–39.
3. He T, et al. J Magn Reson Imaging 2006;24:580–585.

567. B0 AND B1-INSENSITIVE SATURATION PULSE FOR QUANTITATIVE FIRST-PASS MYOCARDIAL PERFUSION MRI AT 3T*

Daniel Kim, Oded Gonen, Leon Axel. ***New York University, New York, NY, USA.***

Introduction: Quantitative, first-pass myocardial perfusion MRI is a promising modality for the assessment of coronary artery disease. Performing perfusion MRI at 3T provides a means to increase the signal-to-noise ratio (SNR), due to the approximately two times greater magnetization available at 3T than at 1.5T. However, the static magnetic field (B_0) and transmit radiofrequency field (B_1) inhomogeneities, as well as dielectric effects, are greater at 3T than at 1.5T. These factors pose a greater challenge to perform accurate T1-weighting using a saturation pulse at 3T than at 1.5T. While a composite B_1-insensitive rotation (BIR-4) (1) pulse has been shown to effectively saturate the magnetization in the heart at 1.5T (2), its effectiveness has not been validated at 3T. The purposes of this study were to evaluate and compare the effectiveness of the BIR-4 saturation pulse against the conventional saturation pulse at 3T.

Methods: Pulse Sequence: The single and BIR-4 saturation pulses were implemented on a 3T whole-body MR scanner (Trio; Siemens) equipped with an 8-channel phased array RF coil. The durations for the single and BIR-4 pulses were 2 ms and 8.2 ms, respectively. The two saturation pulses were compared using a TurboFLASH pulse sequence with identical imaging parameters, including: field of view = 340 $\times$ 255 mm, acquisition matrix = 192 $\times$ 108, in-plane resolution = 1.77 $\times$ 2.36 mm, slice thickness = 8 mm, TE/TR = 1.1/2.45 ms, TD = 12 ms, image acquisition time = 133 ms, flip angle = 10°, TSENSE (3) parallel imaging acceleration factor = 2, and bandwidth = 740 Hz/pixel. The disturbed recovery time between the end of TD and immediately before the acquisition of the center of k-space was 66.2 ms. Image acquisition was repeated for 10 heart

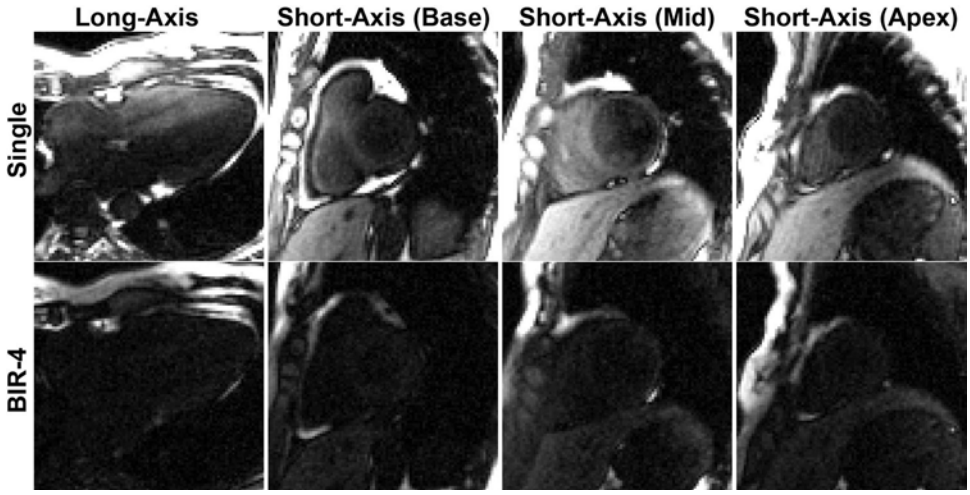

FIG. 1. Representative non-contrast images of the heart comparing the effectiveness of the single (top row) and BIR-4 (bottom row) pulses at 3T. Images are displayed with identical grayscales (0-40 a.u.)

beats in order to average images across repetition. The manufacturer's standard RF calibration was performed prior to the image acquisition.

Phantom Imaging: Phantoms with T1 values of 19, 49, 148, 291, 495, 778, 1130, 1610 ms were imaged, with electrocardiogram gating simulated with the heart rate set to 60 beats per minute. For analysis, the ten repeatedly acquired images were averaged. The mean signal of intensities was calculated for each region of interest (ROI). The relative difference between the mean signal (Single vs. BIR-4) was calculated for each ROI.

Non-Contrast Cardiac Imaging: Five healthy human subjects were imaged in 3 short-axis (apical, mid-ventricular, basal) and 1 long-axis views of the heart. For each saturation pulse, ten repeated acquisitions were acquired within a breath-hold duration of 10 heartbeats. For analysis, the ten repeatedly acquired images were averaged. The mean signal of intensities was first calculated for each ROI (left ventricle) per slice, and then the mean and standard deviation were calculated across ROIs ($n = 20$ total).

Results: The relative difference in signal intensity was negligible for T1 of 19ms but large for T1 $>$ 50 ms (Table 1). Fig. 1 shows representative non-contrast, saturation-recovery cardiac images comparing the effectiveness of magnetization saturation between the single and BIR-4 pulses. The mean left ventricular signal was 135.9% higher for the single pulse than for the BIR-4 pulse (12.6 ± 4.3 vs. 5.3 ± 0.7; $p < 0.001$).

Discussion: This study demonstrates that a single saturation pulse can yield significant signal errors for T1 $>$ 50 ms and that a BIR-4 pulse can be used to perform accurate T1-weighting for quantitative first-pass myocardial perfusion MRI at 3T.

**This abstract has been withdrawn.*

TABLE 1
Comparison of mean signal intensities of T1 phantoms between the single and BIR-4 saturation pulses at 3T.

T1 (ms)	Single Pulse (a.u.)	BIR-4 Pulse (a.u.)	Relative Difference (%)
19	203.6	202.9	0.3
49	200.0	190.0	5.1
148	122.4	100.7	21.5
291	91.5	57.0	60.4
495	69.2	26.8	158.7
778	47.1	18.7	152.2
1130	36.9	14.1	162.2
1610	36.5	10.6	244.2

REFERENCES

1. Staewen RS, et al. Investigative Radiology 1990;25:559–567.
2. Kim D, et al. Magn Reson Med 2005;54:1423–1429.
3. Kellman P, et al. Magn Reson Med 45:846–852.

568. THE ROLE OF KERNEL-BASED METHOD FOR PREDICTIVE CARDIAC MOTION MODELING

Qian Wu, Guang-zhong Yang. ***Imperial College, London, United Kingdom.***

Introduction: Respiratory motion compensation is essential for high resolution cardiac imaging. Subject specific respiratory patterns are a significant problem for motion management in *in vivo* imaging. Existing research has shown that *a priori* subject-specific physiological motion modeling combined with low-dimensional real-time sensing is possible to provide effective deformation prediction. The technique proposed by Ablitt et al. (1) relies on multiple input traces to capture intrinsic patterns of surface deformation in relation to cardiac deformation by partial least squares regression (PLSR). However, PLSR is fundamentally a linear technique. Because of the complexity of the myocardial motion, it is possible that a nonlinear relationship can exist between the measured respiratory traces and

the deformation of the heart. This paper compares PLSR and its kernel-based implementation [2] for extracting the intrinsic relationships between respiratory induced cardiac deformation and real-time surface traces. *In vivo* results show that compared to linear prediction, kernel-based method can improve the overall prediction accuracy.

Method: Kernel-based regression technique is to first map the input space into a high dimensional space by a non-linear mapping function and then construct a linear regression model in that space. The implementation of the nonlinear form of PLSR depends on the kernel function without the explicit computation of the non-linear mapping function.

To examine the effect of the kernel-based technique for motion prediction, data from ten normal subjects acquired from a Siemens Sonata 1.5T MR scanner were used. A segmented 3D TrueFISP sequence was used to acquire short-axis image volumes in free breathing with navigator-echoes and over-sampling. The imaging parameters used include an RF flip angle of 65°, in plane matrix size of 256 × 102, pixel size of 1.56 mm × 2.70 mm × 8.78 mm, and FOV of 400 mm × 275 mm × 123 mm. The 3D stack comprised 14 short axis slices from the valve plane to the apex throughout the full respiratory range. For each subject, a total of six or seven volumes covering different respiratory positions from end-inspiration to end-expiration were created. Leave-one-out cross-validation was used to assess the prediction accuracy. In this study, Gaussian kernel was chosen.

Results: The normalized predictive errors from PLSR and kernel-based PLSR for the ten subjects studied are shown in Fig. 1. It is evident that kernel-based PLSR has introduced a marked reduction of the averaged prediction error compared to the linear approach. The figure also reveals the fact that a nonlinear predictive model can better describe the intrinsic relationship between respiratory induced cardiac deformation and the surface traces.

Conclusion: In this paper, PLSR and its kernel-based implementation are used to extract the intrinsic relationships between respiration induced cardiac deformation and real-time surface traces. Their relative performance of predicting the implicit deformation model is validated on ten *in vivo* data sets. Compared to linear prediction, the results from this study have shown that kernel-based method can improve the overall prediction accuracy, and thus is better suited for extracting the underlying subject specific respiratory pattern.

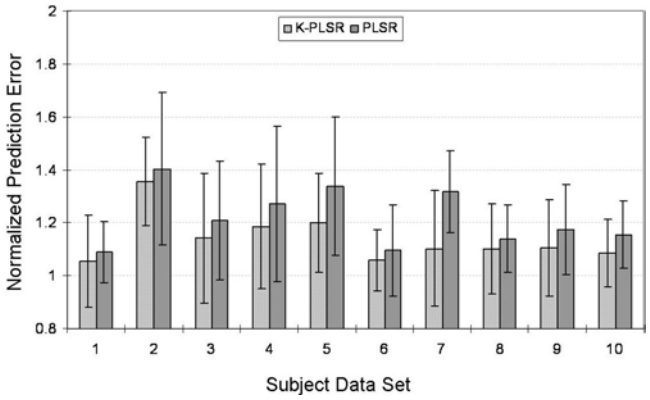

FIG. 1.

REFERENCES

1. Ablitt N, Gao J, Keegan J, Stegger L, Firmin DN, Yang GZ. Predictive Cardiac Motion Modeling and Correction with Partial Least Squares Regression. IEEE Trans Med Imag 2004;23:1315–1324.
2. Rosipal R, Trejo LJ. Kernel Partial Least Squares Regression in Reproducing Kernel Hilbert Space. Journal of Machine Learning Research 2001;2:97–123.

569. MRI STUDY IN ISOLATED LEFT VENTRICULAR NONCOMPACTION

Levente Toth,[1] Akos Varga-Szemes,[1] Reka Faludi,[1] Attila Toth,[2] Lajos Papp,[1] Tamas Simor.[1] [1]***Heart Institute, Pecs, Hungary,*** [2]***Semmelweis University, Budapest, Hungary.***

Introduction: Isolated left ventricular noncompaction (ILVNC) is still an unclassified cardiomyopathy having an unknown prevalence. Our first aim was to evaluate the occurrence of ILVNC in the population of patients (pts) referred for MRI in Hungary. The correlation between the extent of noncompaction and LV function parameters has not been studied using MRI. Thus, our second aim was to determine the correlation between the extent of noncompaction and LV function parameters.

Methods: Total number of cardiac MRI studies in Hungary from 2003 till 2005 was 2867. ILVNC was found only in 39 pts (1.4%, 26 male, mean age: 49.8 ± 16 years, 13 female mean age: 49.8 ± 18 years). The familial form was found in 10 pts (3 families). The diagnosis of ILVNC was already established in 29 pts (74.4%), while using echocardiography and the diagnosis was strengthened using MRI. In 10 pts (25.6%), however, the diagnosis was established only by MRI and not detected by ECHO. The extent of noncompaction was studied in the 17 segments model. Noncompaction was established if the ratio of noncompacted/compacted thickness in end-systole was larger, then 2. EDV, ESV, SV, LVM and their BSA normalised values and EF was measured using MASS 6.1 (Medis, The Netherlands) software.

Results: Four, 12 and 23 ILVNC pts were studied in 2003, 2004 and 2005, respectively. The average number of noncompacted segments per pts was 6.8 ± 2.5 (3–13), and an increased number was found in the cases having familial forms (8.5 ± 3.2). The ratio of noncompacted and compacted thickness was 2.77 ± 0.72. Positive correlation was found between the extent of noncompaction and EDV ($R = 0.324$), EDV/BSA ($R = 0.321$), ESV ($R = 0.352$), ESV/BSA ($R = 0.346$), IT ($R = 0.335$), IT/BSA ($R = 0.357$) parameters. EF and the extent of noncompaction, however, showed a negative correlation ($R = -0.343$).

Conclusions: Increased occurrence of ILVNC was found from 2003 till 2005. The sensitivity of cardiac MRI detecting noncompaction was higher as compared to ECHO. The number

of noncompacted segments was increased in proportion with the values of EDV and ESV indicating the higher risk of increased number of heart failure and sudden cardiac death. The morphological extent of the disease in the LV wall was higher in the familial forms of ILVNC, and thus a worse prognosis might be indicated in this group.

570. PHASE SENSITIVE IMAGING OF INVERSION TAGS FOR IMPROVED CNR AND TAG LONGEVITY

J. Andrew Derbyshire, PhD,[1] Smita Sampath, PhD,[1] Maria J. Ledesma-Carbayo, PhD,[2] Elliot R. McVeigh, PhD.[1] ***[1]LCE, NHLBI, NIH, Bethesda, MD, USA, [2]ETSI Telecomunicacion, Universidad Politecnica de Madrid, Madrid, Spain.***

Introduction: Quantitative regional function is often assessed using tagged, segmented k-space imaging. A well-defined pattern of tag-lines is introduced into the magnetization by application of a tagging preparation sequence (e.g., SPAMM) at the R-wave under ECG synchronization, to be tracked either visually or by post-processing.

Typically, the tagging preparation generates saturated bands of magnetization (i.e., total tagging flip angle is approximately 90 degrees). In principle, improved dynamic range, tagging contrast and, therefore, better longevity throughout the cardiac cycle can be achieved by using tagging preparations that invert the magnetization (i.e., total tagging flip angle: 180 degrees). However, inversion is seldom performed because the longitudinal recovery of the DC magnetization and the rectification of the inverted spins during standard magnitude reconstruction confound the interpretation of the tagging pattern.

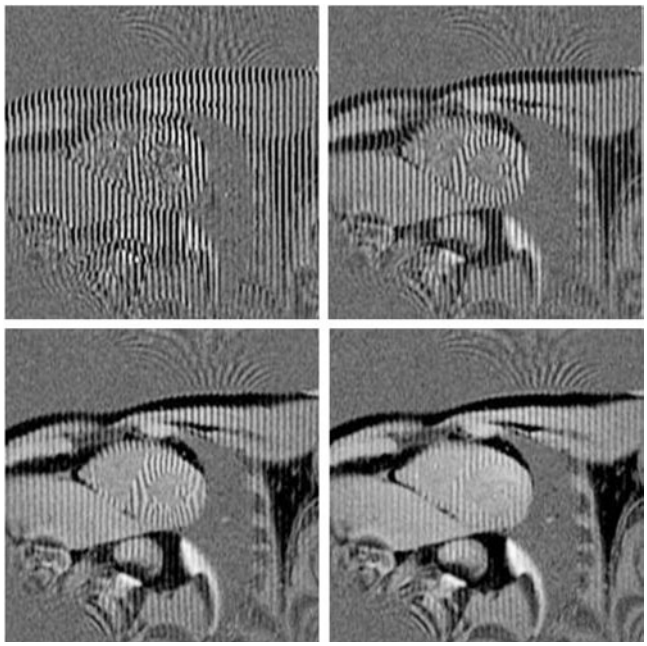

FIG. 1.

Here, we propose and demonstrate the use of fully inverted magnetization in combination with phase sensitive reconstruction of the MRI data acquired using a balanced SSFP imaging sequence employing a ramped flip angle acquisition.

Methods: CMR imaging was performed using a 1.5T Siemens Espree scanner (Siemens Medical Solutions, Erlangen, Germany) equipped with gradient coils rated for amplitudes of 33 mT/m and slew rates of 100 T/m/s. A gated, sequential, multiphase 2D balanced-SSFP ramped-flip-angle imaging sequence with a 90-90 SPAMM tagging preparation was employed. At the end of the 80% R-R acquisition window, the flip angle was ramped down to zero to allow for magnetization recovery.

All in-vivo studies were approved by the IRB of the NHLBI, with informed consent from all subjects. Data was obtained from 5 normal healthy (no prior history of cardiac disease or chest pain) volunteers of age 30–50 and heart rates within the range of 45 – 80 bpm. Typical imaging parameters were: 6 mm tag separation; 300×300 mm imaging FOV; 256×130 acquisition matrix; TE/TR = 5.0/2.5 ms; 5 mm slice thickness; and 5 TRs-per-segment for a temporal resolution of 25 ms.

Phase sensitive reconstruction was performed separately for each receiver coil. A phase reference data set was obtained by applying a 2D Fermi-filter to the k-space data to select only the DC-peak, suppressing the tagging peaks, followed by Fourier transformation to provide low-resolution, untagged images. A rectangular ROI over the heart was identified from which zero and first-order (gradient) phase estimates were found using a linear phase estimation algorithm. This 2D linear phase model served as a phase-reference for the main reconstruction by Fourier transforming the full k-space datasets and removing the linear phase. The corresponding images from each receiver coil were then combined in a phase-sensitive fashion using a magnitude squared weighting for each receiver at each pixel.

Results: Example images obtained by the sequence using conventional magnitude reconstruction and phase sensitive reconstruction are shown in Fig. 1.

Discussion: Note that the early cardiac phases have very small DC signal (due to the use of 90-90 SPAMM tagging), so a single phase reference was used based on the latter 50% of the cardiac cycle. The phase reference map is simply a 2D linear function over the cardiac region, extended to the entire image. No problems were found from using a non-temporally varying phase correction.

While CSPAMM tagging also employs inversion tags, the problem of the DC-peak is removed by performing a 2-step phase cycle of the tagging sequence, requiring twice the imaging (and therefore breath-hold) time of a conventional tagged sequence. The phase sensitive reconstruction method presented here has an acquisition time equal to that of a conventional tagged imaging sequence.

Conclusions: The use of phase sensitive imaging of inversion tags was demonstrated. The method provided well-resolved tags with excellent contrast from onset and throughout an acquisition window of 80% of the cardiac cycle.

571. ATHEROSCLEROSIS AND INFLAMMATION: CORRELATION BETWEEN DYNAMIC CONTRAST ENHANCED MRI PERFUSION PARAMETERS AND PLAQUE NEOVASCULARIZATION IN ATHEROSCLEROTIC RABBITS

Claudia Calcagno, MD,[1] Jean-Christophe Cornily, MD,[1] Fabien Hyafil, MD,[1] Venkatesh Mani, PhD,[1] Karen Briley-Saeboe, PhD,[1] William S. Kerwin, PhD,[2] Zahi A. Fayad, PhD.[1] [1]***Mount Sinai School of Medicine, New York, NY, USA,*** [2]***University of Washington, Seattle, WA, USA.***

Introduction: Atherosclerotic plaque inflammation has been shown to correlate with high-risk disease (1). Previous reports showed a relationship between inflammation and neovessel density, thus indicating that the extent of neovascularization can assess the risk of the atherosclerotic lesion (1). Furthermore it has been shown that plaque perfusion parameters evaluated by bright blood Dynamic Contrast Enhanced (DCE) MRI correlate with plaque neovessels density (2, 3). Bright blood techniques have important advantages while studying plaque perfusion, but might not allow clear vessel wall visualization during injection. Black blood DCE-MRI might allow for better delineation of vessel wall after contrast agent arrival. In this study we correlated plaque perfusion parameters calculated from black blood DCE-MRI with neovascularization in the abdominal aorta of 6 atherosclerotic New Zealand White rabbits.

Methods: Atherosclerosis Induction: New Zealand White rabbits 3–4 months old were fed an atherogenic diet for 5 weeks (1% cholesterol, 6% peanut oil) and then shifted to normal-chow diet for 8 weeks. After the first week, lesion formation was accelerated in the abdominal aorta by baloon-induced injury using a 4F Fogarty embolectomy catheter.

MR Imaging: All animals were imaged approximately 14 weeks after diet initiation in a 1.5 T clinical system (Siemens, Sonata) after sedation with Ketamine/Xylazine. One location per animal was imaged by DCE-MRI (Black Blood Double Inversion Recovery TSE sequence, TE = 5.6, TR = 250, slice thickness = 3 mm, matrix size = 256 × 256, time resolution = 4.8 s, number of images = 150). After the 5th image, 0.2 mmol/Kg of Gd-DTPA were injected at a rate of 2 mL/s followed by saline flush.

Histological analysis: Following MRI, rabbits were euthanized. Aortas were excised, fixed in 4% Para formaldehyde and embedded in paraffin. Five μm thick slices were sectioned and stained with hematoxylin-eosin. An additional section from each location was stained with antiCD31 antibody for neovessels identification. Using a magnification of X 40, neovessels were manually counted in plaque and adventitia; plaque and total neovessels density were calculated.

DCE-MRI Parameters: Semi-quantitative pixel-by-pixel maps of Blood Volume (BV) and Blood Flow (BF) were calculated. BV was calculated as the area under the signal intensity versus time curve (AUC), while BF was calculated as the first moment of the AUC. A single region of interest covering the whole plaque was selected. Average values of BV and BF in the ROI were extracted and correlated to plaque and total neovessel counts using Pearson's test.

Results: Statistical analyses showed positive correlation between plaque neovessels count and both contrast agent DCE-MRI parameters blood volume and blood flow. Correlation between blood volume and plaque neovessels count was strong and significant ($p < 0.05$; $R = 0.858$). Blood volume positively correlated with the total neovessels count ($R = 0.8$, $p = 0.56$). None of the parameters correlated with the neovessels count in the adventitia (Table 1).

Conclusions: The correlation found in this study between perfusion parameters extracted from black blood DCE-MRI and neovessels count in plaques confirms that black blood DCE-MRI is able to reproduce the results previously reported by

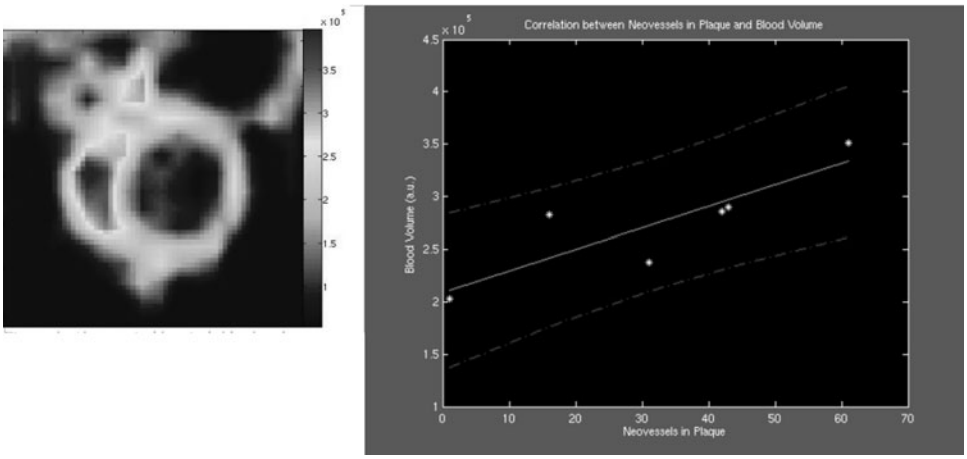

FIG. 1. Above pixel-by-pixel blood volume map detailed view of the aorta of one representative rabbit values are represented in colorscale of a.u. Hot colors represent higher values, while cold colors represent lower values. Right: correlation between blood volume and neovessels count in plaque. Yellow stars: corresponding values of BV and neovessels count. Green: regression line. Red: 95% confidence intervals.

TABLE 1
Correlation parameters between DCE-MRI and histology

	Neovessels in Plaque	Neovessels in Adventitia	Total Neovessels
Blood Volume	R = 0.858 (p = 0.029)	R = 0.186 (p = 0.724)	R = 0.8 (p = 0.56)
Blood Flow	R = 0.755 (p = 0.082)	R = -0.13 (p = 0.981)	R = 0.627 (p = 0.183)

other researchers with the use of bright blood DCE-MRI of atherosclerotic plaques (2, 3). Furthermore, the results reported in this study confirm the role of DCE-MRI in the noninvasive evaluation of plaque inflammatory burden and the high-risk plaque.

REFERENCES

1. Moreno PR, Purushothaman KR, Zias E, Sanz J, Fuster V. Neovascularization in human atherosclerosis. Curr Mol Med 2006;6:457–77.
2. Kerwin WL, Hooker A, Spilker M, Vicini P, Ferguson M, Hatsukami T, et al. Quantitative magnetic resonance imaging analysis of neovasculature volume in carotid atherosclerotic plaque. Circulation 2003;107:851–6.
3. Kerwin WS, O'Brien KD, Ferguson MS, Polissar N, Hatsukami TS, Yuan C. Inflammation in Carotid Atherosclerotic Plaque: A Dynamic Contrast-enhanced MR Imaging Study. Radiology 2006.

572. VAC THERAPY OF A STERNOTOMY WOUND INDUCES AN INCREASE IN WOUND EDGE TISSUE FLUID CONTENT WHILE BLOOD FLOW IN THE MAMMARY ARTERY IS UNALTERED—ASSESSMENT WITH MRI

Rainer Petzina, MD,[1] Martin Ugander, MD, PhD,[1] Henrik Engblom, MD,[1] Roland Hetzer, MD,[2] Richard Ingemansson, MD. PhD.[1] Hakan Arheden, MD, PhD,[1] Malin Malmsjo, MD, PhD.[1] [1]***Lund University Hospital, Lund, Sweden,*** [2]***Berlin Heart Center, Berlin, Germany.***

Introduction: Cardiac surgery is complicated by poststernotomy mediastinitis in 1% to 5% of all procedures and this complication has a mortality of up to 25%. Vacuum assisted closure (VAC) therapy has recently been introduced and effectively reduced mortality to 0%. The mechanisms by which negative pressure facilitate wound healing are to a large extent unknown.

Purpose: To investigate the effects of VAC therapy on the fluid content in the wound edge and the mammary artery blood flow.

Methods: A sternotomy wound was treated with VAC therapy, at a negative pressure of 125 mm Hg, in eight pigs (50 kg). Quantitative assessment of sternal bone marrow and pectoral muscle tissue properties (0–10 mm from the wound edge) was undertaken in a transverse plane at the midventricular level using a T2-weighted short tau inversion recovery (STIR) sequence. Quantification was undertaken as the signal intensity ratio between a given tissue and remote skeletal muscle. Flow in the contralateral internal mammary artery was measured using a velocity encoded gradient echo sequence in a transverse plane at the midventricular level, bisecting the artery. Data are presented as mean ± SEM.

Results: VAC elicited an immediate increase in the STIR signal intensity ratio in the sternal bone marrow (before: 1.3 ± 0.1, at 4 minutes: 2.3 ± 0.3, p = 0.002), and a tendency towards increase in the pectoral skeletal muscle (before: 0.9 ± 0.1, at 4 minutes: 1.2 ± 0.2, p = 0.19). The increase in the sternum came immediately, leveled off after 4 minutes and remained unchanged for the ensuing 40 minutes. The blood flow in the internal mammary artery was similar before and after application of negative pressure (n = 5, before: 37 ± 10 mL/min, after one minute: 36 ± 12 mL/min, p = 1.0).

Conclusions: VAC therapy increases wound edge tissue fluid content. Presumably VAC causes a pressure gradient which may draw fluid from the surrounding tissue to the sternal wound edge which is possibly drained into the vacuum source. This might be one of the mechanism by which VAC facilitates wound healing. VAC application does not alter blood flow in the internal mammary artery and thus does not appear to influence the change in sternal bone marrow fluid content.

573. REPRODUCIBILITY OF RIGHT VENTRICULAR MASS AND VOLUMES IN PATIENTS WITH PULMONARY HYPERTENSION

William Bradlow, Niall Keenan, Raad Mohiaddin. ***Royal Brompton Hospital, London, United Kingdom.***

Introduction: Right ventricular (RV) mass and volume measurements by CMR have been proposed as endpoints in trials of new drug therapy in pulmonary hypertension (PH). While RV reproducibility has been studied previously in the PH population, the historical sequences used limit current relevance. Contemporary sequences have been used in similar work in patients with heart failure, left ventricular hypertrophy and repaired tetralogy of Fallot but not this population.

TABLE 1
Coefficient of Variation for RV Measurements

Measure	Coefficient of Variation (%)
Mass	5.1
EDV	2.2
ESV	2.0
SV	8.9
EF	2.0

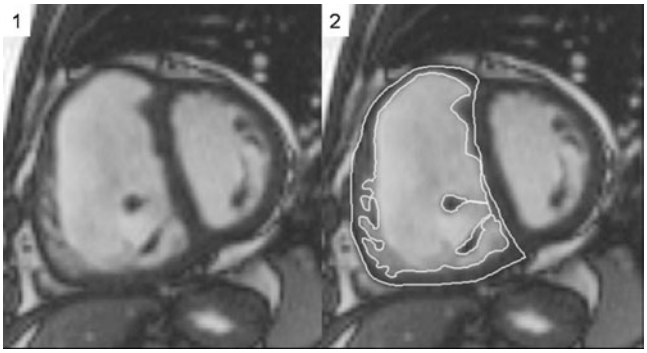

Purpose: Our aim was to define reproducibility in this group.

Methods: SSFP cines were acquired in 10 PH patients (7 females; 3 males, mean age; 45.1 ± 18.3 years, eight pulmonary arterial hypertension; two chronic thromboembolic disease). All patients were in sinus rhythm. The first frame of the four chamber cine served to guide short axis slice prescription. The basal slice was located immediately distal to both anterior and posterior atrioventricular grooves and the contiguous stack completed once the apex was cleared to ensure complete biventricular coverage. Simpson's rule was employed in standard fashion to provide volumetric and mass data for the RV. The septomarginal trabeculation, marginal band and non-uniformities on the RV side of the septum were considered part of the RV myocardium and excluded from the blood pool (Fig.; (1) without and (2) with contours). Analysis was performed on two separate occasions by the same observer to give intraobserver variability.

Results: Coefficient of variation (calculated by dividing the standard deviation of the differences between two observations by their mean and expressing the result as a percentage) are shown for each measurement in the Table.

Conclusions: Despite the complex and unpredictable nature with which the RV hypertrophies and dilates in PH, this work demonstrates that acceptable intraobserver reproducibility is achievable for all RV measurements with experienced observers. On this basis, potential changes in the RV can be discriminated with this technique.

574. VALUE OF CARDIOVASCULAR MAGNETIC RESONANCE IN THE ASSESSMENT OF COMPLEX CONGENITAL HEART DISEASE: A COMPARATIVE STUDY WITH TRANSTHORACIC ECHOCARDIOGRAPHY

Aloha Meave, MD,[1] Erick Alexanderson, MD,[1] Martha Hernández-González, MD,[2] Julio Ermenger, MD,[1] Clara Vázquez, MD,[1] Sergio Solorio, MD,[2] Carlos Sierra, MD,[1] Patricio Cruz, MD,[1] José Antonio Talayero, MD,[1] Alfonso Buendía, MD.[1] [1] *Instituto Nacional de Cardiologia, Mexico D.F., Mexico,* [2] *Unit of Clinical Epidemiology, Medical Unit of High Speciality 1, Mexican Institute of Social Security, León, Guanajuato, Mexico.*

Introduction: Multiple non-invasive imaging techniques have been used in the morphologic and physiologic assessment of complex congenital heart disease. For this purpose, echocardiography is the non-invasive method most commonly used. Recently, Cardiac Magnetic Resonance (CMR) has become an excellent non-invasive technique for the morphologic and functional evaluation of multiple heart diseases.

Purpose: Evaluate the utility of CMR in the morphologic study of complex congenital heart disease compared with transthoracic echocardiography (TTE).

Methods: Forty-five pediatric patients with clinical suspicion of severe congenital cardiopathy were included in this study. A CMR and TTE were performed in all patients and the anatomy and size of cardiac chambers assessed with both methods were compared. Descriptive statistics and Bland-Antman test was used to analyze concordance between methods. *Results:* There were no significant differences in the measurements obtained with both techniques, except for the left ventricle ejection fraction (66.56% ± 9.47 with TTE vs. 52.32% ± 13.85 with CVMR, $p>0.01$) and the diameter of the left branch of the pulmonary artery (9.77 mm ± 6.80 with TTE vs. 13.83 mm ± 8.46 with CVMR, $p = 0.05$). The sensitivity, specificity, positive predictive value and negative predictive value of CMR were superior in the analysis of atrioventricular and ventriculoarterial connection. There was a good concordance of ejection fraction measures, McGoon index, and size of the right ventricle when assessed with CVMR and TTE.

Conclusions: CMR is superior to TTE in the study of extracardiac structures and equally precise in the morphologic and functional assessment of patients with complex congenital heart disease.

575. VISUAL SEMIQUANTITIVE ASSESSMENT OF DELAYED ENHANCEMENT (DE) AND FIRST PASS (FP) PERFUSION DEFECTS: CORRELATION WITH PLANIMETRIC DATA AND GLOBAL FUNCTIONAL OUTCOME AT FOLLOW UP

Luigi Natale, Antonio Bernardini, MD, Agostino Meduri, MD, Antonella Lombardo, MD, Filippo Crea, MD, Lorenzo Bonomo, MD. *Catholic University of Sacred Heart, Rome, Italy.*

Introduction: MRI DE has a strong correlation with infarct size (IS) determined in autoptic studies. Exact "planimetric" IS quantification is time-consuming, requiring ROIs tracing on several images using dedicated software.

Purpose: To use a semiquantitative method to quantify IS and FP and to correlate these data with planimetric measures and global functional indexes assessed 4–6 months after infarction.

Methods: Twenty-two patients with reperfused AMI underwent MRI within 7 days to assess global and regional function

and perfusion. FIESTA for contractile function, FGRET for first pass and IR-prep-FGRE sequences for DE were obtained.

A dose of 0.1 mmol/Kg Gd-DTPA was injected at 3 mL/sec for FP study, immediately followed by equivalent dose for DE.

Additional 4 patients with chronic infarction were studied with the same protocol. Twenty-four patients were studied after 4–6 months to assess functional recovery. FP and DE were scored on a visual scale, based on number of segments involved and on transmural extent (FP-Score, DE-Score), then compared with planimetric-FP and DE measurements, expressed as percentage of myocardial mass.

Results: DE Score had good correlation with planimetric-DE ($R = 0.68$, $p < 0.001$), often underestimating IS in larger infarcts (mean difference -3.4 ± 21). FP score had less strong correlation with planimetric-FP ($R = 0.46$, $p = 0.015$), overestimating small defects (mean difference 4.9 ± 15).

At follow up, DE Score had significant correlation with global function (EDV:$R = 0.75$; ESV:$R = 0.67$; EF:$R = -0.54$) even accounting for initial volumes (EDV:beta $= 0.46$; ESV:beta $= 0.46$; EF:beta $= -0.6$. $p < 0.05$).

FP-score didn't show any significant correlation.

Conclusion: Visual semiquantitative assessment of DE is feasible and has good correlation with global function at follow-up.

576. NON-LINEAR POWER LOSS DURING EXERCISE IN SINGLE VENTRICLE PATIENTS AFTER THE FONTAN-INSIGHTS FROM COMPUTATIONAL FLUID DYNAMICS

Kevin K. Whitehead, MD, PhD,[1] Kerem Pekkan, PhD,[2] Hiroumi Kitajima, MS,[2] Stephen M. Paridon, MD,[1] Mark A. Fogel, MD,[1] Ajit P. Yoganathan, PhD.[3] [1]***Children's Hospital of Philadelphia, Philadlephia, PA, USA,*** [2]***Georgia Institute of Technology, Atlanta, GA, USA,*** [3]***Georgia Institute of Technology and Emory University, Atlanta, GA, USA.***

Introduction: We have previously demonstrated that power loss (PL) through the total cavopulmonary connection (TCPC) in single ventricle patients having undergone a modified Fontan operation can be calculated by computational fluid dynamic (CFD) analysis using 3-D MRI anatomic reconstructions. PL through the TCPC may play a role in single ventricle physiology and their long-term survival. This power loss has been shown to vary significantly with TCPC geometry. In addition, PL is a function of cardiac output (CO) and may increase in a non-linear fashion.

Purpose: We sought to study the effects of simulated exercise conditions on the PL through the TCPC by doubling and tripling the baseline flow measured by through-plane phase contrast MRI (PC-MRI). It was our hypothesis that PL through the TCPC is a function of CO and the relationship between CO and PL may be important in characterizing the function of the TCPC.

Methods: MRI data of 8 pts with a TCPC were analyzed to obtain 3D geometry as well as flow rates through the SVC, IVC, LPA and RPA. Steady flow CFD simulations were performed

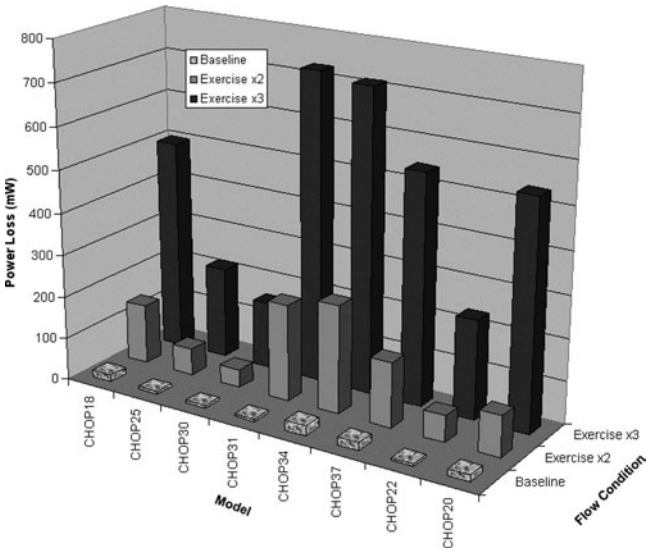

at baseline conditions using the CFD mesh and MRI-derived flow conditions. Simulated exercise conditions of twice ($2\times$) and three times ($3x$) baseline MRI flow were performed by increasing IVC flow. PL through the TCPC was calculated for each condition.

Results: For each model, PL increases in a dramatically nonlinear fashion with increasing cardiac output (Fig.). On average, there was a 9 fold (6–12) increase from baseline to the $2\times$ and 33-fold (29–45) to the 3x conditions. Baseline power loss did not always predict the exercise power loss.

Conclusions: The relationship between CO and PL is nonlinear, with as much as a 45-fold increase in power loss from baseline to simulated maximal exercise. Additionally, the relationship is very dependent on TCPC geometry. This study demonstrates the potential importance of studying the TCPC under exercise conditions, as studying baseline conditions may not adequately characterize the TCPC.

577. EVALUATION OF THE EFFECT OF SLICE THICKNESS AND IMAGE RESOLUTION ON POSITIVE SIGNAL ENHANCEMENT FROM IRON OXIDES USING A WHITE MARKER (GRASP) SEQUENCE

Venkatesh Mani, PhD, Karen C. Briley-Saebo, PhD, Daniel D. Samber, PE, Claudia Calcagno, MD, Zahi A. Fayad, PhD. ***Mount Sinai School of Medicine, New York, NY, USA.***

Introduction: Iron oxides are used for stem-cell tracking and identifying macrophages in atherosclerotic plaques. On conventional T2* gradient echo (GRE) images, iron oxides appear dark and it is often difficult to distinguish signal loss caused by iron-oxides from other artifacts. Recently, techniques have been developed to obtain positive enhancement from iron-oxides (1-3). One such technique is an adaptation of the white marker imaging technique called Gradient echo acquisition for

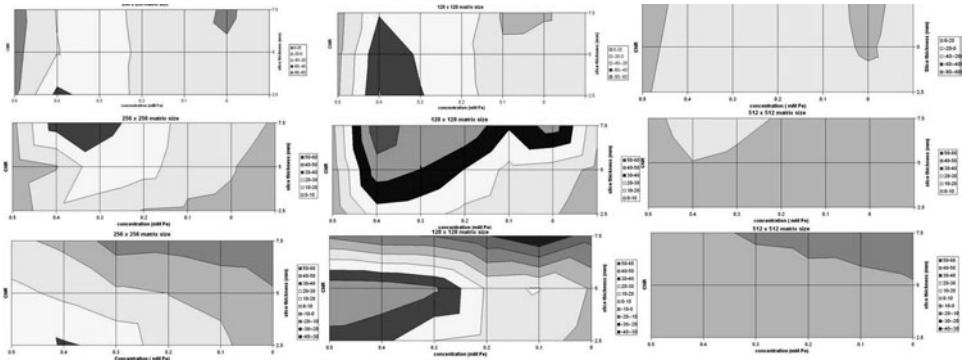

Superparamagnetic Particles (GRASP) that involves reducing z-gradient rephasing to compensate for local negative gradients created in the presence of superparamagnetic particles (4). Though the effect of echo time (TE), z-gradient rephasing and concentration of iron oxide on the signal enhancement using GRASP have been studied (4) the effect of slice thickness and image resolution on the positive contrast generated by this technique have not been evaluated.

Purpose: The purpose of this study was to experimentally quantify and compare the changes in signal enhancement obtained using GRASP, with the signal loss obtained on conventional T2* images using membrane phantoms containing different concentrations of iron-oxides due to changes in slice thickness and image resolution.

Methods: Membrane phantoms containing 6 different concentrations of iron-oxide were imaged using a 1.5 T scanner using T2*-GRE and GRASP sequences. Contrast-to-noise ratios (CNR) between the iron oxide laden membranes and surrounding gel were determined as a function of three different slice thicknesses (2, 5, 7.5 mm) and three different image resolutions (matrix size: 128^2, 256^2, 512^2). The other imaging parameters were as follows: TR = 500 ms, TE = 10 ms, BW = 500 Hz/pixel, FOV = 25 × 25 cm and 1 signal average.

Results: Fig. shows CNR values obtained as surface plots. Lower resolution images produced greater signal loss on T2*-images and greater signal enhancement with GRASP. Thinner slices produced greater signal loss on T2*-images, whereas thicker slices produced greater signal enhancement using GRASP.

Conclusions: Thicker slices of lower resolution generate greater positive enhancement using GRASP.

REFERENCES

1. Seppenwoolde, et al. MRM 2003;50:784–90.
2. Bakker, et al. MRM 2006;55:92–7.
3. Stuber, et al. ISMRM 2006;1193.
4. Mani, et al. MRM 2006;55:126–35.

578. PREDICTION OF REGIONAL FUNCTIONAL IMPROVEMENT AFTER ACUTE MYOCARDIAL INFARCTION: COMPARISON BETWEEN DOBUTAMINE ECHOCARDIOGRAPHY AND CONTRAST ENHANCED MAGNETIC RESONANCE

Luigi Natale, Antonio Bernardini, MD, Agostino Meduri, MD, Antonella Lombardo, MD, Filippo Crea, MD, Lorenzo Bonomo, MD. ***Catholic University of Sacred Heart, Rome, Italy.***

Introduction: Functional recovery is crucial in patients prognosis after acute myocardial infarction.

Purpose: To predict segmental functional recovery after Acute Myocardial Infarction (AMI) with Dobutamine Stress Echocardiography (DSE) and Contrast Enhanced Magnetic Resonance (CE-MRI).

Methods: Fifteen consecutive patients with first AMI (65 ± 8 years) underwent DSE and CE-MRI (GE Signa Excite 2) within 7 days after successful PTCA. Dobutamine was infused stepwise from 10 to 40 mcg/kg. Cine-MRI was performed in short axis (6–8 slices, FIESTA sequences) with additional HLA or VLA slices; delayed imaging (IR-prep FGRE) was obtained in short axis 15 min after 0.2 mmol/Kg Gd-DTPA. Regional function was evaluated using a 16-segments LV model (total 240 segments). Delayed Enhancement (DE) was classified as: absent or transmural extent < 50% (Pattern 1) and transmural extent > 50% (Pattern 2).

Segmental function was visually assessed with DSE and cine-MR. After 6 months echocardiography and cine-MRI assessed functional recovery as improvement of segmental WMSI. Segments without functional improvement after DSE and without recovery of WMSI at follow up were considered as necrotic.

Results: There was a significative agreement between DSE and CE-MRI in prediction of functional LV improvement. Specificity of DSE in the evaluation of necrosis was about 80%, and negative predictive value (NPV) was 88%; specificity of DE with transmural extent >50% was about 87% and NPV was 87%.

Conclusion: Functional improvement after DSE and absent or <50% delayed enhancement are highly predictive of functional improvement at follow up. Both techniques showed significant specificity and NPV in the assessment of myocardial necrosis and showed a significant concordance.

579. RELATIONSHIP OF MRI ESTIMATION OF MYOCARDIAL IRON TO LEFT VENTRICULAR SYSTOLIC AND DIASTOLICFUNCTION IN THALASSEMIA

Leonardi Benedetta, MD, Steven D. Colan, MD, Andrew J. Powell, MD, Renee Margossian, MD. ***Children's Hospital, Boston, MA, USA.***

Introduction: Patients with beta-thalassemia are at risk for myocardial dysfunction secondary to transfusion related hemochromatosis. Although chronic chelation therapy has been helpful in preventing cardiac iron injury, improved methods of guiding this therapy through monitoring for myocardial iron accumulation and predicting the onset myocardial dysfunction are needed. Recent data have indicated the potential utility of both the myocardial T2 relaxation time (T2*) on magnetic resonance imaging (MRI) and tissue Doppler (TD) assessment of diastolic ventricular function for this purpose.

Purpose: To define the relationship between echocardiographic diastolic function indices and MRI T2* with systolic ventricular function in patients with thalassemia.

Methods: Between 2000 and 2006, 24 patients age 27 $\pm$ 10 managed on chronic chelation therapy were prospectively evaluated with echocardiography (ECHO) and have had MRI assessment of T2*.

Results: Findings on echocardiography (ECHO) were: EF = 53 $\pm$ 12, Tei index = 0.56 $\pm$ 0.15, E' = 15 $\pm$ 5, E/E' = 7 $\pm$ 5, and E/A = 2 $\pm$ 0.7. All patients had a restrictive filling pattern (E/A $\leq$2 or 1< E/A <2 with early deceleration < 140 ms) and normal relaxation (E/E' < 10). There was a significant correlation between EF versus E', E/E', and E/A, but not Tei index. None of the diastolic function indices were predictive of deterioration in systolic function. MRI T2* = 20 $\pm$ 14, and 11 subjects had normal T2*. Comparison of MRI and ECHO obtained within 2 months of each other showed:

T2* correlated significantly with MRI EF (r = 0.48) and ECHO EF (r = 0.65) but not with Tei index, or any of the diastolic function indices. In patients with T2* < 9, 8/12 had EF < 50 compared to 0/31 with T2* >9 ($p < 0.001$).

Conclusions: This cohort of adult patients with thalassemia major managed on chronic chelation therapy have normal systolic function, normal relaxation, but restrictive filling pattern and most have abnormal MRI T2*. As previously reported, there is a high level of agreement between MRI and ECHO for EF, but they provide correlate but dissimilar values for ventricular volume. All instances of EF < 50 were found in conjunction with MRI T2 * < 9, whereas T2 * < 9 was unusual in patients with normal ventricular function. T2* is useful for tracking iron content and assessing risk for left ventricular systolic dysfunction whereas diastolic function indices were abnormal in all subjects and were not predictive of systolic dysfunction.

	Echo	MRI	r value
Diastolic Volume	155 $\pm$ 55	173 $\pm$ 63	0.93
Systolic Volume	63 $\pm$ 36	78 $\pm$ 44	0.96
Ejection Fraction	57 $\pm$ 10	57 $\pm$ 10	0.90

580. CARDIOVASCULAR MAGNETIC RESONANCE ANGIOGRAPHY USING TIME-RESOLVED IMAGING OF CONTRAST KINETICS (TRICKS): EXPERIENCE IN CONGENITAL HEART DISEASE

Roberto Sasdelli Neto, Walther Y. Ishikawa, Ibraim M. F. Pinto, Ieda B. Jatene, Luiz C. B. Souza, Adib D. Jatene, Prof. ***Hospital do Coração-Associação do Sanatório Sírio, São Paulo, Brazil.***

Introduction: Standard 3D Magnetic Resonance Angiography (3D-MRA) sequences may at times not to reveal the entire anatomical abnormalities because of incorrect timing of peak enhancement. For a better display of the cardiovascular findings, it would also be desirable if one could reconstruct such structures at different contrast transit times. With the introduction of the 3D-MRA with Time-Resolved Imaging Of Contrast Kinetics (TRICKS), available in GE MR scanners (General Electric, GE Healthcare, Milwaukee, WIs, US), sequential MRA Gadolinium-enhanced series are obtained and allow the selection of the best contrast-enhanced series to study a determined vascular structure.

Purpose: To show the diagnostic benefit and follow-up of the Congenital Heart Disease (CHD) patients with 3D-MRA using TRICKS.

Methods: We evaluated the 3D-MRA with TRICKS in 100 patients with suspected CHD. Mean age was 1.2 years (0–12), 56 males end 44 females.

Results: All images were of diagnostic quality, and the patients had no complications, even those who needed sedation. All images underwent extensive time-resolved reconstructions at dedicated workstations and 3D Volume-rendering data sets were reconstructed in order to unravel the anatomy of the different cardiovascular organs.

Conclusions: The TRICKS adds value to 3D-MRA examinations, because it allows the imager to obtain excellent enhancing-time in child patients, even in those who had complex vascular malformations.

581. CARDIAC MR IN COMPARISON WITH ECHOCARDIOGRAPHY FOR THE IMAGING ASSESSMENT OF CARDIAC MASSES

Gurpreet S. Gulati, MD, Sanjiv Sharma, MD, Shyam S. Kothari, DM, Rajnish Juneja, DM, Vinay K. Bahl, DM. ***All India Institute of Medical Sciences, Ansari Nagar, New Delhi, India.***

Introduction: Cardiac MR (CMR) has emerged as an alternative technique to echocardiography (ECHO) for the imaging of cardiac masses. This is because CMR is less operator dependant, has a large field of view, provides orthogonal images in any plane and allows tissue characterization.We report our 11-year experience with the use of CMR in this group of patients.

Purpose: To compare the efficacy of CMR and ECHO in the evaluation of cardiac masses.

Methods: Over an 11 year period, 35 patients (age range, 16 days–64 years, mean, 26 years; 24 males, 11 females) with a suspected intracardiac mass on ECHO (transthoracic in all; transesophageal in 10) underwent a CMR examination. Ten patients had a contrast-enhanced MRI. Parameters compared on ECHO and CMR included technical adequacy of the modality, ability to detect and suggest the likely etiological diagnosis, and provide additional information (including masses not seen with the other technique, obstruction to the inflow or outflow, and detection of intramural component of an intracavitary lesion). With CMR, the image morphology (including signal intensity characteristics on the various sequences) and extracardiac manifestations were also evaluated. Confirmation of the diagnosis was based upon histopathology in 21, surgical inspection in 8, follow-up imaging on conservative management in 5, and typical extracardiac manifestations of the disease in 1 patient.

Results: Nineteen (54%) patients had tumors (of which 15 were benign and 4 were malignant), 5 had a thrombus or hematoma, 6 had infective and 5 had vascular lesions. Forty one masses (16 in ventricle, 11 in interventricular septum, 9 in atrium, 4 on valve and 1 in pulmonary artery) were seen on CMR, of which ECHO detected 34. Transthoracic ECHO (TTE) and CMR were technically optimal in 82% and 100% cases respectively. Ten patients required an additional transesophageal ECHO (TEE).Overall, CMR showed a mass in all patients, while ECHO missed it in 3 cases. In cases with a mass being shown on both modalities, CMR detected 4 additional masses not visualized on ECHO. CMR suggested the etiology in 26 (74%) cases, while the same was possible with ECHO (TTE and TEE) in 10 (29%) cases. Intramural component, extension into the inflow or outflow, outflow tract obstruction, and associated pericardial or extracardiac masses were better appreciated on CMR.

Conclusions: CMR is advantageous over a combination of TTE and TEE for the detection, characterization and complete morphological and functional evaluation (hemodynamic effects) of cardiac masses.

582. MR- GUIDED STEM CELL ARTERIOGENIC THERAPY IN A RABBIT HINDLIMB ISCHEMIA MODEL

Dorota A. Kedziorek, MD,[1] Wesley D. Gilson, PhD,[1] Matthias Stuber, PhD,[1] Gary Huang,[1] Erin Blush, BS,[1] Ana V. Soto, BS,[1] Jeff W. M. Bulte, PhD,[1] Lawrence V. Hofmann, MD,[2] Dara L. Kraitchman, VMD, PhD.[1] [1]***Johns Hopkins University, Baltimore, MD, USA,*** [2]***Standford University, Standford, CA, USA.***

Introduction: The successful treatment of Peripheral Arterial Occlusive Disease (PAOD) relies on restoration of sufficient blood supply to the ischemic tissue. Cell-based therapy (e.g., mesenchymal stem cells (MSCs)) is an attractive alternative to gene and protein therapies to enhance arteriogenesis. Two possible mechanisms to explain the benefits of MSCs transplantation are: the MSCs differentiate into vascular elements (endothelium, myocytes, pericytes), providing the arteriogenic "building blocks," and/or the MSCs release cytokines that promote endogenous arteriogenesis.

Magnetic resonance imaging can be used to monitor the cell delivery as well as to serially interrogate the degree of engraftment. In addition, MRI can be used to visualize the development of new collateral vessels as well as the effect on tissue perfusion to the downstream ischemic tissue bed.

In the present study, magnetically-labeled, allogeneic, bone marrow-derived MSCs were injected intramuscularly into a rabbit hindlimb after percutaneous creation of a superficial femoral artery occlusion. The Inversion Recovery ON resonance water suppression (IRON) pulse sequence was used for positive contrast tracking of the MSCs, and T2-prepared MR angiography (MRA) enabled the monitoring of neovascularization.

Methods: Mesenchymal stem cells were isolated from the bone marrow of male New Zealand White rabbits. The MSCs were expanded (3 passages), trypsinized, mixed with ferumoxide (Feridex, Berlex Laboratories, Inc.) at concentration 2 mg of Fe/mL, loaded into electroporation cuvettes and electroporated (20 pulses, 50 mV, pulse duration 1 ms) for magnetic labeling. After labeling, the cells were incubated for half an hour in cold medium supplemented with 10% serum. Hindlimb ischemia was induced by a minimally invasive, non-surgical, endovascular method where the thrombogenic platinum coils were deployed within the superficial femoral artery. Twenty-four hours after ischemia induction, rabbits were randomized to receive 13×10^6 magneto-electroporation (MEP)-labeled MSCs ($n = 6$) or diluted ferumoxides ($n = 5$) divided into 6 injections ($\sim$0.25 cc/injection) in the left medial thigh. To achieve a similar appearance to the injectates, the ferumoxide concentration was $\sim$15-fold higher in the control animals compared to the MSC-treated animals. MRI was performed on clinical 3T Phillips Achieva scanner immediately after injection, 1 week, and 2 weeks post-injection. A T2-prepared MRA was acquired with the following imaging parameters: TR/TE = 14.0/3.8 ms, FOV = 270×216 mm^2, spatial resolution = $0.34 \times 0.35 \times 1.5$ mm^3, FA = 20°. A fast spin echo with dual iron pulses to suppress water and fat was acquired: TR/TE = 2000/11.6 ms, FOV = 180×135 mm^2, spatial resolution = $0.45 \times 0.45 \times 3$ mm^3, TSE factor = 24. At two weeks, the animals were humanely euthanized and tissue was harvested for histological analysis.

Results: MEP resulted in efficient magnetic cell labeling with a $< 5\%$ decrease in cell viability. Positive enhancement with

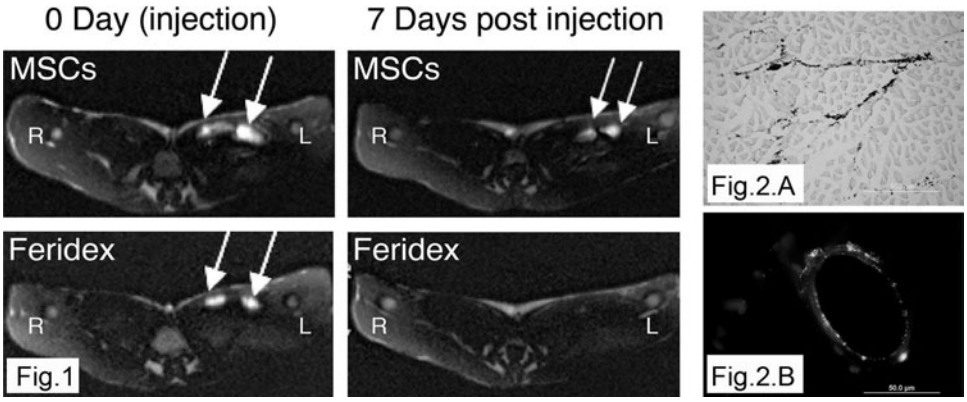

IRON imaging could be detected up to 2 weeks post injection in MEP-treated animals, but not in the ferumoxide only injected control animals (Fig. 1) MRI determined localizations of MEP labeled MSCs were in close proximity of the neovasculature visualized with MRA. Incorporation of the contrast agent laden cells into the small vessel walls was confirmed with Prussian Blue (Fig. 2A) and anti-dextran staining (Fig. 2B).

Conclusion: Detection of positive enhancement by IRON imaging up to 2 weeks post-injection in MSC-treated animals, but not fermuoxide suggests that the bulk of the signal from IRON imaging is from viable labeled MSCs and not free iron. Moreover, histological confirmation of the incorporation into the vessel walls of the MSCs suggests an active role in the induction of new vasculature.

REFERENCES

1. Stuber M, et al. J Cardiovasc Magn Reson 2006;8:13–14.
2. Wagner A. et al. Lancet 2003;361:374–9.
3. Liddell RP, et al. J Vasc Interv Radiol 2005;16:991–8.

583. QUANTITATIVE MYOCARDIAL DISTRIBUTION VOLUME USING FIRST-PASS PERFUSION KINETICS

Nathan Pack, Christopher J. McGann, MD, Edward V. R. DiBella, PhD. ***University of Utah, Salt Lake City, UT, USA.***

Introduction: Delayed Enhanced (DE) MRI has become the gold standard for accurately identifying the presence and extent of myocardial scarring (1). As cardiac myocytes die, the extracellular volume, Ve, increases. Ve is reflected by an accumulation of contrast agent (CA) in the tissue. A quantitative estimate of the magnitude and spatial distribution of Ve may provide a more direct measure of the size and diffuseness of infarcts than DE imaging alone. This information could be used to track changes in infarcts in follow-up studies.

We hypothesize that dynamic contrast-enhanced perfusion MRI may be used to rapidly quantitate Ve in the myocardium. With this method, the kinetics of myocardial blood and tissue enhancement are imaged dynamically during the first-pass injection of CA. The enhancement of the myocardium is assumed to change according to a physiologically derived 2-compartment model. Then, from the kinetics of blood and tissue enhancement in the heart, Ve is estimated in a scan requiring less than 1 minute. In this work, we perform simulations and patient studies to evaluate the model estimates of Ve from first-pass kinetic modeling and compare them to steady-state (Ct/Cb) enhancement estimates (2).

Methods: In 10 patient studies, myocardial perfusion images were acquired with a Siemens Avanto 1.5T MRI scanner using an ECG-gated, hybrid GRE-EPI pulse sequence with T-SENSE (FOV = 360 × 270 mm, matrix = 160 × 90, TI = 40 −70 ms, TR = 6.5 ms, TE = 1 ms, ETL = 4, flip angle = 20°, 8 mm slice thickness). During imaging, each patient was given a low-dose (0.024–0.04 mmol/kg) bolus injection of Gd-DTPA at 6cc/s using a power injector. Three to four short axis (SA) slices of the LV were analyzed in each patient. Offline, the images were manually registered to sub-pixel resolution and regional blood and myocardial tissue regions were selected to obtain dynamic curves for each perfusion series. Estimates of Ve were derived by fitting the enhancement curves to the kinetic model in Equation 1. Here, Ve is defined as the ratio of the rate of influx of Gd

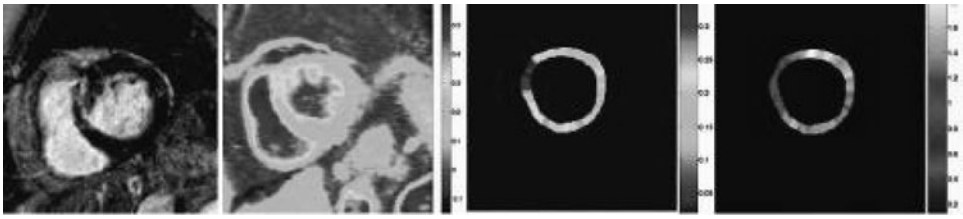

FIG. 1. a) DE image, b) Steady state Ct/Cb (Vc) image, c) Kinetic Ve image, d) Kinetic K_1 image.

(K_1) to the rate of efflux of Gd (k_2) in the tissue curves: Ve = K_1/k_2. Normal regions in each of the patients were manually selected and Ve estimates were compared for the Ct/Cb method and kinetic modeling.

Results: Figure 1a depicts a qualitative contrast-enhanced MR image with an infarct in the anterior-septum of the LV in one patient. Figure 1b shows the Ct/Cb map of Ve values estimated using the steady-state method. Figs. 1c and 1d show the corresponding maps of Ve and blood flow (K_1) derived from kinetic modeling. Ve = 20.2% ± 6.95% from the Ct/Cb model and Ve = 23.7% ± 14.5% from the kinetic models, for the normal regions in each patient.

Conclusions: Preliminary results reveal a close match between estimates of Ve from first-pass kinetic modeling and Ct/Cb studies. Both have a mean normal value of Ve near 22%, which shows promise of the kinetic modeling method to estimate Ve in a fast and reproducible manner. It is also evident from Fig. 1 that the Ve maps from kinetic modeling parallel the distribution of scarring in DE images. The larger standard deviation of Ve estimates from kinetic modeling is likely due to the lower SNR in the dynamic first-pass images and increased patient motion during the scan, which may make model curve-fitting less accurate. Here we demonstrate that kinetic perfusion modeling can be successfully used to quantitate Ve in the myocardium. Additional studies are in progress to further assess the accuracy and utility of Ve measurements in patients with diffuse or patchy necrosis (ie, myocarditis) that are not easily identified nor sized using DE-MRI alone.

REFERENCES

1. Kim RJ, et al. Circ 1996;94:3318–3326.
2. Moran GR, et al. Mag Res Med 2002;48:791–800.

584. COMPLEX MRI EVALUATION OF PORCINE REPERFUSED MYOCARDIAL INFARCTION USING A MULTI-MODALITY APPROACH

Balazs Ruzsics, MD,[1] Pal Suranyi, MD,[2] Pal Kiss, MD,[2] Thomas S. Denney, Jr, PhD,[3] Silvio H. Litovsky, MD,[4] Brigitta C. Brott, MD,[5] Tamas Simor, MD, PhD,[2] Steven G. Lloyd, MD,[6] Gabriel A. Elgavish, PhD,[2] Himanshu Gupta, MD, FACC.[6] ***[1] University of Alabama at Birmingham, Department of Biochamistry and Molecular Genetics, Birmingham, AL, USA, [2] University of Alabama at Birmingham, Department of Biochamistry and Molecular Genetics; Elgavish Paramagnetics Inc., Birmingham, AL, USA, [3] Auburn University, Department of Electrical and Computer Engineering, Auburn, AL, USA, [4] University of Alabama at Birmingham, Department of Anatomic Pathology, Birmingham, AL, USA, [5] University of Alabama at Birmingham, Department of Cardiology, Birmingham, AL, USA, [6] University of Alabama at Birmingham, Division of Cardiovascular Disease, Birmingham, AL, USA.***

Purpose: Characterization of myocardial infarcts using myocardial perfusion and strain analysis of area at risk (viable peri-infarct region) as defined by delayed contrast enhancement (DE) and T2-weighted (T2w) increased signal intensity (ISI).

Methods and Materials: In five pigs, one week after reperfused myocardial infarction, tagged-cine-gradient-echo images and T2w-images were generated using double-inversion-recovery (black-blood) fast-spin-echo sequence. Next, first-pass T1-weighted (T1w) perfusion-imaging was done after 0.1 mmol/kg Gd(DTPA), followed by additional 0.1 mmol/kg Gd(DTPA) and conventional delayed-contrast-enhanced (DE) imaging at 15 minutes. Mean + 2SD of remote signal-intensity was used to define threshold limit for enhancement. Enhanced pixels were counted and the ratio of infarcted or injured to total area of a given slice yielded the Percent-Infarcted-area-per-Slice(PIS_{DE}) and Percent-Enhanced-area-per-Slice(PES_{T2w}). Short-axis slices were divided into 6

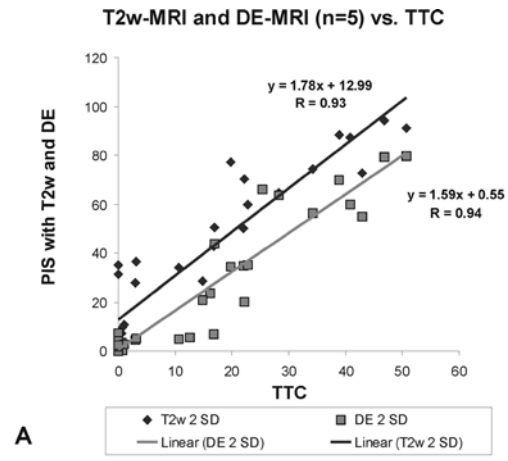

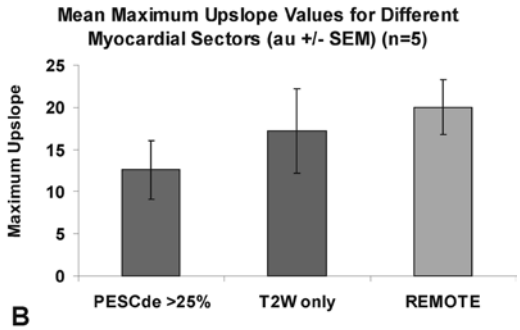

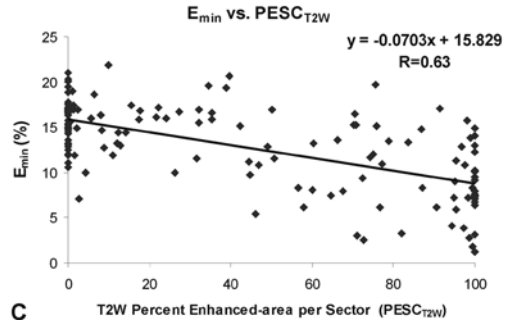

circumferential sectors. Transmurality was calculated as the percentage of enhanced vs. all pixels of sectors (Percent-Infarcted-area-per-Sector($PISC_{DE}$) or Percent-Enhanced-area-per-Sector($PESC_{T2w}$)). For each sector, strain (E_{min}) was determined from tagging. Sectors were categorized based on the presence or absence of T2w-enhancement or DE and maximum-upslope of Signal-Intensity was determined from first-pass images. Postmortem TTC histochemistry was used for validation.

Results: T2w-imaging overestimated infarcts more than DE (Fig. 1a). Fig. 1b shows maximum-upslope values in various compartments. Qualitatively, bulls eye diagram of perfusion and strain-map showed good agreement regarding location of ischemic injury. Sectors severely affected by infarction ($PISC_{DE} > 25\%$) showed reduced strain when compared to the peri-infarct regions as determined by T2w imaging. E_{min} was also depressed in the peri-infarct-region, with fair correlation with $PESC_{T2w}$ (Fig. 1c).

Conclusion: The peri-infarct region has complex pathophysiological characteristics and altered mechanics. Combinations of techniques are needed for its evaluation.

585. EFFECTS OF LOADING CONDITIONS ON THE LEFT VENTRICULAR MECHANICS

Himanshu Gupta, MD,[1] Thomas S. Denney, Jr, PhD,[2] Steven G. Lloyd, MD, PhD,[1] David A. Calhoun, MD,[1] Gilbert J. Zoghbi, MD,[1] Cecilia Corros, MD,[1] Hosakote Nagaraj, MD,[1] Louis J. Dell'italia, MD.[1] [1]***University of Alabama at Birmingham, Birmingham, AL, USA,*** [2]***Auburn University, Auburn, AL, USA.***

Introduction: Torsion, wall stress and strain define important left ventricular (LV) mechanical properties that can be accurately assessed by cardiac MRI. Prior studies suggest that patients with aortic stenosis have increased LV torsion. Here we evaluated the differences in the LV mechanical properties in two physiologically distinct conditions: increased preload due to primary mitral regurgitation and increased afterload due to resistant hypertension.

Purpose: We hypothesized that the differences in the mechanical properties in the two groups as compared to controls may be due to the differences in the LV structural and functional remodeling.

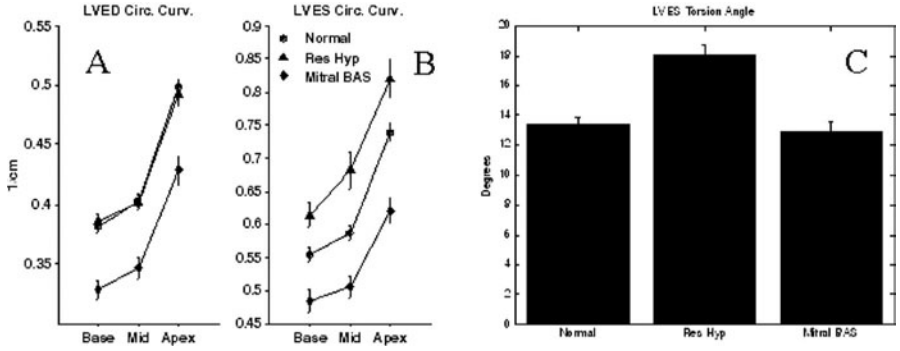

FIG. 1. A & B) Decreased circumferential curvature is noted in MR; C) HTN results in increased torsion.

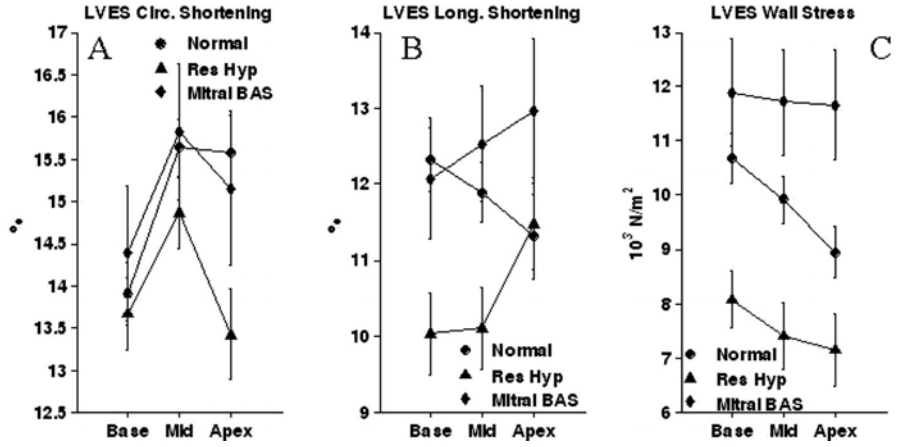

FIG. 2. A, B & C) HTN results in lower longitudinal strain and wall stress. MR results in increased wall stress.

Methods: Primary mitral regurgitation (MR) (n = 20), resistant hypertension (HTN) (n = 50) and normal volunteers (C) (n = 36) were enrolled. Comprehensive MRI evaluation including three-dimensional tagged MRI of the myocardium was performed and analyzed using custom-written and commercial software.

Results: LV ejection fraction was well above normal ranges in both MR (65 ± 6) and HTN (73 ± 11) groups. MR group had eccentric remodeling as indicated by decreased circumferential curvature but increased LV radius: wall thickness ratio ($p < 0.05$). HTN had concentric LV remodeling but with decreased longitudinal strain in spite of an LV systolic wall stress that was decreased below normal ($p < 0.05$). MR resulted in increased systolic wall stress but with no effect on longitudinal strain, circumferential strain or indices of torsion. In contrast, the HTN group there were increases in twist (i.e., torsion/length), mean systolic twist velocity and mean diastolic untwist velocity compared to normals ($p < 0.05$).

Conclusions: Volume as compared to pressure overload results in differential LV remodeling process that is associated with changes in the LV systolic stress, strain and torsion. These differences may be important in planning targeted drug therapy that prevents progressive LV remodeling.

586. TISSUE MAGNETIC RESONANCE IMAGING DEMONSTRATES REGIONAL DIASTOLIC DYSFUNCTION IN REMOTE TISSUE EARLY AFTER INFERIOR MYOCARDIAL INFARCTION

Bernard P. Paelinck, MD, PhD,[1] Christiaan Vrints, MD, PhD,[1] Jeroen Bax, MD, PhD,[2] Johan M. Bosmans, MD, PhD,[1] Albert de Roos, MD, PhD,[2] Hildo J. Lamb, MD, PhD.[2] [1]***University Hospital Antwerp, Edegem, Belgium,*** [2]***Leiden University Medical Center, Leiden, The Netherlands.***

Introduction: Impairment of longitudinal diastolic function is an early sign of myocardial dysfunction. Myocardial infarction of the inferior wall exhibits a smaller functional loss as opposed to similar sized myocardial infarction of the anterior wall. In myocardial infarction of the inferior wall, regional left ventricular (LV) diastolic function, the relation between regional and global diastolic function, and the relation between regional diastolic and systolic function is largely unknown.

Purpose: To test the hypothesis that, in transmural inferior myocardial infarction, longitudinal diastolic function of the remote tissue is impaired, while systolic function is preserved.

Methods: Early diastolic transmitral flow velocity (E), and regional, longitudinal, myocardial systolic (Sa) and early diastolic (Ea) velocities were measured by velocity encoded MR imaging in 15 patients with a recent transmural inferior myocardial infarction due to single proximal right coronary artery disease and 15 age and LV mass index matched control subjects.

Results: Global systolic LV function (ejection fraction 46 ± 7% versus 57 ± 4%, $p < 0.01$) and global diastolic LV function (average Ea of infarcted, adjacent and remote myocardium 6.8 ± 1.7 cm/s versus 10.4 ± 1.5 cm/s, $p < 0.01$) were impaired in patients as compared to controls. Regional systolic and diastolic LV velocities were impaired in infarcted and adjacent tissue in patients. However, in remote tissue, systolic velocities were preserved (Sa 6.6 ± 2.0 cm/s versus 6.8 ± 1.4 cm/s, $p > 0.05$), but diastolic velocities were impaired in patients as compared to controls (Ea 7.2 ± 2.3 cm/s versus 10.2 ± 2.5 cm/s, $p < 0.01$).

Conclusions: Regional diastolic velocities early after inferior myocardial infarction are impaired in the infarcted, adjacent and remote tissue. However, regional systolic velocities are preserved in remote tissue. Therefore, impairment of regional diastolic velocities is an early marker of dysfunction in remote tissue after inferior myocardial infarction.

587. UTILITY OF CARDIOVASCULAR MAGNETIC RESONANCE TO PREDICT LEFT VENTRICULAR RECOVERY AFTER PRIMARY PERCUTANEOUS CORONARY INTERVENTION FOR PATIENTS PRESENTING WITH ACUTE ST-SEGMENT ELEVATION MYOCARDIAL INFARCTION

Michael Shapiro, Koen Nieman, Cesar Nomura, Khuram Nasir, Thomas J. Brady, Ricardo C. Cury. ***Massachusets General Hospital, Boston, MA, USA.***

Introduction: Cardiovascular magnetic resonance (CMR) is established as a major technique in evaluating left ventricular function, myocardial perfusion, infarct size, and myocardial viability and may likely be the optimal modality to predict left ventricular recovery (LVR) after acute myocardial infarction. We investigated the utility of CMR to predict LVR after primary percutaneous coronary intervention (PCI) in patients presenting with first acute ST-segment elevation myocardial infarction (STEMI).

Purpose: The aim of this study was to clarify the value of various CMR parameters for the prediction of LVR in patients presenting with acute STEMI.

Methods: Seventeen patients (mean age 60 ± 10 years, 14 males) presenting with first acute STEMI treated with primary PCI (average door to balloon time 81 ± 34 minutes) were studied. Each patient underwent CMR twice. The baseline examination was performed between 2–6 days (mean 2.9 ± 1.0 days) after presentation and the follow-up examination was performed at an average of 6 ± 1.5 months later. Steady state free precession cines, 1st pass (FP) perfusion, and delayed hyperenhancement (DHE) images were obtained on a 1.5 T system (GE Twinspeed, General Electric, Milwaukee, WI, USA) using an 8-channel phased array cardiac coil. Two blinded observers analyzed data from both CMR examinations for ventricular volumes, ejection fraction (EF), LV mass, and FP perfusion

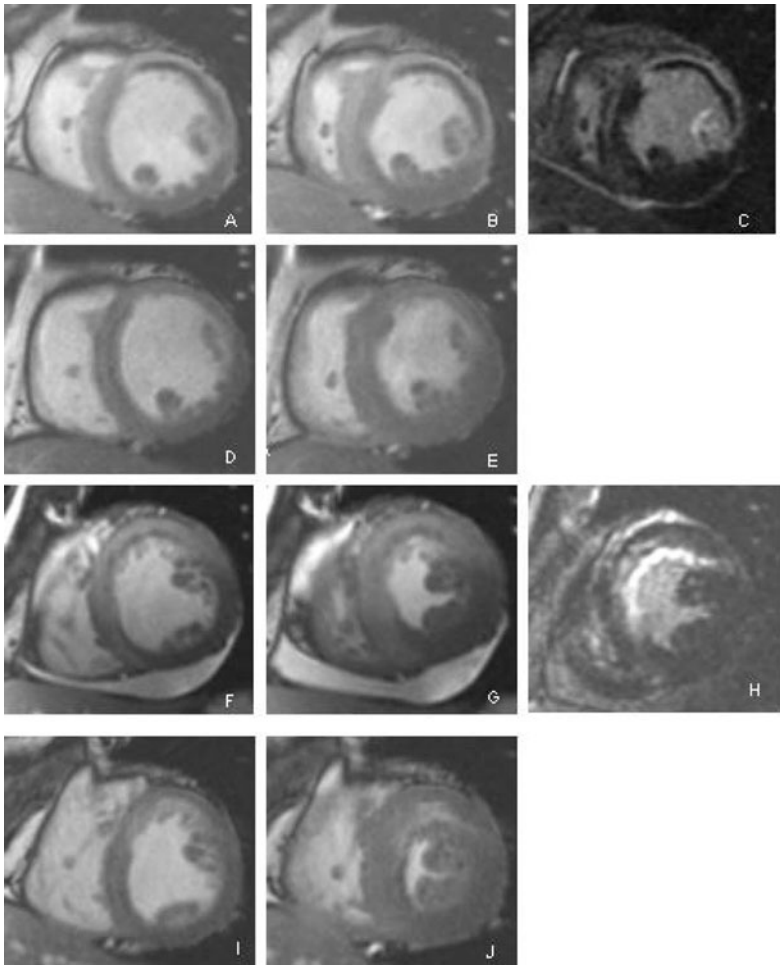

FIG. 1. Patient 1 (A–E) demonstrates akinesis of the anteroseptal, anterior, and anterolateral walls on cine imaging on the baseline MRI (A, B). Delayed enhancement imaging (C) revealed a near transmural infarct with a high degree of microvascular obstruction in the same territory as the regional wall motion abnormalities. The follow-up MRI (D, E) revealed no improvement in regional LV function. Patient 2 (F–J) demonstrates hypokinesis of the anteroseptal and anterior walls on the baseline MRI (F, G). Delayed enhancement imaging (H) revealed an infarct of $< 50\%$ transmurality and no microvascular obstruction. The follow-up MRI (I, J) revealed improvement in regional LV function.

defects. Additionally, microvascular obstruction (MO) and DHE were analyzed on both a global and regional level and compared to the change in regional LV function. Segmental LV function was assessed using a semiquantitative scale (4 = normal, 3 = mild hypokinesis, 2 = severe hypokinesis, 1= akinesis, 0 = dyskinesis). Coregistered segments from MRI #2 were evaluated for change in regional left ventricular function relative to MRI #1 and an improvement by one category or more in the regional wall motion score was considered evidence of LVR.

Results: A total of 680 segments were evaluated of which 267 (39%) demonstrated areas of delayed hyperenhancement. In segments displaying DHE, 169 (63%) demonstrated improved regional LV function and 98 (37%) either demonstrated the same or worsening LV function on MRI #2. In segments with <50%, 51–75%, and >75% transmurality of DHE, 80%, 68% and 2%, respectively, demonstrated LV recovery ($p < 0.0001$ for trend). In patients who demonstrated $\geq 50\%$ transmurality of DHE, the presence of MO was associated with LVR in only 36% of segments and the absence of MO was associated with LVR in 70% of segments ($p < 0.0001$). There was a good correlation between the size of the perfusion defect on FP imaging with the size of MO as determined by the DHE technique ($R = 0.78$). In logistic regression analysis, taking into account baseline LV function, DHE, and presence of MO, the odds ratio for LVR with presence of DHE $\geq$ 50% was 0.10 (95% CI: 0.04–0.22, $p < 0.00001$) and appeared stronger than the presence of MO (OR: 0.33, 95% CI: 0.16-0.67, $p = 0.002$).

Conclusions: CMR is an excellent technique for providing detailed information regarding all aspects of cardiac morphology and function after acute STEMI. We found that the degree of infarct transmurality as determined by DHE is a more powerful predictor of LVR then MO by CMR.

588. MRI ENHANCEMENT OF ATHEROSCLEROSIS USING GADOLINIUM IMMUNOMICELLES IS RELATED TO THE MACROPHAGE CONTENT OF ATHEROSCLEROTIC PLAQUES IN APOLIPOPROTEIN E DEFICIENT MICE

Smbat Amirbekian,[1] Vardan Amirbekian, MD,[2] Karen C. Briley-Saboe, PhD,[3] Juan G. S. Aguinaldo, MD,[3] Fabien Hyafil, MD,[3] Esad Vucic, MD,[3] Michael J. Lipinski, MD,[4] Juan C. Frias, PhD,[3] Zahi A. Fayad, PhD.[3] [1]***Emory University School of Medicine, Mount Sinai School of Medicine, Imaging Science Laboratories, New York, NY, USA,*** [2]***Johns Hopkins University School of Medicine, Mount Sinai School of Medicine, Imaging Science Laboratories, New York, NY, USA,*** [3]***Mount Sinai School of Medicine, Imaging Science Laboratories, New York, NY, USA,*** [4]***University of Virginia School of Medicine, Mount Sinai School of Medicine, Imaging Science Laboratories, New York, NY, USA.***

Introduction: The ability to quantify biological activity of atherosclerosis using MRI holds great promise for noninvasive risk-stratification based on plaque composition. Macrophages play a central role in the pathogenesis of atherosclerosis. Gadolinium-containing immunomicelles (micelles linked to a specific antibody targeting macrophages) have been shown to improve in-vivo assessment of macrophages using MRI.

Purpose: The goals of the current study were to evaluate whether there is a relationship between macrophage density of atherosclerotic plaques and MRI enhancement of plaques using gadolinium-immunomicelles targeting macrophages. We also evaluated the efficacy of imaging atherosclerosis using macrophage-targeted immunomicelles as compared to several well-structured controls.

Methods: Immunomicelles, micelles and standard-Gd-DTPA MRI contrast agents were tested in ApoE-/-mice. Mice were imaged at baseline with a 9.4 T MRI system using a high spatial resolution SE sequence. The mice were then imaged at intervals following tail injection of immunomicelles (n = 9), untargeted micelles (n = 9) or standard agent (n = 4). Immunohistochemistry(IHC), laser-scanning confocal-microscopy, standard pathology were performed to co-localize immunomicelles and atherosclerosis.

Results: Using targeted immunomicelles the signal intensity(SI) increase, measured by the Normalized-Enhancement-Ratio (NER), in the aortic wall post-contrast was an average of 1.65 ± 0.11 (65% enhancement) at 1 hr post-contrast, 1.79 ± 0.1 (79% enhancement) at 24 hrs post-contrast (Fig. 1). Using untargeted micelles SI increase was an average of 1.41 ± 0.12 (41%) at 1 hr, 1.34 ± 0.1 (34%) at 24 hrs (Graph 2). Using Gd-DTPA there was minimal (2 to 19%) enhancement in ApoE-/-mice. Confocal microscopy showed co-localization of macrophages and NBD-chromophore-labeled immunomicelles in plaque. Using the macrophage-stained IHC sections, there was a correlation between the number of macrophages per High Powered Field (HPF) and the change in MRI signal intensity observed on the imaged matched sections of the atherosclerotic aorta (as shown in Graph 1; $R2 = 0.75$ $p < 0.01$).

Conclusions: Immunomicelles show promising results for in-vivo assessment of atherosclerosis using molecular-MRI. The MRI signal-intensity using immunomicelles as the contrast agent is related to macrophage content. Immunomicelles may prove useful in detection of high macrophage density typical of high-risk plaques.

589. DELAYED HYPERENHANCEMENT CORONARY VESSEL WALL IMAGING IN PATIENTS WITH ACUTE MYOCARDIAL INFARCTION: A FOLLOW-UPSTUDY

Tareq Ibrahim, MD,[1] Antanas Jankauskas, MD,[2] Markus Schwaiger, MD,[2] Albert Schomig, MD,[1] Warren J. Manning, MD,[3] David Maintz, MD,[4] René M. Botnar, PhD.[2] [1]***Department of Cardiology, Technical University Munich, Munich, Germany,*** [2]***Department of Nuclear Medicine, Technical University Munich, Munich, Germany,*** [3]***Division***

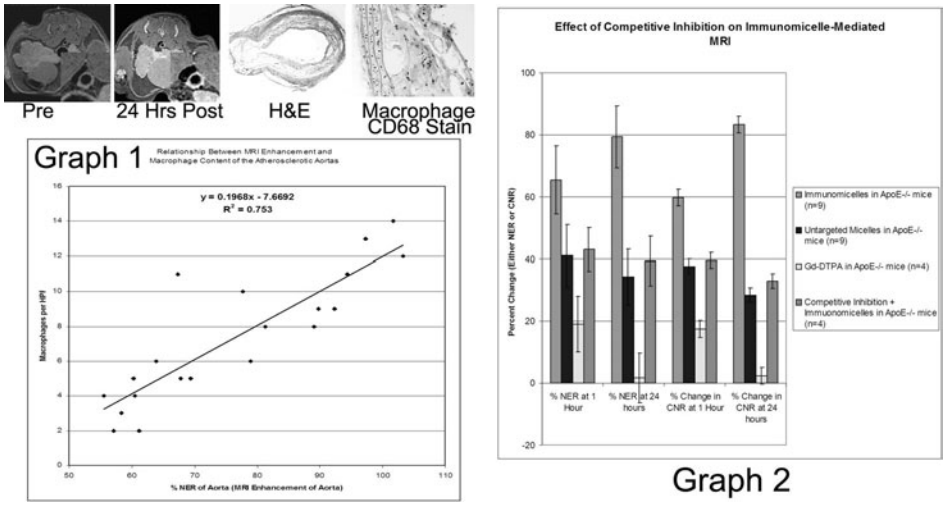

FIG. 1.

of Cardiology, Beth Israel Deaconess Medical Center, Boston, MA, USA, [4]Department of Radiology, University of Münster, Munster, Germany.

Background: Today, it is generally believed that inflammation plays a key role in the initiation, progression and complication of atherosclerosis (1), and that it is closely linked to plaque rupture, the underlying cause of most sudden deaths and acute coronary syndromes (2). Contrast enhanced MRI has been found to be useful for the assessment of acute inflammation in patients with giant cell arteritis (3) and Takayasu's (4) disease. In a preliminary study of delayed coronary wall hyperenhancement (DE–MRI) (5), we could demonstrate that contrast uptake correlates with the severity of coronary atherosclerosis as assessed by MSCT and x-ray angiography (6).

Purpose: We sought to investigate the change in delayed hyperenhancement in the wall of the coronary artery and aorta in patients with acute myocardial infarction (AMI) by performing serial CMR studies 1 week and 2 month post MI.

Methods: Serial DE–CMR of the coronary arteries was performed in 10 patients (56 ± 5 y, 9 M) with AMI $\sim$1 week and again at 2 months post MI. For improved contrast between the coronary artery wall and blood, DE–CMR was performed $\sim$45 minutes after administration of 0.2 mmol/kg Gd–DTPA (Magnevist, Schering). Image acquisition was performed during mid—diastole using a free—breathing ECG triggered T1 weighted inversion recovery (IR) fast gradient echo technique with navigator gating and correction for respiratory motion correction. Imaging parameters included spatial resolution $= 1.25 \times 1.25 \times 3$ mm, TR/TE $= 6.1/1.9$ ms, flip angle $= 30^\circ$, and slices $= 20$. For determination of the optimal inversion time for blood signal nulling, a Look-Locker sequence was used. Contrast-to—noise (CNR) between vessel wall and blood was then calculated in 5 coronary segments (LM, prox. LAD, LCX, mid. LAD, LCX) and the ascending aorta on reformatted images. Strong enhancement was defined as CNR > 9. For clinical correlation, CRP was measured in all patients at the same time intervals.

Results: Two month post MI, the number of all coronary segments with strong enhancement decreased from 36% to 18% and the median CRP value decreased from 1.6 to 0.0 mg/dL. This decrease was most prominent in segments without angiographic CAD or wall irregularities (34% to 11%). In contrast, the number of stenotic segments with strong contrast uptake remained unchanged (40% to 40%). There was a trend for decreased (12.2 ± 5.0 vs. 10.3 ± 6.4; $p < 0.4$) aortic enhancement at the 2 month scan (Fig. 1). Representative images of the LAD, LCX, and aorta are shown in Fig. 2.

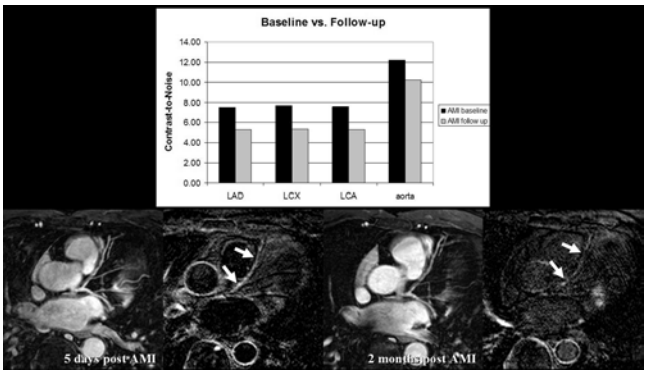

FIG. 1. and 2.

Conclusion: Serial DE–MRI of the coronary arteries and aorta in patients with AMI revealed a decrease of the spatial extent and intensity of strong contrast enhancement at the 2 month post MI scan. This decrease in hyperenhancement may be related to the overall reduction of systemic inflammation and appears to parallel declines in CRP. Larger serial studies in patients with stable CAD appear warranted to better understand the temporal and spatial change in DE-CMR in patients with coronary disease and AMI.

REFERENCES

1. Ross R. New Engl J Med 1999;340:115–26.
2. Virmani R, Burke AP, Farb A, et al. J Am Coll Cardiol 2006;47:C13–8.
3. Bley TA, Wieben O, Uhl M, et al. Am J Roentgenol. 2005;184:283–7.
4. Desai MY, Stone JH, Foo TK, et al. AJR Am J Roentgenol. 2005;184:1427–31.
5. Maintz D, Ozgun M, Hoffmeier A, et al. Eur Heart J. 2006;27:1732–6.
6. Yeon SB, Sabir A, Clouse M et al. SCMR 2005.

590. THE ROLE OF VASCULAR RESISTANCE AND EXTRAVASCULAR COMPRESSIVE FORCES IN CORONARY MICROVASCULAR DYSFUNCTION IN SYMPTOMATIC HYPERTROPHIC CARDIOMYOPATHY

Tjeerd Germans,[1] Paul Knaapen, MD,[1] Paolo G. Camici, MD, PhD,[2] Ornella E. Rimoldi, MD, PhD,[2] Folkert J. Ten Cate, MD, PhD,[3] Jurrien M. Ten Berg, MD, PhD,[4] Pieter A. Dijkmans, MD,[1] Ronald Boellaard, PhD,[1] Willem G. van Dockum, MD,[1] Marco J. W. Goette, MD, PhD,[1] Jos W. R. Twisk, PhD,[1] Adriaan A. Lammertsma, PhD,[1] Frans C. Visser, MD, PhD,[1] Albert C. van Rossum, MD, PhD.[1] ***[1]VU University Medical Center, Amsterdam, The Netherlands, [2]MRC Clinical Sciences Centre, Hammersmith Hospital, London, United Kingdom, [3]Thorax Erasmus Medical Center, Rotterdam, The Netherlands, [4]St Antonius Hospital, Nieuwegein, The Netherlands.***

Background: Hypertrophic cardiomyopathy (HCM) is characterized by both myocardial hypertrophy, and microvascular dysfunction in the absence of any systemic disease likely to cause this hypertrophy and normal epicardial coronary arteries. Microvascular dysfunction is an important determinant of prognosis in HCM patients, and may be the net result of both increased vascular resistance by increased left ventricular hypertrophy and increased extravascular compressive forces, mainly through obstruction of the left ventricular outflow tract (LVOT).

Purpose: The aim of the present study was to determine the relative contribution of both vascular resistance and extravascular compressive forces to microvascular dysfunction in HCM.

Methods: Eighteen patients with symptomatic HCM and normal coronary arteries, and 10 age matched healthy volunteers were studied with PET to quantify resting and hyperemic myocardial blood flow (MBF) at a subendocardial and subepicardial level. In all HCM patients, cardiovascular magnetic resonance imaging (CMR) was performed to determine LV mass (LVMI) and volumes and to measure left atrial maximum volume (LAI).

In addition, echocardiography was used to determine diastolic perfusion time, and heart catheterization was performed to measure LVOT gradient and LV pressures. Also, serum NT-proBNP was used as a biochemical marker of LV wall stress.

Results: Hyperemic MBF was blunted in the HCM patients versus controls (2.26 ± 0.97 vs. 2.93 ± 0.64 mL min^{-1} g^{-1}, $p < 0.05$). In contrast to controls, the endo-to-epi MBF ratio decreased significantly in HCM patients during hyperemia (1.38 ± 0.15 to 1.25 ± 0.19, p = NS and 1.20 ± 0.11 to 0.88 ± 0.18, $p < 0.01$ respectively). This pattern was similar for the hypertrophied septum and lateral wall. Hyperemic MBF was inversely correlated with LVOT gradient, NT-proBNP, left atrial volume index, and LVMI in a univariate regression analysis (all $p < 0.01$). Multivariate regression analysis, however, revealed that only LVMI and NT-proBNP were both independent predictors of hyperemic MBF, with greater impact at the subendocardial myocardial layer.

Conclusions: Hyperemic MBF is more severely impaired at the subendocardial level in HCM patients. The level of impairment is related to LVMI and NT-proBNP, suggesting that both vascular resistance and extravascular compressive forces determine microvascular dysfunction.

591. REGIONAL INTRAMYOCARDIAL FUNCTION: A COMPARISON BETWEEN SPECKLE TRACKING ECHOCARDIOGRAPHY (2D-STI) AND MR TAGGING.

Laura Ernande,[1] Geneviève Derumeaux,[2] Joost Kuijer,[3] Magalie Viallon,[4] Pierre Clarysse,[5] Pierre Croisille.[6]
[1]Departement of Echocardiography, Departement of Radiology, Louis Pradel Hospital, Creatis UMR CNRS, 630, Lyon, France, [2]Departement of Echocardiography, Louis Pradel Hospital, Lyon, France, [3]Departement FMT, VU University Medical Center, Amsterdam, The Netherlands, [4]Siemens, Paris, France, [5]Creatis UMR CNRS, Lyon, France, [6]Departement of Radiology, Louis Pradel Hospital; Creatis UMR CNRS, Lyon, France.

Introduction: Doppler tissue imaging (DTI) is a widely validated method for echographic assessement of regional myocardial deformation. DTI-derived strains are however inherently limited to a 1D, angle-dependent analysis of myocardial deformation. Two dimensional strain based on speckle tracking imaging (STI) has been recently proposed to overcome such limitations allowing to calculate 2D strains in an angle-independent way. Only preliminary results on small groups of patients with coronary artery disease (CAD) or hypertrophic cardiomyopathy have been published to date. Recently, a great deal interest have been focusing on the existence of subtle impairements of regional myocardial function without alteration of global systolic left ventricular function in patients with diabetes mellitus (DM) that could be a pre-clinical marker of diabetic cardiomyopathy (1).

Purpose: To assess circumferential strain changes using STI and MR-tagging in a type-2 DM population, as compared to CAD patients and healthy volunteers (HV).

Methods: Twenty-seven subjects (53 ± 14 years) were included in this study: 3 HV, 14 patients with type-2 DM and no history of cardiac pathology and 10 patients with CAD and left ventricular ejection fraction $\geq$50%. Regional myocardial systolic left ventricular function was assessed by wall motion score (WMS) and by circumferential maximal systolic strain (ε_c) measured by STI and MR-tagging. The delay between echography and MRI was 3 ± 1 days. WMS analysis was performed on echographic B-mode and cine-MR images on matching short axis views at the basal, mid and apical level of the left ventricle. Using standard echographic 2D images and a dedicated software package (EchoPac PC;GE Healthcare, Waukesha, WI, USA), ε_c by STIwas measured in 16 AHA-derived segments. The measure was repeated 3 times on 3 different cardiac cycles. TrueFISP tagging cine-MRI sequences (TR/TE: 30/1.3 ms; tag spacing 6 mm, FOV 280 mm; slice thick 7 mm; FA 20°) were performed on a 1.5 T MR scanner (Avento, Siemens Medical Systems, Erlangen, Germany); images were analyzed using a dedicated post-processing tool (Intag, CREATIS, Lyon, France). $\varepsilon_c$was measured in the same segments as with the STI method.

Results: The feasibility of STI and MR tagging were 98.9% and 93.5%, respectively. After WMS analysis, segments were assigned to one of the following groups: (i) normal segments (WMS 1) of HV (group N-HV); (ii) normal segments (WMS 1) of patients with DM (group N-DM); (iii) normal segments (WMS 1) of patients with CAD (group N-CAD); and

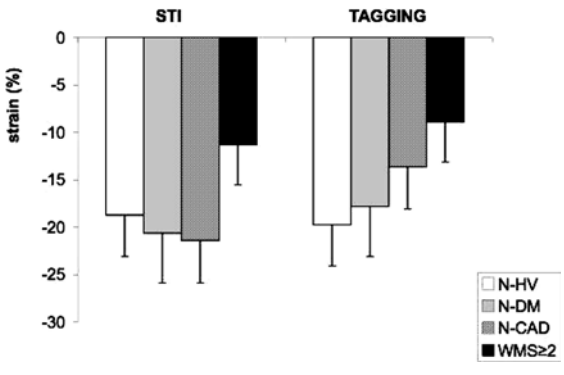

FIG. 1. Circumferential systolic strain (ε_c) assessed by (STI) and MR tagging. N-HV: healthy volunteers; N-DM: type 2 diabetes mellitus patients. N-CAD: normal segments of CAD patients. WMS $\geq$ 2:dysfunctional segments.

(iv) dysfunctional segments (WMS 2, 3 or 4) of the patients with CAD (group WMS $\geq$ 2). Results are expressed as ε_c mean in each group $\pm$ standard deviation and shown in figure. ε_c assessed by STI and MR-tagging discriminated normal segment (WMS 1) and dysfunctional segments (WMS $\geq$ 2) ($p < 0.05$ group WMS $\geq$ 2 vs other groups). ε_c in group N-DM and N-HV were comparable. However, we observed heterogeneous ε_c results in normal segments of patients (group N-DM and N-CAD) with a trend to higher values in ε_c assessed by STI than by tagged MRI in group N-CAD.

Conclusion: Both methods were able to differentiate dysfunctional from normal segments. Circumferential shortening may not be an early marker of intramyocardial dysfunction in type 2 DM patients. Heterogeneous strain values were observed with both imaging methods in remote normal regions suggesting in upcoming studies the use of disease-specific normal range values.

REFERENCE

1. Andersen NH, et al. Clinical Science 2003;105:59–66.

592. MRI-BASED VESSEL WALL PARAMETERS DIFFERENTIALLY CORRELATE WITH CAROTID IMT AND CACS

Karen B. Weinshelbaum,[1] Venkatesh Mani, PhD,[1] Silvia H. Aguiar, MD,[1] John E. Postley, MD,[2] Hiroaki Taniguchi, MD,[1] Rob van der Geest, PhD,[3] J. H. Reiber,[3] Valentin Fuster, MD, PhD,[1] Zahi A. Fayad, PhD.[1] ***[1]Mount Sinai School of Medicine, New York, NY, USA, [2]Columbia University, New York, NY, USA, [3]University of Leiden, Leiden, The Netherlands.***

Introduction: Studies have shown that coronary artery calcium score (CACS) and carotid ultrasound intima media thickness (IMT) measurements are predictors of cardiovascular events. More recently high-resolution black blood MRI has been used for both qualitative and quantitative non-invasive evaluation of arterial walls.

Purpose: The purpose of this study was to compare black blood MRI quantitative vessel wall parameters with CACS and IMT measurements.

Methods: Two groups were studied. One group of twenty-one patients at moderate to high Framingham risk for cardiovascular events underwent both CT and rapid extend coverage double inversion recovery black blood MRI (REX)of the common carotid arteries (CC) and thoracic aorta (TAO). A second group of twenty patients with similar Framingham risk underwent the same MRI imaging, but also underwent carotid ultrasound. MRI-based vessel wall parameters including wall thickness, wall area, and wall area normalized to total vessel area were obtained from manually traced MR cross-sectional images. CACS and IMT were obtained from the CT and ultrasound images.

TABLE 1
Differential correlation between MRI vessel wall parameters and CACS, IMT

MRI Vessel Wall Parameter	Correlation with CACS (R^2)	Correlation with Mean IMT (R^2)	Correlation with Max IMT (R^2)
Common carotid minimum wall thickness	.52	.55	.45
Common carotid maximum average wall thickness	NS	.47	.57
Common carotid average wall thickness	NS	.47	.57
Thoracic aorta maximum wall thickness	NS	.47	.55
Thoracic aorta average wall thickness	NS	NS	NS
Thoracic aorta minimum wall thickness	NS	NS	NS

Results: MRI-based vessel wall parameters in the carotid and aorta showed unequal correlations with CACS and IMT. Table 1 shows the differential correlation between MRI wall thickness parameters and CACS and IMT. Significant correlations at p value $< .05$ are highlighted in bold (Table 1).

Conclusions: Carotid IMT and CACS are widely used for serial measurements and as end points in clinical trials. Black blood MRI is a technique which allows direct quantitative and qualitative evaluation of vessel walls and atherosclerotic disease. A new finding here is that MRI's high-resolution vessel wall imaging allows for multiple types of quantitative measurements which in these cohorts differentialy correlate with CACS and IMT. This suggests that cardiovascular MRI may yield multiple types of distinct and significant information regarding the state of atherosclerosis in an individual.

593. NON-INVASIVE IN VIVO MOLECULAR MAGNETIC RESONANCE IMAGING OF MATRIX METALLOPROTEINASES TO ASSESS AHTEROSCLEROSIS

Smbat Amirbekian,[1] Juan G. S. Aguinaldo, MD,[2] Vardan Amirbekian, MD,[3] Fabien Hyafil, MD,[2] David B. Weinreb,[2] Esad Vucic, MD,[2] Marc Sirol, MD,[2] Eric Lancelot, PhD,[4] Claire Corot, PhD,[4] Zahi A. Fayad, PhD.[2] ***[1]Emory University School of Medicine, Mount Sinai School of Medicine, Imaging Science Laboratories, New York, NY, USA, [2]Mount Sinai School of Medicine, Imaging Science Laboratories, New York, NY, USA, [3]Johns Hopkins University School of Medicine, Mount Sinai School of Medicine, Imaging Science Laboratories, New York, NY, USA, [4]Guerbet, Paris, France.***

Introduction: Matrix Metalloproteinases (MMPs) play an important role in the pathogenesis of atherosclerosis. MMPs play

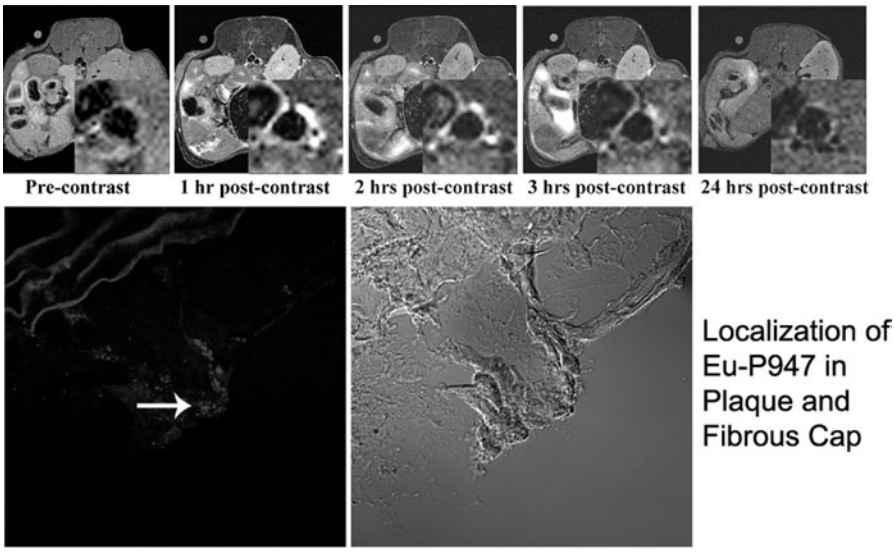

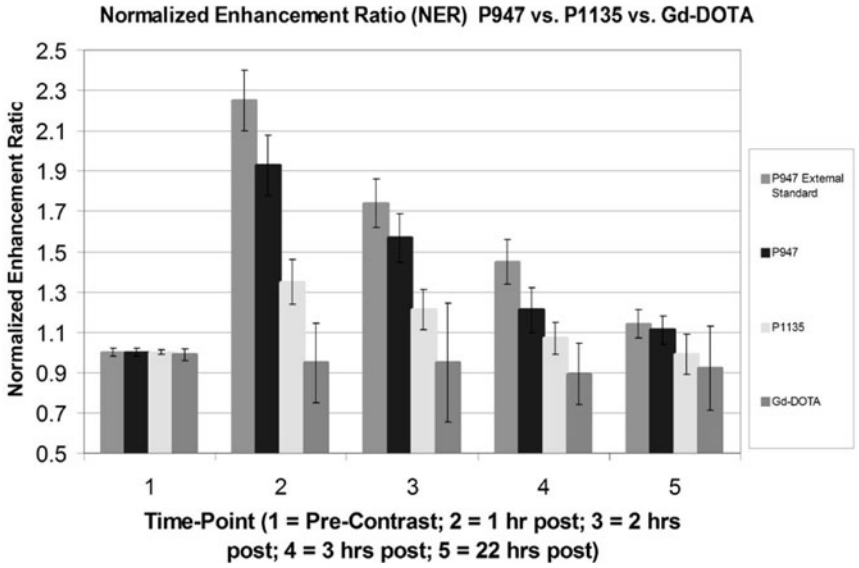

FIGS. 1. and 2.

a vital role in vascular remodeling and stenosis/re-stenosis phenomena. Over-expression of MMPs is associated with plaque rupture and instability. MMPs are often highly expressed at the shoulder regions of plaques that rupture. P947 (Guerbet) is a short peptide ligand for MMPs. P947 has a DOTA-Gadolinium chelate attached to it using a linker, making it into an MRI contrast agent.

Purpose: Here we investigated the in-vivo efficacy of P947 in detecting atherosclerotic plaques using several well-structured controls. We investigated biological specificity by performing localization studies of fluorescent Eu-P947 and co-localization studies using fluorescent Eu-P947 and specific MMP fluorescent immunostaining.

Methods: Using ApoE-/-mice (n = 15), pre-contrast-enhanced (CE) and post-CE MRI was performed at 1, 2, 3 and 22 hrs post-injection. P947 was injected via the tail vein. As one control (n = 4), we used the peptide contrast agent P1135, which is P947 with the peptide sequence completely scrambled. By scrambling the peptide sequence specificity for MMPs is lost. As a second control, another group of ApoE-/-mice (n = 5) were injected with the nontargeted Gd-chelate Gd-DOTA. Fluorescent Eu-P947 was made using Europium instead of Gadolinium. Eu-P947 was injected in ApoE mice to track where P947 goes using laser-scanning confocal-microscopy. Co-localization experiments were performed by using Eu-P947 and fluorescent immunostaining for specific MMPs, including MMP-2, MMP-3, and MMP-9.

Results: In ApoE-/-mice, using P947 the change in MRI signal measured by the Normalized-Enhancement-Ratio (NER) was 2.25 ± 0.19 (125% enhancement) at 1 hr, 1.74 ± 0.14 (74%) at 2 hrs, 1.31 ± 0.13 (31%) at 3 hrs, and 1.18 ± 0.06 (18%) at 24 hrs (Figs. and Graph). Using P1135 (P947 scrambled) we saw enhancements of only 1.31 ± 0.14 (31% enhancement) in the ApoE-/-mice at 1 hr, 1.19 ± 0.11(19%) at 2 hrs, 1.09 ± 0.1

(9%) at 3 hrs, and 1.07 ± 0.05 (7%) at 24 hrs. MMP Zymography demonstrated significant MMP activity in imaged sections (controls were negative). Laser-scanning confocal-microscopy revealed localization of fluorescent Eu-P947 in atherosclerotic plaques of ApoE mice (Figs.). Laser-scanning confocal fluorescence microscopy experiments revealed significant overlap or co-localization between areas of specific MMP staining (MMP-2, MMP-3, MMP-9) and Europium-P947 localization indicating significant specific binding and retention.

Conclusions: Targeting MMPs with P947 showed highly significant MRI enhancement of aortic atherosclerotic plaque in ApoE-/- mice. The enhancement of atherosclerosis using P947 was excellent compared to controls including P1135 and Gd-DOTA. Eu-P947 localized to atherosclerotic plaques and co-localized with specific MMPs.

594. EVALUATION OF GROWTH CHARACTERISTICS OF THE AORTIC ARCH IN CHILDREN WITH HYPOPLASTIC LEFT HEART SYNDROME USING CARDIAC MAGNETIC RESONANCE (CMR) AT 3 TESLA

Inga Voges, Michael Schumacher, Chris Hart, Traudel Hansen, Hans-Heiner Kramer, Carsten Rickers. ***University Hospital, Kiel, Germany.***

Introduction: Hypoplastic left heart syndrome (HLHS) is a fatal disease of the newborn (1:5000) if left untreated. Surgical treatment of HLHS includes a staged reconstruction. The first (Norwood operation) of three stages involves formation of a neo-aorta using aortic homograft or other graft material. Stage 2 aims to create a bidirectional cavopulmonary connection which is converted into a total cavopulmonary connection (Stage 3). Echocardiography and cardiac catheterization have been the standard imaging modalities for pre-operative assessment and long term follow-up. However, it has been shown that the sensitivity of echocardiographic assessment of the neo-aorta is low and that cardiac catheterisation is associated with considerable morbidity in these patients.

Purpose: We sought to use high field CMR (3 Tesla) to evaluate the growing characteristics of the neo-aorta in children with HLHS. We also compared our findings with normal values.

Methods: Ten patients (age range 2 month-10 years) with HLHS after second or third stage operation underwent a CMR study at 3 Tesla. Gradient echo cine and black blood spin echo imaging was performed to delineate neo-aortic anatomy. The images were used for measuring diameters of the reconstructed aorta at five selected segments (aortic root, ascending aorta, aortic arch, aortic isthmus, descending aorta). Additionally high resolution contrast enhanced MR angiography was performed using centra keyhole technique.

Results: The diameters of the reconstructed aortic arch (mean value 12.9 mm, > 2 SD) and the aortic root (mean value 20 mm, > 2 SD) after the Norwood operation was significantly dilated

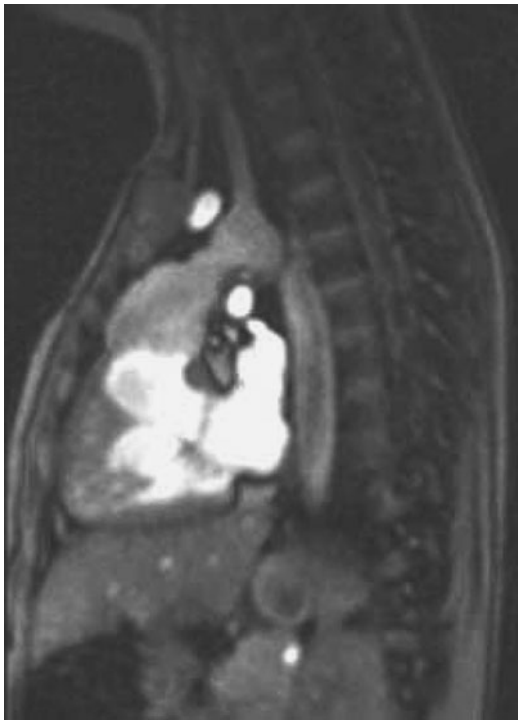

as compared to normal values generated by echocardiography and cardiac catheterisation. However, we did not observe any further increase of aortic dilatation after a period of four to five years. In two patients, we found flow acceleration at the distal anastomosis which was considered borderline requiring close follow up examinations.

Conclusion: In this study we have demonstrated that high field CMR provides a comprehensive imaging modality for the assessment of neoaortic anatomy and flow in pts. with hypoplastic left heart syndrome after Norwood operation.

We found that the neo-aorta is significantly dilated (75%) as compared to normals but did not further dilate over an observation period of 4 to 5 years as compared to pre-operative cardiac catheterisation. Two pts. showed a borderline narrowing of the distal stenosis. In the future CMR has the potential to replace invasive aortic evaluation in these patients.

595. ASSESSMENT OF MECHANICAL DYSSYNCHRONY USING CARDIOVASCULAR MAGNETIC RESONANCE AND SEMI-AUTOMATIC BORDER DETECTION: INITIAL EXPERIENCE

Harald P. Kühl,[1] Ralf Koos,[1] Mirja Neizel,[1] Georg Schummers,[2] Tienush Rassaf,[1] Malte Kelm.[1] ***[1]University Hosptial, Aachen, Germany, [2]TomTec Imaging, Unterschleißheim, Germany.***

Introduction: Assessment of mechanical dyssynchrony is clinically important in patients with reduced left ventricular function and symptoms of heart failure to select patients who

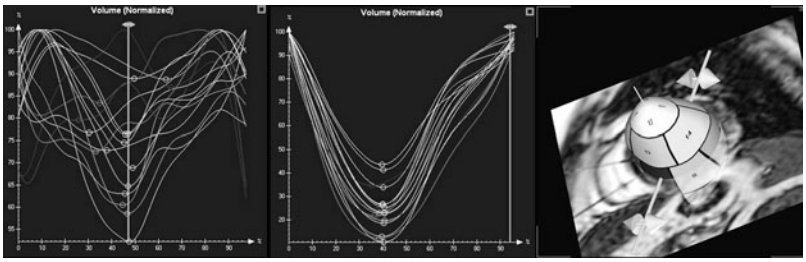

FIG. 1.

may benefit from cardiac resynchronization therapy (CRT). Two-dimensional echocardiography using tissue velocity and strain/strain-rate imaging have shown promising results for the assessment of mechanical asynchrony. However, these techniques have important technical limitations. More recently volumetric real-time three-dimensional echocardiography has been used in conjunction with semi-automatic border detection algorithms to evaluate heart-failure patients for the presence of mechanical asynchrony. The systolic dyssynchrony index (SDI), defined as the standard deviation of the time to minimal systolic volume of all 16 ASE segments (normalized to the RR interval), was introduced as a measure of mechanical asynchrony. This index has shown to be potentially useful for the selection of patients who may benefit from CRT. However, three-dimensional echocardiography may be inadequate in a number of patients with suboptimal acoustic window.

Purpose: In this preliminary study, we investigated 15 patients with reduced left ventricular function for the presence of mechanical asynchrony using CMR and a semi-automatic border detection algorithm. Results were compared to a group of 10 healthy control subjects with normal LV function.

Methods: Mean EF of the patient population was 25 ± 13%. For cine imaging a standard SSFP imaging sequence (TE/TR 1.8/3.6 ms, spatial resolution 1.8 × 1.5 mm^2, slice thickness 8 mm, gap 2 mm) was used with a temporal resolution of 40 frames per RR-interval. Three long-axis images and a stack of 10 to 12 short-axis images covering the complete left ventricle were acquired in repeated breath-holds. The data set was transferred to a separate workstation and transformed off-line into a voxel based 3D data set. Quantitative analysis was performed using a preliminary semi-automatic border detection software adapted from 3D echocardiography (4D MR-LV-Analysis, TomTec, Unterschleißheim, Germany). After manual outlining of endocardial borders in the three long-axis images at end-diastole and end-systole LV casts are automatically calculated for each of the 40 time frames per RR interval providing a global volume-time-curve. The cast can be further subdivided into 16 or 17 subsegments resulting in volume-time curves for each of these subsegments. Global volumes, ejection fraction and SDI were calculated in each patient.

Results: Figure 1 gives an example for a patient with marked mechanical dyssynchrony (SDI 11%, left panel) and a normal control subject (SDI 3%, middle panel) as well as a view of the LV cast at end-diastole. The mean SDI differed significantly between patients and controls (9.6 ± 2.8% vs. 3.2 ± 2.2%; $p < 0.001$). These values are in good agreement to previously published data using real-time 3D echocardiography (1).

Conclusions: The results of this preliminary study suggest that CMR with semi-automatic border detection may be useful for the assessment of mechanical dyssynchrony in patients with poor left ventricular function and poor echo image quality.

REFERENCE

1. Kapetanakis S, et al. Circulation 2005;112:992.

596. LATE GADOLINIUM ENHANCEMENT IN EISENMENGER SYNDROME IS COMMON BUT NOT ASSOCIATED WITH VENTRICULAR DYSFUNCTION, DEGREE OF CYANOSIS, OR EXERCISE CAPACITY

Craig S. Broberg, MD,[1] Sanjay Prasad, MD,[2] Henry Kafka, MD,[3] Michael Gatzoulis, MD, PhD.[3] [1]***Oregon Health and Science University, Portland, OR, USA,*** [2]***Royal Brompton Hospital, Imperial College London, London, United Kingdom,*** [3]***Royal Brompton Hospital & Imperial College London, London, United Kingdom.***

Introduction: Late gadolinium enhancement (LGE) has been demonstrated in the pressure loaded right ventricle (RV) of several forms of congenital heart disease and relates to function. Similar findings in Eisenmenger syndrome (pulmonary hypertension with right-to-left shunt and cyanosis) have not been reported.

Purpose: To determine the frequency and significance of LGE in patients with Eisenmenger syndrome.

Methods: Forty-eight patients with confirmed Eisenmenger syndrome underwent cardiovascular magnetic resonance (1.5 T Siemens Sonata) for assessment of right ventricular (RV) and left ventricular (LV) volumes and LGE (0.1 mmol/kg). Measurement of oxygen saturation, hemoglobin, serum neuropeptides, and exercise capacity (treadmill exercise with measured oxygen consumption) was also performed on the same day.

Results: The right and left ventricles were structurally and functionally similar. All patients had severe RV hypertrophy (RV mass index 65 ± 24 g/m^2 compared to 68 ± 24 g/m^2 for the LV). There was a strong correlation between RV and LV ejection fraction ($r = 0.74$, $p < 0.001$). Gadolinium was

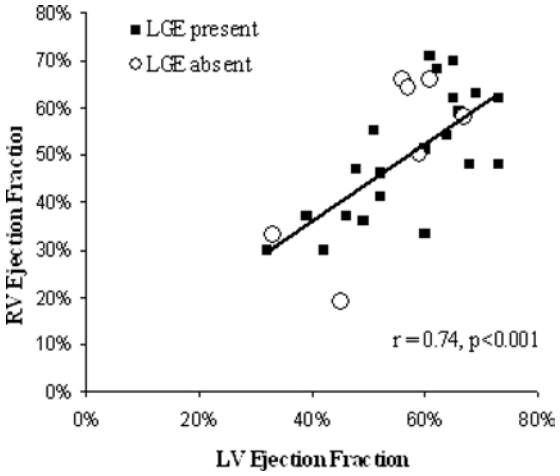

administered to 28 patients, and LGE was present in 18 (64%). Enhancement was most often seen in small quantities within the RV subendocardium. Trabecular pooling in the RV was found in 10 (36%). Papillary muscle fibrosis (RV or LV) was found in 8 (29%) patients, and enhancement at the RV-LV junction was present in 7 (25%). Comparing those with and without LGE there was no difference in age, shunt size, shunt type, RV or LV mass, volumes, ejection fraction, or pulmonic/systemic flow ratio, even controlling for location and type of enhancement present. There were no differences in oxygen saturation, hemoglobin, hematocrit, atrial natriuretic peptide, brain natriuretic peptide, history of arrhythmia, six minute walk test, treadmill exercise duration, or peak oxygen consumption in those with enhancement.

Conclusions: In patients with Eisenmenger syndrome, there is a strong interventricular relationship such that ventricular dysfunction progresses in both ventricles simultaneously. Small quantities of LGE are common, and typically present in areas most susceptible to ischemic injury. However, in contrast to other forms of RV pressure overload, presence of fibrosis does not correlate with ventricular size or function, degree of cyanosis, or exercise capacity.

597. NON-INVASIVE MEASUREMENT OF CORONARY ARTERY VASOREACTIVITY USING 3T MRI

Glenn A. Hirsch, MD,[1] Robert G. Weiss, MD,[1] Gary Gerstenblith, MD,[1] Michael Schar, PhD,[2] Matthias Stuber, PhD.[1] [1]***Johns Hopkins University, Baltimore, MD, USA,*** [2]***Johns Hopkins University/Phillips Medical Systems, Baltimore, MD, USA.***

Introduction: Numerous studies have demonstrated that brachial artery reactivity predicts cardiovascular event rates. Although coronary artery endothelial dysfunction is likely a stronger predictor of coronary atherosclerosis and cardiac events, there is unfortunately no current non-invasive means for assessing endothelial function of the coronary arteries. Endothelial-independent vasodilatation was documented in a previous study using MRI at 1.5T following the administration of nitroglycerin (1).

Purpose: Because isometric handgrip exercise has well-established endothelial-dependent effects on vasoreactivity, we hypothesized that endothelial-dependent coronary vasoreactivity could be measured non-invasively by combining 3T coronary MRI and isometric handgrip exercise.

Methods: We enrolled 7 healthy adult subjects (4 female, 3 males) average age 28.1 $\pm$ 3.8 years. Subjects were placed prone in a commercial 3T coronary MRI scanner and a 6-element phased array coil was used for signal reception. For handgrip exercise, an MR compatible dynamometer (2) was used and maximum grip strength was identified in each individual prior to scanning. Using a series of scout scans, the course and the 3D orientation of the major proximal left (left main [LM]; left anterior descending [LAD]) and right coronary (RCA) segments were identified. The coronary artery that had the least motion and that was most easily imaged in a perpendicular plane was then assessed at baseline using a dedicated segmented gradient echo cine sequence perpendicular to that coronary artery of interest (FOV = 320 mm, Matrix = 512×461, Spatial Resolution = $0.8 \times 0.8 \times 8$ mm^3, temporal resolution = 37 ms TR = 6.1 ms, TE = 3.6 ms, RF excitation angle = 15°, BW = 434 Hz). In all subjects, cross-sectional high-resolution MRA was subsequently repeated during a 3 minute isometric handgrip stress. Continuous handgrip exercise in the scanner was performed for 3 minutes at 30% of each individual's maximum grip. In recovery (at least 3 minutes following the handgrip acquisitions), we repeated the measurements in 5 subjects. Coronary artery cross-sectional areas at baseline, during handgrip and in recovery were then measured for comparison using automated software employing full-width-half-maximum criteria (Cine version 3.15.17) (Fig. 1). To minimize adverse effects of coronary motion on cross-sectional area computations, the analysis was limited to visually inspected periods of minimal myocardial motion (Figs. 1B and C).

Results: All seven subjects had sufficient image quality during isometric exercise, and data during recovery was obtained in five. The LAD artery was used for measurements in 3 subjects, the LM in one subject, and the RCA in 3 of the subjects. In healthy subjects, isometric handgrip induced significant changes in coronary cross-sectional areas as compared to baseline values (baseline 16.6 $\pm$ 3.4 mm^{2}vs. stress 19.1 $\pm$ 3.9 mm^2, $p = 0.02$). The average percent area change was 16.6 $\pm$ 7.6%. In the 5 subjects with coronary cross-sectional areas measured following the stress, there was no significant difference between this measurement and the baseline cross-sectional area (baseline 19.9 $\pm$ 3.8 mm^{2}vs. recovery 20.0 $\pm$ 4.1 mm^2, $p = 0.91$).

Conclusions: Non-invasive measurement of endothelial dependent coronary artery vasoreactivity is now possible using 3T coronary MRI and isometric handgrip exercise. Additional studies are needed to test the feasibility and prognostic value in patients with underlying coronary artery disease.

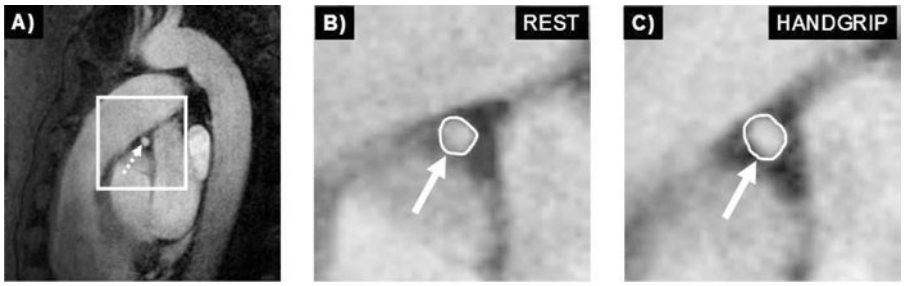

FIG. 1. A cross-sectional view of the left main coronary artery is shown by the dotted arrow in A). The area in the white box is zoomed in B) and C) demonstrating cross-sectional area changes with isometric handgrip compared to the baseline.

REFERENCES

1. Terashima M, Meyer CH, Keeffe BG, et. al. Noninvasive assessment of coronary vasodilation using magnetic resonance angiography. J Am Coll Cardiol 2005;45:104–10.
2. Brown BG, Lee AB, Bolson EL, Dodge HT. Reflex constriction of significant coronary stenosis as a mechanism contributing to ischemic left ventricular dysfunction during isometric exercise. Circulation 1984;70:18–24.
3. Weiss RG, Bottomley PA, Hardy CJ, Gerstenblith G. Regional myocardial metabolism of high-energy phosphates during isometric exercise in patients with coronary artery disease. N Engl J Med. 1990;323:1593–600.

598. EVIDENCE FOR PAPILLARY MUSCLE INVOLVEMENT IN HYPERTROPHIC CARDIOMYOPATHY BY CARDIAC MAGNETIC RESONANCE

Caitlin J. Harrigan, BA,[1] Evan Appelbaum, MD,[2] C. Michael Gibson, MD, MS,[2] James E. Udelson, MD,[3] Warren J. Manning, MD,[2] Barry J. Maron, MD,[4] Martin S. Maron, MD.[3]
[1] PERFUSE CMR Core Laboratory, Harvard Medical School, Boston, MA, USA, [2] Department of Medicine, Cardiovascular Division, Beth Israel Deaconess Medical Center, Harvard Medical School, Boston, MA, USA, [3] Hypertrophic Cardiomyopathy Center, Division of Cardiology, Tufts-New England Medical Center, Boston, MA, USA, [4] The Hypertrophic Cardiomyopathy Center, Minneapolis Heart Institute Foundation, Minneapolis, MN, USA.

Background: Increased thickness of the left ventricular (LV) wall is considered the predominant phenotypic expression of hypertrophic cardiomyopathy (HCM). Whether other prominent myocardial structures such as the LV papillary muscles are also involved in the hypertrophic process remains unclear. Cardiac magnetic resonance (CMR) provides superior spatial resolution with tomographic coverage of the heart. Therefore, we used CMR to characterize the morphology of the papillary muscles in a large, consecutive cohort of HCM patients.

Methods: Cine and delayed enhanced CMR were performed on 100 consecutive HCM subjects from two HCM referral centers using a 1.5 T Philips or Siemens whole body CMR system. ECG-gated, breath-hold cine images were acquired in 3 long-axes and contiguous 10 mm thick short axis slices achieving full coverage of the LV. On the end-diastolic short-axis images, the contours of the papillary muscles and epicardial and endocardial borders were traced manually. Papillary muscle mass, total LV mass, maximal wall thickness and volumes were automatically calculated. Delayed enhancement was performed 15 minutes after the intravenous administration of 0.2 mmol/kg of gadolinium-DTPA (Magnevist, Schering; Berlin, Germany) with a breath-hold inversion sequence (TI = 240–300 ms), acquired in the same views as the cine images. The presence of hyperenhanced myocardium was assessed on the short-axis, contrast-enhanced images using an image intensity $\geq$6 SD above the mean of remote myocardium.

Results: In the HCM patients, LV papillary muscle mass was 11.8 ± 4.8 g (range 3 to 27 g). When included as part of overall LV hypertrophy, the papillary muscles contributed 5% of total LV mass in 43% of patients, 6–10% of mass in 53% of patients and $>$10% in 4% of patients. The mean number of papillary muscles was 2.8 ± 1.0 for the HCM patients, including 38% patients with three, and 21% patients with four or more (up to five). There was a significant correlation between total papillary muscle mass and total LV mass ($R^2 = 0.1$; $p = 0.001$). Four patients (4%) showed delayed hyperenhancement representing fibrosis of $\geq$ 1 papillary muscle.

Conclusions: Morphologic abnormalities of the papillary muscles including increased mass and fibrosis are present in a substantial number of HCM patients. These CMR data demonstrate that the cardiomyopathic process is more diffuse than previous regarded, and can now be considered to involve the papillary muscles.

599. CORRECTION FOR T1 NONLINEARITY IN MYOCARDIAL SIGNAL INTENSITY IMPROVES FIRST-PASS PERFUSION QUANTIFICATION

Li-Yueh Hsu, Peter Kellman, Andrew E. Arai. ***NIH, Bethesda, MD, USA.***

Introduction: The nonlinear T1 saturation recovery in first-pass contrast-enhanced MR myocardial perfusion imaging is an important issue which affects quantification of myocardial

MBF: mL/g/min, SLP and CER: a.u.

Mean (n = 10)	Rest PreLUT	Rest PostLUT	Rest % of correction	Stress PreLUT	Stress PostLUT	Stress % of correction
TD70_MBF	0.95	1.00	4.8%	3.34	3.89	16.3
TD70_SLP	0.36	0.38	6.1%	0.75	0.80	11.9%
TD70_CER	1.69	1.78	5.5%	2.43	2.70	11.2%
TD150_MBF	0.91	0.97	6.8%	2.92	3.72	27.1%
TD150_SLP	0.35	0.40	14.5%	0.71	0.88	24.1%
TD150_CER	1.51	1.71	13.2%	2.13	2.60	22.4%

blood flow. Despite many efforts focused on improving the linearity of the LV blood pool signal intensity, relatively little work has been published with regard to nonlinearity in the myocardium.

Purpose: We hypothesize that T1 nonlinearity is significant in the myocardium, and it will affect both semi and fully quantitative perfusion estimates. This nonlinearity will affect a long saturation recovery delay more than a short one, and a nonlinear correction of the myocardial signal intensity will improve quantitative perfusion estimates. Semiquantitative perfusion indices underestimate perfusion independent of T1 nonlinearity.

Methods: Ten normal volunteers went through 40 dual-bolus (Gd-DTPA 0.005 and 0.1 mmol/kg) perfusion studies on a 1.5T Siemens Espree scanner to cover the interplay of rest vs. stress states and short vs. long saturation recovery delays (TD 70 and TD150 ms) for quantitative perfusion estimates. Rest perfusion was performed 4 hours after the dipyridamole (0.56 mg/kg over 4 minutes) stress study. TD70 and TD150 studies were acquired on separate days. A look-up-table (LUT) for signal intensity versus T1 magnetization was calculated based on the following imaging parameters: 90° prep, 25° readout, TR 7.5 ms, TE 1.48 ms, 8 mm slice, acquisition matrix 128 × 80, FOV 360 × 270. The T1 value was converted to the contrast concentration using the equation $1/T1 = 1/T1_{init} + \gamma$ [Gd] ($T1_{init}$: 850 ms, γ: 4.5 L/mmol). The time-signal intensity curves were analyzed on 6 sectors of a mid ventricular slice. Semiquantitative perfusion indices of intensity upslope (SLP) and contrast enhancement ratio (CER) were measured. Fully quantitative myocardial blood flow (MBF) was estimated using a Fermi model constrained deconvolution. All perfusion estimates were compared before and after the LUT correction and correlated against the MBF of the LUT corrected TD70.

Results: Fig. 1 shows the relationship between myocardial signal intensity and contrast concentration for TD70 and TD150. Raw time-signal intensity plot shows the LUT correction has the largest effect near peak contrast enhancement. Table 1 summarizes the results of fully quantitative MBF and semiquantitative CER and SLP before and after the LUT correction. Both fully quantitative and semiquantitative measurements were significantly improved after the LUT correction for the stress perfusion but to a lesser extent for the rest study. The degree of correction required for TD150 was higher than TD70 due to more severe nonlinearity. Fig. 2 shows semiquantitative SLP and CER still underestimated vasodilated MBF even after the LUT correction. The effects of underestimation were of similar magnitude for TD70 and TD150.

Conclusions: The effect of T1 nonlinearity between myocardial signal intensity and contrast concentration significantly affects perfusion quantification. This nonlinearity leads to underestimation of all quantitative perfusion measures studied. The effects are more severe for TD150 than TD70. A LUT correction based on acquisition specific relaxivity models of signal intensity versus contrast concentration can correct the signal intensity curves for perfusion quantification. However, semiquantitative perfusion indices still underestimated vasodilated blood flow despite correction of the T1 nonlinearity.

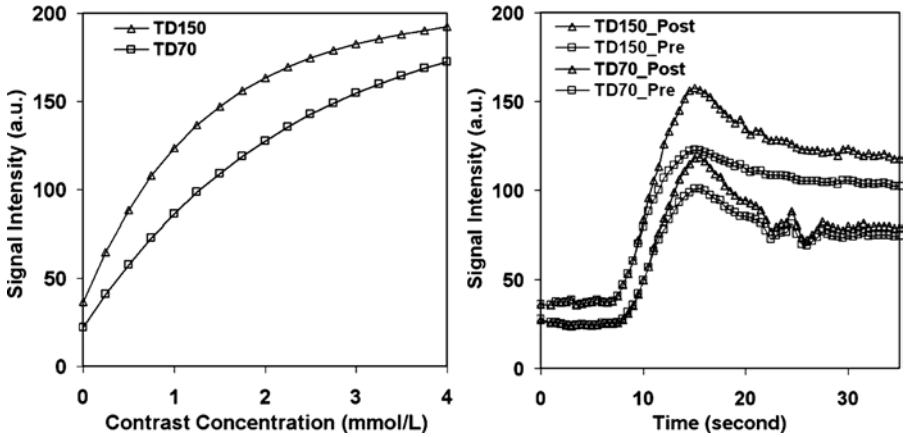

FIG. 1.

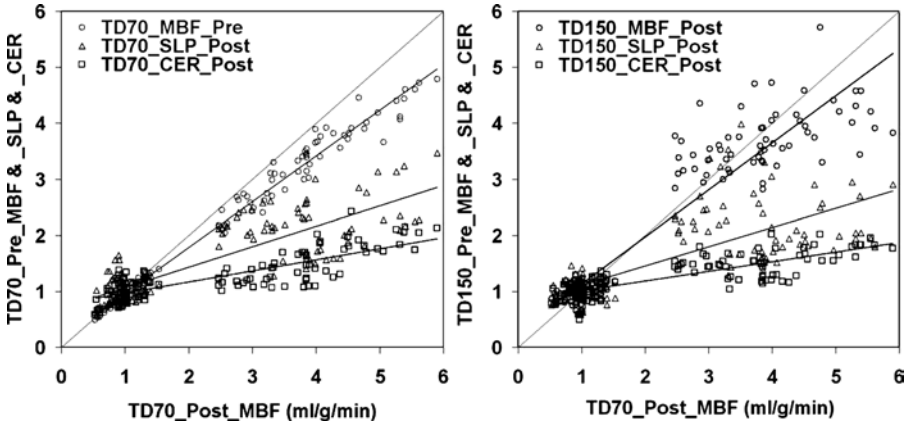

FIG. 2.

600. SUBCLINICAL ATHEROSCLEROTIC DISEASE IN HIGH RISK CHILDREN AND YOUNG ADULTS AS ASSESSED BY MAGNETIC RESONANCE IMAGING

Silvia H. Aguiar, MD,[1] Venkatesh Mani, PhD,[1] Karen B. Weinshelbaum,[1] John E. Postley, MD,[2] R. J. van der Geest, PhD,[3] J. H. Reiber, PhD,[4] Zahi A. Fayad, PhD.[1] [1]***Mount Sinai Medical Center, New York, NY, USA,*** [2]***Columbia University, New York, NY, USA,*** [3]***Leiden University Medical Center, The Netherlands, Leiden, The Netherlands,*** [4]***Leiden University Medical Center, Leiden, The Netherlands.***

Introduction: Cardiovascular Risk Factors by themselves are imprecise measures of extent of vascular pathology or disease burden. There had been controversy over age and timing for initiation of specific early interventions in young adults and children. Direct subclinical atherosclerotic disease visualization with MRI may help identify individual risk in this population.

Purpose: Vascular MRI may be used to evaluate burden of atherosclerotic disease (as direct subclinical atherosclerosis quantification) in children and adolescents at a high-risk distribution and may be equivalent to subclinical atherosclerosis of adult population at an intermediate to high 10 year risk by Framingham Risk Score (FRS).

Methods: Black-blood MRI of the aorta and extracranial carotid arteries was performed in 196 subjects (ages 8 to 87, 67 females) distributed into 5 age groups: Group 1 ($n = 40$, 14.12 ± 5.51 years, age 8–19, all at high-risk cardiovascular distribution); Groups 2, 3, 4, 5 consisting of 10 year increments ($n = 156$, 60.0 ± 21.5 years, ages 20 to 87, FRS $12\% \pm 0.12$). For each subject, 36 to 48 cross-sectional images of the aorta and 12 to 24 images of carotids were analyzed. Average arterial wall area (AWA) was calculated and normalized with lumen diameter (nAWA) in each resulting image to compensate for age-related arterial size variation. Average imaging time was 50 minutes.

Results: Analysis of 3,853 aortic and 3,352 carotid imaging slices showed that nAWA increases with age earliest in common carotid arteries followed by descending thoracic aorta in risk Groups 2 to 6. Post-Hoc ANOVA showed a bimodal distribution in that nAWA of Group 1 (Carotid 0.32 ± 0.05; Aorta 0.21 ± 0.03) is not significantly different from those of adults in their 50s and 60s, Groups 4 and 5 (Carotids 0.34 ± 0.06; Aorta 0.20 ± 0.03).

Conclusions: Atherosclerotic Disease Burden in children and adolescents with high-risk distribution is equivalent to the adult population at intermediate to high risk as assessed by high-resolution MRI. Our data may establish basis for future population studies. MRI is a rapid, non-invasive, and highly reproducible and may facilitate risk-stratification and monitoring of affected young patients.

601. QUANTIFICATION OF THE REGIONAL MYOCARDIAL FUNCTION AFTER DOBUTAMINE IN RAT USING CINE AND TAGGED MRI

Jean-Luc Daire, PhD, Jean-Pascal Jacob, Jean-Noel Hyacinthe, PhD, Karin Montet-Abou, Benoit Maricot, Matthieu Leptit-Coiffé, PhD, Denis Morel, MD, PhD, Jean-Paul Vallée, MD, PhD. ***Geneva University Hospital, Geneva, Switzerland.***

Introduction: The clinical hallmarks of hibernating myocardium include regional contraction deficit while retaining an inotropic

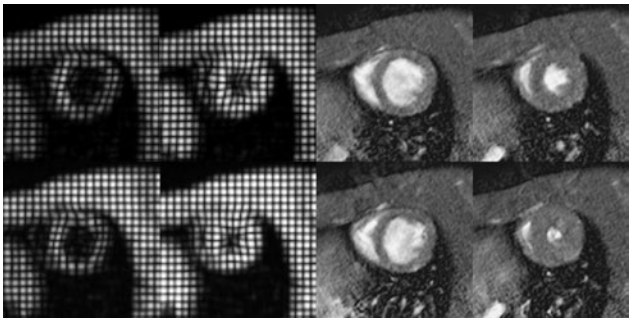

FIG. 1. Representative example of tagged and cine images at rest (first row) and stress under dobutamine (2nd row) in diastolic and systolic phases.

TABLE 1
Values of wall thickening and circumferential strains for each dose (mean ± SD)

Dobutamine dose (μg/min/kg)	0	2.5	5	10
Wall thickening	1.15 ± 0.22	1.34 ± 0.22*	1.47 ± 0.16*	1.84 ± 0.42*
Endocardium	0.38 ± 0.09	0.47 ± 0.13*	0.53 ± 0.15*	0.56 ± 0.14*
Midwall	0.28 ± 0.06	0.32 ± 0.07*	0.35 ± 0.08*	0.37 ± 0.10*
Strain epicardium	0.21 ± 0.05	0.23 ± 0.06. *	0.26 ± 0.06*	0.27 ± 0.08**

*$p < 0.001$; **$p < 0.018$.

reserve during a low dose dobutamine challenge. Experimental models on rodent aiming to reproduce myocardial hibernation require an accurate quantification of the cardiac function after dobutamine. MRI using both cardiac cine and tagged images has been recognized as a robust method to assess the cardiac function in rat. However, the respective advantage of both MRI methods regarding dobutamine challenge has never been investigated.

Therefore, the purpose of this study was to measure the regional contractile function in the normal rat using cardiac cine and tagged images during incremental doses of dobutamine.

Material and Method: Eight normal rats were imaged on a clinical 1.5 T MR system using a segmented turbo field echo cine sequence (11-16 phases per cycle, acquired voxel size 0.28/0.28/2 mm, TR/TE 12/7.6 ms, FA 45°, acquisition time per slice 2′45″) and a C-SPAMM tag preparation segmented cine fast field echo sequence (18–25 phases per cycle, acquired voxel size 0.63/1.79/3 mm, tag spacing 1.25 mm, TR/TE 7.8/3.6 ms, FA 10°, acquisition time per slice1′30″). After imaging at rest, three doses of dobutamine were injected (IV): 2.5, 5 and 10 μg/min/kg. Two short axis views were analysed per animal. For each slices, wall thickening using manual contour definition, circumferential and radial strains using semi-automated tracking software were calculated.

Results: Good cine and tagged images were obtained in all the rats even at higher dose of dobutamine associated with high heart rate (300–440 bpm) (Fig.). Measured from the cine MRI, ejection fraction and left ventricle end-systolic volume exhibit significant changes after each dobutamine perfusion dose ($p < 0.001$). Similar differences were observed with tagged MRI at both the endocardium and the mid-wall.

Both wall thickening and circumferential strains show significant difference between contractile function for each dose of dobutamine and reference contraction without dobutamine (Table). For wall thickening measurements and circumferential strain at endocardium and midwall levels, relative changes between each dose are significantly different ($p < 0.05$) except between 5 and 10 μg/min/kg for circumferential strain.However, radial strains and circumferential strain at epicardium level do not allow to separate all changes induced by dobutamine.

Conclusion: Both cardiac cine and tagged MRI can quantify the effect of incremental doses of dobutamine on the regional cardiac function in rat. Cine imaging with an increased spatial resolution allows in addition an accurate measurement of end diastolic and end systolic volume as well as cardiac mass. Tag MRI, despite a lower spatial resolution, yields accurate measurements in the subendocardium in a short amount of time. Therefore, both methods needs to be performed in the cardiac function assessment on rat to improve the robustness of cardiac MRI.

602. END DIASTOLIC LEFT VENTRICULAR MASS PREDICTS SURVIVAL BETTER THAN END SYSTOLIC MASS

Erik B. Schelbert, MD, MS, Jie J. Cao, MD, MPH, Andrew E. Arai, MD. ***National Institutes of Health, Bethesda, MD, USA.***

Introduction: Increased left ventricular mass (LVM) occurs in most disease states of the heart and is associated with increased mortality. LVM is conventionally measured in end diastole. Alternatively, LVM at end systole can also easily be measured, although there increased chance of including trabeculae and papillary muscle. It is not clear which method is preferable.

Purpose: Thus, we sought to compare LVM measurements at end systolic (ES) and end diastole (ED) and characterize their association with mortality.

Methods: From September 2001 to July 2006, 2,339 adult patients referred for cardiac MRI had left ventricular mass measured in both ED and ES using 1.5 T MRI scanners with SSFP cine pulse sequences. LVM was measured on a volumetric stack of manually-traced short axis images which excluded trabeculae and papillary muscle. Bland-Altman plots and linear regression assessed agreement between LVM measured at ED and ES. Survival analysis was performed in a subset of patients (n = 1,185) who were scanned between September 2001 and December 2004, the last update of vital status by the US National Death Index. The association of subsequent mortality with LVM measured either at ED or ES was quantified by Cox regression models where mass was indexed to body surface area.

Results: Most patients were male (67%); the mean age was 54 years (interquartile range 45–66). Mean mass was 111 g measured at ED and 116 g at ES. LVM at ED and ES were highly correlated ($R = 0.94$; $p < 0.0001$) and yielded the following relation: LVM-ES (grams) = (1.01) × LVM-ED (g) + 4.2. Bland-Altman analysis, however, revealed that as the mass increased, agreement deteriorated slightly, with a bias towards higher LVM at ES compared to ED (Fig. 1). In the survival analysis subset, there were 45 deaths (4%) over a median follow-up of 1.4 years (interquartile range 0.6–2.4). End diastolic LVM measurement was more associated with mortality in Cox regression analysis (LVM-ES/BSA: Chi square = 3.7, $p = 0.055$; LVM-ED/BSA: Chi square = 4.7, $p = 0.031$) although the differences were not significant.

Conclusions: Despite overall close correlation between end diastolic and end systolic mass, a bias in estimating end systolic

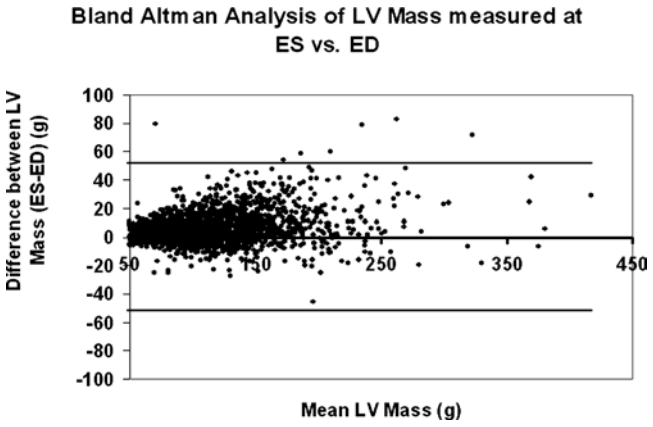

FIG. 1.

mass was observed. Since LV hypertrophy is associated with worse prognosis, it is interesting to note that end systolic mass had slightly less prognostic value than end diastolic mass.

603. MR ASSESSMENT OF POTENTIAL RIGHT VENTRICULAR REMODELLING ONE YEAR AFTER PERCUTANEOUS PULMONARY VALVE IMPLANTATION IN PATIENTS WITH PULMONARY REGURGITATION

Philipp Lurz,[1] Johannes Nordmeyer,[1] Louise Coats,[1] Graham Derrick,[1] Sachin Khambadkone,[1] Fiona Walker,[2] Philipp Bonhoeffer,[1] Andrew Taylor.[1] [1]***Great Ormond Street Hospital, London, United Kingdom,*** [2]***The Heart Hospital, London, United Kingdom.***

Introduction: Pulmonary regurgitation is a common condition in patients with congenital heart disease late after surgical repair. Percutaneous pulmonary valve implantation (PPVI) can treat this condition without cardiopulmonary bypass.

Purpose: We have described the acute improvements in ventricular performance after PPVI, and now present our 1-year follow-up data using CMR imaging to assess mid-term ventricular performance.

Method: We selected 31 patients (24.4 $\pm$ 10.8 years), from our total population of 137 who had undergone PPVI for various indications, because they had moderate/severe PR (regurgitant fraction $>$20% on magnetic resonance [MR]) and an echocardiographic gradient $<$50 mm Hg across the right ventricular (RV) outflow tract at echocardiography. CMR assessments of ventricular volumes and great vessel blood flow prior to PPVI, immediately after PPVI and 1 year after PPVI were performed and analysed. Data are expressed as mean $\pm$ standard deviation. Data were compared using ANOVA statistics, with paired Student t-testing and Bonferoni correction between groups. A p value of < 0.05 was regarded as significant.

Results: Although there was an significant acute improvement in indexed right ventricular end-diastolic volume (iRVEDV), indexed effective right ventricular stroke volume (iERVSV), pulmonary regurgitant fraction (RF), further significant benefits one year after PPVI were not seen.

Acutely following PPVI indexed left ventricular stroke volumes (iLVSV) increased from 41.0 $\pm$ 8.2 mL/m^2 to 48.6 $\pm$ c5.6 mL/m^2 immediately after the procedure. At one year there was no significant further increase in iLVSV $-$52.1 $\pm$ 7.7 mL/m^2 (ANOVA post 1 year, p = n.s.).

Conclusion: One year after PPVI initially chance in ventricular performance and dimensions are well maintained, but no statistically significant further improvement was observed. No evidence for right ventricular remodelling was seen. These results demonstrate that at 1 year the PPVI functions well, but the lack of long-term re-modelling may suggest that we should intervene at an early stage in patients with chronic pulmonary regurgitation before the development of irreversible ventricular dysfunction.

604. VALIDATION OF AUTOMATIC DETECTION OF LEFT VENTRICULAR POSITION AND ORIENTATION

Xiang Lin, Brett Cowan, Alistair A. Young. ***University of Auckland, Auckland, New Zealand.***

Introduction: Virtually all cardiac MRI investigations include a functional study to determine left ventricular (LV) ejection fraction, volumes and mass. This requires the segmentation of the LV endocardial and epicardial boarders which can require considerable time from busy clinicians.

The automatic identification of the LV in true-FISP MRI cines would remove the need for users to perform this step and allow more time for powerful image segmentation algorithms to work on the data prior to display to the clinician. Present techniques to determine the position and orientation of the LV use either low level segmentation or feature recognition techniques and suffer from the disadvantages of computational expense or unacceptable failure rates when tested on large data sets.

Purpose: To develop and test an algorithm to determine the position and orientation of the LV from short axis (SA) true-FISP cine images.

TABLE 1

	Pre-PPVI	Immediately post-PPVI	1 year post PPVI	ANOVA post 1 year
iRVEDV	103.2 $\pm$ 8.6 mL/m^2	86.2 $\pm$ 10.3 mL/m^2	86.8 $\pm$ 7.9 mL/m^2	p = n.s.
iRVSV	37,80 $\pm$ 5.8 mL/m^2	43,70 $\pm$ 8.8 mL/m^2	45,30 $\pm$ 11.8 mL/m^2	p = n.s.
RF	33.3 $\pm$ 12.6%	4.0 $\pm$ 4.3%	4.1 $\pm$ 4.2%	p = n.s.

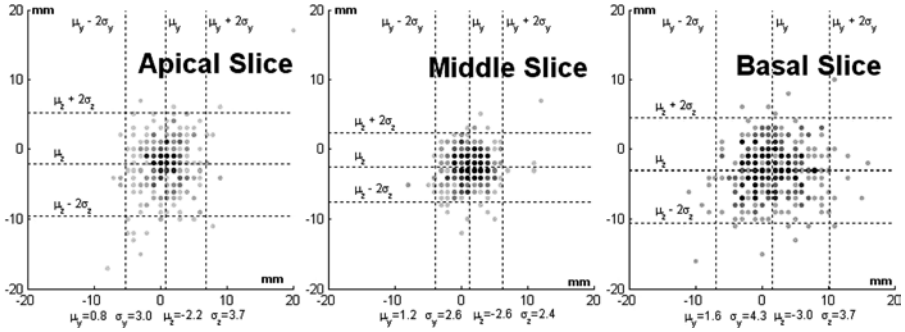

FIG. 1. Errors in the automated method for each of the apical, middle and basal SA slices.

Methods: The most striking and distinguishing feature of the LV is its movement at the frequency of the cardiac cycle. The method is based on using the Fourier transform to detect the position and orientation of the LV. The method can be summarized in the following six steps:

Step 1: The Fourier transform is calculated for each pixel through time and images representing the magnitude of the DC component (average cine image) and first harmonic at the frequency of the cardiac cycle (H1) are created for each of the SA slices. In all cases, the first harmonic image clearly localises the heart.

Step 2: An initial long axis line is fitted through the centroids of the SA H1 images in 3D.

Step 3: A radius defining a circular region of interest (ROI) for each SA slice is defined with its origin at the intersection of initial long axis and each SA slice. The size of the ROI is determined from the H1 image (after filtering) and is used to crop the DC image.

Step 4: The LV blood pool on the middle SA slice is segmented on the DC image using an adaptive thresholding technique and the contour forced to be convex to include the papillary muscles with the blood pool.

Step 5: The contour is then transferred to the adjacent slices, and the most similar region chosen until the LV blood-myocardial boarder has been defined on all SA images.

Step 6: The final long axis of the LV is obtained by fitting a line to the centroids of the segmented regions on each slice.

The method was applied to 330 cases from the ONTARGET cardiac MRI trial obtained from sites in six countries and a range of scanner manufacturers. Two skilled independent analysts defined the long axis of the LV for the purposes of comparison with the automatic method.

Results: The automated method was successful in 329/330 cases. The errors in position on each of the basal, middle and apical slices are shown in Fig. 1.

The average difference in the long axis angle between the two analysts was 3.5°. The average difference between the automated method and each of the two analysts was 6.1° and 6.4° respectively.

Conclusion: An method for the automated determination of the position and orientation of the LV has been validated and found to be successful in 329/330 cases.

605. SERIAL HIGH RESOLUTION MRI OF CAROTID ARTERY: A NOVEL METHOD TO ASSESS MEASUREMENT VARIABILITY DUE TO MIS-REGISTRATION

Niranjan Balu, William S. Kerwin, Chun Yuan. ***University of Washington, Seattle, WA, USA.***

Introduction: Accuracy of serial measurement of carotid atherosclerotic plaque is important for monitoring lesion progression and regression. Measurement accuracy on axial images are confounded by the orientation of the artery relative to imaging plane, positioning of bifurcation between the scans, SNR, flow artifacts etc. In order to improve measurement accuracy, the contribution of these factors to the overall measurement error needs to be quantified.

Purpose:

a) To mathematically model the factors contributing to measurement error in serial axial carotid MRI with parameters derived invivo;
b) To assess the contribution of mis-registration to overall measuement error.

Methods: Model parameters were measured from 19 subjects scanned twice within 4 weeks on a 1.5T GE Signa with a quadruple inversion recovery T1w sequence with TR/TE/FOV/Thickness/Matrix/NEX of 800/8/16 × 12/2/0/256 × 256/2. Lumen and outerwall were drawn on all slices using custom-built software. Total measurement error was modeled with two additive components: segmentation error (including SNR, flow artifacts, reviewer training etc); 2) mis-registration error which includes the error in repositioning the carotid artery relative to the imaging plane (positioning error); and error in positioning the carotid bifurcation (slice-offset error). Segmentation error was modeled as a zero mean gaussian with variance measured by outlining each slice twice (2-week interval between

TABLE 1

Error component	Probability Model	Est. model parameters	Effect of 50% reduction of model parameters on total error: Lumen area	Effect of 50% reduction of model parameters on total error: Outer wall area
Lumen segmentation	Gaussian	$\mu = 0, \sigma = 2.2$ mm^2	6%	NA
Outer Wall segmentation	Gaussian	$\mu = 0, \sigma = 5.5$ mm^2	NA	4%
Initial angle	Gaussian	$\mu = 28.68, \sigma = 12.86$ degrees	25% for combined 50% reduction in all components	24% for combined 50% reduction in all components
Angle difference	Gaussian	$\mu = 0, \sigma = 7.12$ degrees		
Slice offset	Uniform	On (−1 mm, 1 mm)	3%	1%

sessions). Positioning error has two subfactors: angle that the carotid makes with the imaging plane at the first scan (θ) and the difference in angle between two scans (α). θ was calculated by fitting 3D regression lines to the centroids of the internal (ICA) and common (CCA) carotids and finding the angle of this line to the imaging plane. The average of the ICA and CCA angles was considered as distribution of θ. To determine α which needs more precision, centerlines by 3D chamfer masks wre fitted to 3D models of the carotid. The center lines were registered and rotation off the z-axis determined from the registration rotation matrix. Slice-offset error is caused by misalignment of the bifurcation less than the slice thickness (modeled by uniform distribution) and differential change in plaque along the length of the artery. This change was calculated for each slice from invivo data using the first scan. Simulations for artery and slice based data were compared to invivo measurements. Contribution of each component was determined by simulating its reduction by 50%. Components were ranked according to the reduction in overall measurement error.

Results: The resulting model parameters are summarized in Table 1 along with the effect on the total error of reducing each error component by 50%. Simulated data for 40 arteries with 320 slices (8 slices per artery) were compared to actual measurements on 36 arteries and 325 slices (Fig. 1). Standard deviations of the lumen measurement error for were 3.76 mm^2(simulated) versus 3.78 mm^2 (actual) at the artery level and 5.38 mm^2 (simulated) versus 3.75 mm^2 (actual) at the slice level. For outerwall, simulated and actual standard deviations were 4.90 vs. 6.52 mm^2 for the artery and 8.78 vs. 7.21 mm^2 for the slice.

Conclusions: Total measurement error in serial carotid MRI is a complex interplay of segmentation and mis-registration errors (positioning, difference angle and slice-offset subcomponents). We have demonstrated a novel model that can quantify the relative importance of each of these components. The model is consistent with actual measurements in qualitative distribution and quantitative measurements of standard deviation. Therefore, it serves as a good model for systematically testing the effect of improved acquisition methods on error in serial measurements.

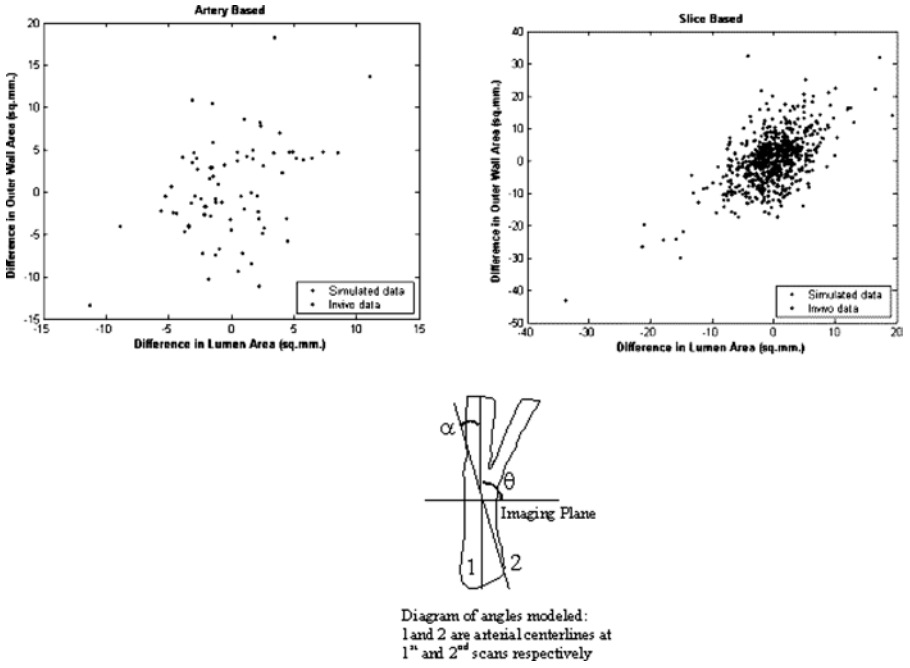

FIG. 1.

Such testing suggests that for improved measurement accuracy, the most benefit will be obtained by optimizing the protocol to reduce errors in angular positioning. Improvements segmentation tools will have a lesser impact.

606. LEFT ATRIAL VOLUME BY ECHOCARDIOGRAPHY CONSISTENTLY UNDERESTIMATES VOLUME BY CARDIOVASCULAR MAGNETIC RESONANCE EVEN USING IDENTICAL METHODS.

Craig S. Broberg, Matthew Witlock, MD, Anuj Garg, MD. ***Oregon Health and Science University, Portland, OR, USA***

Introduction: Left atrial volume has been shown to predict adverse cardiovascular events. Because of growing clinical significance of this measurement, there is a need to better define the level of agreement between imaging modalities. Echocardiographic atrial volumes are calculated using the area length method, which has been shown to consistently underestimate volume by Simpson's method using cardiovascular magnetic resonance (CMR) or computed tomography as gold standards. It is not clear whether this difference is due to erroneous geometric assumptions required by the area length method, or to other discrepancies between imaging modalities.

Purpose: To compare left and right atrial volumes calculated using the area-length method with both echocardiography and CMR.

Methods: Patients underwent both CMR (1.5 Tesla GE Excite) and echocardiography within one month. Atrial long axis dimension and area were measured offline from both the 4 chamber view (right and left atria), and two chamber view (left atrium only). All measurements were made by the same observer. Biplane volume of the left atrium was calculated using the formula $\text{Area}_{\text{echo}} \times \text{Area}_{\text{CMR}} \times 0.849/\text{average length}$, whereas right atrial volume was calculated from single plane data. Values were indexed to body surface area. Results between echo and CMR were compared using Pearson's correlation coefficient as well as mean difference and range between methods according to Bland-Altman methods. Selected patients also had atrial volumes measured using Simpson's method from contiguous short axis cines by CMR.

*Results:*Images from 54 patients were included, representing a wide range of atrial volumes. Five echocardiograms and 2 CMR scans were excluded because of image quality. There was a strong correlation between echocardiography and CMR for both the left and right atrial volumes ($r = 0.92$, $p < 0.001$ and $r = 0.82$, $p < 0.001$, respectively). However, echocardiography consistently underestimated atrial volume compared to CMR (percent difference 31% and 33% for left and right atria respectively). By Bland-Altman analysis, the mean difference in left atrial volume index (CMR-Echo) was 25 mL/m^2, with considerable variability (95% CI of the mean 60 mL/m^2). Similarly, mean difference for right atrial volume was 7.3 mL/m^2 (95% CI 69 mL/m^2). Differences in area rather than length accounted for most of the discrepancy. There was better agreement between area-length method and Simpson's method using only data from CMR for both the left and right atria.

Conclusion: Despite strong correlation, echocardiography consistently and significantly underestimates atrial volume compared to CMR using the area-length method. With growing clinical interest in this measurement, it is important to recognize disagreement, and clinical values and normal ranges should not be compared between modalities. Alternative methods for quantification by echocardiography may be favorable.

607. DIAGNOSTIC ACCURACY OF INVERSION RECOVERY SINGLE SHOT SSFP VS SEGMENTED GRE ON DETECTING THE PRESENCE OF LATE MYOCARDIAL ENHANCEMENT

Jonathan Lyne, MRCP, Didier Locca, Chiara Bucciarell, MD, Ravi Assomull, MRCP, Dudley Pennell, MD, FRCP, FACC, FESC. ***Royal Brompton Hospital, London, United Kingdom.***

Introduction: Inversion recovery preparation with segmented gradient echo readout (GRE) is considered the gold standard sequence for the detection of late myocardial enhancement. However, to ensure full ventricular coverage it requires multiple breath holds and can be time consuming, taking on average 15–20 cardiac cycles per slice with 8–10 slices required to provide

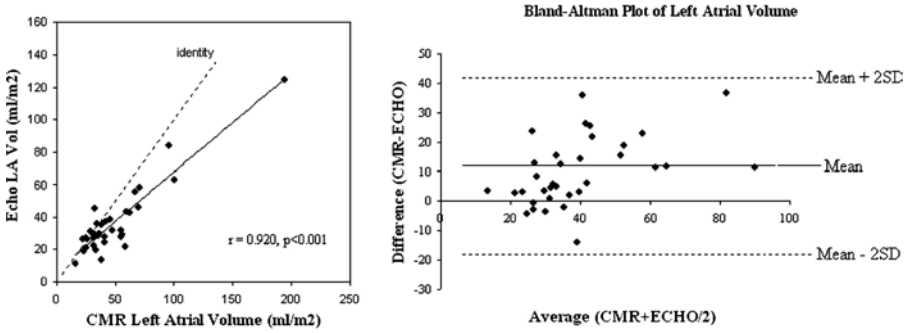

full ventricular coverage. Multislice single shot steady state free precession (SSFP) allows rapid coverage of the entire left ventricle (~9–10 slices) in a single acquisition. A reliable single shot readout mulitislice inversion recovery imaging sequence would permit rapid viability imaging improving scanning efficiency.

Purpose: To evaluate the diagnostic accuracy of the multislice single shot SSFP inversion recovery sequence in detecting the presence or absence of late enhancement compared with segmented GRE images.

Methods: We studied 86 consecutive patients with and without known coronary aretery disease undergoing clinical cardiovascular magnetic resonance imaging for viability assessment. Images were acquired 10 minutes following intravenous injection of 0.1 mmol/kg gadolinium-BMA. The inversion time was progressively optimized to adequately null normal myocardium. Imaging with the GRE sequence consisted of consecutive single slice breathold acquisitions whereas the SSFP imaging was in a single multislice single breathold acquisition. Both sequence acquisitions were ECG gated to end diastole and sufficient acquisitions were made to provide full ventricular coverage. Typical imaging parameters for GRE were: read field of view (FOV) 320 cm, phase FOV 75%–100%, repetition time (TR) of 700 ms, echo time (TE) 3.8 ms, in-plane pixel size 2.2 × 1.3 mm, flip angle 20°, slice thickness 8 mm, segments 23. Base resolution 256 × 60%. Bandwidth 230 Hz/pixel. In the SSFP sequence similar FOV was used but in plane spatial resolution was lower, base resolution 192 × 75%, in-plane pixel size 2.5 × 1.8 mm. Slice thickness 8 mm, TR 700 ms, TE 1.08 ms, flip angle 50°. Bandwidth 1180 Hz/pixel. Images were analyzed by two blinded observers for the presence or absence of late myocardial enhancement.

Results: On segmented GRE imaging 45 out 1462 segments were scored as having late enhancement. Blinded observers were concordant as to the presence or absence of any ventricular late myocardial enhancment in all cases. In 36 cases, they were concordant in scoring the presence of late myocardial enhancment with both imaging sequences. In the remaining 50 cases, there was concordance as to the absence of late myocardial enhancment with both sequences.

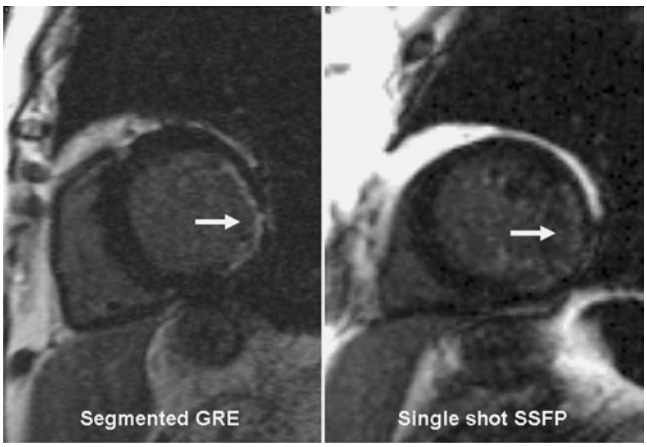

Conclusions: Despite its lower spatial resolution, the SSFP single shot mutlislice imaging sequence was capable of detecting the presence or absence of late enhancement compared to the segmented single slice GRE sequence. Potentially as a rapid imaging sequence it may be applied to screen for the presence or absence of late myocardial enhancement as a first line sequence. If required this may then be followed by higher resolution segmented GRE images. These results are also reassuring in cases were it is not possible to use a segmented GRE sequence such as patients unable to breath hold or children. A single shot multislice SSFP inversion recovery sequence may be applied before considering further acquisitions.

608. DELAYED ENHANCEMENT AFTER ACUTE MYOCARDIAL INFARCTION AS A PREDICTOR OF LONGTERM REMODELLING

Ana G. Almeida, MD, PhD, Pedro C. Silva, MD, Henrique Mesquita-Gabriel, MD, Antonio N. Diogo, MD, Cláudio David, MD, Mário G. Lopes, MD, PhD. ***University Hospital Santa Maria, Lisbon, Portugal.***

Introduction: Delayed enhancement (DE) is a well known useful sequence to assess the extent of myocardium necrosis in the acute (AMI) and chronique phase of myocardial infarction. However, its clinical value in prognosis assessment is not well established.

Purpose: We hypothesized that the extent of necrosis as assessed by DE in the early phase after AMI in patients treated by primary angioplasty, could predict late remodelling.

Methods: Twenty-six patients (18 males, 53 ± 11 years old) with a first AMI related to LAD and treated with primary angioplasty with stenting were included. All were in sinus rhythm. All underwent two CMR examination, the first 5 to 7 days after angioplasty and the second at 6 months after intervention. A 3 T Philips Achieva Philips scanner was used.The first study included: steady-state free precession in short sxis covering all left ventricle, for end-diastolic and end-systolic volumes and ejection fraction assessment, using Simpson's; a contrast DE sequence using a T1 weighted inversion recovery with a prepulse delay to null the normal myocardium, with aquisition of 12-15 short-axis slices, horizontal and vertical long-axis views, 10 minutes after contrast injection. Contours were draw to obtain the extension of DE as a percentage of left ventricle mass (EDE). At six months this protocol was repeated. At this time, a 20% increase of on the end-diastolic or end-systolic volumes or a 20% decrease on the ejection fraction were considered as criteria for remodelling.

Results: All patients yielded TIMI 3 flow after angioplasty and none showed no-reflow by clinical or CMR criteria. Maximum CK was 1650 ± 1100 mg/dL, maximum TNT was 35.1 ± 26.3 and mean EDE was 25.4% ± 11.1%. At six months, the mean EDE was 15.2% ± 10.7%, and eight patients yielded

criteria for remodelling. We found a positive correlation between EDE and late end-diastolic volume ($p = 0.02$), end-systolic volume ($p = 0.002$) and negative with ejection fraction ($p = 0.01$). Using ROC curves, a cutoff of 19.8% for early EDE could identify patients with remodelling criteria with 89% sensitivity and 88% specificity. Multivariate analysis using clinical, laboratory and CMR variables yielded EDE as the only independent predictor for late remodelling (end-diastolic volume, p = 0,02, end-systolic volume, $p = 0.001$, ejection fraction $p = 0.02$).

Conclusions: Early quantitative assessment of necrosis after primaty angioplasty by means of delayed enhancement evaluation is a promising tool for prediction of late remodelling. The use of this method should allow the assessment of new therapeutic modalities in order to prevent remodeling and improve prognosis.

609. REGIONAL MYOCARDIAL PERFUSION IN AN ANIMAL MODEL OF RIGHT VENTRICULAR HYPERTROPHY ASSESSED WITH FIRST PASS MRI

Carsten Rickers, MD,[1] Michael Jerosch-Herold, PhD,[2] Hans Heiner Kramer, MD,[1] Xudong Hu, MD,[3] Naveen Murthy, MD,[3] Myra Urness, BSC,[3] Norbert Wilke, MD.[4]
[1] University Hospital Kiel, Kiel, Germany, [2] University Oregon, Portland, OR, USA, [3] University of Minnesota, Minneapolis, MN, USA, [4] University of Florida, Jacksonville, FL, USA.

Introduction: Right ventricular hypertrophy (RVH) is common in patients (Pts.) with congenital heart disease. The myocardial perfusion patterns in chronically pressure overloaded right ventricles as a possible determinant of congestive symptoms and sudden cardiac death are unknown.

TABLE
Myocardial perfusion in an animal model of RVH

	Rest	Stress	MPR
RV free wall	0.7 ± 0.2	1.5 ± 0.5	2.1
Septum	0.8 ± 0.3	2.7 ± 0.4	3.3
LV free wall	0.8 ± 0.2	2.9 ± 0.3	3.6
p	ns	<0.05	<0.05

Purpose: We sought to investigate myocardial blood flow of the right and left ventricle in an animal model of progressive RV pressure load.

Methods: Eight piglets (12 ± 2.2 kg) received operative pulmonary artery banding via a left lateral thoracotomy. Over 5 to 6 months all pigs increased their body weight significantly (85 ± 17 kg). MR-first pass perfusion imaging (0.03 mmol/kg Gd-DTPA; TR/TE/α= 1.8/0.9/18) and cine MR-imaging was performed in all pigs using a 1.5 T cardiac MR-scanner (Siemens, Sonata) with perfusion scans both at baseline and during stress (Adenosine 140 ug/kg/min). Myocardial blood flow (mL/g/min) and Perfusion Reserve (MPR = hyperemic over resting myocardial flow) were calculated in 4 segments of the RV and 4 segments of the LV per slice (2–3/per animal, depending on heart rate). Blood flow was derived from signal intensity curves with a Fermi-model for constrained deconvolution for the tissue contrast-enhancement curves. For validation of myocardial perfusion, microphere studies were performed in 3 pigs. Invasive pressure measurements have be taken in all animals prior to MRI.

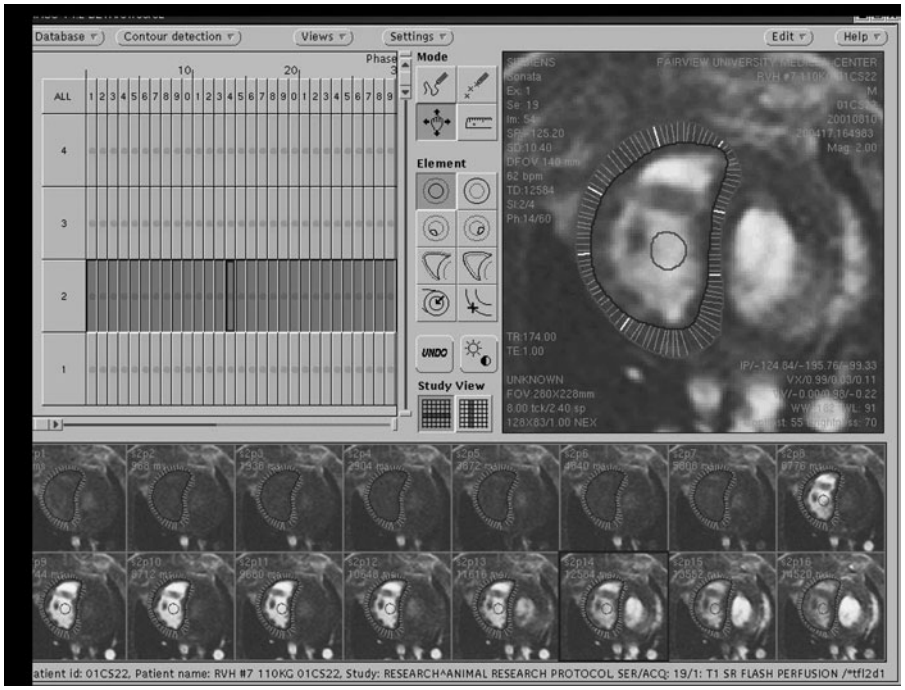

Results: Invasive right and left ventricular pressures were found to be almost identical (RV/LV pressure = 1 ± 0.2) after 24–28 weeks post banding. First pass perfusion imaging at rest showed that the myocardial perfusion of the right ventricle was not significantly reduced as compared to the left ventricular free wall or the septum. But hyperemic blood flow and perfusion reserve of the right ventricular free wall were significantly reduced (Table). Microphere measurement showed a good correlation with MR measurements.

Conclusions: In this animal model of RVH we have demonstrated that right ventricular perfusion can be measured with first pass perfusion MRI. We found that right ventricular hypertrophy due to chronic pressure overload leads to impaired myocardial perfusion reserve of the right ventricular free wall. MR perfusion imaging has the potential to improve our understanding of microvascular circulation in pts. with congenital heart disease and RVH.

610. REGIONAL WALL MOTION AND EJECTION FRACTION PREDICT MYOCARDIAL INFARCTION BETTER THAN QUANTITATIVE CORONARY ANGIOGRAPHY

Erik B. Schelbert, MD, MS, Federico E. Mordini, MD, Tariq Haddad, MD, Andrew E. Arai, MD. ***National Institutes of Health, Bethesda, MD, USA.***

Introduction: It is unclear how cardiac tests compare in their ability to predict myocardial infarction.

Purpose: We sought to quantify the diagnostic performance of invasive quantitative coronary angiography (QCA) relative to noninvasive tests such as left ventricular ejection fraction (LVEF) and regional wall motion abnormality (RWMA) for detecting chronic MI as defined by delayed enhancement (DE) by cardiac magnetic resonance (CMR).

Methods: Patients referred for angiography (n = 68) by their cardiologist underwent CMR studies on a 1.5 T scanner. Patients with prior ST elevation MI patients were excluded. MRI measures included: quantification of LVEF using a volumetric stack of manually-traced short axis images and RWMA as observed on FISP cine CMR as well DE imaging using phase sensitive inversion recovery sequences performed 15 minutes after gadolinium-DTPA administration (0.15 mmol/kg). Invasive X-ray quantitative coronary angiography (QCA) yielded the maximal percent stenosis of the coronary arteries. Logistic regression models evaluated whether variables could predict MI as indicated by DE in a typical coronary distribution. Model discrimination was compared with the c statistic, and a c statistic above 0.90 was considered robust.

Results: Most patients were male (n = 42; 69%); the mean age was 60 years (interquartile range 54–66). Mean LVEF was 59% (range 18%–77%), and 16 patients had regional wall motion abnormalities (n = 16; 26%). There were 25 patients with MI (37%). In univariable logistic regression models, RMWA, LVEF, and QCA were all significant predictors of MI ($p < 0.05$), whereas other clinical variables such as age, diabetes, hypertension, hypercholesterolemia, tobacco use were not ($p > 0.05$). RWMA was a better discriminator of MI than QCA maximal coronary luminal stenosis (c statistic: 0.86 vs. 0.78), even when patients who received prior percutaneous intervention (n = 18) were excluded (c statistic: 0.85 vs. 0.81). A model containing both noninvasive parameters (LVEF and RWMA) further improved discrimination (c statistic: 0.87). When QCA was dichotomized, a cut point of 50% stenosis yielded the best discrimination (c statistic: 0.71). For detecting MI, the sensitivity/specificity of RMWA was 76%/95%, while the sensitivity/specificity of QCA (maximum stenosis < 50%) was only 12%/47%.

Conclusions: In patients without prior ST elevation MI, noninvasive tests such as ejection fraction and regional wall motion appear to have better discrimination for detecting chronic myocardial infarction than quantitative coronary angiography. These data highlight the limitations of angiography for detection of chronic myocardial infarction. Moreover, since no test robustly predicted myocardial infarction on DE magnetic resonance scanning with high clinical certainty, these data also underscore the inherent utility of DE imaging.

611. SIMPLIFIED DETERMINATIONS OF LEFT ATRIAL VOLUMES AND PULMONARY VENOUS DIMENSIONS IN ATRIAL FIBRILLATION PATIENTS AND NORMAL SUBJECTS BY CARDIAC MAGNETIC RESONANCE

Paul S. Lee,[1] Jeffrey L. Anderson, MD,[2] Kurt R. Jensen, MS,[2] Gerri K. Jelaco,[2] Duane D. Blatter, MD.[2] [1] ***University of Utah, Salt Lake City, UT, USA,*** [2] ***LDS Hospital, Salt Lake City, UT, USA.***

Background: Increasingly, cardiac magnetic resonance (CMR) is used to image the left atrium (LA) and pulmonary veins (PV) in association with radiofrequency catheter ablation (RFCA) for atrial fibrillation (AF). CMR is used for pre-procedure cardiovascular assessment, as a baseline for post-ablation comparisons (e.g., to assess disease regression or PV stenosis), and as a template to guide placement of ablation lesions. Optimal interpretation of CMR requires information about dimensions in health and disease. Moreover, LA size is increasingly recognized as an indicator of chronic left ventricular pressure and prognosis. LA volume is proposed as a better predictor than 1- or 2-dimensional measurements of LA size. However, traditional short axis stack assessment (using Simpson's rule) is too time consuming for routine practice.

Purpose: The purpose of this study was to measure and compare LA volumes by 2 simplified methods in normal volunteers and consecutive patients with either chronic (CAF) or

TABLE

Measure	Normals	Atrial Fibrillation	p value
No.	30	48	—
Age/Male%	47 y/50%	63 y/54%	—
LA vol: A-L (mL)	69.1 (30.7, 120)	108 (54.0, 205)	<0.001
LA vol: ellipsoid (mL)	—	90.3 (52.3, 140)	—
PV diameter (mm)	13.9 (10,18)	16.9 (11, 21)	<0.001
PA diameter (mm)	31.6 (23.6, 42.5)	31.2 (24.0, 41.2)	0.37
RPA diameter (mm)	19.3 (13.6, 24.0)	21.2 (17.0, 30.0)	0.012
LPA diameter (mm)	20.5 (15.6, 25.0)	22.5 (18.0, 27.0)	0.002

paroxysmal (PAF; defined as sinus rhythm at study) AF referred for RFCA.

Methods: Thirty normal adult volunteers and 48 AF patients (pts) were studied. Normals were younger, but sexes were equally represented in both groups. CMR included axial and sagittal scout views and short- and 2, 3, and 4 chamber long-axis SSFP cines on a GE 1.5 Tesla magnet (EXCITE platform, v 11.0). AF pts also underwent MR angiography (MRA). LA volumes were determined by biplane (2, 4 chamber) area-length (A-L: 2[A1 $\times$ A2]/L1 + L2) and 3-axis ellipsoid methods (π/6[AP $\times$ SI $\times$ RL]). Pulmonary venous diameters were measured at their ostia with the LA. The 5th and 95th percentile confidence intervals (CI) in volunteers were taken to define the normal range.

Results: Results are shown in the Table as means (5, 95% CI).

All but 1 atrial and pulmonary vascular measures were increased in AF pts, including LA volume and PV, RPA and LPA diameters. PV diameters were larger with CAF than PAF (+1.2 mm, $p = 0.01$), and LA volume (A-L) tended to be larger (median 111 vs. 96 mL, $p = 0.09$). Small (1.6 mm) but significant differences in average diameters among the 4 PV were noted among pts and controls. LA volumes were somewhat smaller by the ellipsoid method but correlated moderately well with the LA-AL method (Pearson's $r = 0.42$, $p = 0.004$).

Conclusion: Simple measures, obtained during routine CMR examination, enable estimates of LA volume and pulmonary vascular dimensions that distinguish between normals and AF pts and between PAF and CAF pts. An LA A-L volume of $\leq$ 120mL (vol index $\leq$ 65 mL/m^2) and PV diameter of $\leq$ 18 mm characterize the normal population and are distinct from those reported by echocardiography, with greater values suggesting progressive AF burden. Future studies should explore additional diagnostic and prognostic applications of these measures.

612. COMPARISON OF METHODS OF QUANTIFICATION OF LEFT ATRIAL VOLUME BY CINECARDIOVASUCLAR MAGNETIC RESONANCE

Cecilia Corros, MD,[1] Himanshu Gupta, MD,[1] Thomas S. Denney,[2] Louis J. Dell'Italia, MD,[1] Steven G. Lloyd, MD.[1] *[1] University of Birmingham Alabama, Birmingham, AL, USA, [2] University of Auburn, Auburn, AL, USA.*

Introduction: Left atrial (LA) enlargement has been previously documented as a strong predictor of cardiovascular outcomes. Traditionally, LA size has been documented using M-mode echocardiography expressing LA size through linear dimensions, but it has been shown that LA volume is a more powerful measure of LA size and allows an accurate assessment of the asymmetric remodeling of LA chamber.

Cine MRI (CMRI) is a well-tolerated non-invasive technique. Recent published studies have been shown that LA enlargement can be reliably identified by CMRI (1).

Purpose: We sought to compare the agreement between two methods for evaluation LA volumes: a biplane area-length method and Simpson's method of disk summation, using CMRI.

Methods: One hundred sixty-eight CMRI studies were performed in 140 patients (49% men). Of these, 67 (49% men) were resistant hypertensive patients, 28 (54% men) were patients with non ischemic mitral regurgitation (MR) and 45 (44% men) were healthy subjects without previous history of cardiac disease. CMRI was performed with a 1.5T scanner (GE Healthcare) using a phased array surface coil and prospective electrocardiographic triggering. LA contours, on the 2 and 4 chamber views, were manually drawn at end-ventricular systole which corresponds to the largest LA area, the pulmonary veins and the LA appendage were excluded. The length was obtained from the middle of the plane of the mitral annulus to the posterior wall. Volumes were then computed using the Dodge area-length formula (2). LA volumes were also computed using a biplane Simpson integration method from the same contours. For each contour, an LA long-axis centerline was computed. The LA axial diameter was then measured perpendicular to the centerline at a set of points spaced 0.5 mm apart. The cross-sectional area at each point was computed by assuming that the corresponding diameters measured in each image were the major and minor axes of an ellipse. The LA volume was computed by summing the cross-sectional areas multiplied by the point spacing (0.5 mm). In all cases the LA volumes were indexed for the body surface area.

Results: Regression analysis reveal reasonable agreement between the Biplane Area-Length and Simpson's methods with all patients at low volumes, but the values diverge at large volumes ($R^2 = 0.97$, $p < 0.0001$). LA volumes are overestimated by the area-length method as compared to Simpson's method with mean difference of 12.0 ± 7.0 mL/m^2 (Fig. 1A). The difference between the two methods increased with increasing LA volumes (Fig. 1B). Correlation and error analysis resulted in a relationship between the two methods of LA volume (area-length) = 3.3 mL + 1.12 $\times$ LA volume (Simpson) with 95% confidence limits of the slope between 1.35 (upper limit) and 1.03 (lower limit). Patients were divided into subgroups (hypertensive, mitral regurgitation and normal) and analyses were repeated. The area-length method overestimated LA volume in all groups as compared to the Simpson's technique (difference 19 ± 8 in MR

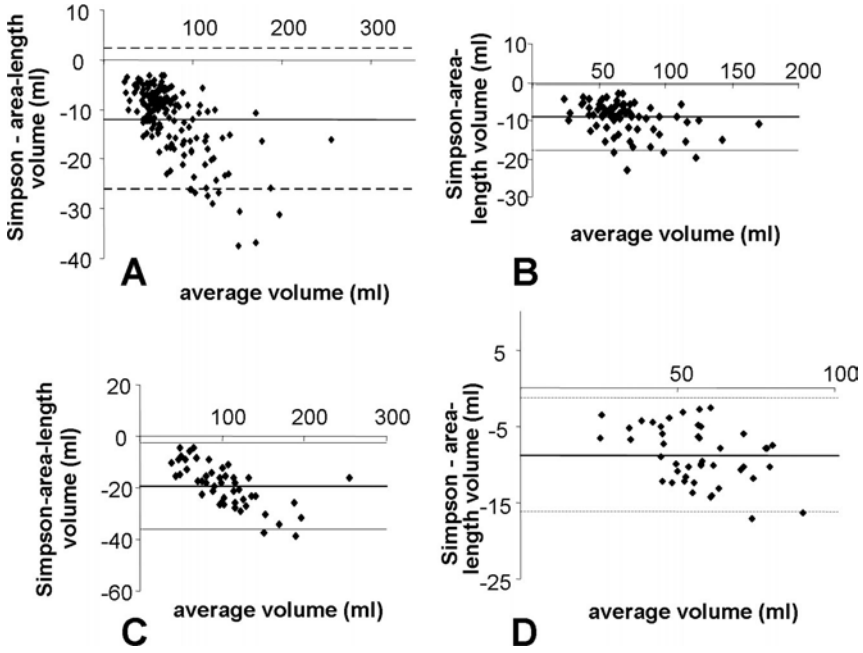

group, 9 ± 4 in hypertensive and 9 ± 3 in normal subjects) (Fig. 1B, C, D).

Conclusions: The agreement between the area-length method and Simpson's method for evaluation of LA volume is reasonable for small volumes but when a more precise result is required, particularly in the case of increased in LA volumes, Simpson's method is preferable.

REFERENCES

1. Rodevand O, Bjornerheim R, Ljosland M, et al. Left atrial volumes assessed by three and two-dimensional echocardiography compared to MRI estimates. Int J Card Imaging 1999;15:397–410.
2. Hudsmith LE, Petersen SE, Francis JM, Robson MD, Neubauer S. Normal human left and right ventricular and left atrial dimensions using steady state free precession magnetic resonance imaging. J Cardiovasc Magn Reson 2005;7:775–782.

613. QUANTITATIVE CARDIAC MAGNETIC RESONANCE PERFUSION IMAGING CORRELATED TO FRACTIONAL FLOW RESERVE WITH INVASIVE ANGIOGRAPHY

Norbert Wilke, Christopher Klassen, Franz von Ziegler, Alan Siuciak, Brad Shoemaker. ***University of Florida Health Science Center Jacksonville, Jacksonville, FL, USA.***

Cardiac magnetic resonance (CMR) perfusion imaging is a promising technique to assess the presence of coronary artery disease (CAD). Our objective was to evaluate the accuracy of various CMR parameters to detect significant CAD as compared with angiography or fractional flow reserve (FFR). We prospectively enrolled 37 patients who underwent coronary angiography, FFR and MRI perfusion. Stress was induced using adenosine for CMR and FFR tests. Semi-quantitative assessments, namely maximum up-slope and peak-intensity indexes, derived from time-intensity ratios between rest and stress. Myocardial perfusion reserve (MPR), calculated using Fermi deconvolution technique, was the quantitative CMR parameter. Accuracy of quantitative, semi-quantitative, and qualitative CMR data was compared with quantitative coronary angiography (QCA) in 108 coronary segments and FFR in 44 coronary segments. Sensitivity and specificity for detection of hemodynamically significant CAD (FFR $\leq$ 0.75) were 92.9% and 56.7% for MPR (cutoff 2.06). Area under the curve (AUC) to detect FFR $\leq$ 0.75 was 0.78 for MPR ($p < 0.01$), 0.63 for up-slope ($p = NS$) and 0.66 ($p = NS$) for peak-intensity index. Sensitivity and specificity for detection of anatomically significant CAD (> 50% DS) were 87.2% and 49.2% for MPR (cutoff 2.06). AUC was 0.75 for MPR, 0.69 for up-slope and 0.65 for peak-intensity indexes to detect > 50%DS (all $p < 0.05$). Visual assessment yielded a sensitivity of 78.6% and specificity of 65.5% to predict FFR $\leq$ 0.75, and sensitivity of 74.5% and a specificity of 67.2% to predict > 50% DS. In conclusion, MPR appears to be the most accurate index to detect anatomical and hemodynamically significant CAD. Standardization of such quantitative methods, with minimal operator dependency, would be useful for clinical and research applications.

614. 3D FREE-BREATHING CARDIAC FUNCTION COMPARED WITH THE 2D BREATH-HOLD APPROACH

Dana C. Peters,[1] Reza Nezafat,[1] Yuri Ishihara,[1] Holger Eggers,[2] Christian Stehning,[2] Warren J. Manning.[1] ***[1]Beth Israel Deaconess Medical Center, Boston, MA, USA, [2]Philips Research Laboratory, Hamburg, Germany.***

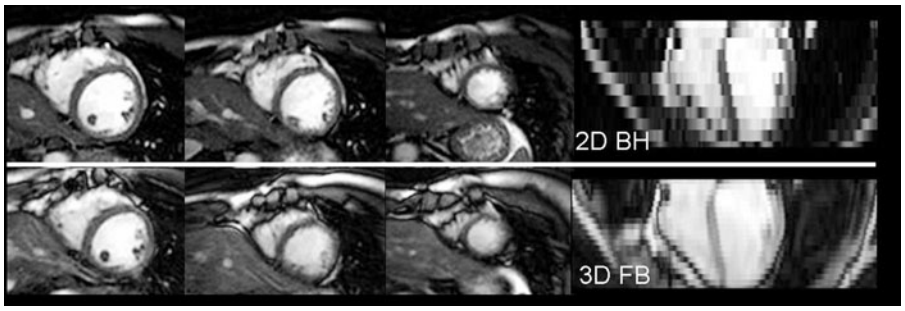

FIG. 1. Comparison of 2D breath-hld cardiac function (top) vs. 3D free-breathing radial cardiac function (bottom). The 3D method provides similar image quality but no slice mis-registration. The reformats illustrate the slice mis-registration of the 2D scan.

Introduction: Cardiac magnetic resonance (CMR) provides state-of-the-art assessment of myocardial function, using a 2D breath-hold balanced SSFP approach. However, recent work has focused on 3D methods, to shorten exam time, potentially improve SNR, and allow for registered slices without gaps in coverage in a single breath-hold (1–5). We have developed a 3D free-breathing acquisition, which can provide greater temporal resolution compared to breath-hold 3D. However, the acquisition of a respiratory navigator signal disturbs the steady state and the respiratory information is quickly outdated. To meet these challenges, the 3D cardiac and navigator (NAV) gated cine sequence employs the recently introduced dual-NAV technique (6–7). In this method, the NAV is acquired once per heart-beat in late diastole. The k-space data collected during a specific heartbeat are only retained if the current and previous heart-beats' navigator data both fall within the acceptance window.

Methods: All imaging was performed on a 1.5 T Philips Achieva (Philips Medical Systems, Best, The Netherlands). Seven healthy adult subjects were imaged (4F/3M, average age = 25) using a multiphase ECG-triggered 3D balanced SSFP sequence. A single NAV was placed at end-diastole to monitor the diaphragmatic position. The scan acquired radial projections in the kx-ky plane and partition-encoding in kz. Scan parameters were: 3D radial SSFP, 160 × 160 Np, TR/TE/θ= 3.4/1.7/45°, 32 cm FOV, 13 10 mm slices zero-filled to 5 mm, 16 cardiac phases. A 6–8 mm acceptance window around end-expiration was used for the dual NAV approach. A linear ramp start-up series preceded the first phase. The last phase was terminated with an α/2–TR/2 sequence. Two dimensional breath-held short axis images of cardiac function were also obtained for comparison. Scan parameters were the same as for 3D except: 30 cardiac phases, retrospective ECG-gating. Slice misregistration of the 2D data was visually assessed by using reformatted long-axis views.

Results: The 3D image quality was good in 5/7 subjects although the quality of the first cardiac phase was reduced due to the interruption of steady state by the immediately preceding navigator. In 5/7 subjects, the dual NAV technique reduced respiratory motion artifacts with an average NAV efficiency of 43 ± 12% (average total scan time was 7 minutes 5 s ± 1 minute 44 s). One subject had a very rapid breathing pattern. Visible slice mis-registration on the 2D images was present in 6/7 studies in multiple slices, as previously reported for breath-hold imaging (8). Fig. 1 compares approximately matched slices of the 2D (top) and 3D (bottom) studies in late diastole. The long-axis reformat shows slice mis-registration typical of 2D multiple breath-hold imaging. Preliminary measurements of SNR of blood and myocardium showed that blood SNR and CNR were lower for the 3D acquisition compared with 2D.

Discussion: In this study, we have presented a high temporal and spatial resolution 3D cardiac function imaging sequence using a dual navigator strategy. This 3D sequence has lower SNR and CNR compared to the 2D acquisition, likely attributable to reduced flip angles, necessary for reducing SAR, less inflow signal enhancement, and some radial streaks. However, with future work to reduce the 3D scan times and improve the transition to steady state, this technique will provide a free-breathing measurement of cardiac function, with registered slices and high temporal resolution.

REFERENCES

1. Alley MT, JMRI 1999;9:751.
2. Barger AV, et al. MRM 2000;44:821.
3. Peters DC, et al. JMRI 2004;20:411.
4. Jung BA, et al. MRM 2002;48:921.
5. Kozerke S, et al. MRM 2004;52:141.
6. Stehning C, et al. ISMRM 2005;1616.
7. Nezafat R, et al. SCMR 2005;424.
8. Swingen C. Int J Cardiovasc Imaging 2003;19:325–36.

615. QUANTITATIVE TAGGED MAGNETIC RESONANCE IMAGING STRAIN ASSESSMENT OF MECHANICAL DYSSYNCHRONY IN PATIENTS WITH BOTH NARROW AND WIDE QRS COMPLEXES

Kenneth C. Bilchick, MD, Robert H. Helm, MD, Katherine C. Wu, MD, Robert Weiss, MD, Joao A. Lima, MD, Ronald D. Berger, MD, PhD, Henry R. Halperin, MD, David A. Kass, MD, Albert C. Lardo, PhD. ***Johns Hopkins Medical Institutions, Baltimore, MD, USA.***

Introduction: Cardiac resynchronization therapy (CRT) is associated with a number of benefits in patients with heart failure,

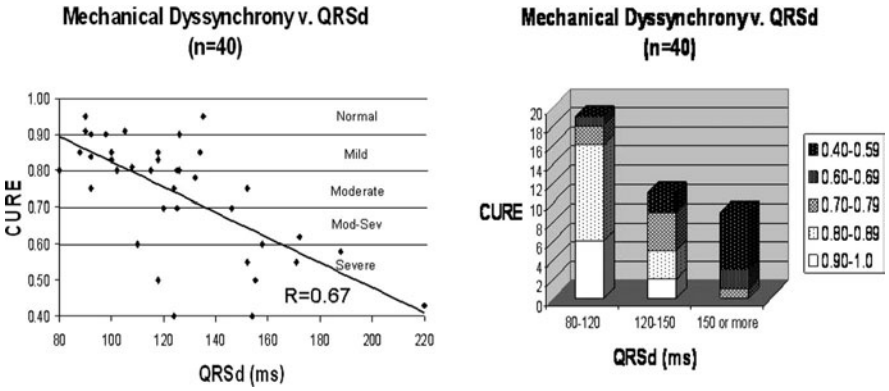

FIG. 1.

including improved exercise capacity and improved survival. Despite these benefits, only 70% of patients meeting criteria for CRT demonstrate a clinical benefit and it is believed that others not meeting strict criteria based on QRS duration (QRSd) may also benefit. The likely reason for this is that QRSd is used to select patients for CRT but does not directly measure mechanical dyssynchrony. MRI myocardial tagging (MRI-MT) measures regional strain very well and has the potential to become a useful clinical tool for the assessment of mechanical dyssynchrony. The circumferential uniformity ratio estimate (CURE) (0–1; 0 = asynchrony, 1 = perfect synchrony) is a previously validated MRI-MT index of mechanical dyssynchrony.

Purpose: We sought to address the hypothesis that the MRI-MT-based CURE is useful for identifying mechanical dyssynchrony in both patients with ischemic and nonischemic cardiomyopathies, as well as define a normal range for CURE. In addition, since QRSd is the current standard for diagnosing dyssynchrony in patients who may be CRT candidates, we also aimed to describe the relationship between MRI-MT assessment of mechanical dyssynchrony and the QRSd.

Methods: We performed a retrospective analysis of patients referred for implantable cardioverter defibrillators (ICDs). The decision to implant an ICD capable of CRT in a given patient was made on clinical grounds by the treating physician. Regional strains were measured based on MRI-MT and the CURE calculated (as previously published) based on the zero-order and first-order terms of the Fourier transform of the spatial distribution of strain.

Results: Forty cardiomyopathy patients (Reynolds Study, age 63 ± 11 years, 68% ischemic cardiomyopathy, LVEF $23 \pm 10\%$) referred for ICDs had MRI-MT and 12-lead electrocardiograms. In 7 control subjects (age 47 ± 13 years), MRI-MT showed that CURE approached unity ($CURE_{normals} = 0.95 \pm 0.025$ [SD]). Based on this, a normal CURE was defined as at least 0.90 and abnormal CUREs were graded from mild to severe as shown in Fig 1. The cardiomyopathy patients had QRSd 124 ± 31 ms (80-220 ms) with CURE as follows: $CURE_{<120\ ms} = 0.83 \pm 0.019$ (SEM), $CURE_{120-150\ ms} = 0.74 \pm 0.049$, and $CURE_{>150\ ms} = 0.55 \pm 0.035$ ($p < 0.01$ v. $CURE_{normals}$ for all). Although CURE tended to decrease as QRSd increased ($R = 0.67$), there was significant scatter in patients with QRSd 100–150 ms. As shown in the Fig., patients with both narrow and wide (>120 ms) QRSd had varying degrees of mechanical dyssynchrony, ranging from normal to moderately severe in patients with QRSd < 120 ms and from normal to severe in patients with QRSd > 120 ms. Although patients with QRSd > 150 ms had mostly severe mechanical dyssynchrony and the majority received CRT, 2/10 with moderate or moderately severe dyssynchrony and 5/21 with normal or mild mechanical dyssynchrony received CRT.

Conclusions: Although patients with wider QRSd tended to have more severe mechanical dyssynchrony, there was prominent variation in the degree of mechanical dyssynchrony for most of the range of QRSd, particularly for those patients with QRSd in the 100–150 ms range. Although QRSd > 150 ms predicted more significant mechanical dyssynchrony, CURE was particularly useful in identifying patients with borderline or moderately wide QRSd and significant mechanical dyssynchrony. Further investigation into MRI-based assessments of mechanical dyssynchrony for CRT selection is warranted.

616. DEEP SEDATION VERSUS GENERAL ANESTHESIA: SAFETY AND EFFICACY IN PEDIATRIC PATIENTS UNDERGOING CARDIAC MAGNETIC RESONANCE IN A LARGE COHORT

Mark A. Fogel, MD, Paul M. Weinberg, MD, Elicia Parave, CPNP, CEN, Christine Harris, Lisa Montenegro, MD, Mikael Concepcion. ***Children's Hospital of Philadelphia, Philadelphia, PA, USA.***

Purpose: To assess the safety and efficacy of deep sedation in the pediatric age range in patients undergoing cardiac magnetic resonance (CMR) for congenital heart disease (CHD).

Background: Remaining motionless during CMR is problematic in pediatrics yet important for image quality and ventricular mass/volume calculation. Recently, there has been a shift away from sedation in pediatric patients undergoing CMR towards general anesthesia (GA) citing safety concerns, making a non-invasive test very invasive.

Methods: A retrospective review of hospital records and images of CMR cases at our institution from 1997–2006 was undertaken.

Results: The 1521 pts who underwent CMR during the study period were aged 8.5 ± 6.1 years old (range 2 days-18 years, median = 8.8 years, mode = 3 months). Six hundred sixty CHD patients (4.3 ± 4.3 years of age) underwent deep sedation and 161 CHD patients underwent GA (3.7 ± 4.8 years of age). Diagnoses included a broad spectrum of CHD including single ventricle, transposition of the great arteries and tetralogy of Fallot.

Deep Sedation Patients: There were no serious adverse events including no mortalities, hospitalizations or emergency room visits because of deep sedation. There were 18 (2.8%) self-limited events including 12 (1.9%) "paradoxical" reactions and 6 patients (0.8%) who vomited. Of patients who were sedated, 14 failed the sedation regimen and awoke prior to scan completion (11 of these patients had enough information obtained from their scans that it was not repeated and 3 needed to undergo GA to obtain further imaging). This represented a deep sedation success rate of 97.9%.

GA Patients: Of the 161 patients, 8 records could not be located so the study group consisted of 153 patients. All GA cases were completed successfully. There were 6 AEs which represented 3.9% of all patients undergoing GA. Two patients (1.3%) had oxygen desaturation, one with endotracheal tube dislodgement and one with accompanying tachycardia. Both were treated without incident. Two patients (1.3%) needed an overnight stay in the hospital; one had stridor after extubation, and one had a fever. One patient had a rhythm disturbance while undergoing CMR and one patient had bronchospasm following an adenosine stress perfusion study, both of which resolved on their own. No sequelae from these events occurred. There were no mortalities due to GA for CMR.

Image Quality: Observers blinded to the patient's status found no difference between images obtained with deep sedation, general anesthesia or no sedation. Average score for steady state free precession imaging was 8.5 ± 0.7, 8.2 ± 0.7 and 8.7 ± 0.6 for patients undergoing deep sedation, GA and no drug regimen respectively. For cine images, average score was 8.3 ± 0.6, 8.1 ± 0.9 and 8.4 ± 0.6 for patients undergoing deep sedation, GA and no drug regimen respectively. Intraobserver variability was 3.8% and 3.9% and intraobserver variability was 8.7% and 9.2% for "static" steady state free precession images and cine images. Differences between deep sedation, GA and no drug regimen groups was not considered clinically significant. With free breathing using a smaller field of view and signal averaging, even in young infants, we were able to obtain excellent image quality for the various types of CMR imaging. With free breathing using a smaller field of view and signal averaging, even in young infants, we were able to obtain excellent image quality (Fig. 1).

Conclusions: Sedation of appropriately screened pediatric patients with CHD undergoing CMR is safe, well tolerated and yields high quality images. GA should be considered for patients with CHD and hemodynamic or airway compromise, who have failed sedation or have other special circumstances.

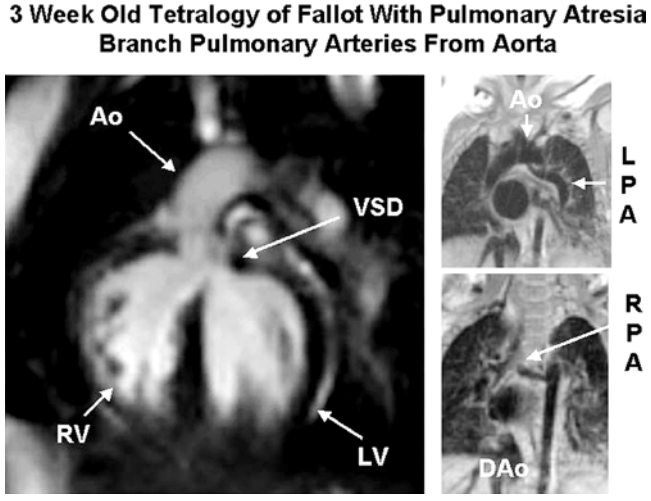

FIG. 1.

617. EPICARDIAL FAT MEASURED DURING ROUTINE CARDIAC MAGNETIC RESONANCE PREDICTS CORONARY ARTERY DISEASE

Eric Larose, Julie Côté, Josep Rodes-Cabau, Peter Bogaty, Jean Champagne, Bernard Brochu, Santiago Miro, Bernard Noel, Olivier Bertrand, Jean-Pierre Despres. ***Quebec Heart Institute at Laval Hospital, Quebec, PQ, Canada.***

Introduction: Obesity is gaining epidemic proportions. While the body-mass index (BMI) may be associated with cardiac morbidity in epidemiological studies, this measure does not consistently predict cardiovascular events in smaller trials. However, visceral abdominal fat is consistently superior to BMI for risk stratification. Visceral fat has been highly correlated to systemic markers of inflammation and cardiometabolic risk. Growing numbers of patients benefit from cardiac magnetic resonance (CMR), which concurrently identifies visceral cardiac fat and subcutaneous fat reliably.

Purpose: We investigated whether measures of visceral cardiac (pericardial and epicardial) and subcutaneous fat obtained during routine CMR predicted coronary artery disease.

Methods: We prospectively studied 95 subjects by CMR, recruited into 2 groups: angiographically confirmed coronary artery disease (CAD); orno evidence of CAD on screening treadmill exercise test. T1-weighted imaging was performed (TE = 10 ms, TR = 1 RR) in the axial plane with 5 mm slice thickness and 5 mm gap. Measurements were consistently performed at the same level in all subjects, identified by the visualization of both mitral leaflets in axial plane. Fat was identified by its characteristic bright signal in T1. The dark stripe of the pericardial space separating bright epicardial fat from bright pericardial

fat was identified and the maximum diameter was measured for both epicardial and pericardial fat. Maximum diameter of subcutaneous fat was also measured above the mid-sternum. Visceral epicardial and pericardial fat and non-visceral subcutaneous fat were compared in groups with CAD and without CAD.

Results: Sixty subjects with CAD were compared to 35 controls without CAD. CAD subjects were significantly older (59 vs. 50 y, $p < 0.01$) and had higher fasting glucose (6.63 vs. 5.54 mmol/L, $p < 0.01$), but both groups were comparable for LDL-cholesterol, triglycerides, hypertension, smoking, gender, BMI, and family history. CAD subjects had significantly greater epicardial fat maximum thickness compared to those without CAD (6.95 vs. 4.94 mm, $p < 0.01$). Pericardial fat and subcutaneous fat maximum thickness were comparable in CAD and no CAD subjects. After controlling for age and fasting glucose in multivariate analysis, epicardial fat maximum thickness remained an independent predictor of CAD (OR 1.4, 95 CI 1.1–1.8, $p = 0.04$).

Conclusions: Epicardial fat maximum thickness is a significant predictor of CAD, independent of classic risk factors. Epicardial fat maximum thickness measured on routine axial T1-weighted CMR may further refine cardiometabolic risk stratification.

618. COMPARISON OF MRI AND ECHOCARDIOGRAPHY FOR ASSESSMENT OF MECHANICAL DYSSYNCHRONY

Kenneth C. Bilchick, MD, Robert H. Helm, MD, Theodore Abraham, MBBS, MD, Albert C. Lardo, PhD. ***Johns Hopkins Medical Institutions, Baltimore, MD, USA.***

Introduction: The measurement of regional cardiac strains has become increasingly important for the evaluation of cardiac mechanical dyssynchrony and the need for cardiac resynchronization therapy (CRT). Although echocardiographic measurements of longitudinal strain and time to peak strain are readily available and clinically validated for cardiac mechanical dyssynchrony, MRI with myocardial tagging (MRI-MT) also has the ability to evaluate dyssynchrony with the advantages of high spatial/temporal resolution and assessment of circumferential strain. Recently it has been shown that circumferential strain (as assessed by MRI-MT) rather than longitudinal strain (the strain usually assessed by echocardiography) is the predominant strain in the heart.

Purpose: Given that clinical data comparing MRI and echo for assessment of dyssynchrony are very limited, we sought to compare these modalities for the assessment of dyssynchrony in normal subjects and subjects with heart failure. In this way, with comparison to MRI as the gold standard, we aimed to discover the limitations and strengths of echocardiographic measurements of regional longitudinal strain for dyssynchrony assessment and evaluate the MRI-based circumferential uniformity ratio estimate (CURE, described below) for the grading of mechanical dyssynchrony.

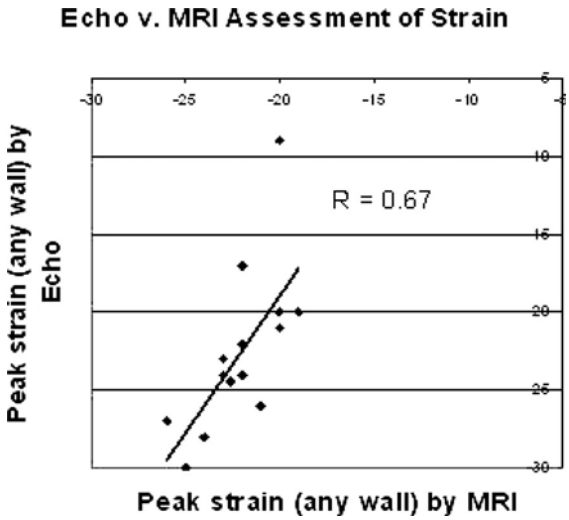

FIG. 1.

Methods: Fifteen subjects (11 normals, 2 with dilated cardiomyopathy, and 2 with heart failure with normal ejection fraction) underwent both echo and MRI-MT assessment of mechanical dyssynchrony, including measurement of strain and time to peak strain in the septal and posterolateral walls. From these measurements, the septal-posterolateral wall delay in time to peak strain (SPLWD, currently one of the most widely used criteria for dyssynchrony), the standard deviation of time to echo peak strain in six segments (Ts-SD6) and the MRI circumferential uniformity ratio estimate (CURE; 0–1, 0 = asynchrony, 1 = perfect synchrony) were calculated.

Results: Mechanical dyssynchrony as measured by CURE was significantly greater in normal subjects as compared to dilated cardiomyopathy (0.95 ± 0.01 v. 0.72 ± 0.12; $p = 0.002$), but was not significantly different between normal subjects and those with heart failure with normal ejection fraction ($p = NS$). In normal subjects, peak longitudinal strain in any wall as calculated by echo was similar to that calculated by MRI (-22.6 ± 0.61 v -24.5 ± 0.96; $p = NS$). There was also a good correlation between peak strain in any wall as measured by echo or MRI for all subjects (Fig. 1; $R = 0.67$). The MRI-based CURE showed a significant correlation with the echo-based SPLWD ($R = 0.62$), but did not correlate well with the Ts-SD6 calculated in a limited number of subjects.

Conclusions: Assessment of regional longitudinal strains by echocardiography and regional circumferential strains by MRI offer complementary information for the evaluation of cardiac mechanical dyssynchrony. Further comparison between these two modalities with additional patients promises to have important clinical implications in patient selection for CRT.

619. OFF-RESONANCE IMAGING OF SUPERPARAMAGNETIC IRON-OXIDE NANOPARTICLES IN INFARCTED MOUSE MYOCARDIUM AT DILUTE

CONCENTRATIONS AND HIGH MAGNETIC FIELD STRENGTHS

Christian T. Farrar, PhD, Guangping Dai, PhD, Bruce R. Rosen, MD, PhD, David E. Sosnovik, MD. ***Massachusetts General Hospital, Charlestown, MA, USA.***

Introduction: Iron-oxides such as MION are usually imaged with T2* based techniques, which produce negative contrast around the nanoparticle. Positive contrast off-resonance imaging (ORI) techniques have recently been developed and have been used to image cells, densely loaded with iron-oxides, at 1.5 T. Our aims in this study were to characterize the behavior of ORI at high field strengths and in the presence of more dilute concentrations of iron-oxides, such as those produced by targeted in-vivo agents. The ability of the off-resonance technique to detect the endogenous accumulation of the macrophage-targeted nanoparticle MION in a healing myocardial infarct was thus studied.

Methods: Prior to in-vivo imaging, aqueous MION solutions ranging from 8–256 ug Fe/mL were imaged at 4.7 and 14 T. Spin-echo images were acquired with varying on-resonance water suppression bandwidths (WSBWs). The mean chemical shift induced by MION was determined from fits of the dependence of the off-resonance signal intensity on the WSBW. In-vivo, fat suppressed ORI was then performed at 4.7 T in 3 control mice and in 4 mice with healing myocardial infarcts. Myocardial infarction was induced by ligation of the left coronary artery and the mice were injected through the tail vein with 15 mg Fe/kg of MION 48 hours later. In-vivo off-resonance imaging of the heart and thorax was performed a further 48 hours later (96 hours post ligation) with the following parameters: FOV = 35 × 30 mm, matrix = 128 × 128, TR = 2000 ms, TE = 2.9/5.8/8.7/11.6 ms, NA = 4.

Results: The mean induced chemical shift was linear with MION concentration (Fig. 1a). In contrast, significant non-linearity was observed in the ORI signal intensity (Fig. 1b). This is due to the large reduction in T2 with higher MION concentrations at these fields, even at relatively short echo times. Positive contrast was consistently seen at air-fluid interfaces, in-vitro, and at air-tissue interfaces in-vivo (Fig. 2a,b). However, positive contrast was not seen in the myocardium in any of the control mice, even with a WSBW of 200 Hz (Fig. 2a). Positive contrast was seen in the injured anterolateral myocardium of all 4 infarcted mice, consistent with the uptake of MION by macrophages infiltrating the healing infarct (Fig. 2b). The contrast-to-noise ratio between the injured anterolateral wall and uninjured septum was significantly higher in the infarcted mice than in control mice (Fig. 2c). Increasing the WSBW to 400 Hz reduced much of the background off-resonance signal, however, the sensitivity to MION accumulation in the myocardium was lost.

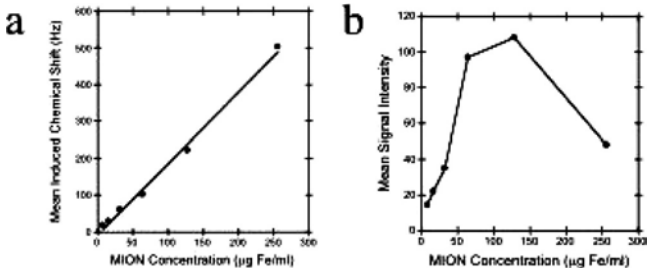

FIG. 1. Dependence of the mean induced chemical shift (a) and off-resonance signal intensity (b) on MIQN concentration for an aqueous MION phantom imaged at 4.7T. The mean off-resonance signal intensity was determined from images acquired with a 250 Hz water suppression bandwidth.

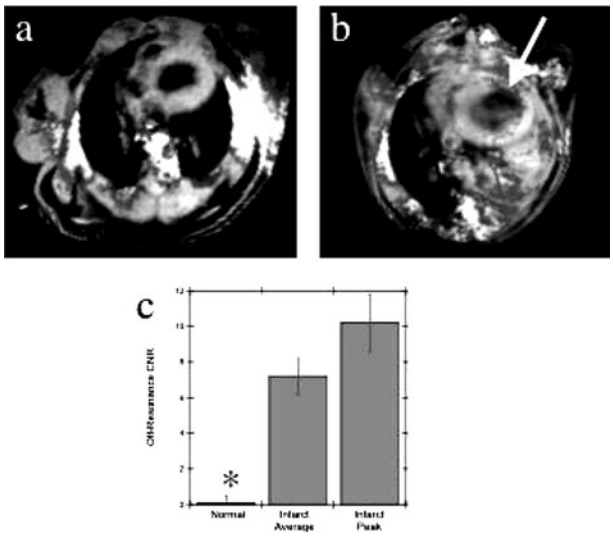

FIG. 2. Off-resonance images of normal (a) and intarcted (b) mice acquired at 4.7T with a water suppression bandwidth of 200 Hz. The off-resonance images have been mapped to a color scale and overlaid onto conventional spin-echo images. Iron-oxide accumulation within macrophages infiltrating the injured myocardium produces positive off-resonance contrast (arrow). Significantly greater CNR between the infarcted anterolateral myocardium and the uninjured septal wall was seen in the off-resonance images of the infarcted mice than in control mice (c).

Conclusion: Post-infarction myocardial inflammation and MION accumulation could be successfully imaged in-vivo with a positive contrast off-resonance technique. The detection of dilute concentrations of targeted iron oxides at high fields is thus possible but requires the use of narrow water suppression bandwidths and short echo times to maintain high sensitivity.

620. ACCURACY OF CMR PERFUSION AND VIABILITY ASSESSMENT IN THE DIAGNOSIS OF CORONARY ARTERY DISEASE

Jonathan Lyne, MRCP,[1] Ravi Assomull, MRCP,[1] Stuart Watkins, MRCP,[1] Joanna Petryka,[1] Karen Symmonds, MSc,[1] Julian Collinson, MRCP,[2] Peter Gatehouse, PhD,[1] Dudley Pennell, MD, FRCP, FACC, FESC.[1] ***[1]Royal Brompton Hospital, London, United Kingdom, [2]Chelsea and Westminster Hospital, London, United Kingdom.***

Introduction: A number of previous studies have compared CMR perfusion data to invasive and non invasive techniques used in the diagnosis and assessment of coronary artery disease (CAD). As the diagnosis of CAD has frequently been used as an outcome measure almost all of these studies have excluded patients with known CAD. Therefore these studies may not be a true reflection of this tests routine clinical utility in the assessment of patients with known CAD.

Purpose: To prospectively evaluate the accuracy of CMR perfusion and viability assessment against quantitative coronary angiography in the diagnosis and evaluation of patients with and without known coronary artery disease.

Methods: This study was approved by the local ethics committee. In 85 prospectively enrolled patients (74 male, average age 62 years) with recent or awaiting invasive xray coronary angiography, dual sequence, first pass perfusion images were acquired using a 1.5T MR scanner (Siemens Avanto, Erlangen, Germany). Only patients with contraindications to magnetic resonance imaging were excluded. A non selective square saturation recovery, interleaved segmented-EPI sequence (factor 4) with RF spoiling, incorporating TSENSE (acceleration rate 2) and fat saturation was used for myocardial imaging. Flip angle 30°, TR 5.8 ms/TE 1.22 ms, bandwidth 1860 Hz/pixel. Read field of view (FOV) 34–40 cm; phase FOV 75% of the read FOV; base matrix 128 × 96; pixel size range 2.4 × 2.4–3.1 × 3.1 mm, slice thickness 8 mm. An accurate arterial input function was obtained using a fast GRE sequence for the AIF image, TR 1.08 ms/TE 0.58 ms, flip angle 10° using a 0.10 ms RF pulse, 10 mm slice thickness, 128 frequency-encode (FE) × 48 phase-encode (PE) raw data, including × 2 FE FOV oversampling, 3900 Hz/pixel in the same plane as the middle of the three myocardial image slices. Subjects abstained from caffeinated products for 24 hours prior to scanning. Gadolinium-BMA (Omniscan) 0.1 mmol/kg body weight was injected at 7 mL/s (Spectris, Medrad, Indianola, PA) via an 18-gauge cannula. Three short axis slices were acquired over 50 consecutive cycles during adenosine (140 mcg/kg/min for 4 minutes) and 20 minutes after at rest. This permitted a 16 segment analysis with dedicated software (CMRtools; Cardiovascular Imaging Solutions, UK). For late enhancement imaging inversion recovery images were obtained with a segmented read out gradient echo sequence. Three long axis and adequate short axis images were acquired to ensure full ventricular coverage. Perfusion images were scored by blinded observers for the presence and absence of late myocardial enhancement and the presence or absence of an inducible perfusion defect. Quantitative coronary angiography (QCA) measurments were made with stand alone software (Medcon Inc.)

TABLE
Patient demographics

Male	Hypertension	Current or Exsmoker	Aspirin	Beta blocker	Statin therapy
74 (87%)	17 (20%)	27 (32%)	42 (49%)	38 (45%)	55 (65%)

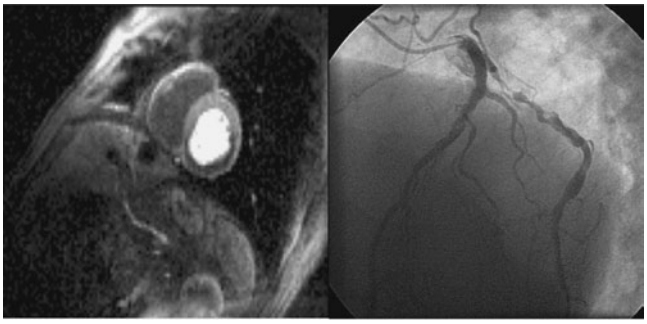

Results: Observer scoring as to the absence or presence of CAD on the results of the perfusion and late enhancement images were correlated against the results of QCA (>50% stenosis in 1 or more main epicardial vessel). The sensitivity was 87%, specificity 88%. With QCA parameters of >70% in one or more vessel sensitivity was 94%, specificity 80%. Only 3 of the 85 patients were diagnosed with CAD on the basis of late enhancment alone without a perfusion defect.

Conclusions: In an unselected group of patients, perfusion and late enhancement CMR is highly accurate in the diagnosis of coronary artery disease. In this study patients with known CAD and revascularistion were not excluded therefore providing a better indicator of this techniques performance in the clinical setting.

621. DECREASE IN ATRIAL VOLUME AND SYSTOLIC FUNCTION AFTER PULMONARY VEIN ISOLATION

John V. Wylie, MD, Vidal Essebag, MD, PhD, Mark E. Josephson, MD, Warren J. Manning, MD, Thomas H. Hauser, MD, MMSc, MPH. ***Beth Israel Deaconess Medical Center, Boston, MA, USA.***

Introduction: Catheter ablation of atrial fibrillation (AF) involves extensive radiofrequency ablation (RFA) of the left atrium (LA) at the ostia of the pulmonary veins (PV).

Purpose: We hypothesized that resultant LA scar would lead to a decline in LA volume and systolic function.

Methods: We evaluated LA volume prior to and one month after PV isolation in 30 consecutive patients with paroxysmal AF referred for RFA using steady-state free-precession ECG-gated cine cardiovascular magnetic resonance. All patients were in sinus rhythm at both studies. LA volume was calculated using the area-length method from the 2-chamber and 4-chamber views at end ventricular systole (maximum LA size), ventricular mid-diastole (prior to LA contraction), and at ventricular end-diastole (minimum LA size). LA ejection fraction (LAEF) was defined as (mid-diastolic volume–end-diastolic volume)/mid-diastolic volume. All patients underwent RFA PV isolation using an 8 mm tip catheter around each PV until bi-directional block was confirmed.

Results: Both maximum LA volume and mid-diastolic volume declined after the procedure, as did the LAEF (Table,

TABLE
LA Measures Pre- and Post- RFA PV isolation

	Pre-RFA	Post-RFA	P
Maximum LA Volume, mL	117 ± 31	98 ± 23	<0.001
Volume prior to LA Contraction, mL	85 ± 24	76 ± 21	0.015
Minimum LA Volume, mL	59 ± 21	55 ± 17	0.219
LA Ejection Fraction, %	32 ± 11	27 ± 8	0.010

$p < 0.02$ for both). The majority (73%, $n = 22$) of subjects had a decline in LA EF ($p < 0.01$). There was no change in minimum LA volume and no patient developed PV stenosis.

Conclusions: PV isolation using RFA is associated with decreased LA size and impaired systolic function. This finding may have implications for post-procedure thromboembolic risk and for procedures employing more extensive LA RFA.

622. SEPARATING NORMAL STRUCTURES FROM PATHOLOGY IN THE ASSESSMENT OF INTRACARDIAC MASS BY CARDIAC MAGNETIC RESONANCE

W. Patricia Bandettini, MD, Andrew C. McUsic, Andrew E. Arai, MD. ***National Institutes of Health, Bethesda, MD, USA.***

Background: In a review of the literature searching for articles involving the use of MRI to assess patients with cardiac mass, only five original articles were found in which the sample size was greater than 15 patients with actual cardiac masses, and only two had samples sizes 50 or greater (50 and 55 respectively). One of these two studies collected patients over a 13 year period, and the other was performed prior to 1989 which was also prior to the common use of gadolinium first-pass perfusion and delayed enhancement techniques.

Objective: The purpose of this study was to determine the prevalence of normal structures, thrombus, or tumors in a large patient group specifically referred for assessment of intracardiac mass after another imaging technique.

Methods: Patients ($n = 116$) were referred specifically for CMR assessment of intracardiac mass based on findings from echocardiography, computed tomography, or PET. All CMR studies were performed on a 1.5 T scanner using either a 4-element phased array coil or a 12-element surface coil array. All patients underwent volumetric cine CMR of the heart, including an additional stack of images acquired parallel to the 4-chamber view, extending from before the insertion of the inferior vena cava up through the top of the aortic arch. Most patients also underwent first-pass perfusion with gadolinium contrast and delayed enhancement (DE) imaging. Any structure defined as lipoma or lipomatous hypertrophy was documented through the use of fat saturation techniques applied to a fast spin echo sequence. Lipomatous hypertrophy of the interatrial septum was defined as greater than 1.5 cm fat within the interatrial groove. The crista terminalis was defined as the ridge of tissue that extends from the inferior vena cava to the superior vena cava along the posterior wall of the right atrium. Potential masses were also imaged with a black blood fast spin echo sequence (proton density weighted and T2-weighted).

TABLE 1
Most common findings

	Number of Patients (%)
Benign/Normal Variants	
Crista terminalis	9 (8%)
Lipoma	5 (4%)
Lipomatous hypertrophy (interatrial)	4 (3%)
Accessory papillary muscle or trabeculation	4 (3%)
Tumors or Thrombus	
Cardiac metastases	30 (26%)
Extracardiac masses adjacent to heart	12 (10%)
Primary cardiac tumors	11 (9%)
Thrombus	13 (11%)

Results: Twenty-six of the 116 patients had "masses" that were determined to be benign or normal variants (22% prevalence). The most common normal or normal variant structures identified were the crista terminalis, lipomas, lipomatous hypertrophy of the interatrial septum, and accessory papillary muscles or dense trabeculae. Other normal structures identified included the Eustachian valve, a prominent left atrial appendage ridge (also known as the "warfarin ridge"), and abnormal inflow of the IVC along an interatrial septal patch.

The 68 masses identified that were not considered normal structures or variants included metastatic lesions, thrombi, extracardiac metastases, and primary cardiac masses. Four structures that were non-malignant included an extracardiac mass that was biopsied and identified as reactive lymphoid tissue, a large right coronary artery aneurysm that was originally diagnosed as a pericardial cyst by echocardiography, and two pericardial cysts. There were two patients in whom CMR was able to clarify that both metastases and thrombi were present.

Conclusion: CMR can differentiate solid tumors, lipomas, thrombi, pericardial cysts, and normal cardiac structures. The use of first-pass perfusion and gadolinium DE assists in the differentiation of thrombus from solid masses, the separation of vascular structures from pericardial cysts, and in the characterization of vascularity of a solid tumor. In 22% of this study's patients, the CMR diagnosis of a normal structure or normal variant avoided more invasive evaluation or treatment. In our experience, the ability to distinguish between a normal structure, a thrombus, and a tumor greatly impacts the management of patients with suspected intracardiac masses.

623. QUANTITATIVE ANALYSIS OF CARDIAC T2 RELAXATION TIME FEASIBLY PREDICTS LEFT VENTRICULAR FUNCTIONAL RECOVERY IN PATIENTS

WITH REPERFUSED ACUTE CORONARY SYNDROME-201TL AND 123I-BMIPP DUAL SPECT VALIDATION

Toshiaki Kadokami, MD, Natsumi Kawamura, MD, Hidetoshi Momii, MD, Takaya Fukuyama, MD, Shin-ichi Ando, MD. ***Saiseikai Futsukaichi Hospital, Chikushino, Japan.***

Introduction: Acute myocardial ischemic injury has been shown to result in regional hyperintensity in T2-weighted cardiovascular magnetic resonance (CMR) while only infarcted region can be detected as delayed gadrinium (Gd)-enhancement. Areas with increased T2 in the absence of delayed enhancement (DE), which can be defined as mismatch region, may indicate stunned but viable tissue.

Purpose: Thus, we hypothesized that extent of the mismatch region is associated with left ventricular (LV) functional recovery in reperfused acute coronary syndrome (ACS).

Methods: CMR imaging was performed 4 ± 2 days after revascularization and repeated six months later in fifteen patients with ACS. Patients with prior myocardial infarction were excluded. Each CMR protocol consisted of cine MRI for LV functional analysis, dual fast-spin-echo sequence (TE1 = 18, TE2 = 100) for myoccardial T2 measurement, and Gd (0.15 mmol/kg) enhanced inversion-recovery gradient echo technique for detecting DE. Regional T2 value and DE extent was evaluated from the three standard short-axis slices using a 16-segment LV model. Segmental DE extent score was determined as follows: no DE = 0, 1–25% of transmural extent = 1, 26–50% = 2, 51–75% = 3, > 76% = 4. T2 score for each segment was determined as follws: < 70 ms = 0, 71–80 ms = 1, 81–90 ms = 2, 91–100 ms = 3, >101 ms = 4. Then the mismatch score was calculated as follows: Mismatch score = T2 score-DE score. Sum of the mismatch score for each segment was used for analysis.

Results: Larger mismatch score was closely associated with LV ejection fraction amelioration (Table). In addition, the MS in CMR correlated well with the mismatch extent in 201Tl and 123I-BMIPP dual SPECT, which had been shown to be useful in predicting functional recovery of stunned myocardium.

Conclusions: These results suggest that the discrepancy between abnormal T2 and DE, which indicates stunned but viable tissue, can predict global cardiac functional recovery in patients with ACS after reperfusion.

TABLE
Relationship between proportional EF change and mismatch score

Proportional EF change	n	Mismatch score
>10%	9	7 ± 5
<9%	6	2 ± 4

624. ANGIOGRAPHIC ESTIMATES OF MYOCARDIUM AT RISK DURING ACUTE MYOCARDIAL INFARCTION: A VALIDATION STUDY USING CARDIAC MAGNETIC RESONANCE IMAGING

Jose T. Ortiz, MD, Sheridan N. Meyers, MD, Charles Davidson, MD, Daniel C. Lee, MD, Preeti Kansal, MD, Edwin Wu, MD. ***Northwestern University, Chicago, IL, USA.***

Background: The extent of an acute area of myocardial necrosis following coronary occlusion is largely dependent on the distal distribution of coronary arteries. Previous experimental studies showed that as early as 40 minutes after coronary occlusion, the circumferential extent of necrosis is established and encompasses the lateral boundaries of the area at risk. Subsequent increases in infarct size are dependent on the transmural extent of necrosis. We tested the ability of two different angiographic scores to measure the anatomical area at risk of infarction and finally predict the final infarct size in subjects with transmural infarct. We also hypothesized that myocardial salvage provided by early reperfusion or angiographic collateral flow occurs primarily by means of reduction in infarct transmural extent.

Methods and Result: The anatomical area at risk by angiography was determined in 82 subjects with first acute ST-segment elevation myocardial infarction presenting with an occluded artery at the time of primary percutaneous coronary intervention. The myocardium at risk by Myocardial Jeopardy Index (BARI score) and a modified version of the Alberta Provincial Project for Outcome Assessment in Coronary Heart Disease (APPROACH score) ranged from 9.1% to 60.0% and from 12.0% to 47.8% of the left ventricular (LV) wall volume, respectively. Contrast-enhanced cardiovascular magnetic resonance (Ce-CMR) was performed within a week to measure the infarct size (range 2.9% to 57.5% of total LV mass), the infarct endocardial surface area (infarct-ESA) (range 6.8% to 63.9% of total LV endocardial surface area), and infarct transmural extent.

Among 21 subjects with transmural infarcts (mean infarct transmurality > 75% of the LV wall), the total infarct size by ce-CMR matched the myocardium at risk by BARI and APPROACH scores ($r = 0.90$ and $r = 0.92$ respectively, $p < 0.0001$). The myocardium at risk by the BARI and APPROACH scores also matched the infarct-ESA in the whole group ($r = 0.90$ and $r = 0.87$ respectively, $p < 0.0001$). Bland-Altman analysis showed a mean bias of 1.66% and 2.81% between infarct-ESA and BARI or APPROACH score respectively. APPROACH score overestimated the infarct-ESA in small infarcts and underestimated it in cases of large infarcts, whereas BARI score was more sensitive to individual differences throughout the entire group.

Additionally, subjects with well developed collaterals or time-to-reperfusion < 3 hours had fewer segments with transmural infarct and less mean infarct transmurality score ($p < 0.05$

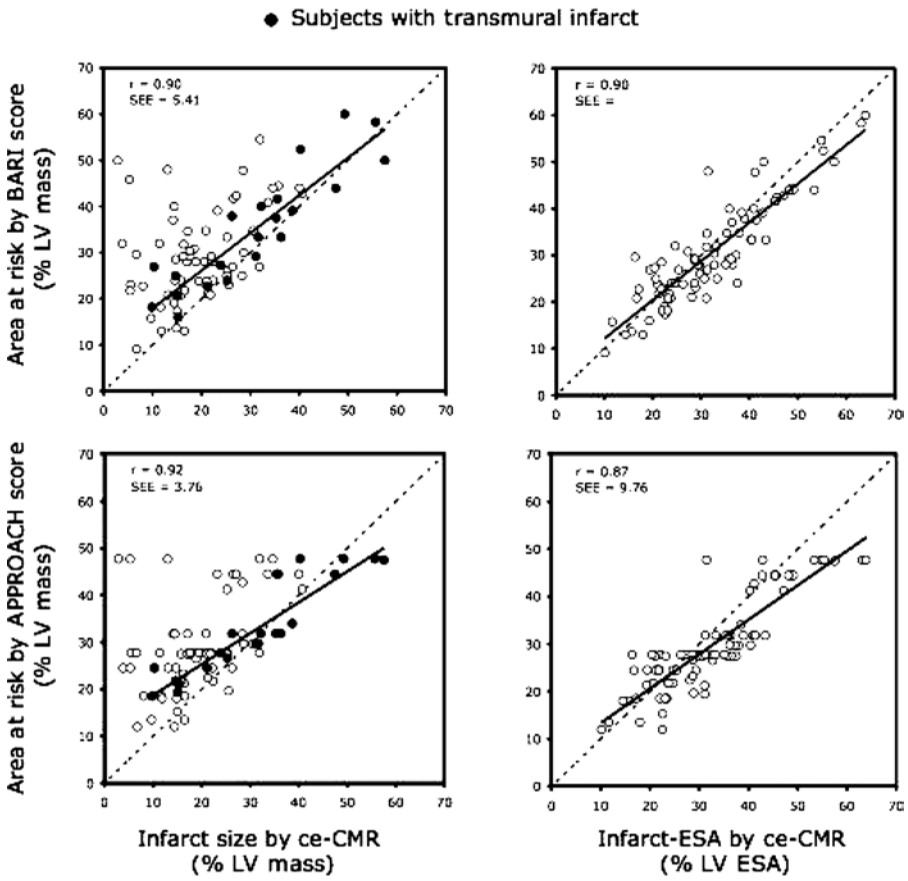

for all), but there was no difference in the initial area at risk and infarct-ESA between groups.

Conclusions: Both BARI and APPROACH scores provide accurate measurements of anatomical area at risk of infarction as evident in patients with transmural infarcts and absent salvage. BARI score calculation may be preferred when accuracy is the priority, and APPROACH is a simple and fast score to apply in retrospective studies. Myocardial salvage provided by early reperfusion or angiographic collateral flow occurs primarily by means of reduction in infarct transmurality. Therefore, the infarct endocardial surface area measured by CMR can be a surrogate measure of the area at risk of infarction.

625. A NOVEL METHOD TO ASSESS DIASTOLIC DYSFUNCTION FOLLOWING MYOCARDIAL INFARCTION BASED ON CINE CARDIAC MAGNETIC RESONANCE IMAGING

Michael A. Morse, MD,[1] Jose T. Ortiz, MD,[1] Xiaoming Bi, PhD,[2] YiuCho Chung, PhD,[2] Sven Zuehlsdorf, PhD,[2] Renate Jerecic, PhD,[2] Daniel C. Lee, MD,[1] Edwin Wu, MD.[1]
[1]Northwestern University, Chicago, IL, USA, [2]Siemens Medical Solutions, Chicago, IL, USA.

Background: Steady-state free precession cine has a high myocardial to blood pool signal contrast, and therefore, frame-to-frame changes in pixel intensities can be used to evaluate global left ventricular (LV) wall motion throughout a cardiac cycle. A rapid and novel approach was developed to evaluate diastolic dysfunction by analyzing these pixel intensity changes and constructing left ventricular motion time curves (LVMTC). The aim of this study was to compare this novel approach to the standard mitral inflow phase-contrast velocity time curves (PVTC) to assess diastolic dysfunction in patients following acute myocardial infarction.

Methods: Short and long-axis cine and delayed contrast-enhanced imaging to encompass the entire left ventricle were performed on 55 subjects within a week following reperfused STEMI. Using a self-developed analysis tool in ImageJ (NIH, Bethesda, MD), a region of interest (ROI) was traced along the epicardial border for 3 long axis and a mid-ventricular slice. Within the ROI, the differences in pixel intensities between subsequent cine frames were summed ($\Sigma\ I_N$-I_{N+1}) and averaged to construct a LVMTC. Mitral inflow velocity images were assessed using a phase-contrast velocity sequence set perpendicular to the mitral valve leaflet tips. The ratio between early (E′) and late (A′) diastolic motion peaks and the Deceleration Time (DT) of the E′ wave from the LVMTC were compared to the early (E) and late (A) peak velocities ratio and DT of the E wave

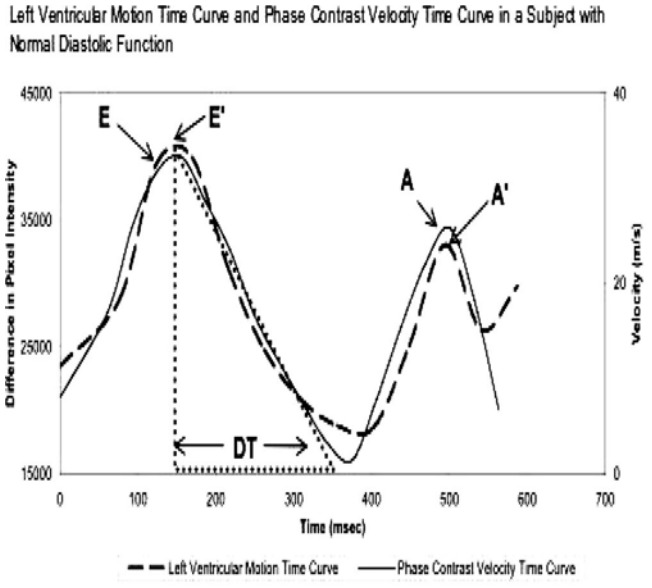

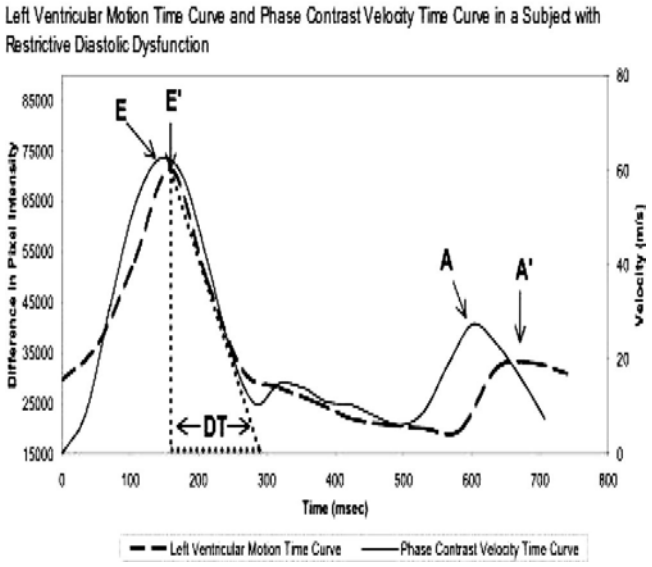

from the PVTC. The E/A ratio and DT for both LVMTC and PVTC were used to classify subjects into four diastolic dysfunction categories: normal (E/A = 1–2 and DT > 200 ms), impaired relaxation (E/A < 1), pseudonormal (E/A = 1–2 and DT < 200 ms), and restrictive (E/A > 2 or E/A 1-2 and DT < 160 ms).

Results: There was a good correlation between the E/A and E′/A′ ratios ($r = 0.60$, $p < 0.001$) and DT ($r = 0.75$, $p < 0.001$) between LVMTC and PVTC. Bland-Altman analysis between LVMTC and PVTC showed a bias of 0.05 ± 0.6 and 8.7 ± 22.6 ms for E/A ratio and DT, respectively. When dividing patients into the 4 diastolic dysfunction categories, the LVMTC were able to correctly identify patients 85% of the time. The LVMTC and PVTC agreed for 89% of normal, 50% of impaired, 100% of pseudonormal, and 80% of restrictive subjects. The new modality had 100% sensitivity and 89% specificity in detecting any diastolic dysfunction. In 7 subjects with E and A wave fusion on PVTC, LVMTC analysis was able to identify distinct E′ and A′ peaks. Furthermore, DT from LVMTC ($r = 0.46$, $p < 0.01$); and PVTC ($r = 0.52$, $p < 0.001$) had good correlation with myocardial infarct size.

Conclusions: LV motion time curves are a rapid and accurate novel approach for detecting diastolic dysfunction in post-MI subjects and can be retrospectively applied to existing cine data. As with mitral inflow velocity measurements, the severity of diastolic dysfunction increases with larger acute infarct sizes. Furthermore, diastolic dysfunction severity can be correctly classified retrospectively without the need for additional phase-contrast velocity imaging, and may have additional value in patients with E and A wave fusion.

626. A COMPARISON OF TWO DIFFERENT FIELD INSENSITIVE SATURATION PULSES FOR IMPROVED UNIFORMITY IN MYOCARDIAL PERFUSION IMAGING AT 3T

Sven Zuehlsdorff, PhD,[1] Peter J. Weale, BA, DCR(R),[1] Aya Kino, MD,[2] James C. Carr, MD,[2] Renate Jerecic, PhD.[1] [1]***Siemens Medical Solutions, Inc., Chicago, IL, USA,*** [2]***Northwestern University, Chicago, IL, USA.***

Introduction: Quantification or semi-quantification of myocardial perfusion requires spatially homogenous saturation of magnetization across the heart. In particular, variation in flip angle of a saturation preparation will impose a spatially varying difference in contrast which may compromise the accuracy of quantitative or semi-quantitative perfusion and potentially reduce CNR.

Kim et al. (1) demonstrated improved performance of saturation at 1.5 T using a B1-insensitive rotation pulse (BIR4) (2) and a composite pulse compared to a single pulse.

At higher field strength, e.g., 3T, perfusion images show higher SNR but at the expense of increased susceptibility to field in homogeneity. This potentially impairs both qualitative and quantitative assessment of perfusion to a greater degree than at 1.5T.

Purpose: In this work the performance of two different field insensitive saturation pulses is compared in-vivo and in-vitro to the standard pulse on a clinical 3T scanner (MAGNETOM Trio, Siemens, Erlangen, Germany).

Methods: The three saturation pulses evaluated in this study were:

(I) single non-selective saturation recovery pulse; (II) a train of three non-selective saturation pulses utilizing dedicated time intervals and crusher gradients to eliminate stimulated echoes; and (III) a BIR4 adiabatic pulse. Each pulse flip angle has been optimized in phantoms to achieve maximum saturation.

Clinical perfusion protocols have been performed (turboFLASH readout, echo spacing = 2.4 ms, α=12 deg, 128 × 83 matrix, GRAPPA factor 2 using a homogenous water phantom to

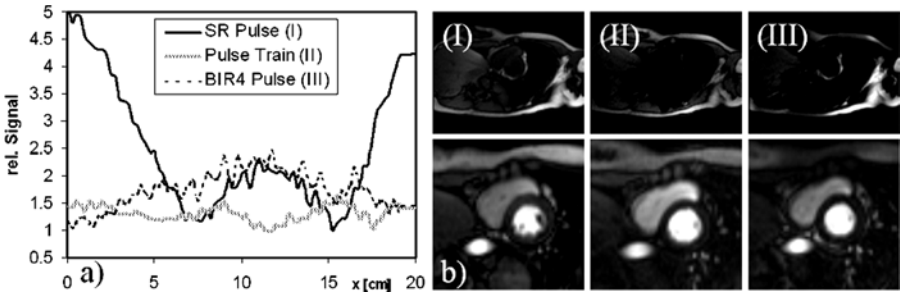

FIG. 1. a) Normalized profiles of saturated images in a water phantom using a single saturation recovery (SR) pulse (I), a three-pulse train (II) and a BIR4 pulse, respectively. The uniformity of the saturation is improved by using pulse train (II) and BIR4 (III) as alternative to the single SR pulse (I). b) In-vivo images of a healthy volunteer pre-contrast and during first pass perfusion.

assess the performance of the saturation pulses. The maximum relative signal variation over a 20 cm profile was determined as a measure of the pulse uniformity. All three described pulse schemes were examined in the same healthy volunteers and the image results were analyzed for uniformity of saturation. Contrast agent was administered at a rate of 4 mL/s at a dose of 0.075 mmol/Kg under rest and perfusion images were acquired over 50 heartbeats.

Results: The maximum relative signal variation in a water phantom using the three saturation schemes was calculated as (I) 5.1, (II) 1.6 and (III) 2.4, respectively.

Preliminary in-vivo results demonstrate non-uniform saturation with pulse (I) over a large FOV, which is better visualized within homogenous structures like the liver whereas the effect in the heart is less easy to detect. Initial evaluation of the myocardial signal time curves (spread of base-line signal intensity, peak signal intensity and of the myocardial signal intensity in the "plateau" phase) shows that there may be a non uniform saturation across the heart with pulse (I) which is not seen with the two B1 insensitive pulses (II) and (III).

Conclusion: Both alternatives (II) and (III) to a single saturation pulse (I) yield a more uniform saturation at 3T, as previously demonstrated at 1.5T (1). However, the differences between pulse (II) and (III) are small showing little qualitative differences in in-vivo studies. Further in-vivo evaluation is required to quantify this effect.

Use of a B1 insensitive saturation pulse (pulse train or BIR4 pulse, respectively) mitigates the detrimental effects of B1 inhomogeneity that are exacerbated at high field strengths. Adoption of these pulse schemes will be desirable to enable the development of quantitative myocardial perfusion methods at high field strengths.

REFERENCES

1. Kim D, et al. Magnetic Resonance in Medicine 2005;54:1423–1429.
2. Tannus A, Garwood M. NMR in Biomedicine 1997;10:423–434.

627. CORRELATION ANALYSIS OF TIME-SIGNAL INTENSITY HISTOGRAM CAN AUTOMATICALLY DISTINGUISH CHANGES IN PERFUSION AND LATE ENHANCEMENT: GADOLINIUM MRI ASSESSMENT OF AN ISCHEMIC RAT HIND-LIMB MODEL AT 7 TESLA

Li-Yueh Hsu, Andrew Wragg, Stasia Anderson, Robert S. Balaban, Manfred Boehm, Andrew E. Arai. ***National Institutes of Health, Bethesda, MD, USA.***

Introduction: MRI at high field strength is a promising method for assessing ischemia and the consequences of ischemia in small animal models treated with various stem cells. MR measurements of skeletal muscle perfusion have been published using endogenous or exogenous contrast agents in rats and humans. There is still a need for objective image analysis methods which can detect differences in perfusion and late enhancement in the entire dynamic contrast-enhanced study.

Purpose: To develop automated analysis of dynamic gadolinium-enhanced MR images suitable for detecting differences in perfusion and late enhancement in an ischemic rat hind-limb model.

Methods: This 7T MRI pilot study used animals in a double-blind placebo-controlled experiment comparing MAPC-Derived Progenitor Cells (MDPC) treated (n = 6), phosphate buffered saline (PBS) injected (n = 6), and sham operated (n = 3) rats. Gd-DTPA (0.3 mmol/kg) was delivered through a tail vein catheter. Sequential images were acquired at 3 s/image over 4 minutes. An axial cross section above the knee was imaged using a T_1-weighted spoiled fast gradient echo pulse sequence (TR 50 ms, TE 2.2 ms, flip angle 30°, FOV 3.4 × 3.4 cm, matrix 128 × 64, thickness 2.0 mm) and resulted an in-plane resolution of $265 \times 531\ \mu m^2$. All images were post-processed to correct signal intensity bias caused by the transmitting and receiving surface coil based on a pre-contrast image. An automated computer segmentation algorithm was developed to encircle the cross section of both limbs. Time-signal intensity histograms of the right and left limbs were then calculated separately for all images in the time series. The correlation coefficient of the time-signal intensity histograms (ischemic vs. non-ischemic limb) and semi-quantitative parametric maps of contrast enhancement were analyzed.

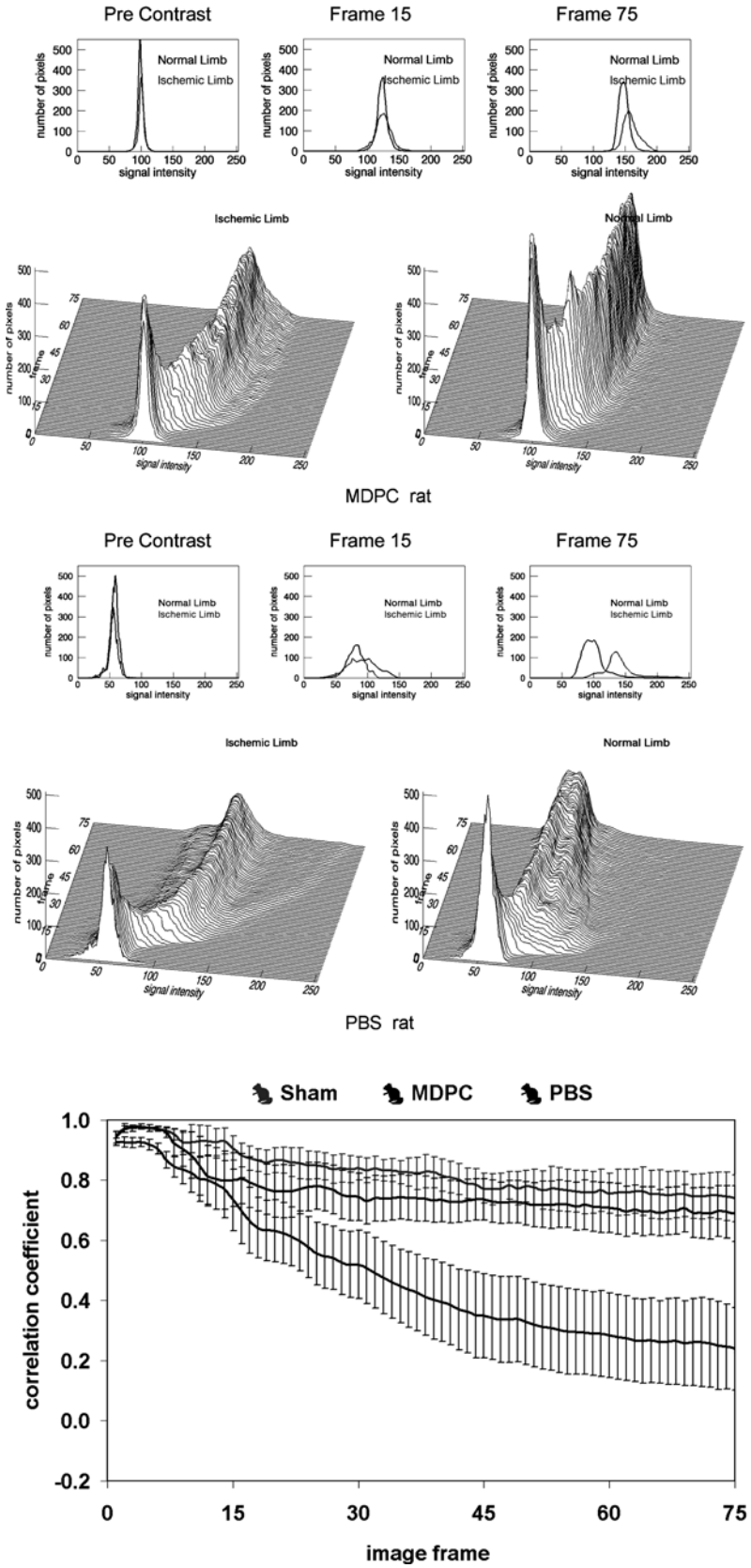
Pre Contrast
Frame 15
Frame 75
Normal Limb
Ischemic Limb
number of pixels
signal intensity
Ischemic Limb
Normal Limb
frame
MDPC rat
PBS rat
Sham
MDPC
PBS
correlation coefficient
image frame

FIGS. 1, 2, and 3.

Results: In time-signal intensity histogram analysis, the MDPC treated limbs correlated well with their corresponding non-ischemic limbs while the PBS control group did not (Figs. 1 and 2). There was a significant reduction of the correlation coefficient ($p < 0.05$) in the ischemic PBS control group compared to either ischemic MDPC treated or non-ischemic sham operated group at late image time frames (Fig. 3, > 108 seconds post-contrast). In parametric map analysis, there was no significant difference of hypo-enhanced area between MDPC and PBS groups at early perfusion dependent time frames. However, the late enhancement area was significantly larger in the PBS than the MDPC group.

Conclusions: A novel dynamic MR image analysis method was developed, based on the correlation coefficient of the time-signal intensity histograms of ischemic and normal limb muscles. This method automatically processed the images and distinguished the MDPC treated animals from PBS controls. The differences were primarily reflected by more late contrast enhancement on PBS treated limbs. The new computerized method can be generalized for assessing myocardial perfusion and late enhancement in contrast-enhanced MRI.

628. CARDIAC MAGNETIC RESONANCE CHARACTERIZATION OF CARDIAC ABNORMALITIES ASSOCIATED WITH HYPEREOSINOPHILIA

W. Patricia Bandettini, Amy D. Klion, MD, Andrew E. Arai, MD. ***National Institutes of Health, Bethesda, MD, USA.***

Background: Hypereosinophilic syndromes (HES) are a rare group of heterogeneous disorders that may be complicated by cardiac manifestations, including fatal endomyocardial fibrosis. Although pathological studies suggest that the development of endomyocardial fibrosis occurs in 3 stages: 1) an acute necrotic phase in which there is eosinophilic and lymphocytic infiltration of the myocardium; 2) the formation of thrombi along the endocardium of either ventricle and on the atrioventricular valves; and 3) fibrosis of the endocardium, restrictive cardiomyopathy, and entrapment of chordae tendinae causing regurgitant valvular lesions, there is little grouped data regarding the cardiac magnetic resonance (CMR) characteristics that may be seen in this disease process.

Objective: Using the strengths of CMR's multiple imaging planes, its high resolution, and its ability to discriminate between various tissue types, we sought to prospectively characterize the cardiac manifestations of HES in a series of patients evaluated in a clinic specializing in HES.

Methods: Seven patients with known HES were imaged on either a GE 1.5T CV/i scanner or a Siemens 1.5T Avanto scanner. Imaging consisted of steady state free precession (SSFP) short and long axis cine, gradient echo echoplanar (GRE-EPI) first pass perfusion, and phase sensitive inversion recovery delayed enhancement. The patients received a cumulative dose of 0.15–0.20 mmol/kg dose of Gadolinium-DTPA for the perfusion and delayed enhancement imaging. Velocity encoded phase contrast imaging was also performed on an individualized basis to better assess valvular function.

Results: The results for all 7 patients are summarized in Table 1. The mean age was 50 ± 8 years. The mean left ventricular ejection fraction (EF) was 55 ± 6%. Valvular thickening and regurgitant lesions were most commonly noted with 5 of 7 patients having abnormal posterior mitral valve leaflets and 3 of 7 having moderate to severe mitral regurgitation. Ventricular cavity fibrosis was observed in 2 patients (patients 1 and 3), and both of these patients had both the right and left ventricles affected. In total, 4 of 7 patients had abnormal DE studies. The 2 patients with ventricular cavity fibrosis also demonstrated restrictive physiology. The 3 symptomatic patients had at least 4 out of 5 major CMR findings as listed in Table 1. The 4 asymptomatic patients all had only 0–1 findings. None of the 7 patients had any definite findings of thrombus. Figure 1 illustrates Patient 3's biventricular filling in an SSFP cine still-frame and the bright signal intensity characterizing endomyocardial fibrosis on DE in a 3-chamber view.

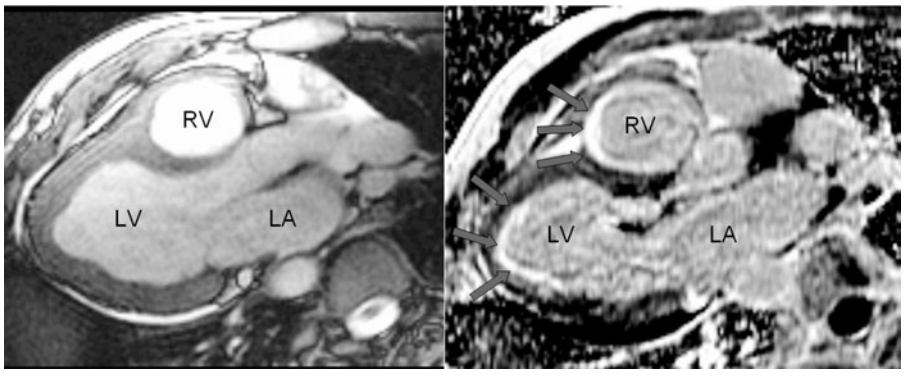

FIG. 1. Patient #3: Cine MRI in a 3-chamber view using steady-state free precession (left) and delayed enhancement (right). Note the abnormal thickness of the usually thin left ventricular apex and the abnormal filling within the mid-right ventricular chamber. There is a bright white rim of enhancement lining both the left and right ventricules (arrows) which is suggestive of fibrosis.
Abbreviations: LV = left ventricle, RV = right ventricle, LA = left atrium.

TABLE 1
Summary of patient CMR characteristics

Symptomatic	Gender	Age	Right ventricle	Left ventricle	Mitral Valve	Tricuspid Valve	Abnormal late gadolinium
Patient 1	Male	29	Abnormal apical thickening	Abnormal inferolateral and apical thickening, EF 60%	Adherence of posterior leaflet; severe regurgitation	Severe regurgitation	Focal, atypical DE of basal inferior wall
Patient 3	Male	32	Abnormal filling of mid to apical cavity	Mild hypertrophy with filling of apical cavity, EF 60%	Adherence of posterior leaflet with severe regurgitation	Severe regurgitation	Biventricular DE pattern lining the endocardium, consistent with fibrosis
Patient 5	Female	54	Unremarkable	Moderate dilatation, severe systolic dysfunction, EF 23%	Restricted posterior leaflet motion and moderate regurgitation	Moderate regurgitation	Subendocardial thin rind of DE in a diffuse distribution
Asymptomatic							
Patient 2	Male	47	Unremarkable	EF 64%	Thickening and adherence of posterior leaflet with moderate regurgitation	Mild regurgitation	None
Patient 4	Female	70	Unremarkable	EF 55%	No thickening or regurgitation	No thickening or regurgitation	Atypical intermediate signal intensity in a patchy pattern
Patient 6	Male	35	Unremarkable	EF 67%	No thickening or regurgitation	Mild regurgitation	None
Patient 7	Male	81	Unremarkable	EF 57%	Thickening and adherence of posterior leaflet with mild regurgitation	Mild regurgitation	None

Conclusion: In addition to structural information regarding the cardiac chambers and valves, CMR offers the capability of tissue differentiation, e.g., thrombus versus fibosis and the ability to assess for restrictive physiology. The most common valvular abnormality involves adherence and thickening the posterior leaflet of the mitral valve. Restrictive physiology appears to be associated with extensive endocardial fibrosis as demonstrated by DE, and the most symptomatic patients appear to have pathology of multiple valves and fibrosis involving both ventricles. In our experience, which is the largest case series described to date, we conclude that CMR is able to comprehensively characterize the extent of cardiac involvement in patients with hypereosinophilia.

629. THE RELATIVE VALUE OF CARDIAC MAGNETIC RESONANCE AND ECHOCARDIOGRAPHY FOR DIAGNOSING MYXOMA IN PATIENTS WITH CARNEY COMPLEX

W. Patricia Bandettini, MD, Andrew C. McUsic, Douglas R. Rosing, MD, Constantine A. Stratakis, MD, Andrew E. Arai, MD. ***National Institutes of Health, Bethesda, MD, USA.***

Background: Echocardiography is currently the most commonly used imaging tool in screening for intracardiac mass. Cardiac magnetic resonance (CMR) has the ability to perform high resolution imaging with volumetric coverage and discriminate between different tissue types. Carney complex is a multiple neoplasia syndrome that includes recurrent cardiac myxoma as one of its main manifestations.

Objective: The purpose of this study was to assess the additional benefit of performing CMR in conjunction with echocardiography as a screening tool in a patient group that has a known predisposition to developing cardiac myxoma.

Methods: Twenty-six patients diagnosed with Carney complex were imaged by both echocardiogram and CMR. The patients were part of an ongoing study defining the

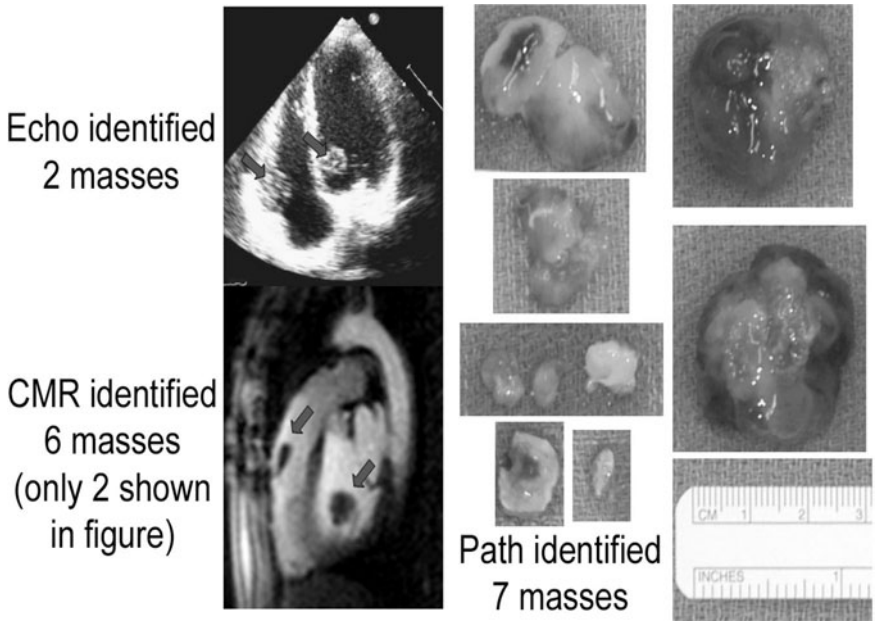

FIG. 1.

genotype and clinical phenotype of this disorder. Echocardiography included standard long and short axis views with 2-D, M-Mode and Doppler techniques. CMR included cine techniques, T2-weighted imaging, first pass perfusion, and post-contrast delayed enhancement inversion recovery gradient echo methods.

Results: The mean age was 28 ± 12 years, and the imaged group included 11 males (15 females). Fifteen (58%) had a prior history of myxoma resection. On a per patient basis, CMR identified 12/26 patients as having at least one intracardiac mass, and echocardiography identified 6/26 patients as having at least one intracardiac mass. On a per mass basis, CMR identified 20 masses, and echocardiography identified 8 masses. Fig. 1 demonstrates the echocardiography, CMR, and surgical pathology findings of one patient. In this patient, echocardiography identified 2 masses, CMR identified 6 masses, and surgical pathology identified 7 masses. All 7 masses were myxoid stroma. In two patients, there were 2 mobile masses that were seen more clearly by echocardiography than by CMR. One mass identified by both techniques was proven to be a lipoma by CMR. The distribution of locations for all presumed myxomas was: 1 right atrial, 4 left atrial, 11 right ventricular, and 3 left ventricular. All presumed myxomas hypoenhanced with perfusion, but there were variable patterns of delayed enhancement (DE) (10 hypoenhanced, 4 hyperenhanced, 3 showed heterogenous/intermediate enhancement, and 3 were not seen by DE). Six patients were found to have small regions of DE within the left ventricle that were consistent with subclinical embolic events. One patient had a transmural myocardial infarction which was previously known; cardiac catheterization at the time of the myocardial infarction demonstrated normal epicardial coronary arteries, suggesting an embolic event as a possible etiology.

Conclusions: CMR more clearly identifies intracardiac masses and provides additional information not seen by echocardiography.

1. CMR is more sensitive than echocardiography in the identification of intracardiac masses, on both a per mass and a per patient basis.
2. In the Carney complex patients, myxomas presented in all four cardiac chambers; however, the right ventricle was the most common location which is in contrast to patients diagnosed with sporadic myxoma.
3. The DE patterns were quite variable. These findings differ from the textbook description of myxoma in that myxoma was previously thought to hypoenhance on DE. These mixed patterns may represent various stages of the myxoma or different underlying histology.
4. There was a higher incidence of subclinical infarctions in this population which is likely reflective of embolic phenomena.
5. Two masses that were characterized better by echocardiography were highly mobile, suggesting that the random, mobile nature of the masses may not be seen as well by averaged CMR imaging.

Although echocardiography is a good screening tool, CMR demonstrates superior sensitivity. This study represents the largest collection of Carney complex patients with myxoma characterized by CMR. Both echocardiography and CMR should be performed in all patients with a high suspicion of intracardiac mass.

630. INFARCT TRANSMURALITY AND THE PRESENCE OF MICROVASCULAR OBSTRUCTION BY CONTRAST ENHANCED CARDIAC MAGNETIC RESONANCE TO

PREDICT REGIONAL WALL MOTION RECOVERY AFTER MYOCARDIAL INFARCTION

Jose T. Ortiz, MD, Daniel C. Lee, MD, Preeti Kansal, MD, Chiara Bucciarelli-Ducci, MD, Paula Tejedor, MD, Edwin Wu, MD. ***Northwestern University, Chicago, IL, USA.***

Background: Contrast-enhanced cardiac magnetic resonance (CMR) has been shown to predict recovery of left ventricular (LV) function after myocardial infarction. The relative contribution of microvascular obstruction (MO) in addition to infarct transmurality is unknown. Accordingly, we performed a segmental analysis in patients with an acute ST-segment elevation myocardial infarction (STEMI) to study the ability of infarct transmural extent and microvascular obstruction to independently predict segmental wall motion recovery.

*Methods:*A standard contrast-enhanced CMR was performed within 1 week in 85 patients after their first STEMI and repeated at a mean of 6 ± 4 months. Initial and follow-up infarct transmural extent were separately assessed using a 5-grade scale on a 17-segment model as follows: 0 = no hyperenhancement (HE); 1 = 1–25% transmural HE; 2 = 26–50% transmural HE; 3 = 51–75% transmural HE; 4 = 76–100% transmural HE of total wall thickness. Similarly, segmental wall motion was evaluated in a 5-grade scale: 0 = normal; 1 = mild to moderate hypokinesis; 2 = severe hypokinesis; 3 = akinesis; 4 = dyskinesis. Additionally, those segments with areas of hypoenhancement on delayed contrast-enhancement images were labeled as having microvascular obstruction.

Results: A total of 1496 segments were analyzed, of which 610 were dysfunctional at baseline. Increasing infarct transmurality resulted in an increasing percentage of dysfunctional segments: HE = 0, 14.9%; HE = 1, 65.5%; HE = 2, 84.9%; HE = 3, 100%; and HE = 4, 100%, as well as a decrease in the likelihood of recovery of wall function at follow-up ($p < 0.0001$ for trend) (Fig. 1). Microvascular obstruction was observed in 91 segments on the initial study with HE scores ranging from 2 to 4 with a majority of the segments (72%) occurring with transmural infarcts.

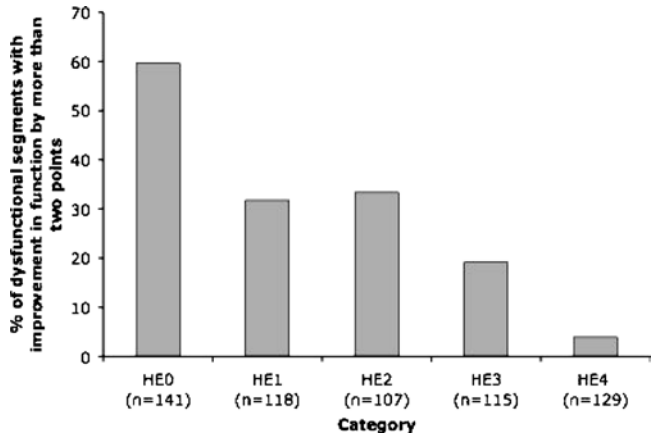

FIG. 1.

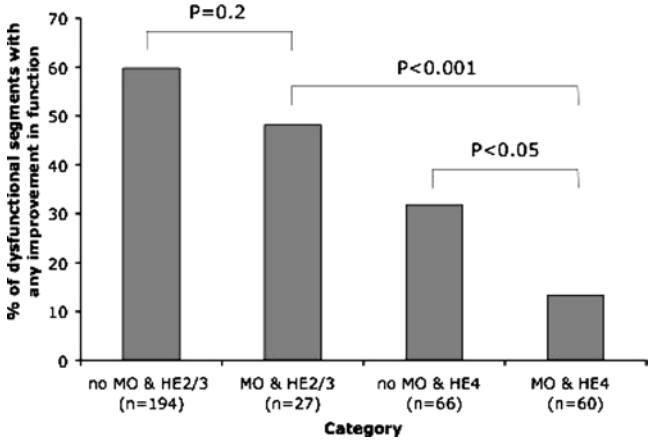

FIG. 2.

When evaluating only segments with microvascular obstruction, the presence of microvascular obstruction was associated with a reduced likelihood of recovery in function at follow-up among segments with HE = 2 or 3, and reached statistical significance among those segments with HE = 4 ($p < 0.05$) (Fig. 2).

Conclusions: We confirmed the importance of preserved myocardial viability as the strongest predictor of segmental function recovery. The presence of microvascular obstruction further decreases the likelihood of functional recovery independent of the infarct transmural extent. The presence of microvascular obstruction confers an ominous prognosis for recovery of function in segments with transmural infarction.

631. ACCURACY AND IMPORTANCE OF PHASE CONTRAST VELOCITY MAPPING FOR PULMONARY BLOOD FLOWS IN BRANCH PULMONARY ARTERIES WITH AND WITHOUT STENOSIS IN THE PRESENCE OF PULMONARY REGURGITATION: COMPARISON WITH NUCLEAR MEDICINE

Matthew A. Harris, MD, Timothy Y. Liu, BA, Matthew J. Gillespie, MD, Paul M. Weinberg, MD, Mark A. Fogel, MD. ***The Children's Hospital of Philadelphia, Philadelphia, PA, USA.***

Introduction: Postoperative pts with conotruncal anomalies often have residual stenosis of the pulmonary arteries which may require intervention. Nuclear medicine pulmonary flow studies are commonly used to assess the net pulmonary blood flows to each lung. Knowledge of the net pulmonary blood flow may not reveal the significance of branch pulmonary artery stenosis in the face of elevated pulmonary vascular resistance in the contralateral lung.

Purpose: To confirm the accuracy of Phase-Contrast Magnetic Resonance Imaging for the quantification of net pulmonary blood flow and to use this technique for the identification of elevated vascular resistance in the contralateral lung of patients with unilateral pulmonary artery stenosis.

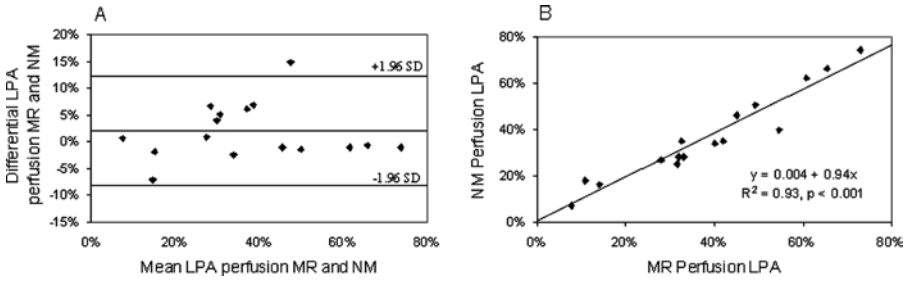

Methods: We retrospectively reviewed 16 consecutive post-operative conotruncal anomalies pts (median age 10.5 years, range 1.5–33.4 years), between 11/03 through 9/06 who underwent both nuclear medicine and phase-contrast MRI for the assessment of branch pulmonary artery blood flows. Both studies were performed within 2 years of each other without any catheter or surgical intervention occurring in the interim. All pts had pulmonary regurgitation identified in one of the branch pulmonary arteries. Six of the 16 patients had catheterization data available for review.

Results: There was a strong correlation between the net pulmonary blood flows measured by both nuclear medicine and phase-contrast MRI ($R = 0.93$, $p < 0.001$), as demonstrated by Bland-Altman (A) and Pearson Correlation plots (B). Phase-contrast MRI measurements of the sum of the net flows of each branch pulmonary artery correlated strongly with the net flow measured in the main pulmonary artery ($R = 0.88$, $p < 0.001$) and the aorta ($R = 0.78$, $p < 0.001$). There were two pts with unilateral branch pulmonary artery stenosis, who had relatively small differences in their net pulmonary blood flows ($> 33\%$ to the stenotic pulmonary artery), with $> 80\%$ of the total regurgitant volume observed in the non-stenotic pulmonary artery. At catheterization, using a combination of hemodynamic catheter data and nuclear medicine differential net pulmonary flow data, there was elevated vascular resistance in the contralateral lung.

Conclusions: Phase-Contrast Magnetic Resonance Imaging accurately measures the net branch pulmonary artery blood flow in patients with pulmonary regurgitation without the use of ionizing radiation. This method identifies elevated vascular resistance of the contralateral lung in patients with unilateral pulmonary artery stenosis.

632. FEASIBILITY OF MRI TO QUANTIFY BLOOD FLOW RESERVE IN LOWER EXTREMITIES

Hosakote M. Nagaraj,[1] Amol Pednekar,[2] Cecilia Corros,[1] Himanshu Gupta,[1] Steven G. Lloyd.[1] ***[1]University of Birmingham Alabama, Birmingham, AL, USA, [2]Phillips Medical Systems North America, Bothell, WA, USA.***

Introduction: Blood flow in exercising skeletal muscle is a highly integrated process involving arteriolar dilatation, capillary permeability, various vasodilating metabolites, mechanical factors and functional sympatholysis (1, 2). Evaluating the perfusion reserve is different from other modalities such as absolute flow measurements because it circumvents variability due to baseline flow and inter-individual anatomic variations. Although various techniques have been used to evaluate the severity and significance of peripheral artery disease (PAD), systematic estimation of the flow reserve is not routinely done. A reliable and easy quantification of the flow reserve would be of immense practical importance in the management of patients with PAD. The exercise induced flow reserve in the abdominal aorta as measured by Phase Contrast MRI (PC-MRI) has been demonstrated (3). But the flow at this location is remote from the site of stenosis in the lower extremities in patients with PAD. Thus, a method to assess the exercise induced flow reserve at the more distal site would be preferable.

Purpose: Here, we propose a system that uses PC-MRI to estimate the exercise induced blood flow reserve in the lower-extremity.

Methods: PCMRI was done on 5 normal volunteers to assess the blood flow in the superficial femoral artery (SFA) in legs at mid thigh level. An ECG-gated cine PC-MRI sequence was used (QFlow; segmented k-space gradient echo sequence with 7 lines per segment; VENC 100 cm/s, matrix 192×96; field of view 45 cm; 10 mm slice thickness; TR 3.8 ms, TE 1.8 ms, Total image acquisition time 25 s) on a 3 Tesla MR scanner (Intera, Philips Medical Systems). A specially designed, MRI compatible ergometer to allow resistive plantar flexion of the foot was positioned inside the bore of the MR unit. The subjects performed unilateral plantar flexion for 4 minutes with a rate of 40/min. The mechanical power was set to 0.5 watts. This was followed by repeat MR Imaging immediately and after 3 minutes of recovery. Following semiautomatic contour detection, peak flow velocity, average blood flow and flow reserve were analyzed and presented as mean with standard deviation. The mean flow reserve calculated as (post exercise flow-pre-exercise flow)/ pre-exercise flow).

Results: Fig. A demonstrates an example of the peak velocity signals in the exercising leg SFA at baseline, post-exercise and after 3 minutes of recovery. Absolute blood flow in exercising leg SFA at different stages of the experiment in individual volunteers is summarized in the Fig. B. The mean blood flow in the exercising leg SFA ($n = 5$) at pre-exercise, immediately post-exercise and 3 minutes after recovery period was 93 ± 51.1 mL/min, 209.7 ± 43.8 mL/min and 107.5 ± 42.8 mL/min

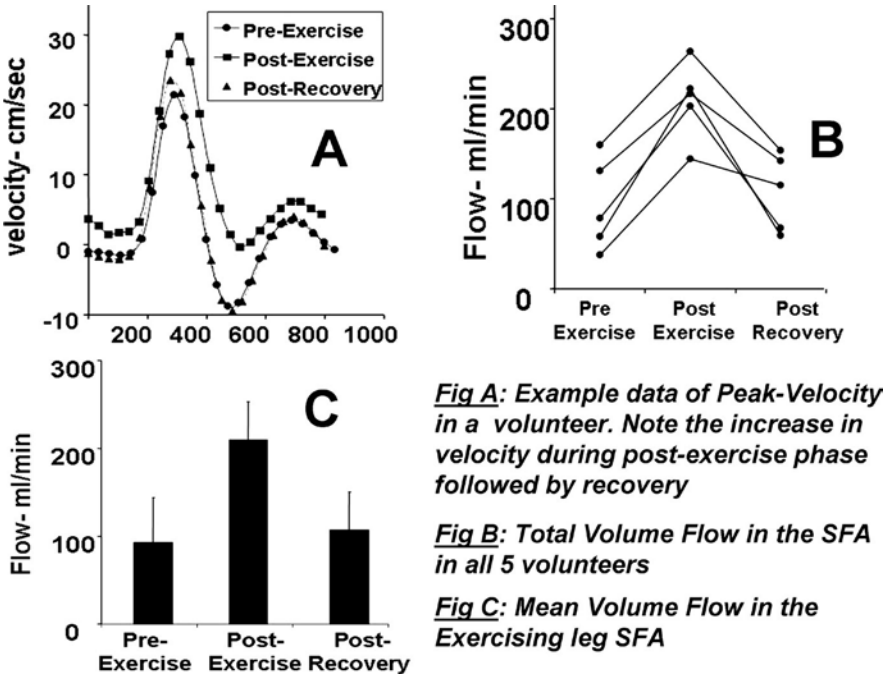

Fig A: Example data of Peak-Velocity in a volunteer. Note the increase in velocity during post-exercise phase followed by recovery

Fig B: Total Volume Flow in the SFA in all 5 volunteers

Fig C: Mean Volume Flow in the Exercising leg SFA

respectively as shown in Fig C. The mean flow reserve was 170 ± 109%.

Conclusions: Regional blood flow in the SFA is increased with calf exercise during unilateral plantar flexion at submaximal levels of exercise and returns to the baseline after a brief recovery. This technique of using PC-MRI for quantification of exercise induced flow reserve may be useful for the study of patients with PAD.

REFERENCES

1. Dinenno FA, et al. J Physiol 2003.
2. Rosenmeier JB, et al. Physiol 558:351–36.
3. Pederson EM, et al. Mag Res Imag 17:489–494.

633. CMR MARKERS FOR FOCAL AND GLOBAL INFLAMMATION IN ACUTE MYOCARDITIS ARE RELATED TO PATIENT AGE AND LEFT VENTRICULAR FUNCTION

Myra S. Cocker, BSc,[1] Hassan Abdel-Aty, MD,[2] Matthias G. Friedrich.[1] [1] *Stephenson CMR Centre, University of Calgary, Calgary, AB, Canada,* [2] *Franz-Volhard-Klinik, Berlin, Germany.*

Background: Cardiovascular magnetic resonance (CMR) allows differentiation between focal and global myocardial inflammation. Focal inflammation has been observed in myocarditis, yet its relationship to LV function and patient characteristics is not well defined.

Methods: We studied 61 patients (40 males, age range 43 ± 15 years) with CMR evidence for acute myocarditis, using a 1.5 T MRI system (Avanto, Siemens Medical Solutions, Erlangen, Germany). Patients were included if they met at least two of the following: presence of non-subendocardial late enhancement (LE) (indicating irreversible injury); elevated global early enhancement (EE) reflecting hyperemia; elevated T2 signal (indicating edema). Patients were divided based on the presence or absence of high focal T2 signal.

Left ventricular (LV) function was assessed using standard methods. Myocardial edema was imaged with a T2-weighted STIR sequence. Free-breathing T1-weighted spin echo images were acquired before and early (over 4 minutes) after administration of 0.1ml/kgBW Gd-DTPA. Irreversible injury was demonstrated using an inversion-recovery prepared gradient echo sequence 10 minutes after Gd-DTPA infusion. As a marker for tissue inflammation, normalized contrast early enhancement (EE) was quantified. LV volumes were measured using standard sequences. The presence of focal edema was assessed qualitatively.

Results: Patients in the group with focal T2 were younger (40 ± 15 years vs. 47 ± 15 years, $p < 0.05$). Left ventricular parameters differed significantly between patients with or without focal T2. In patients with focal T2, end-systolic volume index (0.39 vs. 0.59, $p < 0.05$) was lower, and ejection fraction was higher (59 ± 15% vs. 49 ± 18%, $p < 0.05$). There were no statistically significant differences between groups regarding stroke volume (96 vs. 81 mL $p = 0.07$) and end-diastolic volume index (0.96 vs. 1.05, $p = 0.5$). EE was significantly lower in patients with high focal T2 signal (5.80 vs. 8.52, $p < 0.01$), while global T2 did not differ between patients (1.94 vs. 2.00, $p = 0.8$).

Conclusions: Whereas global inflammation as defined by elevated EE was associated with decreased left ventricular function, patients with focal T2 lesions were more likely to have

a higher ejection fraction. Furthermore, CMR markers of focal tissue inflammation were associated with age. This may reflect possible age-dependent differences in host-immune response to myocarditis.

634. NON CONTRAST ENHANCED MR ANGIOGRAPHY OF CHEST WITH 3D STEADY STATE FREE PRECESSION: INITIAL EXPERIENCE

Mayil S. Krishnam,[1] Roya Saleh, Sr,[1] Lien Tran,[1] Vibhas Despande,[2] Paul Finn,[1] Stefan Ruehm.[1] [1] *UCLA, Los Angeles, CA, USA,* [2] *Siemens Medical Solution, Los Angeles, CA, USA.*

Introduction: Contrast-enhanced MR angiography (CEMRA) is increasingly used to evaluate great vessels and supra aortic arteries. Recently, a three-dimensional navigator gated free breathing selective steady-state free precession (SSFP) sequence has been proposed to display heart and great vessels without contrast administration. The SSFP sequence generates inherent high contrast between blood pool and background tissue in the body due to a high T2/T1 ratio.

Purpose: To assess the feasibility and diagnostic value of non contrast 3D SSFP MR Angiography in the morphological assessment of the heart, coronary arteries, aorta and pulmonary arteries and to compare the results with CEMRA.

Methods: Forty consecutive outpatients referred for cardiovascular MR for various indications including complex congenital heart disease have been studied with a 1.5 T MR scanner. Protocols include non selective free breathing respiratory gated 3D SSFP imaging of the whole chest (TR/TE = 2.3 ms/1.0 ms, flip angle = 90, bandwidth 980 Hz/pix, FOV 400 mm × 400 mm, matrix 320 × 320, slice thickness 3 mm interpolated to 1.5 mm, partitions 88–128, T2 preparation time 40 ms, respiratory gating widow 4 mm, acquisition time 7–15 min) and CEMRA. Two radiologists evaluated both datasets for image quality, visibility and motion artifacts in the heart and 14 vascular segments per patient including the coronary arteries, pulmonary arteries, aorta, and branch arteries of the aortic arch. Stenosis and aneurysm of aorta, main pulmonary arteries and supra aortic arteries were assessed using a 0–4 point score grading system The origin and proximal course of coronary arteries were also evaluated. Intravascular signal-to-noise ratio (SNR) values were determined for 3D SSFP and CEMRA.

Results: The overall image quality and intravascular SNR values of SSFP were comparable to CEMRA ($p > 0.05$). The overall visibility of heart, coronary arteries and extra cardiac great arteries was significantly higher on 3D SSFP compared to CEMRA ($p < 0.05$). Three dimensional SSFP was less prone to motion artifacts compared with CEMRA ($p < 0.05$). Stenosis and aneurysm of the aorta and pulmonary arteries were reliably detected on both modalities with good interobserver agreement (Kappa 0.8) with 100% sensitivity and specificity for SSFP. The anatomy of the coronary arteries was confidently diagnosed in all subjects by 3D SSFP. Supraaortic arteries were better evaluated with CEMRA than SSFP. Two false positive stenosis in the left subclavian artery were seen on SSFP.

Conclusions: Free breathing non contrast 3D MR angiography of chest with SSFP is feasible in clinical patients, and it provides reliable diagnostic information of the aorta and pulmonary arteries. Morphological assessment of the complex congenital heart disease and proximal coronary arteries are better evaluated with 3D SSFP than CEMRA. In addition, 3D SSFP MRA chest can be performed in patients with limited breath-holding capabilities and contraindication to gadolinum.

635. GENDER DIFFERENCES IN THE EXTENT OF IRREVERSIBLE INJURY IN ACUTE MYOCARDITIS

Myra S. Cocker, BSc,[1] Hassan Abdel-Aty, MD,[2] Jordin D. Green, PhD,[3] Matthias G. Friedrich, MD.[1] [1] *University of Calgary, Calgary, AB, Canada,* [2] *Franz-Volhard-Klinik, Berlin, Germany,* [3] *Siemens Medical Solutions, Calgary, AB, Canada.*

Background: Cardiovascular magnetic resonance (CMR) allows visualization of irreversible injury in acute myocarditis. The relationship between irreversible injury and patient characteristics is poorly understood.

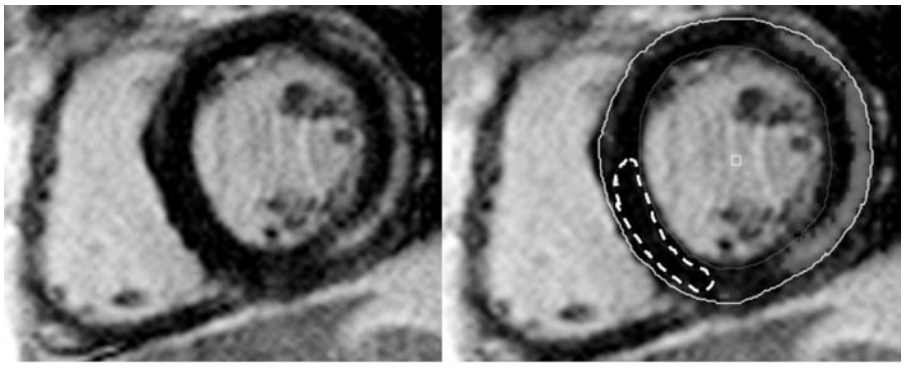

FIG. 1. Automated detection of lateral wall subepicardial late enhancement. 21% of the myocardium is irreversibly injured (Red overlay). Healthy myocardium is identified by the region within the dashed line.

*Methods:*Using a 1.5 T MRI system (Avanto, Siemens Medical Solutions, Erlangen, Germany), we assessed 44 patients (25 males, age range 41 ± 15 years) with CMR evidence for acute myocarditis. Left ventricular (LV) function was quantitatively assessed using standard methods. LE was quantitatively assessed in inversion-recovery gradient echo images (short axis view, complete LV coverage) 10 minutes after Gd-DTPA infusion. Basal slices with less than 75% of myocardium and apical slices with poor image quality were excluded. Automated computer threshold detection was set at 5 standard deviations above the mean of healthy myocardium to identify fibrosis, using non-enhancing myocardium as reference areas.

Results: Men were found to have a statistically larger absolute (8.5 ± 7.0 g vs. 3.5 ± 2.6 g $p = 0.001$) and relative (13.3 ± 8.6 vs. 8.4 ± 4.3% of total LV mass, $p = 0.048$) extent of irreversible injury.

Conclusions: Our results indicate that irreversible injury in myocarditis is more extensive in men, than in women. These gender-dependent differences may provide insight into the pathophysiology of acute myocarditis.

636. EVALUATION OF DIASTOLIC FUNCTION WITH VOLUMETRIC ANALYSIS AND MITRAL INFLOW VELOCITIES FOLLOWING ACUTE MYOCARDIAL INFARCTION

Michael A. Morse, Jose T. Ortiz, MD, Daniel C. Lee, MD, Preeti Kansal, MD, Edwin Wu, MD. ***Northwestern University, Chicago, IL, USA.***

Background: Volume-time-curves (VTC) can be used to evaluate left ventricular compliance. Patients with chronic diastolic dysfunction, when compared to healthy patients, have prolonged left ventricular time to peak filling rate (TPFR) and lower peak filling rates (PFR). Mitral inflow velocity patterns and E wave deceleration times can also be used to evaluate diastolic dysfunction.

We hypothesized that patients with large myocardial infarctions should develop more severe diastolic dysfunction as measured by VTC and mitral inflow velocities. The aim of this study was to compare these two modalities of evaluating diastolic dysfunction and how they relate to acute myocardial infarct size.

Methods: Forty-two subjects underwent CMR within 1 week of acute ST-segment elevation myocardial infarction (STEMI). Standard cine and delayed contrast-enhanced viability images along with a phase-contrast mitral inflow velocity image were obtained. A 3-dimensional Cardiac Image Modeling (CIM) software (Auckland, New Zealand) was applied to the short and long axis cine images to construct a representative 3-dimensional volume time curve (VTC). The first derivative of the VTC was then calculated to assess left ventricular TPFR and PFR. The PFR was then corrected by the end diastolic volume (PFR/EDV) for each subject. Phase-contrast velocity time curves (PVTC) were generated using diastolic mitral inflow velocity data. The deceleration time (DT) was extrapolated by measuring the time interval from the diastolic E wave peak to the baseline.

Results: CMR was performed an average of 2.7 ± 1.4 days (range 0 to 7 days) status post acute STEMI. Mean left ventricular infarct size ranged from 23.5 ± 18.4 grams (range 2.9 to 115.0 grams), which corresponded to a left ventricular infarct percentage of 19.6 ± 13.0% (range 2.9 to 63.3%). Both DT ($r = -0.52$, $p < 0.001$) and EF ($r = -0.84$, $p < 0.001$) were inversely correlated to infarct size. Additionally, volumetric analysis found a significant, although weak, correlation between infarct size and PFR/EDV ($r = -0.40$, $p < 0.01$) and TPFR ($r = -0.34$, $p < 0.05$). On multivariate analysis including age, heart rate, LV mass, EF, EDV and ESV, DT was the only independent predictor of infarct size. However, volumetric analysis for TPFR and PFR were not univariate predictors infarct size.

Conclusions: Infarct size correlated strongly with both markers of systolic, ejection fraction, diastolic dysfunction, and E-wave deceleration time. Although volumetric analysis evaluating TPFR and PFR were independently related to infarct size, their relationships were not as concrete. These subjects were also found to have lower PFR, but in contrast to chronic diastolic dysfunction subjects, a shorter TPFR with larger acute myocardial injury. In summary, volume time curve analysis does not appear to be as reliable and accurate predictor of acute myocardial infarct size when compared to mitral inflow phase-contrast velocity time curves and ejection fraction, and there may be other factors that affect TPFR such as left ventricular, myocardial stunning, and adrenergic tone that can modulate the effect of infarct size on diastolic function.

637. RELATION BETWEEN LEFT ATRIAL VOLUMES, RIGHT VENTRICLE VOLUMES AND REGURGITANT VOLUME IN MITRAL REGURGITATION BY CINE MRI

Cecilia Corros, MD, Himanshu Gupta, MD, Louis Dell'Italia, MD, Nagaraj Hosakote, MD, Steven G. Lloyd, MD. ***University of Birmingham Alabama, Birmingham, AL, USA.***

Introduction: Reliable diagnosis and quantification of mitral regurgitation are important for patient management and for optimizing the time for valve surgery. Regurgitation results in volume overload of the left atrium (LA) followed by left ventricle (LV) and LA dilation with further progressive mitral regurgitation. Thus, LV and LA chamber sizes have been used in assessing the severity of mitral regurgitation (1).

Though studies have shown a relation between severity of mitral regurgitation and right ventricle size using cineventriculography (2) to our knowledge the relation between LA and RV volumes has not been investigated before.

Purpose: The aim of our study is to evaluate the relations between regurgitant volume, LA volume and RV volume

using CMR in patients with mitral regurgitation due to valve prolapse.

Methods: Thirty-one CMR studies were performed in 26 patients with mitral regurgitation secondary to mitral valve prolapse. Patients with greater than mild regurgitant of other valves were excluded. CMR was performed with a 1.5T scanner (GE Healthcare) using phased array surface coil and prospective electrocardiographic triggering. LA contours, on the 2 and 4 chamber views, were manually drawn at end-ventricular systole which corresponds to the largest LA area. The inferior LA border was defined as the plane of the mitral annulus. The pulmonary veins and the LA appendage were excluded. The length was obtained from the middle of the plane of the mitral annulus to the posterior wall. Volumes were then computed using the Dodge area-length formula. Short axis SSFP MRI was performed and the contours of the LV and the RV at end-systole and end-diastole were manually drawn for each slice. LV and RV volumes were calculated by disc summation. Regurgitant volume was calculated through the difference between the LV stroke volume (SV = LV end-diastolic volume—LV end-systolic volume) and RV SV (RV end-diastolic volume—end-systolic volume). LA, LV and RV volumes were indexed by body surface index. Pulmonary arterial systolic pressure (PAP) was determined by Doppler echocardiography from the modified Bernoulli formula on the tricuspid regurgitant velocity.

Results: The mean age was 54 ± 10 years and 62% were men. Mean LA maximum volume was 76.7 ± 28 mL/m^2. Mean LV and RV end-diastolic volumes were 96.0 ± 21.9 mL/m^2 and 69.6 ± 15.5 mL/m^2, respectively. Mean LV and RV end-systolic volumes were 35.4 ± 10.7 mL/m^{2}and 32.7 ± 10.3 mL/m^2, respectively. LV ejection fraction was 64 ± 7% ,and RV ejection fraction was 54 ± 9%. PAP was 39 ± 7 mm Hg, which correspond with mild arterial pulmonary hypertension (PHT). A statistical correlation between LA volume and regurgitant volume was found ($R = 0.60$, $p = 0.039$), with no statistical correlation between LA volume and PAP ($p = 0.3$). LA volume and RV diastolic volume exhibited a statistical correlation ($R = 0.42$, $p = 0.02$), but there was not a statistical correlation between RV volume and regurgitant volume ($p = 0.9$) (Fig. 1).

Conclusions: LA maximal volumes exhibit a statistical correlation with regurgitant volume in patients with chronic mitral valve prolapse. RV and LA volumes are related but there was no relationship between RV volumes and regurgitant volume. These findings could reflect an increase in compliance in LA and pulmonary vasculature which could protect the RV from volume overload in this population without severe PHT.

REFERENCES

1. Burwash IG, Blackmore GL, Koilpillai CJ. Usefulness of left atrial and left ventricular chamber sizes as predictors of the severity of mitral regurgitation. Am J Cardiol 1992;70:774–9.
2. Unterberg R, Rommich P, Volker W, Mauser M, Karsch KR. Effect of volume load of the left ventricle in aortic and mitral insufficiency on the geometry and function of the right ventricle. Z Kardiol 1987;76:761–9.

638. EFFICACY OF COMPREHENSIVE CARDIAC MRI WITH WHOLE MRCA, STRESS PERFUSION AND LATE ENHANCEMENT IN KAWASAKI DISEASE

Yasuyuki Kobayashi, MD, Kentarou Asou, MD, Koutarou Murano, MD, Yukihisa Ogawa, MD, Kunihiro Yagihashi, MD, Yasuo Nakajima. ***St. Marianna University School of Medicine, Kawasaki, Kanagawa, Japan.***

Introduction: Kawasaki disease is an acute vasculitis of unknown etiology that predominantly occurs in young children and leads to the development of coronary artery aneurysms. These patients are also prone to the development of coronary artery stenosis, with subsequent myocardial ischemia and myocardial infarction. In the examination of young children, cardiac MRI has the great advantage of no radiation exposure, unlike CAG, CTCA, and RI studies.

Purpose: The objective here is to present the efficacy of complementary cardiac MRI with whole MRCA, stress/rest perfusion MRI and late enhancement in the assessment of Kawasaki disease.

Methods: The subjects were 12 patients with Kawasaki disease who underwent whole MRCA, pharmalogical stress/rest perfusion and late enhancement MRI. In 3 cases, follow-up MRI examination was performed. The MRI system used was a 1.5T MR imager (Achieva; Philips). IR balanced TFE sequence for perfusion during and without stress was below; TR/TE = 2.8/1.3 ms. And Inversion Recovery 3D-TFE sequence for late enhancement was acquired; TR/TE = 5.0/2.0 ms. Balanced TFE sequence for whole MRCA was below; TR/TE = 4.6/2.3 ms and 0.8 mm thickness. Adenosin was used for phamalogical stress.

Results:

1) In eight cases out of 12, coronary artery aneurysms were clearly observed on whole MRCA. In one case with huge coronary artery aneurysm, severe stenosis has appeared on follow-up MRI examination.
2) Early defect was observed in two cases with coronary aneurysm on stress perfusion MRI was observed again in same patients on follow-up MRI within six months.
3) In one case, late enhancement was observed, which indicated myocardial infarction.

Conclusions: Cardiac MRI is very useful for diagnosis and clinical course observation with Kawasaki disease. Whole MRCA, perfusion MRI and late enhancement are most effective to demonstrate coronary artery and myocardial abnormalities of Kawasaki diseases.

639. MRI TO EVALUATE LEFT ATRIAL REMODELING AFTER MITRAL VALVE REPAIR IN MITRAL REGURGITATION SECONDARY TO VALVE PROLAPSE

Cecilia Corros, MD, Louis Dell'Italia, MD, Himanshu Gupta, MD, David McGiffin, MD, Nagaraj Hosakote, MD,

Steven G. Lloyd, MD. ***University of Birmingham Alabama, Birmingham, AL, USA.***

Introduction: Mitral regurgitation results in volume overload of the left atrium (LA) and the left ventricle (LV) followed by LA and LV dilation with further progressive mitral regurgitation. Increased LA volume has been shown to be a predictor of adverse cardiovascular outcomes.

Improvement in LA volumes has been reported previously after mitral valve repair in patients with mitral regurgitation due to ischemic and dilated cardiomyopathy (1–2). However, this remodelling has not been investigated in patients with mitral regurgitation due to mitral valve prolapse.

Purpose: The aim of our study is to evaluate the LA volume before and 6 months after mitral valve repair surgery in patients with mitral regurgitation secondary to mitral valve prolapse and without other cardiac disease.

Methods: Fifteen patients with mitral regurgitation secondary to mitral valve prolapse were evaluated with cine MRI (CMRI) before and six months after the mitral valve repair surgery. CMRI was performed with a 1.5 T scanner (GE Healthcare) using a phased array surface coil and prospective electrocardiographic triggering. LA contours, on the 2 and 4 chamber views, were manually drawn at end-ventricular systole which corresponds to the largest LA area. The inferior LA border was defined as the plane of the mitral annulus. The pulmonary veins and the LA appendage were excluded. The length was obtained from the middle of the plane of the mitral annulus to the posterior wall. Volumes were then computed using the Dodge area-length formula. Short axis SSPF MRI was performed and the contours of the LV and the RV at end-systole and end-diastole were manually drawn for each slice. LV and RV volumes were calculated by disk summation. LA, LV and RV volumes were indexed by body surface index.

Results: The mean age was 54 ± 10 years and 67% were men. Mean LV diastolic volume before surgery was 100.1 ± 27.0 mL/m^2 and postsurgery was 73.3 ± 25.2 mL/m^2 ($p = 0.004$). LV ejection fraction before surgery was $64.9 \pm 5.6\%$ and after surgery was $58.8 \pm 12.0\%$ ($p = 0.04$). LA maximum volumes decreased significantly over time (from 78.3 ± 32.9 mL/m^2 to 36.0 ± 10.9 mL/m^2) (Fig. 1).

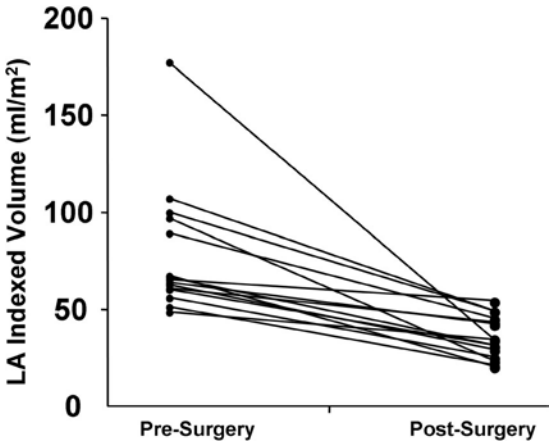

FIG. 1.

Conclusions: Significant improvement occurs in LA volume only six months after mitral valve repair in patients with valve prolapse. The degree of this beneficial remodelling is profound, with final volumes less than half the initial value.

REFERENCES

1. Bax JJ, Braun J, Somer ST, Klautz R, Holman ER, Versteegh M, et al. Restrictive annuloplasty and coronary revascularization in ischemic mitral regurgitation results in reverse left ventricular remodelling. Circulation 2004;110:103–8.
2. Westenberg JJM, Van der Geest RJ, Lamb HJ, Versteegh MIM, Braun J, Doornbos J, De Roos A, Van der Wall EE, et al. MRI to evaluate left atrial and ventricular reverse remodelling after restrictive mitral annuloplasty in dilated cardiomyopathy. Circulation 2005;112:437–42.

640. ANALYSIS OF LEFT VENTRICULAR MYOCARDIAL STRUCTURE USING DTMRI REVEALS SIGNIFICANT REGIONAL HETEROGENEITY

Daniel B. Ennis, PhD,[1] Emma T. Pineda,[2] Patrick A. Helm, PhD,[3] D. Craig Miller, MD,[1] Neil B. Ingels, PhD.[1]
[1]Stanford University, Stanford, CA, USA, [2]University of Notre Dame, South Bend, IN, USA, [3]University of Virginia, Charlottesville, VA, USA.

Introduction: Left ventricular myocardial function is increasingly recognized to be regionally heterogenous (1, 2). Recent work by Zwanenburg (3) illustrates that left ventricular prestretch induced by atrial systole is increased in the lateral wall relative to the septum and is correlated with increased total systolic shortening in the same wall. Such changes are likely due, in part, to differences in regional loading conditions (i.e., the septum is loaded by right and left ventricular pressures) which invokes regional differences in the Frank-Starling mechanism but may also be attributed to regional differences in tissue structural organization and material properties. Recent work suggests that the myocytes are coupled together into thin sheets that provide slippage planes for large myocardial deformations (5). These sheets help explain how myocytes that only shorten $\sim$<15% , resulting in an increased cell diameter by 8% can results in wall thickness changes of $\sim$30–50%. The tensor mode is useful for quantifying the degree to which myocytes are organized into sheet-like structures.

Purpose: To define the regional heterogeneity of myocardial structure in the normal canine heart.

Methods: All animal experiments were in accordance with national and institutional guidelines. Following a separate set of experiments five canine hearts were extracted and fixed with 5% formaldehyde solution prior to imaging and for long-term storage.

DTMRI data were analyzed using recently proposed orthogonal scalar metrics (invariants) of DTMRI tissue structure (4).

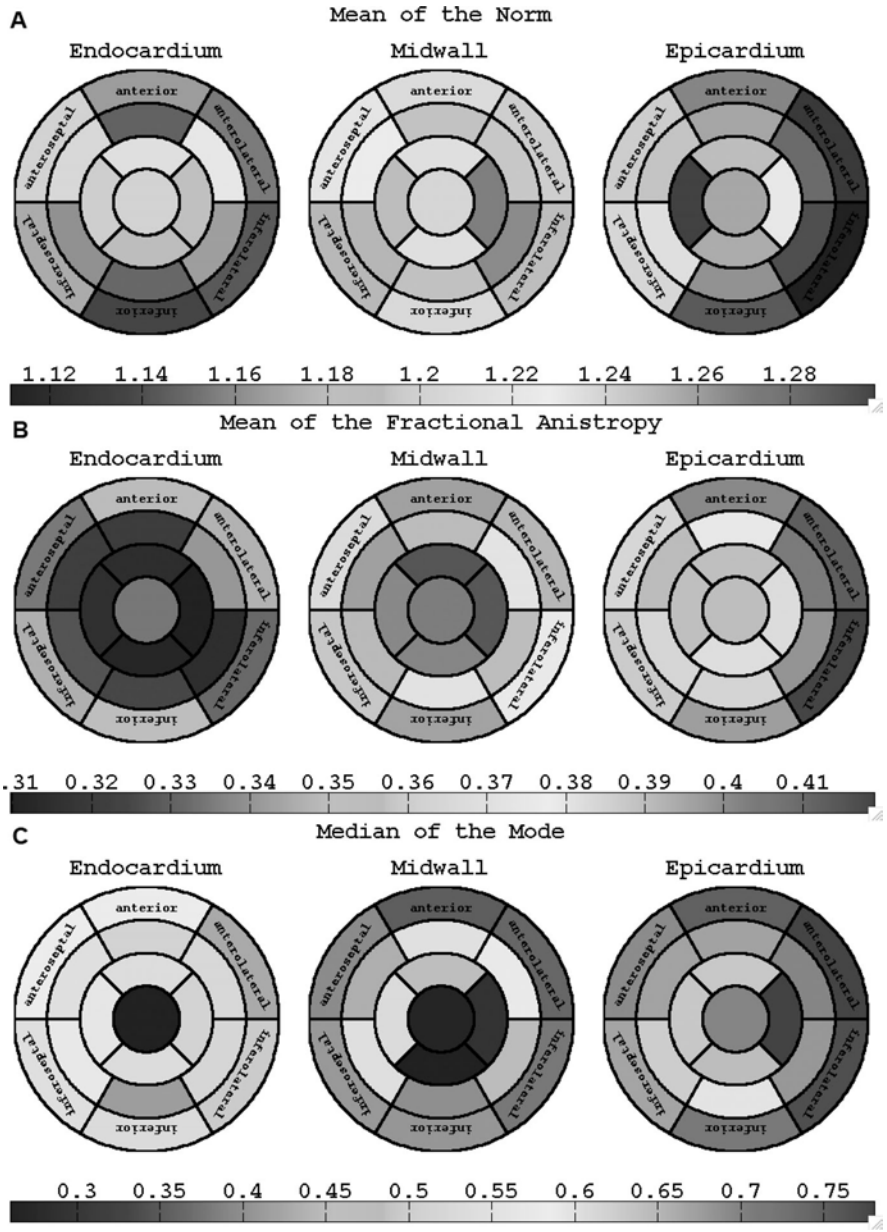

FIG. 1.

Orthogonal tensor invariants decompose the underlying tissue structure into the magnitude of isotropy (tensor norm), magnitude of anisotropy (fractional anisotropy, FA), and the mode of anisotropy (kind of tissue structure, e.g., planar, orthotropic, or linear anisotropy).

Right and left ventricular tissue and papillary-trabecular tissue was manually labeled. The left ventricle was isolated and segmented further for regional analysis. Automated analysis was then used to divide the left ventricle into 17 anatomical segments at epicardial, mid-myocardial, and endocardial wall depths for a total of 51 left ventricular regions, each containing thousands of pixels, for each of five hearts. Within each segment the mean for norm and FA and median for mode data were calculated and these values were averaged across the population. Bullseye plots (base-outer ring, apex-middle disc, septum on left) of the population mean were then generated (Figs. A–C).

Results: The tensor norm data (Fig. 1A) indicate a transmural trend with higher diffusivities found in the endocardium compared to the epicardium. This gradient, however, appears to be less in the septum indicating more uniform magnitudes of isotropic diffusion in the septum. The FA, a measure of structural organization, (Fig. 1B) similarly showed a transmural trend with lower and more uniform FA in the endocardium and higher FA in the epicardium, especially in regions near the basal-lateral wall. The tensor mode (Fig. 1C) data demonstrate a transmural trend of increasing mode from endocardium to epicardium. Mode

values near zero indicate orthotropic tissue structure (myocardial sheets) and mode values near one indicate linear anisotropy (fibrous structure without distinct sheets). Note that the apex appears the most sheet-like, a finding that needs to be confirmed histological.

Conclusions: Clear transmural, base to apex, and circumferential differences are evident in this analysis of myocardial tissue structure, confirming, that myocardial tissue structure is regionally heterogeneous.

REFERENCES

1. Moore CC, et al. Radiology 2000; 214:453–466.
2. Bogaert J, et al. Am J Physiol Heart Circ Physiol 2001; 280:H610–620.
3. Zwanenburg JJ, et al. Am J Physiol Heart Circ Physiol 2005; 288:H787–794.
4. Ennis DB, et al. Magn Reson Med 2006; 55:136–146.
5. LeGrice IJ. Circ Res 1995; 77:182.

641. SERIAL MEASUREMENTS OF INFARCT SIZE USING MAGNETIC RESONANCE IMAGING PREDICT RECOVERY OF VENTRICULAR FUNCTION

Cory M. Swingen,[1] Gilbert L. Raff, MD,[2] Ralph Gentry, RT,[2] Inder S. Anand, MD,[3] Michael Jerosch-Herold, PhD.[4] ***[1]University of Minnesota, Minneapolis, MN, USA, [2]William Beaumont Hospital, Royal Oak, MI, USA, [3]Division of Cardiology, VA Medical Center, Minneapolis, MN, USA, [4]Oregon Health and Sciences University, Portland, OR, USA.***

Purpose: We sought to test the hypothesis that the recovery of LV function is dependent on the change in infarct size (IE) measured with delayed contrast-enhanced MRI (ce-MRI) following myocardial infarct (MI) immediately after reperfusion.

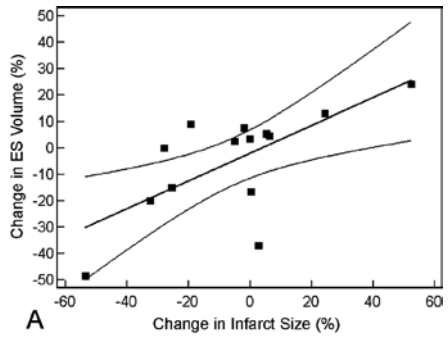

Methods: Fifteen patients underwent cine MRI and ce-MRI at an average of 17 hours and 3 months following an acute MI. Global function was assessed using a 3D MRI-based analysis of the LV and regional wall thickness, wall motion (WM) and wall thickening (WT) calculated. IE and TEI were correlated with global and regional parameters.

Results: At baseline, contractile defect size was significantly greater than IE ($45.2\,g \pm 8.9\,g$ vs. $33.3\,g \pm 7.4\,g$, $p = 0.004$) with no difference at 3 months ($p = 0.3$). Baseline end-systolic volume (ESV) and ejection fraction (EF) correlated with baseline IE ($r = 0.56$, $p = 0.04$ and $r = -0.69$, $p = 0.005$, respectively) and the change in LV mass at 3 months ($r = -0.52$, $p = 0.04$). Baseline IE correlated with regional function at 3 months (WM: $r = -0.65$, $p = 0.03$; WT: $r = -0.76$, $p = 0.006$). Changes in infarct size were associated with changes in EDV ($r = 0.50$, $p = 0.04$), ESV ($r = 0.68$, $p = 0.007$), EF ($r = -0.56$, $p = 0.05$) and WM ($r = -0.69$, $p = 0.03$) independent of baseline IE.

Conclusions: MRI can accurately quantify the recovery of contractile dysfunction in patients with recent reperfused MI. Infarct size change correlates with the recovery of LV function following revascularization therapy.

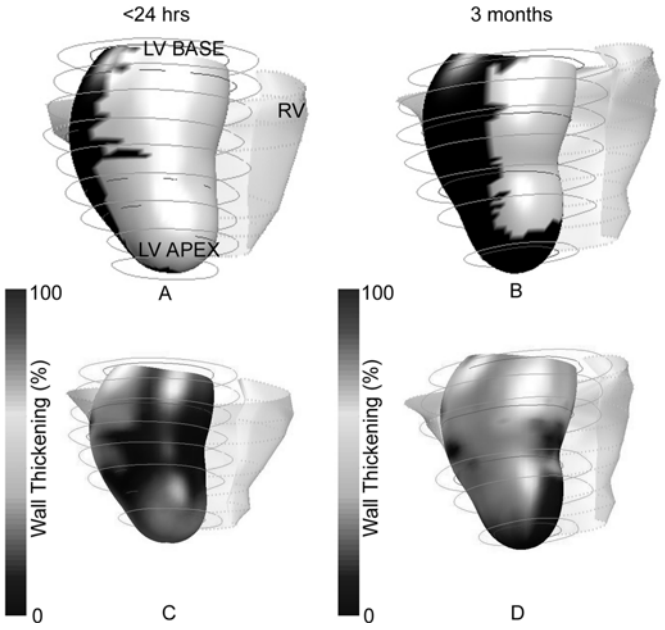

642. DOES MITRAL REGURGITATION CAUSE LEFT VENTRICULAR DYSSYNCHRONY?

Hosakote M. Nagaraj, MD,[1] Thomas S. Denney, Jr, PhD,[2] Steven G. Lloyd, MD, PhD,[1] Chichi Aban, PhD,[1] Cecilia Corros, MD,[1] Louis Dell'italia, MD,[1] Himanshu Gupta, MD.[1] ***[1]University of Birmingham Alabama, Birmingham, AL, USA, [2]Auburn University, Auburn, AL, USA.***

Introduction: Mitral regurgitation (MR) is a frequently present in patients of heart failure and results in worse clinical outcomes as compared to those without MR (1). MR promotes detrimental cardiac remodeling with worsening left ventricular (LV) dilatation, eccentric hypertrophy, and left atrial enlargement. In the presence of LV dyssynchrony, Cardiac resynchronization therapy (CRT) is known to decrease the severity of secondary MR and improve NYHA class, exercise capacity and quality of life. It is unknown if MR on its own contributes to LV dyssynchrony independent of LV dysfunction

Purpose: Here, we hypothesized that in patients with LV remodeling but preserved LV function, moderate to severe MR may cause LV dysynchrony.

Methods: Thirty-seven normal volunteers (n = 37) with no prior history of heart disease and 22 patients with moderate to severe MR (n = 22) were included into the study. Ischemia as a confounding factor was excluded by history in volunteers and by angiographic/nuclear stress testing in MR patients. MRI was performed on a 1.5 T MRI scanner optimized for cardiac application. ECG gated breath- hold steady state free precision technique and tagged MRI (SPAMM) were used to obtain standard (2 and 4 Chamber, Short Axis) views of the heart. The quantification of morphology and fnction was performed on a GE Advantage Workstation with Mass Medis version 2.0 software by highly experienced cardiologists with level 3 training. Time-to-peak-strain (TTPS) was computed for each participant using harmonic phase of tagged MRI images (HARP-analysis). The LV wall in each image was divided into four sectors, and in each timeframe, the median principal strain was computed in each sector over the basal, middle, and apical thirds of the LV. LV dyssynchrony was assessed by comparing the delay between TTPS of the four sectors at 3 different levels.by history in volunteers and by angiographic/nuclear stress testing in MR patients. MRI was performed on a 1.5 T MRI scanner optimised for cardiac application. ECG gated breath hold steady state free precision technique and tagged MRI (SPAMM) were used to obtain standard (2, and 4 chamber, short axis) views of the heart . The quantification of the morphology and function was performed on a GE Advantage Workstation with Mass Medis version 2.0 by highly experienced cardiologist with level 3 training.

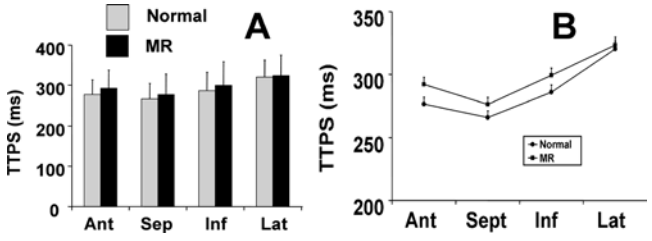

FIG. 1. A&B: Demonstrate a delay in the absolute time to peak strain (TTPS) in the MR group as compared to controls (p-NS). The difference range of the TTPS amongst the various quadrants and also medial-lateral & anterior-posterior quadrants in the two groups was not significant. This indicates absence of LV dyssynchrony in the MR group when compared to controls.

We used either the t-test or the nonparametric Wilcoxon test for comparing two independent samples. The difference between all the myocardial sectors of the 2 groups along with the range difference (lateral-septal and anterior-inferior) at three different locations namely apex, mid and base were analyzed using a generalized linear model for repeated measures via the PROC MIXED procedure of SAS.

Results: All the patients in the MR group had moderate to severe MR and their LV was significantly dilated as compared to controls and both the groups had normal LV ejection fraction. Thus, we excluded LV dysfunction as a confounding factor for dyssynchrony. The difference in the TTPS between various quadrants of the myocardium at corresponding levels was similar amongst the two groups (Fig. 1 A, B).

Conclusions: Moderate to severe MR with dilated LV but preserved function does not contribute to LV dyssynchrony. Therefore, CRT in the absence of LV dyssynchrony may not decrease the severity of MR.

643. MYOCARDIAL STRESS PERFUSION DYNAMIC SIGNAL EVALUATION: COMPARISON BETWEEN UPSLOPE AND FERMI MODEL

Yi Wang, DSc, Raphael Hazel, PhD, Bin Luo, MS, Marguerite Roth, RN, Jing Han, PhD, Nathaniel Reichek, MD.
St. Francis Hospital, Roslyn, NY, USA.

Introduction: Perfusion quantification can improve the diagnostic accuracy in ischemic disease. A simple approach to quantify myocardial perfusion uses dynamic signal (DS) upslope. It has been shown repeatedly that a decrease in upslope is associated with myocardial perfusion defects. However, upslope estimation is sensitive to artifacts. Model based deconvolution methods can also be used to derive absolute perfusion based on the relative intensity and timing of the DS segmental blood and myocardial signal.

Purpose: We applied both algorithms to the same first pass stress and rest perfusion images acquired from normal volunteers with the same endo- and epi-myocardial contours. Variations in regional estimates of flow reserve (FR) or flow reserve index (FRI), defined as the ratio of stress/rest upslope or absolute perfusion value respectively, were studied to see how each algorithm performs.

Methods: To ensure the normality of the data, strict exclusion criteria were used in volunteer recruitment, including exclusion of hypertension, diabetes, smoking, family history of cardiac disease, and EBCT coronary calcium score ≤ 20. Nine volunteers (ages: 20 to 69, 6 females) were enrolled after IRB approval. Using a saturation recovery TrueFISP technique, first pass perfusion studies under adenosine pharmacological stress

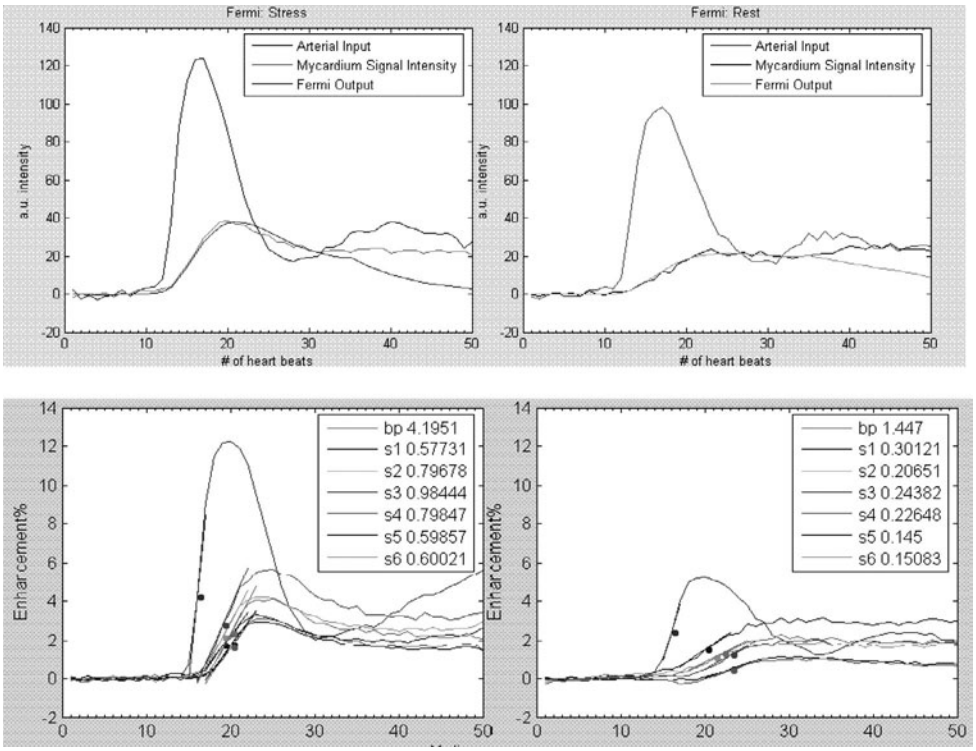

FIGS. 1 and 2.

and at rest were performed on a 1.5 T scanner. A voxel spatial resolution of $1.9 \times 2.8 \times 8$ mm^3 was achieved in 3 rotational long axis slices per heartbeat. Using MASS (Medis, Leiden, the Netherlands), the endo- and epi-myocardial contours were manually drawn on an image showing good myocardial contrast and then automatically propagated at each time point. The myocardium was divided into 6 equal segments. Mean signal intensities of all pixels in each myocardial segment at every time point were transferred to custom developed program that calculated upslope and absolute flow. Segmental upslope was calculated for each time point by taking signal intensity from neighboring time points using least square means. For the model based technique, to solve the deconvolution equation, a Fermi function was selected as the distribution of tracer residence times to search for the best fit of the DS curve for each myocardial sector, with blood as input and myocardial signal as output. The FR or FRI was determined as the ratio of stress to rest perfusion or upslope, respectively. Twenty-four out of total 162 sectors were excluded due to artifacts. Coefficient of variation (CV) was calculated as SD/mean $\times$ 100%.

Results: An example of a pair of DS and Fermi model produced fitting under stress (left) and at rest (right) of one sector are shown in Fig. 1. An example of DS and upslopes under stress (left) and at rest (right) of one slice are shown in Fig. 2. The mean, SD and CV of FR in 9 volunteers were 2.75, 1.11 and 40.21 for Fermi model while those of FRI were 1.43, 0.51 and 35.95 for upslope. The results of four-way ANOVA showed significant difference between Fermi and upslope methods adjusted by the subject, slice and sector ($p < 0.0001$). The association between Fermi and Upslope is significant adjusted by the subject, slice and sector using ANCOVA with partial $R^2 = 0.04$, $p = 0.0007$. The model-based methods showed similar CV and higher FR (than slope-based method) that is closer to reference methods such as PET and invasive Doppler flow wire.

Conclusions: Regional flow reserves (or index) vary with the algorithm chosen for perfusion evaluation. Results from the upslope algorithm showed mean flow reserve index values much lower than Fermi model based FR. Fermi model based FR results were with smaller CV and the mean is more consistent with normal adenosine perfusion in PET literature, suggesting it might be a more useful algorithm than upslope approaches.

644. MR EVALUATION OF CARDIAC AMYLOIDOSIS: LIKELIHOOD EVALUATION OF VARIOUS CRITERIA IN THE DIAGNOSIS

Sanjaya Viswamitra, MB, BS, Kedar Jambhekar, MD, David Quardebitty, RT, Behzad Molavi, MD. ***UAMS, Little Rock, AR, USA.***

Introduction: Amyloidosis, extra-cellular deposition of insoluble fibrillar proteinaceous material in various organs includes cardiac involvement. This is most common and clinically

significant with type AL primary amyloidosis associated with multiple myeloma or other monoclonal gammopathies. Cardiac injury due to amyloid deposition in the myocardium results in atrophy of adjacent myocardial fibers, coronary wall thickening and luminal narrowing, ventricular and atrial wall thickening, reduced ventricular wall compliance, impairment of diastolic filling, and eventual diastolic heart failure and death. The diagnosis of cardiac amyloidosis remains elusive. Cardiovascular MR (CMR) is a powerful tool in its diagnosis.

Purpose: We aim to describe various CMR imaging features that are seen in cardiac amyloidosis and evaluate the frequency with which these occur. We propose that this can be used as an algorithm in improving the confidence to diagnose cardiac amyloid.

Methods: Retrospective review of 36 patients with multiple myeloma were referred for the evaluation of cardiac amyloidosis at our institution between April 2005 and September 2006 was performed. A 3-point clinical grading scale (18 definite, 4 probable, 13 absent) was used to categorize patients suspected of cardiac amyloidosis. This was based on investigations which included myocardial biopsy (3), other organ biopsy (19), ECHO for diastolic dysfunction (16), significant EKG abnormalities (2).

All CMR studies were performed on either a 3T Trio or 1.5T Avanto (Siemens, Erlangen, Germany) MRI systems. Short axis and 4 chamber Tru-Fisp cine MRI was used for function analysis. Delayed hyperenhancement (DHE) images were obtained using a phase sensitive inversion recovery sequence (PSIR) after initially obtaining a time to inversion (TI) scout at approximately 10–15 minutes after injection of gadolinium intravenously. A 4 element phased array coil was used.

The CMR findings evaluated were a 3-point delayed hyperenhancement grading scale (definitely positive, probable and definitely no enhancement); diffuse/focal distribution; difficulty in finding an inversion time; presence of pleural and pericardial effusion; wall thickness; and abnormal ejection fraction.

Results: CMR categorization of amyloidosis in those 18 patients definitely thought to have amyloidosis clinically (true positive -TP and false positive -FP): 19 positive DHE exams have definite amyloidosis (15 TP, 4 FP); 4 DHE probable (1 TP 3 FP); 13 diffuse uptake 13 (11TP 2 FP), 8 focal (4 TP 4FP); 10 with difficulty in finding an inversion time (10 TP 0 FP); pleural effusions (11 TP 1 FP), pericardial effusion (11 TP 1 FP); 5 with septal wall thickening greater than 1.4 cm (3 TP 2 FP), 13 with ejection fraction less than 50% (6 TP 7 FP). The findings that had the highest likelihood of being positive for amyloid involvement of the heart was diffuse delayed hyperenhancement. Though less frequent, inability to get a good inversion time was also highlly predictive for cardiac amyloid. Almost all patients with amyloidosis had pleural and pericardial effusions. Increased wall thickness and decreased ejection fraction were not predictive for presence of cardiac amyloidosis.

Conclusions: Cardiac amyloidosis is a difficult diagnosis to make and one that currently has a poor prognosis. CMR can accurately make the diagnosis. The confidence in making the diagnosis is increased by difficulty in getting an inversion time and diffuse delayed hyperenhancement of the myocardium and the presence of pleural and pericardial effusions, even in the presence of normal ejection fraction and wall thickness.

645. ACUTE MYOCARDIAL INFARCTION: COMPARISON OF TWO IMAGING TECHNIQUES, 201TI SPECT AND CARDIAC MAGNETIC RESONANCE, IN DETERMINING INFARCT SIZE, MICROVASCULAR OBSTRUCTION AND LEFT VENTRICULAR VOLUMES AND FUNCTION

Bernard Noel,[1] Maurice Levy.[2] [1] *Hopital Laval, Ste-Foy, PQ, Canada,* [2] *Hopital European La Roseraie, Paris, France.*

Background: Thallium 201 (201TI) single photon emission computed tomography (SPECT) is widely used in the evaluation and quantification of myocardial necrosis and viability following acute myocardial infarction (MI). In the last years, cardiac magnetic resonance (CMR) gadolinium delayed enhancement (DE) has shown its ability to acutely measure infarct size as well as transmural extension of necrosis, which is a predictor of viability and functional recovery. We tested the hypothesis that CMR was superior to 201TI SPECT in necrosis detection and quantification of transmural extension of necrosis and microvascular obstruction. We also compared accuracy of myocardial gated SPECT and CMR to determine ventricular volumes and left ventricular function.

Methods: Cine-MRI, gadolinium first-pass (FP), inversion recovery DE-CMR and rest-distribution 201TI SPECT images were obtained within 7 days following a successfully reperfused first acute myocardial infarction. All images were analysed using a 17 segment myocardial model (3 short axis slices and 2 long axis). FP images were analysed to document microvascular obstruction. DE-CMR images were compared with uptake defect on redistribution 201TI SPECT images. Primary endpoints were the ability to define the presence of myocardial necrosis and its transmural extent. Secondary endpoints were the ability to measure LVEF and ventricular volumes, to detect regional contractility anomaly and microvascular obstruction.

Results: Forty-three consecutive patients (33 men, 10 women, mean age 58 $\pm$ 14 years) were included in the study and completed both procedures. Infarct territory was anterior in 23, inferior in 17 and lateral in the remaining 3. DE-CMR detected 100% of MI in the proper location (defined by the infarct related artery at angiography) while 201TI SPECT failed to show necrosis in 11 patients (6 inferiors (35%) and 5 anteriors (21%). CMR was superior to 201TI SPECT at detecting necrosis ($p < 0.01$). All infarcts missed by 201TI SPECT were of small size and contained in subendocardium. Ventricular diastolic and systolic volumes did not differ significantly between both techniques and

left ventricular ejection fraction demonstrated a good correlation ($r = 0.76$, $p < 0.01$) between CMR and gated SPECT.

Conclusions: CMR using gadolinium delayed enhancement is superior to 201TI SPECT in detecting myocardial necrosis when performed early after myocardial infarction. Small size subendocardial inferior infarcts are prone to be missed by 201TI SPECT. A good correlation exists between cine-MRI and SPECT tomogating in the determination of LV volumes and function.

646. MR DOPPLER OF HIGH-SPEED JETS THROUGH VALVULAR STENOSES

Adam B. Kerr, PhD,[1] Juan M. Santos, PhD,[1] Bob S. Hu, MD,[2] Daeho Lee,[1] John M. Pauly, PhD.[1] ***[1]Stanford University, Stanford, CA, USA, [2]Palo Alto Medical Foundation, Palo Alto, CA, USA.***

Introduction: Approximately 10% of patients with heart disease in the United States have valvular heart disease. It is important in assessment of these patients to quantify the intracardiac flow velocities. Doppler ultrasound is a noninvasive approach that provides this capabilitybut can be limited by the accessible geometry and by a poor acoustic window. MR Doppler (1–3) is an MRI-based approach analogous to Doppler ultrasound that provides real-time spatial and temporal resolution of velocity distribution along an interrogation cylinder. MR Doppler has the benefit of not being limited by acoustic windows or restrictive geometries, as well as the potential of being simply a part of an integrated comprehensive MRI examination of heart disease. However, MR Doppler imaging of high-speed jets is prone to significant image degradation. We present here a novel interleaved, echo-shifted readout for MR Doppler that is less sensitive to jets and is designed to minimize ghosting artifacts.

Methods: An assumption made in MR Doppler is that the velocity of flowing spins remains constant throughout the acquisition (typically 10–25 ms). However, this assumption is invalid for a high-speed stenotic jet that may accelerate from 1 to 4 m/s over 1 cm. Accordingly, we developed an interleaved readout scheme that reduces the acquisition period at the cost of requiring multiple interleaves.

Figure 1a shows the overlay of a two-interleaf bowtie (1) that form a partial acquisition of k_v-k_z (velocity-position) space. Figs. 1b, c show two overlays of possible gradient interleaf waveforms $G_z(t)$ that both trace out the trajectory of Fig. 1a. The pre-encoding waveform prefacing the train of bipolar lobes is calculated for each interleaf to provide the equal spacing in k_v as shown. Fig. 1c shows the echo-shifted variation where a deliberate delay is introduced following the pre-encoding lobe. The smoother temporal sampling of k_v reduces ghosting artifacts due to off-resonance and T_2^* decay, similar to echo-shifting in interleaved echo planar imaging (4).

Results: The MR Doppler sequence was implemented as part of a real-time system interfaced to a GE 1.5-T Signa scanner

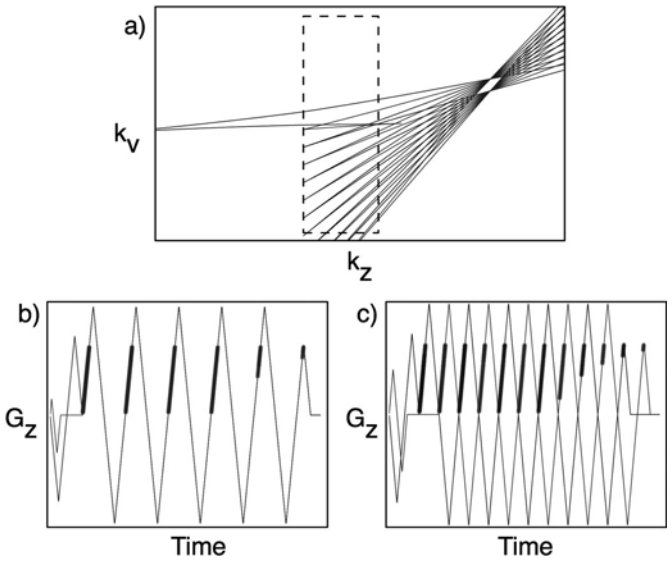

FIG. 1. a: Closeup of central k_v-k_z space as sampled by a two-interleaf trajectory. The dashed box represents the data used for reconstruction. b, c: Gradient waveforms for non- and echo-shifted interleaves overlaid on each other. The thick lines show the readout period that is used for reconstruction.

(40 mT/m, 150 T/m/s). Figure 2 illustrates that high-velocity jets (4 m/s) in a flow phantom at the nozzle of an area reducer are better resolved with the echo-shifted interleaved acquisition compared to a single acquisition with the same total readout duration at the expense of poorer temporal sampling

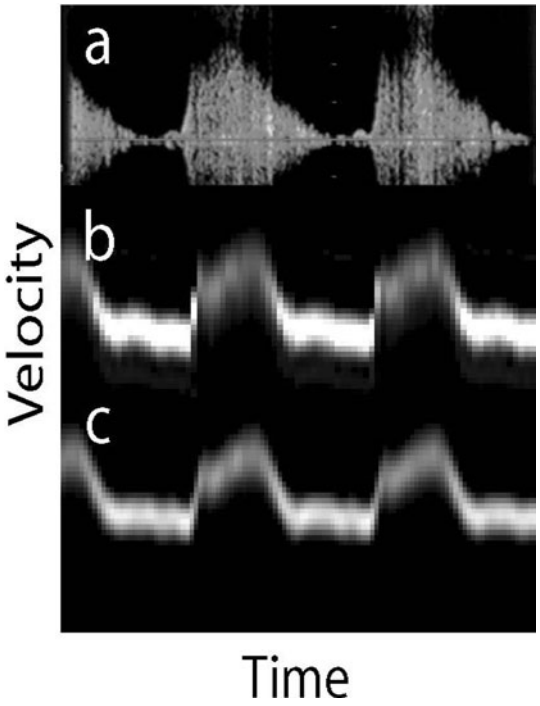

FIG. 2. Velocity-spectrum images from 4 m/s flow at the nozzle of a 3/8-inch to 1/8-inch diameter reducer using: (a) continuous wave Doppler ultrasound, (b) a single 12-ms acquisition and (c) a two-interleaf sequence with 6-ms readout duration. The TRs of the two sequences are 19 and 15 ms, respectively.

of the waveform. Note the absence of N/2 ghosts in the interleaved acquisition, even during periods of rapid flow acceleration.

Conclusions: The echo-shifted interleaved acquisition for MR Doppler provides greater immunity to artifacts from flow acceleration near jets, and has accurately imaged flow up to 4 m/s as validated by continuous-wave Doppler ultrasound. The reduced temporal sampling rate does not present any obvious difficulty in identifying the peak velocity.

REFERENCES

1. Irarrazabal P, et al. Magn Reson Med 1993;30:207–212.
2. MacGowan CK, et al. J Magn Reson Imag 2005;21:297–304.
3. DiCarlo JC, et al. Magn Reson Med 2005;54:645–655.
4. Butts K, et al. Magn Reson Med 1994;31:67–72.

647. MULTIPLE LONG AXIS ACQUISITIONS ARE HIGHLY CORRELATED WITH CORRECTED SHORT AXIS ACQUISITIONS FOR THE EVALUATION OF LV FUNCTIONAL PARAMETERS

Michael L. Ma,[1] Lucia K. C. Ma,[1] Andreas Kumar, MD,[1] Jordin D. Green, PhD,[2] Matthias G. Friedrich, MD.[1]
[1]Stephenson CMR Centre, University of Calgary, Calgary, AB, Canada, [2]Siemens Medical Solutions, Calgary, AB, Canada.

Introduction: Short axis stacks are considered the gold standard for quantifying LV volumes and function. Problems with defining the slice area in the most basal and most apical slices however limit its use, especially by introducing an interobserver variability. Quantification using a long axis may overcome this limitation. We compared interobserver variabilities of a short axis (SAX) approach compared to a multiple long axis approach (LAX).

Materials and Methods: We assessed 46 patients (29 male, 47 ± 18) referred for a functional evaluation on a 1.5 T system (Avanto, Siemens Medical Solutions). Standard SSFP cine sequences were used for all approaches, with a slice thickness of 8 mm and a 2 mm gap for the SAX. SAX was performed as multiple short axes across the entire left ventricle in an imaging plane perpendicular to the long axis of the LV. Basal slices were included using on long axis cross-reference. The LAX slices were performed using 6 slices rotating in 30 degree increments around the anatomical LV long axis.

Endocardial and epicardial contours were drawn for the LV at end systole and end diastole in each data set using a clinically validated software (cmr^{42}, Circle International, Calgary, Canada). Papillary muscles and trabeculations were included into LV mass for the SAX. Contours for LAX excluded trabeculations. The time needed to complete assessments was recorded.

End-systolic (ESV) and end-diastolic volume (EDV), stroke volume (SV), ejection fraction (EF), and LV mass were all assessed by two independent observers. Inter-observer variability was measured by calculating the correlation coefficient and the mean difference of the pair observations using a statistics software (Microsoft Excel for Mac, Microsoft Corporation, USA).

Results: Inter-observer variability coefficients for SAX and LAX are shown in Table 1 along with the mean difference and standard deviation. Correlation between corSAX and LAX is also shown in Table 1. Evaluation of the corSAX took a mean of 9.5 minutes longer than LAX.

Conclusion: Interobserver variability for end-diastolic volume and end-systolic mass is smaller when using a long axis approach instead of a short axis stack-based quantification. Thus, a long axis method may be preferable for follow-up studies.

The small differences between short axis and long axis approach observed for end-diastolic volume and end-systolic mass are likely due to the inclusion of trabecular tissue in the short axis approach.

TABLE 1

Inter-observer Variability Correlation Coefficients					
	SAX		LAX		
	r^2	Mean diff	r^2	Mean diff	p value
EDV (mL)	0.96	14 ± 12	0.99	8 ± 11	< 0.01
ESV (mL)	0.99	8 ± 11	0.98	6 ± 13	0.2
EF (%)	0.99	0.3 ± 4.2	0.95	0.9 ± 3.6	0.5
ES Mass (g)	0.93	31 ± 28	0.96	24 ± 17	< 0.01
	Correlation of LAX vs. SAX				
	Mean + SD LAX	Mean + SD SAX			
EDV (mL)	182 + 101	177 + 95	0.99	3.1	< 0.01
ESV (mL)	94 + 102	91 + 97	0.99	2.7	< 0.05
EF (%)	55 + 16	55 + 15	0.94	0.2	0.9
ES Mass (g)	144 + 64	140 + 62	0.94	1.1	0.056

648. A POINT-SPREAD-FUNCTION (PSF) ANALYSIS TO STUDY THE EFFECT OF PHASE ENCODING ORDER IN DELAYED ENHANCEMENT IMAGING

Raja Muthupillai, PhD,[1] Benjamin Cheong, MD,[2] Scott Flamm, MD.[2] [1]***Philips Medical Systems and Baylor College of Medicine, Houston, TX, USA,*** [2]***Radiology, St. Luke's Episcopal Hospital, Houston, TX, USA.***

Introduction: In typical implementations of delayed enhancement (DE) sequence, a segmented k-space approach is used to acquire all phase encoding steps necessary for image formation. During the readout, the MR signal continues to evolve, and this results in a modulation of signal intensity along the phase encoding direction. This mapping of this signal modulation on k-space depends on the phase encoding order (PEO). The purpose of this study is to investigate the effect of such signal modulation across K_y during the segmented gradient echo readout, for commonly used PEOs via point spread function (PSF) analysis.

Materials and Methods: All imaging was performed on a 1.5 T commercial MR imager (Philips, Intera Achieva). Four vials containing differing concentrations of Gd-DTPA in saline were imaged using an inversion-recovery prepared segmented gradient echo based DE technique. A synthetic ECG signal was used for gating. Specific acquisition parameters were: TR/TE/flip: 5/2.1 ms/ 15°; number of phase encoding steps/RR interval: 16; acquired and reconstructed voxel size: 1 × 1 × 8 mm. In 24 shots, all phase encoding steps from $-K_{ymax}$ to $+K_{ymax}$ were filled. The following profile orders were evaluated: (i) linear (L): the center of k-space was sampled at the middle of the readout, and the acquisition started from $-K_{ymax}$; (ii) low-high (LoHi): the center of k-space (near $K_y = 0$) was sampled at the beginning of the readout, and the acquisition proceeded towards +/- K_{ymax} towards the end of the readout; (iii) reverse-linear (RL): similar to L in that the center of k-space was sampled at the middle of the readout, but the acquisition started from $+K_{ymax}$. In the absence of partial Fourier imaging, the effect of L or RL are similar, and only results from profile order 'L' are presented here. The phase encoding gradient was turned off to directly visualize the effect of amplitude modulation along Ky as an image (Fig. 1, left most panels).

Results: Representative images depicting the amplitude modulation across k-space for linear and low-high PEOs, and the corresponding PSF are shown in Fig. 1.

Discussion: For linear profile orders, all tissues with T_1 values shorter than the tissue that is being nulled, e.g., irreversible injury, have a narrow PSF compared to tissues with longer T_1, e.g., pericardial effusion. For low-high profile order, for all tissues with T1 values shorter than the tissue being nulled, the characteristic amplitude modulation with lower signal intensity in the center of k-space results in a narrow PSF but with significant oscillatory side-lobes resulting in an image with an "edge enhanced" appearance. This analysis can be readily extended to both single shot 2D DE as well as 3D DE techniques.

Conclusions: The results from this study reveal that the shape of the PSF caused by amplitude modulation that occurs along K_y is significantly influenced by PEO. Some characteristic artifacts in DE imaging, e.g., edge enhancement, or ringing in the presence of relatively long T_1 tissue types such as pericardial effusion can be explained by the PSF analysis described.

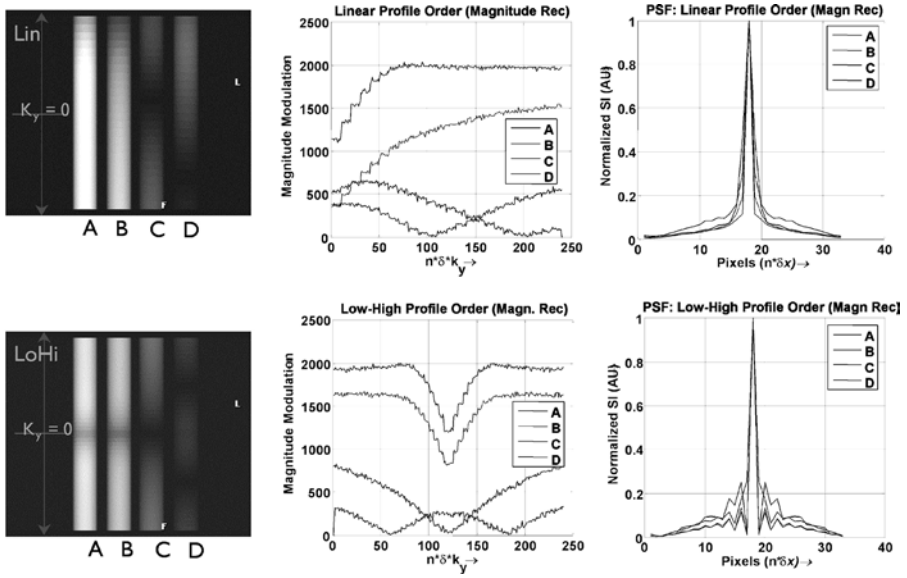

FIG. 1. Amplitude modulation along ky for Vials A-D, and the corresponding effect on PSF for linear profile order (top row), and low-high profile order (bottom row). Note the general broadening of PSF with the linear profile orders for increasing T_1 values, compared to the presence of side-lobes caused by the amplitude modulation in the case of low-high profile orders.

REFERENCES

1. de Roos A, Dornbos J, van der Wall E, van Voorthuisen A. AJR 188;c150:c531–534.
2. Kim RJ, Fieno DS, Chen EL, et al. Circulation 1999; 100:1992–2002.

649. POSITIVE CONTRAST TO EVALUATE STEM CELL VIABILITY AND PROLIFERATION USING OFF-RESONANCE MAGNETIC RESONANCE IMAGING

Yoriyasu Suzuki, MD, Phillip C. Yang, MD. ***Stanford University, Palo Alto, CA, USA.***

Introduction: MRI is emerging as a main diagnostic modality in preclinical investigations of stem cell therapy. Dual ability to track iron-oxide labeled cells and to characterize the treated tissue has enabled longitudinal monitoring of therapeutic efficacy. However, one of the limitations in cell therapy is the inability to confirm the quantity of the delivered cells *in vivo*.

Purpose: To estimate cell quantity *in vivo* using novel off-resonance (OR) MRI sequence designed to generate positive contrast to estimate the volume of iron-oxide labeled cells.

Methods: In vivo correlation between MR- and bioluminescence-guided quantitation of mESC following cell delivery was studied. Using mESC line transfected with Click Beetle Red luciferase reporter gene (mESC-luc$^+$), multimodality MR (1.5T Signa MRI Scanner, GE, WI) and bioluminescence imaging (BLI, Xenogen IVIS System 200, CA) was performed. 3×10^6 iron-oxide labeled viable mESC-luc$^+$ and formalin fixed non-viable mESC-luc$^+$were transplanted into the each hind limb of mice (n = 8). The mice were studied serially on 1, 4, 7, 10, and 16 post-opeartive days (POD) to measure luciferase activity using CCD camera system

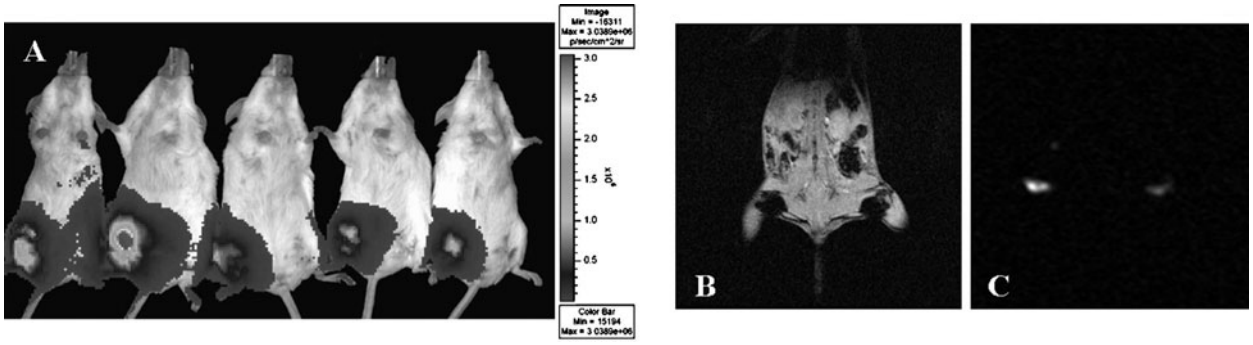

FIG. 1.

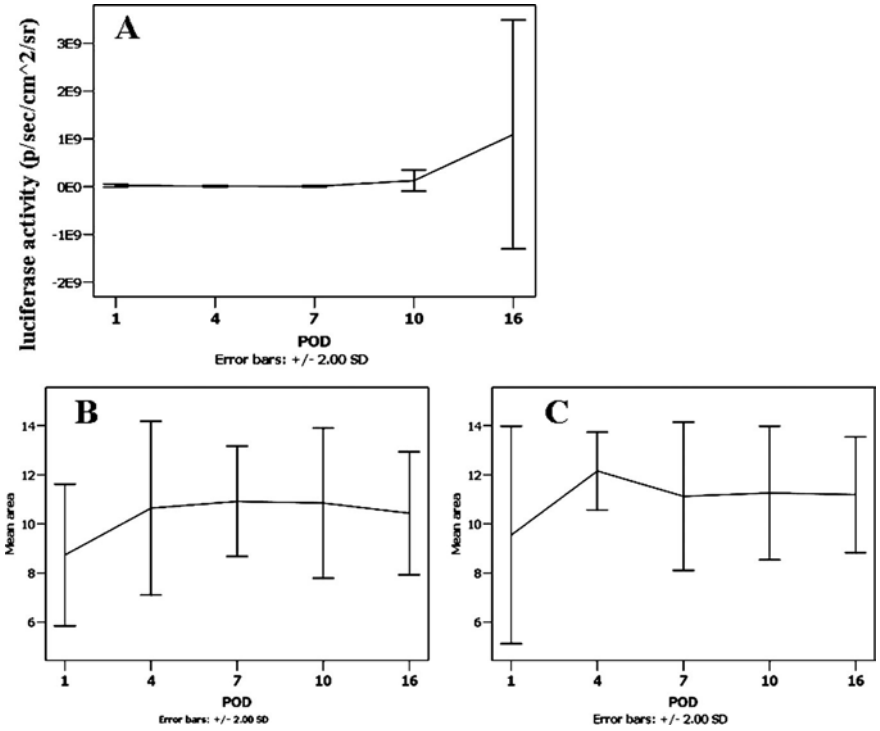

FIG. 2.

(IVIS, Xenogen) and 1.5T MR clinical scanner equipped with 3 inch surface coil. The photons emitted from mESC-luc$^+$ were quantified over 5 minutes. Conventional GRE and OR MRI sequences were applied to measure signal intensity and projectional area.

Results: Typical images of both modalities are shown in Fig. 1. Fig. 1A is BLI, 1B is conventional GRE, and 1C is OR. The BLI measurement of luciferase activity demonstrated no significant change from 1 to10 POD ($2.23 \times 10^7 \pm 0.7 \times 10^7$ vs. $1.26 \times 10^9 \pm 0.2 \times 10^9$ p/sec/cm^2/sr, p = NS). However, significant increase was seen from 1 to 16 POD ($2.23 \times 10^7 \pm 0.7 \times 10^7$ vs. $1.10 \times 10^9 \pm 0.2 \times 10^9$ p/sec/cm^2/sr, $p < 0.05$) indicating proliferation of the transplanted mESC (Fig. 2A). The OR imaging of both viable (Fig. 2B) and formalin-fixed (Fig. 2C) mESC demonstrated steady signal area from 1 to 10 POD (8.7 ± 1.4 vs.10.8 ± 1.5 cm^2, p = NS) and similarly from day 1 to 16 POD (8.7 ± 1.4 vs.10.4 ± 1.2 cm^2, correlation data, p = NS). The OR and BLI signal demonstrated close correlation of cell quantity during 1- 10 POD ($R^2 = 0.275$, $p = 0.009$).

Conclusions: These findings demonstrate that OR may provide a reliable estimation of the quantity of delivered cells during the initial period following cell delivery *in vivo*. These findings may be translated into *in vivo* pre-clinical and clinical investigations of the efficiency of cell delivery.

650. FEASIBILITY STUDY OF MYOCARDIAL PERFUSION WITH ADENOSINE VASODILATOR STRESS USING 3T CMR

Padmini Varadarajan, MD, Ramdas G. Pai, MD, Gerald M. Pohost, MD. ***USC, Los Angeles, CA, USA.***

A denosine CMR using 1.5 T magnet is well established. A 3 T magnet has the potential to provide better spatial resolution and hence a better predictive value for coronary artery disease. We evaluated the feasibility of adenosine CMR at 3 T to evaluate myocardial perfusion.

Methods: Thirty consecutive patients referred for evaluation of myocardial ischemia were evaluated by adenosine CMR using GE 3 T magnet. Adenosine was injected intravenously at 140 mcg/kg/min at a rate of 3 mL/min as a continuous infusion. At 4 minutes, 0.02 mg/kg of Gadolinium chelate was injected using a power injector and first pass evaluation was performed using FGRE notched saturation recovery pulse. A total of 4–6 short axis slices were obtained. Rest perfusion assessment was performed without the injection of adenosine. After a 10 min wait period, myocardial delayed enhancement was performed using inversion recovery sequence, flip angle 13 degrees, 2 NEX, inversion time 200–220. First pass scans were evaluated for a perfusion defect segmentally as well as transmurally. Ischemia was defined as a perfusion defect at stress but not at rest and a diagnosis of infarct was defined as presence of perfusion defect at stress with transmural scar by delayed enhancement imaging.

Results: Six patients had reversible perfusion defects, out of which 5 had significant epicardial coronary artery disease corresponding to the area of perfusion defect. One patient had diffuse subendocardial perfusion defect with normal coronary arteries and diffuse patchy scarring suggestive of microvacular dysfunction.

Conclusion: Our preliminary data indicate the feasibility of performing rest and stress myocardial perfusion using 3T CMR system with a very high diagnostic quality.

651. SPLENIC INVERSION TIME: AN INTERNAL STANDARD FOR CARDIAC INVERSION TIME ESTIMATION

Sanjaya Viswamitra, MB, BS, Kedar Jambhekar, MD, Sanjay Agarwala, MD, Behzad Molavi, MD. ***UAMS, Little Rock, AR, USA.***

Introduction: Delayed hyperenhancment is the gold standard in the evaluation for cardiac viability. This inversion pulse method is based on accentuating contrast in infarcted myocardium by nulling normal myocardium by using an inversion time equal to the null time for normal myocardium. However, the inversion time can be variable. Technical difficulties in the visualizing an

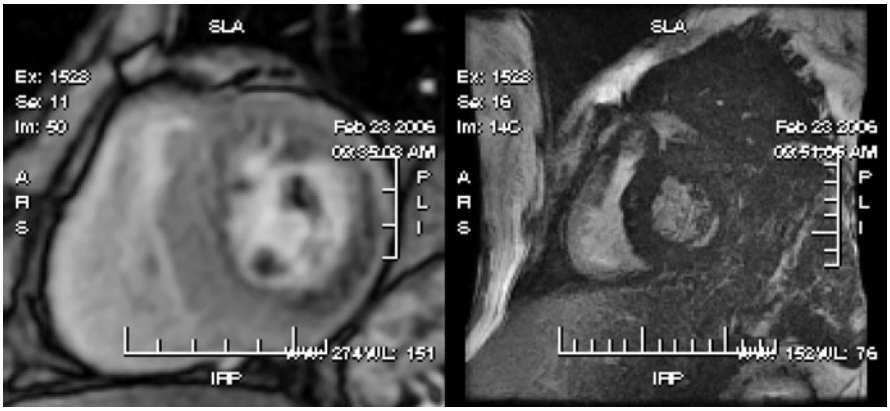

accurate inversion time can lead to improper use of null times and decreased conspicuity of the infarct. This can also be a difficulty when evaluating global disease states such as cardiomyopathy (eg. amyloidosis, hypertrophic cardiomyopathy) where one can accidentally null the pathology.

The null times of various tissues is proportional to the amount of gadolinium uptake, distribution, and kinetics as this has the greatest effect on the rate of recovery and hence null times of tissues after contrast administration.

Purpose: We propose using the spleen as an internal standard to accurately guage the null time for normal myocardium.

Methods: The time to inversion scout (TI scout) was retrospectively reviewed in 15 patients who had cardiac MRI with delayed hyperenhancement. Ten of these had CMR to evaluate viability while the remaining 5 had clinically documented cardiac amyloidosis.

All exams were performed on a 1.5 T Avanto (Siemens, Erlangen, Germany). Exams chosen were those where the spleen and the myocardium could be well visualized together on at least one image. The TI scout was obtained approximately 10 minutes after the intravenous administration of gadolinium contrast. The TI scout sequence is preprogrammed sequence that acquires images at every 25 ms interval between 150 ms and 700 ms. The images were then reviewed and visual note made of the inversion time for normal myocardium and that for the spleen.

Results: All 10 patients evaluated for viability had a TI time similar (equal to or within 25 ms) to that of myocardium. Of the 5 patients with cardiac amyloidosis, 3 had markedly differing null times for myocardium and spleen (>50 ms). Two patients with amyloidosis had inversion times that were less than 50 ms different from spleen but also had less diffuse involvement of the myocardium.

Conclusions: The inversion time of spleen is similar if not identical visually to the inversion time of normal myocardium at approximately 10 minutes from time of injection. The spleen and the myocardium are frequently seen together on at least one image allowing the spleen to be used as a reliable internal standard to guage the efficacy of the inversion time for normal myocardium.

652. IMPLEMENTATION OF CMR SEQUENCES ON A 1.5T CLINICAL SCANNER FOR QUANTITATIVE ASSESSMENT OF CARDIAC STRUCTURE AND FUNCTION IN A RODENT MODEL OF MYOCARDIAL ISCHEMIA

Alexandra Bernshausen, VMD,[1] Alexandra Kaithahn, MD,[2] Constanze Schroller, VMD,[1] Sylvia Schachoff, RT.[2] Markus Schwaiger, MD,[2] Karl L. Laugwitz, MD,[1] René M. Botnar.[2]
[1]Department of Cardiology, Technical University Munich, Munich, Germany, [2]Department of Nuclear Medicine, Technical University Munich, Munich, Germany.

Introduction: With the advent of genetically modified mice, in-vivo investigation of structural, functional, and molecular changes of various cardiovascular diseases such as myocardial infarction, cardiomyopathy, heart failure or atherosclerosis has become feasible under well controlled conditions. Such models offer great potential for quantitative and serial assessment of ejection fraction (EF), regional wall motion or plaque progression/regression after pharmacological or stem cell therapy. Furthermore, histological correlates can be obtained for microscopic validation. To facilitate translational research and to have full access to cardiac MR (CMR) sequences that are readily available on clinical scanners, we sought to optimize clinical MR protocols for murine and rat imaging on a 1.5 T clinical scanner.

Purpose: We sought to implement ECG triggered MR pulse sequences on a 1.5 T clinical scanner for assessment of cardiac structure and function in mouse and rat models of myocardial ischemia.

Methods: For reliable ECG synchronization and high resolution imaging, a dedicated small animal ECG device, 1025-MR, (SA Instruments Inc., Stony Brook, NY) and dedicated microscopy coils (Philips Medical Systems, Best, The Netherlands) were used. All imaging was performed on a 1.5 T Philips Achieva MR scanner using a dedicated cardiac software package (R1.2.2) and a clinical gradient system (30 mT/m, 150 mT/m/ms). Animals were anesthetized with fentanyl, medetomidin, and midazolam and imaged in prone position with the thorax positioned on top of the microscopy single loop surface coil (D = 2.3 mm or D = 4.7 mm). High-resolution MRI sequences for assessment of myocardial function, infarct size, and morphology were implemented. Cine MRI was performed with both prospective and retrospective ECG triggering using a spoiled gradient echo technique. Imaging parameters included TR/TE = 18 ms/6.5 ms, flip angle = 30°, averages = 1, FOV = 35 mm, matrix = 128 resulting in a spatial resolution of 0.22 × 0.22 × 1 mm at a temporal resolution of 18 ms. Delayed enhancement imaging was performed with an inversion recovery (IR) gradient echo sequence with diastolic image acquisition. Imaging parameters included TR/TE = 10 ms/4.8 ms, flip angle = 25°, averages = 4, lines per RR interval = 4, FOV = 70, matrix = 192 resulting in a spatial resolution of 0.36 × 0.36 × 2 mm. Image acquisition was synchronized with every 3rd R-wave to allow for sufficient magnetization recovery. T2* weighted black blood imaging was performed with a double inversion gradient echo technique with the inversion time set to null blood. Imaging parameters included TR/TE = 13 ms/9.2 ms, flip angle = 20°, averages = 5, lines per RR interval = 5, FOV = 100, matrix = 192. Image analysis was performed using a standard cardiac software package on a commercial ViewForum workstation (Philips Medical Systems, Best, The Netherlands). Ejection fraction was calculated for all animals.

*Results:*In the majority (> 90%) of animals, cine MRI could be successfully performed (Fig. 1). Failure of scanning was always related to an insufficient ECG signal. Ejection fraction in

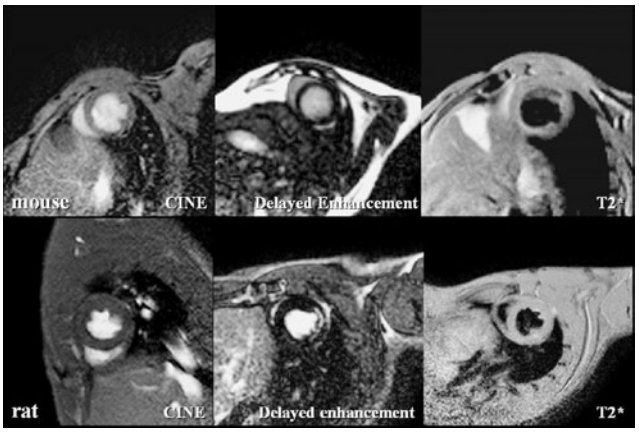

control mice was ~ 60%. Calculation of end-systolic and diastolic volumes was not possible using the clinical post-processing software as data precision was insufficient. Delayed enhancement imaging allowed visualization of infarct size (Fig. 1, bottom row) and black blood imaging provided additional anatomical information. The limiting factors of performing small animal MRI in a clinical scanner are gradient performance and ECG reliability. The first affects TR and thus temporal resolution, while the latter could be reduced by twisting the ECG cables and thereby minimizing gradient coupling. In terms of spatial resolution (~200 μm) and scan time (~2 min/slice), cine MRI on a clinical MR scanner provided similar results as compared to high field animal systems.

*Conclusions:*We successfully demonstrate the feasibility of performing small animal cardiovascular MR in a clinical 1.5T MR scanner with similar spatial resolution as compared to high field small animal systems. With dedicated insert gradient coils, advances in ECG devices, and analysis software, small animal imaging in a clinical scanner may become a valuable alternative to high field animal systems thereby facilitating translational research.

653. FAST 2D FREE-BREATHING, RESPIRATORY-TRIGGERED INVERSION RECOVERY DELAYED ENHANCEMENT: CLINICAL EVALUATION IN CHRONIC INFARCTS

Glenn Yo, MD,[1] Harrie van den Bosch, MD,[1] Johannes Post, MD, PhD,[2] John Wondergem, MD,[1] Jan Verwoerd, MSc,[1] Albert de Roos, MD, PhD.[3] [1]***Catharina Hospital, Department of Radiology, Eindhoven, The Netherlands,*** [2]***Catharina Hospital, Department of Cardiology, Eindhoven, The Netherlands,*** [3]***LUMC, Department of Radiology, Leiden, The Netherlands.***

Introduction: Delayed contrast-enhanced(DE) MRI is now routinely used for the evaluation of (non-)viable myocardium in patients with chronic ischaemic myocardial disease. Accepted techniques apply multiple breathholds in 2D techniques and one-breath-hold acquistions in 3D scans. Therefore, image quality is highly dependant on the patient's ability of breathholding. For viability imaging in extended protocols (for example, stress protocols), and in dyspnoeic patients a free-breathing, respiratory-triggered DE acquisition may be needed.

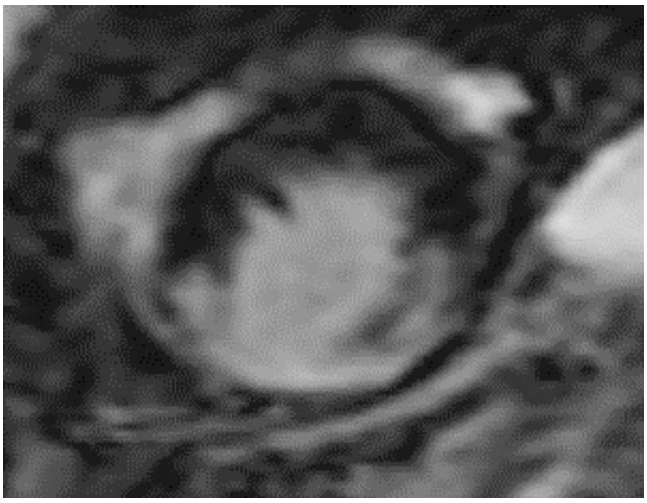

FIG. 1. Two dimensional free-breathing, respiratory-triggered IR B-TFE.

Purpose: Our objective was to evaluate a fast 2D free-breathing, respiratory-triggered Inversion Recovery B-TFE sequence in a clinical setting.

Methods: In this study, 32 consecutive patients (25 men and 7 women; mean age 68 y) were included with known ischaemic myocardial disease. All imaging was performed on a clinical 1.5 T Achieva MR system, software release 1.2. DE-MR protocol consisted of a 3D breathheld IR sequence and a free-breathing, respiratory-triggered 2D B-TFE sequence, both acquired in short axis plane.

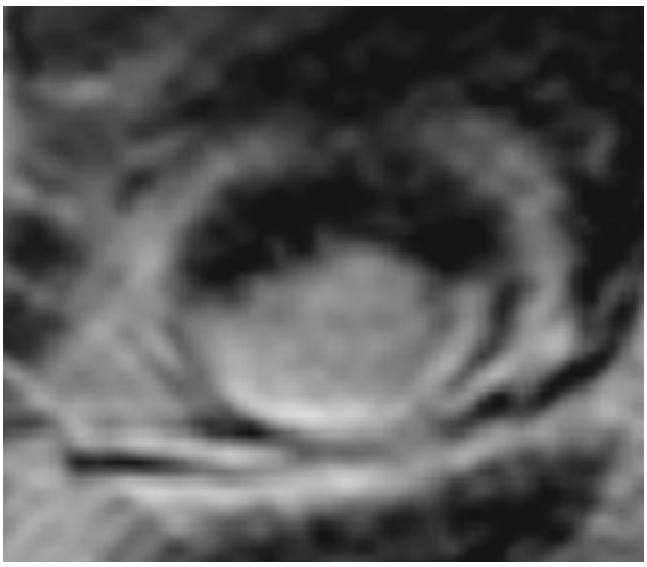

FIG. 2. Three dimensional breathhold IR IR TFE.

Three dimensional breathhold IR-TFE DE parameters: TR/TE = 3.7 ms/1.15 ms; flip angle = 15°; voxel size = 1.50 × 1.50 × 10.0 mm.

Two dimensional free-breathing IR B-TFE DE parameters: TR/TE = 3.0 ms/1.49 ms; flip angle = 45°; voxel size = 1.37 × 1.37 × 10.0 mm.

Data analysis: For statistical analysis we considered only segments that were graded diagnostic in both DE techniques. Analysis of all data was performed by two expirienced cardiac MR radiologists. Image quality was analysed on a 4 point scale. Segmental, transmural extent of non-viable tissue and quantitative analysis (%LV) were obtained.

Results: In 28 of 32 patients, the image quality was good to excellent for both DE techniques. In one patient, the 3D DE scan was non-diagnostic and in one patient 10 out of 16 segments were of non-diagnostic quality. The image quality for the 2D free-breathing scan in these two patients was good and excellent, respectively. In total 486, segments were scored independantly for segmental, transmural extent of non-viable tissue. Good interobserver agreement was obtained for both DE techniques (kappa = 0.70). Quantitative analysis (% LV) showed good correlation for infarctsize between both techniques (r^2= 0.90).

Conclusions: Two dimensional free-breathing, respiratory-triggered IR B-TFE DE sequence can be used as a reliable tool in a clinical setting. This technique maybe a good alternitive in dyspnoeic patients and in extended cardiac MR protocols.